UNIVERSITÀ DEGLI STUDI DI SALERNO

UNIVERSITÀ DEGLI STUDI DI SALERNO
Dipartimento di Farmacia

PhD Program
in **Drug Discovery and Development**
XXX Cycle — Academic Year 2017/2018

PhD Thesis in

Design, synthesis and biological activity of new target selective antitumoral agents

Candidate	Supervisor
Alessandra Russo	Prof. *Ines Bruno*

PhD Program Coordinator: Prof. Dr. *Gianluca Sbardella*

Preface

My three-year PhD course in Drug Discovery and Development at the Department of Pharmacy of Salerno University started in 2014 under the supervision of Prof. Ines Bruno. My research project was mainly focused on the design, synthesis and biological evaluation of small molecules as new modulators of novel emerging targets involved in cancer processes. Specifically, my research activity was focused on the investigation of two major targets:

- the epigenetic family of Macrodomain proteins, in particular, the hydrolases MacroD1 and MacroD2;
- the Bcl-2 associated athanogene 3, BAG3.

The entire work was carried out under the direct supervision of Prof. Ines Bruno and Dr. Stefania Terracciano. The Computational guided design of compounds was performed in collaboration with Prof. Giuseppe Bifulco's research group. Biological screenings were performed in collaboration with Dr. Jon Elkins of the Structural Genomics Consortium (Oxford University), in the case of Macrodomain proteins project, whereas with Dr. Maria Carmela Vaccaro and Prof. Alessandra Rosati, in the case of BAG-3.

Furthermore, to improve my knowledge on Macrodomain proteins, in 2016 I joined Dr. Jon Elkins' research group at the Structural Genomics Consortium where I spent five months. During that period, my research was carried out under the supervision of Dr. Romain Talon and was addressed to the expression, purification and crystallization of human MacroD1 protein, in order to perform a fragment screening, X-ray crystallography based, on the target of interest.

List of publications related to the scientific activity performed during the three years PhD course in Drug Discovery and Development

Papers:

- ➢ S. Terracciano, A. Foglia, M. G. Chini, M. C. Vaccaro, **A. Russo**, F. Dal Piaz, C. Saturnino, R. Riccio, G. Bifulco and I. Bruno. "New dihydropyrimidin-2(1H)-one based Hsp90 C-terminal inhibitors". *RSC Advances,* **2016**, 6, 82330-82340.

- ➢ Stefania Terracciano, **Alessandra Russo**, Maria G. Chini, Maria C. Vaccaro, Marianna Potenza, Antonio Vassallo, Raffaele Riccio, Giuseppe Bifulco, and Ines Bruno, "Discovery of new molecular entities able to strongly interfere with Hsp90 C-terminal domain". *Scientific Reports, 2018, 8, 1709, 1-11;*

- ➢ Simone Di Micco, Luana Pulvirenti, Ines Bruno, Stefania Terracciano, **Alessandra Russo**, Maria C. Vaccaro, Vera Muccilli, Nunzio Cardullo, Corrado Tringali, Raffaele Riccio, Giuseppe Bifulco. "Identification by Inverse Virtual Screening of Magnolol-Based Scaffold as New Tankyrase-2 Inhibitors". **Submitted Manuscript** to *Bioorganic & Medicinal Chemistry,* **2018**.

Conference proceedings:

➢ **A. Russo**, I. Bruno, S. Terracciano, G. Bifulco, G. Lauro. "Design and Synthesis of potential Inhibitors of Macrodomains as new promising candidates in Cancer therapy". European-Winter School on Physical Organic Chemistry, Bressanone (Italy), February, 1-6, 2015;

➢ **A. Russo**, S. Terracciano, G. Lauro, G. Bifulco, R. Riccio, I. Bruno. "Discovery of potential modulators of Macrodomain proteins MacroD1 and MacroD2" XXXVI National Meeting of Italian Chemical Society, Organic Chemistry Division**,** Bologna (Italy), September 13-17, 2015;

➢ **A.Russo**, S. Terracciano, G. Lauro, G. Bifulco, R. Riccio, I. Bruno."Design, synthesis and biochemical evaluation of potential MacroD2 protein modulators" XLI International Summer School on Organic Synthesis "A. Corbella" ISOS 2016 , Gargnano (Italy)**,** June, 12-17, 2016;

➢ **A.Russo**, S. Terracciano, G. Lauro, G. Bifulco, R. Riccio, I. Bruno. "X-ray crystallography based fragments screening on Macrodomain protein MacroD1" XLII International Summer School on Organic Synthesis "A. Corbella" ISOS 2017, Gargnano (Italy), June, 18-22, 2017;

➢ **A. Russo**, S. Terracciano, G. Lauro, M. C. Vaccaro, R. Riccio, G. Bifulco, I. Bruno. "Microsomal Prostaglandin E2 Synthase-1 potential inhibitors: design, synthesis and biological evaluation" XXVI International meeting of Italian Chemical Society, Paestum (Italy), September, 10-14, 201.

Table of contents

Abstract

Cancer development is a complex pathological process that exploits a variety of biological actors. The identification of new molecular entities able to interfere with new biological targets involved in tumorigenesis is strongly needed, both for the development of new promising drug candidates, and as chemical probes useful to further investigate less understood biological aspects. Two main targets, involved at different levels in cancer development, have been thoroughly investigated: the epigenetic Macrodomain proteins, MacroD1 and MacroD2, and the Bcl-2 associated athanogene 3, BAG3 protein. The results obtained are summarized in the two main sections, reported below according to the target of interest:

a) Discovery of new modulators of human Macrodomain proteins, MacroD1 and MacroD2, by structure-based and X-ray crystallography based approaches.

MacroD1 and MacroD2 are two orthologue members of the epigenetic family of the Macrodomain containing proteins which have been recently identified as attractive targets for the treatment of cancer, due to their well-established overexpression in several human tumors.[1-2] These proteins can act as *erasers* of the histone code ADP-rybosilation, a post-translational modification involved in the modulation of gene expression and chromatin remodelling.[3] With the aim of identifying new modulators of these high related proteins, we carried out two different drug discovery approaches: a computer aided structure based drug design on the MacroD2 crystal structure (PDB: 4IQY) and a Fragment screening, based on X-ray crystallography, on the protein MacroD1. Concerning the first approach, starting from the crystal structure of MacroD2 protein in complex with ADP-ribose, its natural ligand, we performed a preliminary virtual screening on a Database of 16 million of 1,4 disubstituted triazoles. Results analysis allowed us to select the most promising molecules in terms of docking score and shape similarity. The next step consisted in the synthesis of the most promising molecules basing on a versatile and suitable synthetic strategy. The synthetized molecules were, then, tested in collaboration with the Structural Genomics Consortium of Oxford, to evaluate their ability to bind the target protein with Alpha Screen, Biolayer interferometry and

Isothermal titration calorimetry. These biophysical methods allowed us to disclose compound **SP2** as a real binder of the protein MacroD2, with a dissociation constant of 2.54±1.1 µM. This promising molecule will be further investigated on MCF-7 cancer cells, overexpressing the protein, to assess its potential antitumoral activity.

Concerning the study of MacroD1 protein, a fragment screening based on X-ray crystallography technique has been carried out, during my stage experience at the University of Oxford; this advanced method allowed the identification of three fragments co-crystallized with the protein MacroD1. Since in the Surface Plasmon Resonance (SPR) assay the binding to the protein was confirmed for two of the three fragments, we decided to start to investigate, *in silico*, the binding mode of the most promising one, compound **3**, in order to develop a collection of high affinity binders for the target protein. These new molecules have been synthesized and then tested again by SPR, against the protein MacroD1 and, in line with the computational predictions, four of them showed to bind the target protein with higher affinity, compared to the lead compound; these results are of great interest since so far no Macrodomain binder has been yet disclosed, hence they can open the way to the discovery of new chemical platforms able to modulate the protein MacroD1, as new attractive candidates for drug development.

b) Design, synthesis and biological evaluation of the first BAG3 modulator as an attractive candidate for the development of a new class of chemotherapeutics.

BAG3 (Bcl-2-associated athanogene 3) is a multidomain protein which, through its BAG domain, is able to interact with several partners, modulating, thus, key signalling pathways involved in physiological and pathological processes.[4] Indeed, BAG3 has been shown to sustain cell survival and to induce resistance to chemotherapy in human cancers, hence, it is recently emerged as a therapeutic target of human malignancies.[5] With the aim of exploring BAG3 protein, basing on a combined approach of *structure-based drug design* and biophysical methods, we screened a huge library of commercially available molecules against the target of interest. Starting from the virtual screening and SPR results, we selected a 2,4

Abstract

thiazolidinedione based molecule (**7**), as a promising BAG3 activity modulator. This compound, indeed, showed to bind with a good affinity both to the full length protein (K_D: 5.2±3.8 nM) and to its isolated BAG domain (K_D: 3.51±2.7 nM), moreover it did not show any binding for two other members of BAG proteins tested, BAG1 and BAG4. Hence, we decided to evaluate the potential antiproliferative activity of the disclosed hit on A375 melanoma cancer cells, which are known to overexpress the BAG3 protein; compound **7** resulted to have a good cytotoxicity (25±1.5 μM) against the cell line tested, in line with our predictions. Starting from these promising outcomes, we developed a collection of synthetic 2,4-thiazolidindiones, as derivatives of the lead compound, in order to expand the chemical diversity around the scaffold and we succeeded to identify a promising molecule (**LK-4**); this compound, indeed, was able to selectively bind BAG domain of BAG3 protein, with high affinity (K_D: 6.4±2.2 nM), interfering with BAG3-Hsp70 protein-protein interaction. **LK-4** showed a high cytotoxicity (IC_{50}: 16±1.5 μM) against A375 melanoma cancer cells, and at the same time, a good selectivity; moreover, it did not affect the cell viability of PMBC human normal cells. A co-immunoprecipitation assay confirmed that **LK-4** interfere with BAG3-Hsp70 complex formation in cell and in a time-dependent manner, representing a valuable chemical probe to further investigate BAG3 protein in the attempt to develop new attractive protein modulators.

INTRODUCTION

CHAPTER 1

Macrodomain proteins: MacroD1 and MacroD2

1.1. Drug discovery in cancer therapy

"Cancer" is a generic term used to describe a large group of related diseases that involve an abnormal cell growth with the potential to spread to other parts of the body. According to the World Health Organization (WHO), more than one hundred types of cancer have been disclosed so far, and owing to the great variety of histological types, and, overall, to its multifactorial etiology, it is a particularly difficult disease to treat. The challenge for a medicinal chemistry project is to design new drugs able to selectively target cancer cells, while avoiding multidrug resistance pathways. In the last decades, the many efforts lavished in this research area provided valuable insights into cancer physiopathology with the disclosure of strategic biological targets which can be of great help for the development of potent and selective chemotherapeutics. These achievements have been made possible thanks to multifaceted approaches requiring the synergistic contribution of several scientific figures, e.g., clinicians, biologists, medicinal and synthetic organic chemists, X-ray crystallographers and other structural biologists, chembioinformaticians, computational experts, and logicians, among others. This tireless joint research provided a great improvement of the technological tools employed in drug discovery programs (**Figure 1.1**). For example, once the molecular target has been selected, the advanced computer-aided approaches provide a fast and cost-efficient lead identification. Moreover, such computational programs are useful also to predict whether the designed molecules are likely to display the desired ADMET (absorption, distribution, metabolism, excretion, and toxicity) properties. In addition, on one side, the progress made in Organic synthesis provides synthetic procedures that allow to rapidly generate a wide structural variety of products, on the other side, the introduction of innovative biophysical and biological techniques enables the rapid screening of a great number of compounds, supplying information useful to outline a SAR profile of the most promising molecules. Basing on these premises, my PhD research project has been focused on the development of new modulators of novel biological targets involved in tumorigenesis. In particular, in the frame of the research lines carried out by the Organic Chemistry group of the Department of Pharmacy, University of Salerno, I decided to investigate two interesting targets such as: the human Macrodomain

proteins MacroD1 and MacroD1 and the Bcl2-associated athanogene 3 (BAG3). The MacroD family proteins are considered epigenetic enzymes whose overexpression, in various cell lines, has been shown to protect against multiple apoptotic signals such as: chemical, biological or physical stimuli. After DNA damage, Macrodomain proteins can inhibit apoptosis by modulating chromatin remodeling activity, through protein ADP-rybosilation, and facilitate DNA repair within a chromatin context.[6] The other target under investigation is the BAG3 protein, a member of BAG family, recently emerged as a key regulator of important physiological processes including cell survival, apoptosis, cytoskeleton organization, and autophagy[7]; through its well conserved domain, BAG3 has also been shown to collaborate with Hsp70 in regulating cancer development through multiple pathways.[8]

Moreover, during my PhD research project, I had the opportunity to go to spend a research period at the Structural Genomics Consortium, in Oxford, where I experienced the innovative technologies of the synchrotron of the Diamond Light Source which allowed to expand my knowledge in the protein crystallization and fragment screening processes.
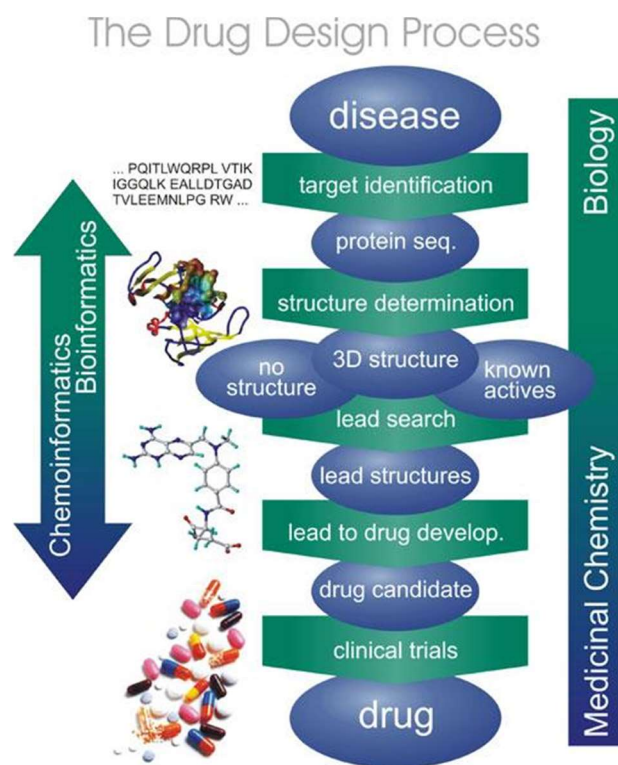
Figure 1.1 *Flow chart of the Drug discovery process*

1.2. Epigenetics

Epigenetics is a genomic branch defined as the study of the structural adaptation of chromatin to exogenous signals; in more detail, it includes all the chromosomal modifications associated with both, DNA repair, or cell-cycle phases, and stable changes maintained across multiple cell generations. In simple words we can say that the epigenetic mechanisms are all the inheritable changes in gene expression with no alterations in DNA sequences.[9] The term epigenetics was first introduced by Conrad Waddington, however many further definitions have been given from 1942 to date. Chemical modifications of DNA and histones are dynamically laid down and removed by chromatin-modifying enzymes in a highly regulated manner (**Figure 1.2**). Four different DNA modifications[10] and 16 classes of histone modifications have been at least well elucidated.[11,12] These modifications can alter chromatin structure by modifying noncovalent interactions within and between the nucleosomes. They also serve as docking sites for specialized proteins with unique

domains, the so called "chromatin readers", that specifically recognize these modifications, and recruit additional chromatin modifiers and remodeling enzymes, which, in turn, act as the effectors of the modification. The information conveyed by the epigenetic modifications plays a critical role in the regulation of all DNA-based processes, such as transcription, DNA repair, and replication. Consequently, abnormal expression patterns or genomic alterations in chromatin regulators can have profound effects and can lead to the induction and maintenance of various cancers. Hence, disruption of the epigenome is a well-recognized fundamental mechanism in cancer, and several epigenetic drugs have been proven to modulate cell survival and to be less toxic than conventional chemotherapy.[13] The great interest evoked by this research area prompted many investigations in the attempt of understanding and clarifying several issues, however, although significant advances have been done in this field, many questions remain still unsolved.
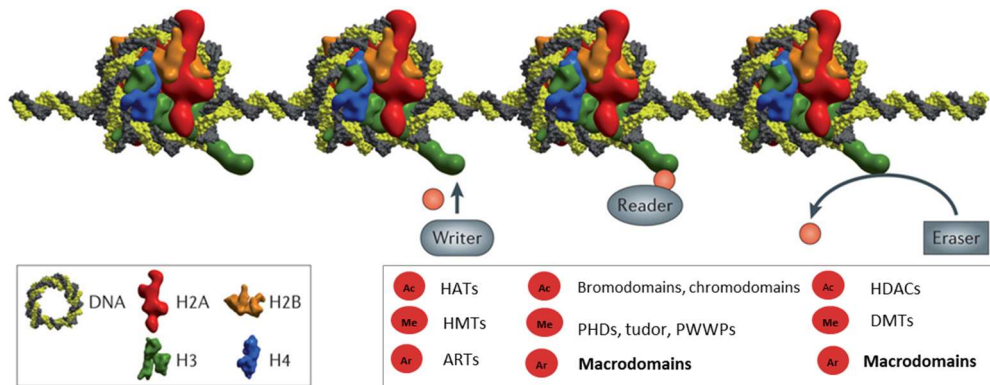
**Figure 1.2** *Epigenetic enzymes involved in regulation of gene expression*

DNA methylation

DNA methylation is a widespread modification in bacteria, plants and mammals; this covalent modification is natural in DNA; it is produced during DNA replication and it is considered as a stable gene-silencing mechanism. In eukaryotic cells DNA methylation takes place at the 5' end of the cytosine nucleotide followed by a

guanine nucleotide (CpG dinucleotide), and requires S-adenosyl-methionine as methyl donor. This reaction is catalyzed by the DNA methyltransferase enzymes family (DNMT family), including DNMT1, DNMT3A and DNMT3B. Cancer-associated DNA hypomethylation is as prevalent as cancer-linked hypermethylation, however, these two types of epigenetic abnormalities, usually, seem to affect different DNA sequences. It has been suggested that tumor-associated DNA hypermethylation contributes to carcinogenesis separately from aberrant DNA hypomethylation[14], and it has been proved to silence tumor suppressor genes; this kind of aberration has been mostly found in CpG-rich 5' gene regions.[15,16] However, the understanding of cellular consequences of normal and aberrant DNA methylation remains a key area of interest, nevertheless, so far, hypomethylating agents represent one of the few epigenetic therapies that have gained FDA approval for routine clinical use.[17]

Histone modifications

Histones including H2A, H2B, H3 and H4 form, together, the histone octamer that is the basic structure of the nucleosome components.[18] Chromatin or histone components are prone to a wide variety of covalent, reversible, post translational modifications, such as acetylation, mono-, di-, and trimethylation on lysine residues, symmetric or asymmetric mono- and dimethylation on arginine residues, phosphorylation on serine and threonine residues, ubiquitination, biotinylation, and SUMOylation (Small Ubiquitin-like Modifier or SUMO) on lysine residues, and finally mono-ADP-ribosylation on arginine and glutamate residues (**Table 1.1**).
Although many examples of modifications within the central domains of histones have been identified, the majority of these post-translational modifications occur on the lysine amino-tails, due to their protruding position from the nucleosome core. These modifications, individually or in combination, are able to influence inheritable epigenetic programs that encode distinct nucleosome functions, such as gene transcription, X-chromosome inactivation, heterochromatin formation, mitosis, and DNA repair and replication.[19,19b] Mechanistically, these functions are exerted either directly, by altering nucleosome interactions with chromatin, or

indirectly, by recruiting effector proteins that, with specific modules, recognize particular histone modifications in a sequence-dependent manner. In addition to their catalytic functions, many chromatin modifying factors also possess ''reader'' domains, allowing them to bind to specific regions of the genome and respond to the information conveyed by upstream signaling cascades. The amino-acidic residues that line the binding pocket of the reader domains can dictate a particular preference for specific modification states, whereas, residues outside the binding pocket, contribute to determining the histone sequence specificity. The basis underlying these epigenetic codes resides in the substrate specificity both, of the enzymes that catalyze the several covalent modifications, and of the enzymes that remove these marks to reverse the modifications. Given that chromatin is the physiological template for all DNA-mediated processes, it is not surprising that histone modifications represent an essential component in controlling the structure and/or function of the chromatin, with different modifications yielding distinct functional consequences. Indeed, site-specific histone modifications have shown to correlate with particular biological functions such as gene transcription, chromatin remodeling and apoptosis regulation (**Figure 1.3**).[20]

Modification	Targets	Enzyme involved	Effect	Reversible
Acetylation	Lysine	Histone acetyltransferases (HATs), Histone deacetylases (HDACs)	Acetylation removes positive charges and reduces histone-DNA interaction	Yes
Methylation	Arginine and lysine	Lysine methyltransferases, arginine methyltransferases, lysine demethylases	Methylation removes positive charges and reduces histone-DNA interaction	Yes
Phosphorylation	Serine, theonine, tyrosine	Kinases, phosphatases	Adds negative charges that can alter chromatin structure and accessibility	Yes
Ubiquitylation/sumoylation	Lysine	E1, E2, E3 add 8 kD ubiquitin or 12 kD SUMO, removal by isopetidase deubiquitin enzymes	Suppress gene expression, possible targeting of histone to proteosome for degradation	Yes
ADP Ribosylation	Glutamate and arginine	Poly-ADP-ribose-polymerase (PARP), poly-ADP-ribose-glycohydrolases	Mono-, poly-ribosylation restricts access, possible role in chromatin stabilization, such as in DNA repair	Yes
Deimination/citrrulination	Arginine, methylated arginine	Peptidyl arginine deiminase 4 (PAD4)	Removes positive charge of arginine, reduces histone-DNA interaction	No
Protein conjugation	Lysine	Transglutaminases	Covalent attachment of molecules to proteins and protein-protein crosslinking	No
β-N- acetylglucosamine	Serine, threonine	*O*-GlcNAc transferase, β-*N*-acetylglucosaminidase (*O*-GlcNase)	Sugar added by transferase, removed by *O*-GlcNcase	Yes

Table 1.1 *Principal Histone modification*

1.3. Main histone modifications

Histone methylation

Lysine methylation of histones H3 and H4 is implicated in both transcriptional activation and repression, depending on the methylation site, while, arginine methylation promotes transcriptional activation. Lysines can be either mono-, di- or tri-methylated, providing functional diversity to each site of methylation. The most extensively studied histone methylation sites include histone H3 lysine 4 (H3K4), H3K9, H3K27, H3K36, H3K79 and H4K20[21], but there are also arginine sites of methylation including H3R2, H3R8, H3R17, H3R26 and H4R3. Several studies demonstrated that histone methylation plays an important role at different levels of the transcriptional regulation, through the recruitment of cell-specific transcription factors and the interaction with initiation and elongation factors.[22]

Histone acetylation

Histone acetylation is an epigenetic mark often associated with an open chromatin structure. This makes chromatin accessible to transcription factors and can significantly increase gene expression. Histone acetylation is largely present at DNA promoter regions. For example, acetylation of K9 and K27 on histone H3 (H3K9ac and H3K27ac) is normally associated with an increase of active genes. However, acetylation low levels are also found throughout transcriptionally active genes, and for this reason, this issue is still under debate. Histone acetyltransferases (HAT) and Histone deacetylases (HDACs) are the enzymes responsible for writing and erasing the acetylation tag on the histone tails. This mechanism has shown to regulate the dynamic chromatin plasticity, and actually, lysine residues within histone H3 and H4 showed to be the preferential targets for HAT complexes.[23]

Histone phosphorylation

Phosphorylation of histone cores is a critical intermediate step in chromosome condensation during cell division, in transcriptional regulation, and in DNA damage repair processes. Unlike acetylation and methylation, histone phosphorylation seems to function by establishing interactions between other histone modifications and serving as a platform for effector proteins, leading to a downstream cascade of events. Phosphorylation of histone H3 at S10 (H3phosphoS10) and histone H2A on T120 are mitotic markers: these modifications, in fact, are involved in chromatin compaction and in chromatin function regulation during mitosis. Phosphorylation of H2AX at S139 (resulting in γH2AX) has been identified as one of the earliest events occurring after DNA double-strand breaking and serves as a recruiting point for DNA damage repair proteins.[24] Actually, histone phosphorylation plays a wide range of roles: H2B phosphorylation, that have been the focus of extensive investigations, for example, facilitates apoptosis-related chromatin condensation, DNA fragmentation, and cell death.[25]

1.4. ADP-Rybosilation

ADP- rybosilation, firstly described in 1960', is a reversible post-translational modification (PTM) of proteins, resulting in the covalent attachment of a single ADP-ribose unit [i.e., mono(ADP-ribose) (MAR)] or polymers of ADP-ribose units [i.e., poly(ADP-ribose) (PAR)] on a variety of amino acid residues on target proteins.[26] ADP-ribosylation reactions are phylogenetically ancient and can be divided into four major groups: mono-ADP-ribosylation, poly-ADP-ribosylation, ADP-ribose cyclization, and formation of O-acetyl-ADP-ribose. When this modification occurs, an ADP-ribose moiety of NAD is transferred to a specific amino acid of an acceptor protein on the histone tails with the consequent release of nicotinamide.[27,28] The reaction can occur through both enzymatic and non-enzymatic mechanisms.[29] The enzymatic type is mediated by diverse groups of ADP-ribosyl transferase (ADPRT) enzymes, which use ADP-ribose units, derived from β-nicotinamide adenine dinucleotide (NAD^+), to catalyze the ADP-

ribosylation reaction. To date there are 22 human gene products possessing ADP-ribosyltransferase activity; these enzymes include bacterial ADPRTs (e.g., cholera toxin and diphtheria toxin) as well as members of three different protein families in yeast and animals: (1) arginine-specific ecto-enzymes (ARTCs), (2) sirtuins, and (3) PAR polymerases (PARPs).[30] This modification has been shown to regulate several cellular functions via different mechanisms. For example, rybosilation of protein substrates can affect protein-protein interactions, the factors repairing recruitment to DNA damage sites, DNA repair processes, moreover, rybosilation of target proteins can also facilitate their ubiquitination, promoting protein degradation via proteasomal pathways. Basing on these considerations and on other growing mass of evidences, ADP-related pathways have been recognized to be implicated in a wide range of cellular processes like transcription, chromatin remodeling, cell proliferation, apoptosis and cancerogenesis.[31,32]
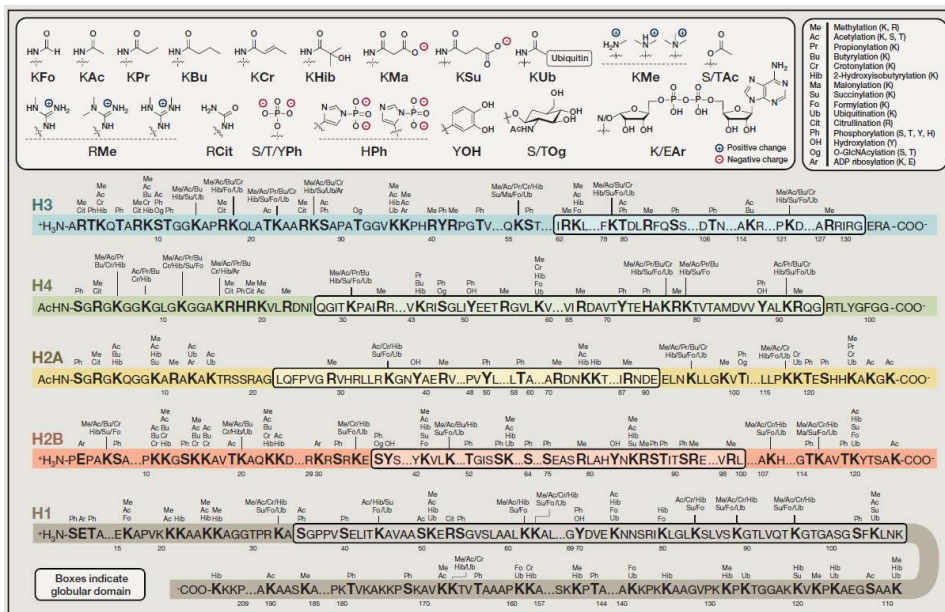


Figure 1.3 *Histone modifications on the histones cores [33]*

Mono-ADP-rybosilation

Mono-ADP-ribosylation is a post-translational modification originally identified as the pathogenic mechanism of several bacterial toxins. This modification is catalyzed by mono-ADP-ribose-protein transferases (MARTs), whereas, mono-ADP-ribose-protein hydrolases (MARHs), are the enzymes able to reverse the reaction by hydrolyzing the protein-ADP-ribose bond.[34,35] The simultaneous presence of both mono-ADP-ribosyltransferase and mono-ADP-ribose-protein hydrolase activities, in the same cell, suggests that the reversible protein mono-ADP-ribosylation represents a regulatory mechanism for the protein substrates.[36] It is known that mono-ADP-ribosylation occurs at different amino acid residues levels, according to the specificity of the individual MARTs. ADP-ribosylation of histones is thought to be linked to DNA repair processes and cell proliferation. When cells are exposed to damage by OH radicals or methylating/alkylating agents, the total covalent mono-ADP-ribosylation of histones increases by a factor from 2 to 12, while the levels of histone H1-ADP-ribosylated are even more higher (more than 30-fold).[37,38] Mono-ADP-ribosylation on H4 seems to occur preferentially when H4 is hyperacetylated[39], suggesting a potential cross talk of histone mono-ADP-ribosylation and histone acetylation. The amino acid residues of the acceptor proteins that are modified by the specific MARTs include arginine, asparagine, glutamate, aspartate and cysteine.[34,40] Conversely, mono-ADP-ribosylation of cellular proteins through non-enzymatic mechanisms mainly occurs on lysine or cysteine residues.[41]Amino acid-mono-ADP-ribose-specific MARHs cleave the ribose unit, leading to the release of free mono-ADP-ribose and to the restoring of the free reactive group on the corresponding amino acid residue.[42] Many evidences suggest that mono-ADP-ribosylation, along with other modifications of histone tails, may regulate several steps in DNA damage response pathways: for example mono-ADP-ribosylation could act, in cooperation with acetylation and phosphorylation, as a DNA damage signal to recruit additional signaling factors and chromatin modifiers.

Poly-ADP-rybosilation

Poly-ADP-ribosylation, as enzymatic reaction, is known since the early sixties of the last century.[43] In the following 20 years, this post-translational modification has been related to several nuclear functions, i.e. histone modification[44], differentiation[44], cell death[45], transcriptional regulation[46] and DNA repair/genome stability. In the enzymatic reaction NAD^+ is cleaved into nicotinamide and ADP-ribose, with the latter attached to glutamate or aspartate via an ester bond[47], or to lysine, forming a ketoamine by a first Schiff-Base formation, followed by an Amadori rearrangement.[48] After attachment of the first ADP-ribose moiety, further units are rapidly added via α-gylcosidic bonds, branches can originate from the growing chain, depending on the synthesizing enzyme and the interaction partners. These reactions are catalyzed by Poly-ADP-rybosil-transferases enzymes (PARPS); this enzymes family consists of 17 members with distinct cellular localizations and functions.[26] As well as for Mono-ADP-rybosilation, also Poly-ADP-rybosilation is a reversible mechanism, indeed, PAR polymers turn over rapidly in the cell[49]. The enzymes that act as "erasers" of this epigenetic mark have evolved to remove covalently linked ADP-ribose and PAR from proteins (**Figure 1.4**). These enzymes include PAR glycohydrolase (PARG), TARG/C6orf130[50], MacroD1 and MacroD2[51,51b] and the NUDIX family of hydrolases.[52] Many of these enzymes contain a macrodomain fold that allows them to interact with ADP-ribosylated substrates. Based on the large size of poly-ADP-ribose, this modification seems to play a direct role in the "histone code". In addition, poly-ADP-ribosylation was suggested to indirectly contribute to the "histone code" by dictating the levels of local chromatin compaction.
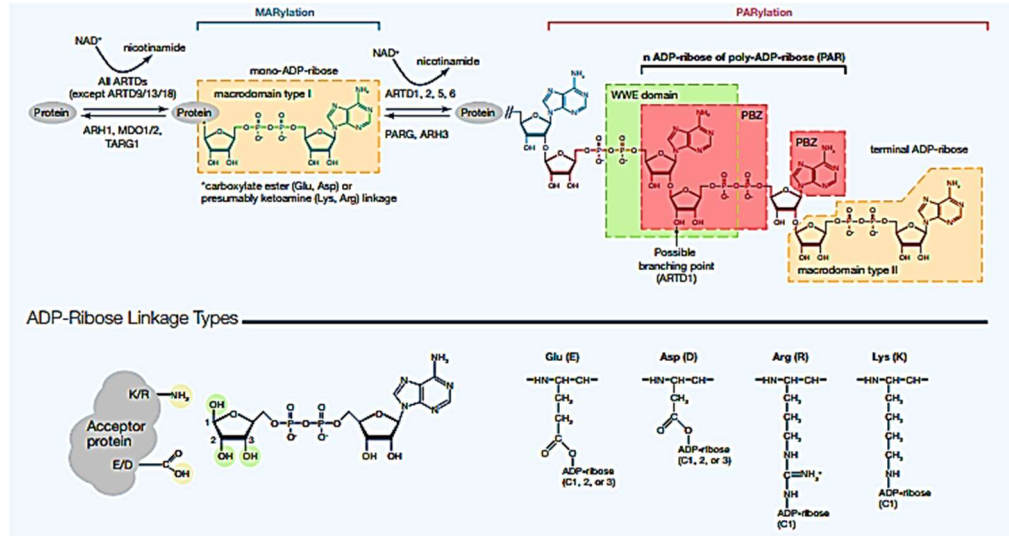
Figure 1.4 *Representative scheme of Mono and Poly-ADP-rybosilation*

1.5. Macrodomain containing proteins

As previously mentioned, several enzymes are involved in the regulation of the ADP-rybosilation cellular pathway. Depending on their activity, these enzymes can be classified as *writers* (e.g. if the enzyme adds an ADP-ribose moiety), *erasers* (e.g. if the enzyme removes an ADP-ribose group) or *readers* (if the enzyme is able to "read or detect" the presence or the absence of the ADP-ribose mark) (**Table 1.2**). Despite these different functions, all these proteins are characterized by the presence of an evolutionarily conserved structural domain of 130-190 a.a. and they are not only found in vertebrates but also in many bacteria, viruses and plants, suggesting their evolutionary conservation.[53] The first macrodomain was identified, through genomic sequencing (initially termed X domain), as "a domain of considerable conservation" within the genomes of the murine hepatitis virus (MHV) and infectious bronchitis virus.[54] Shortly thereafter, a homologous domain was identified as part of the rat MacroH2A protein, a histone variant that consists of a fusion between histone H2A and a domain of unknown function.[55] Because MacroH2A was the largest histone variant, the novel domain was defined *macrodomain*. In contrast to many other modification recognition domains, which

are adapted to recognize a single or a small number of modification types, macrodomains can recognize ADP-ribose (ADPr) in both its free and protein-linked forms, in related ligands, such as *O*-acyl-ADP-ribose (*AAR*), and even in ligands unrelated to ADPr.[56] The macrodomain containing proteins exert regulatory influence on inter- and intracellular signalling, transcription, DNA repair pathways, maintenance of genomic stability, telomere dynamics, cell differentiation and proliferation, as well as on necrosis and apoptosis.[57]

WRITERS

Name	Alternative Names	Enzymatic Activity (automodification)	Cellular Localization[1]
ARTD1	PARP1	PARylation, branching	N
ARTD2	PARP2	PARylation	N >> C
ARTD3	PARP3	MARylation	N > C
ARTD4	PARP4, vPARP	MARylation	C > N
ARTD5	PARP5A, tankyrase 1	OARylation	C >> N
ARTD6	PARP5B, PARP6, tankyrase 2	OARylation	C >> N
ARTD7	PARP15, BAL3	MARylation	C
ARTD8	PARP14, BAL2, CoaSt6	MARylation	C > N
ARTD9	PARP9, BAL1	no activity reported	C >> N
ARTD10	PARP10	MARylation	C >> N
ARTD11	PARP11	MARylation	N and C
ARTD12	PARP12, ZC3HDC1	MARylation	C >> N
ARTD13	PARP13, ZC3HAV1, ZAP1	no activity reported	C
ARTD14	PARP7, tiPARP, RM1	MARylation	C and N
ARTD15	PARP16	MARylation	C
ARTD16	PARP8	MARylation	C
ARTD17	PARP6	MARylation	C
ARTD18	TPT1	no activity reported	unknown

[1]during interphase (N, nuclear; C, cytoplasmic)

READERS

Domain Names	Characteristics of Domain	ADP-Ribosylation Structure Recognized	Proteins that Contain This Domain
Macrodomain	Conserved domain of 130-190 amino acids	-Terminal and protein-bound ADP-ribose of PAR (type II) -MAR (type I)	MacroH2A variants, ARTD7 (BAL3), ARTD8 (BAL2), ARTD9 (BAL1), ALC1, GDAP2
PAR-binding zinc finger (PBZ)	Cys and His-coordinated Zn, aromatic residues	Adjacent ADP groups. Zinc-coordinated fold recognizes the $\alpha(1-2)$ O-glycosidic bond. Can also bind to the phosphates and the adenine ring of the more distal ADP-ribose.	CHFR, APLF
WWE domain	Domain containing the conserved amino acid sequence Trp-Trp-Glu	iso-ADP-ribose of PAR	RNF146 (Iduna), ARTD8, ARTD11, ARTD12, ARTD13, ARTD14 (tiPARP) Deltex 1, Deltex 2, Deltex 4, HUWE1, TRIP12, DDHD2
PAR-binding motif (PBM)	Consensus sequence $[HKR]_1-X_7-[AIQVY]_1,-[KR]_5-[KR]_8-[AILV]_7,-[FILPV]_9$	Long and branched PAR, possibly due to high negative charge	XPA, MSH6, DNA Ligase III, XRCC1, DNA polymerase ϵ, DNA-PK catalytic subunit, Ku70, ERRCC-6, MR11, ATM, CENP-A, Condensing 1, p21, p53, a.o.
RNA recognition motif (RRM)	Structurally highly variable beta-sheet with conserved RRM motif	Long PAR chains	A wide variety of RNA and ssDNA-binding proteins (e.g., hnRNP A1, NONO, and RBMX)

ERASERS

Name	Alternative Names	Activity and Reported Specificity	Cellular Localization
PARG (111,102, 99 kDa isoforms)		-Exo- (primarily) and endoglycohydrolytic activity towards PAR -60 and 55 kDa isoforms are inactive	N (111 kDa), C (102, 99, 60 kDa), Mitochondria (55 kDa)
ARH1	ADPRH	MAR (Arg)	C
ARH2	ADPRHL1	no activity reported	
ARH3	ADPRHL2	-Glycohydrolytic activity towards PAR, possibly exo only -Hydrolyzes O-acetyl-ADP-ribose	N, C, Mitochondria
MacroD (MDO1)	LRP16	MAR (Glu)	N, C
MacroD2 (MDO2)	C20orf133	MAR (Glu)	N, C
C6orf130	TARG1, OARD1	-MAR (Glu) -Exoglycohydrolytic activity towards PAR	N, C

Table 1.2 *ADP-rybose signaling proteins*

Humans contain 10 genes encoding for 11 members of the macrodomain family, which includes macroH2A (and its various isoforms including macroH2A1/macroH2A2), MACROD1 (LRP16), MACROD2 (C20orf133), C6orf130, MACROD3 (GDAP2), ALC1 (CHD1L, CHDL), and macroPARPs (PARP-9; PARP-14; PARP-15)[6] (**Figure 1.5**). All of these proteins contain a macro domain near their N-terminus or C-terminus domains, except for macro-PARPs in which 2–3 macro domains are linked. In addition to the conserved macrodomain, these proteins also contain a variety of additional domains, which allow them to interact with specific target proteins or target them to specific chromatin structure regions. For example, macroPARPs also contain a PARP catalytic domain and are the only described proteins with both a PARP-like domain and a macrodomain. Basing on an accurate analysis of the topology of macrodomain proteins, composed by diverse domains ecompassed by N- and C-terminal tails, it is possible to grasp the important and intricate role of these proteins in the regulation of diverse cellular functions. The macrodomain proteins might be viewed as molecular bridges that bring together the target proteins, via interactions with the variable domains, and the metabolites of NAD^+, including PAR, via binding to the conserved macro domain.[58]
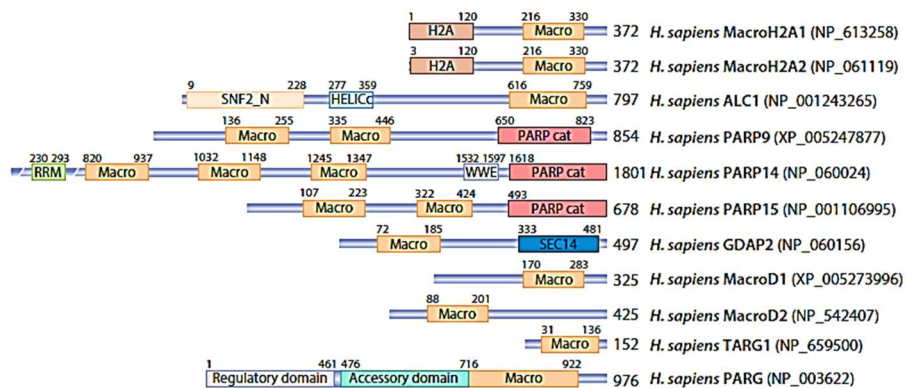

Figure 1.5 *Human Macrodomain proteins*

1.6. Macrodomains structure and functions

Three-dimensional (3D) structures of the ADP-ribose (ADPr) binding fragments of macrodomains have been recently solved; this allowed a comparison with the previously published structures of members of the macrodomain family, providing additional evidence of the high structural similarity inside this protein class.[58] As revealed by structure determination, macrodomains adopt a globular α/β/α sandwich fold composed of a central six-stranded mixed β-sheets, flanked by five α-helices (**Figure 1.6a**)[3,58], while the substrate binding occurs via a deep cleft on the crest of the domain. The macrodomain fold shares some resemblance to the DNA-binding domain of leucine aminopeptidases, as well as to the P-loop nucleotide hydrolase. The stable interaction between the ligand and the macrodomain can trigger a variety of downstream effects, including recruitment to DNA damage sites (hot spots of PAR generation) or formation of protein complexes.[59] Although there is a relatively high degree of sequence similarity (approximately 30–40%) among the macrodomain proteins family members[6], the small sequence variation between the domains is probably responsible for the selectivity of the different macrodomains for specific binding partners. Indeed, further structural and biochemical characterization showed that ADPr and its derivatives can be accommodated within the cleft (**Figure 1.6 b-c**).[60] The interaction between ligand and macrodomain is stabilized by several conserved interactions within the binding pocket: (*a*) the adenosine moiety readily undergoes π-π stacking with a conserved aromatic residue, whereas its N6 nitrogen is further coordinated by an aspartate residue;[56,61] (*b*) the central part of the cleft stabilizes the substrate binding by several side-chain/backbone-pyrophosphate contacts, which induce a more closed conformation of the macrodomain;[32] (*c*) The pyrophosphate and the distal ribose are accommodated between two substrate-binding loops (termed loop 1 and 2). Although both loops contribute to substrate specificity, loop 1 harbors the catalytic residues of most macrodomains, exhibiting hydrolase activity (for this reason it has been also termed catalytic loop). Loop 2 provides further coordination of the pyrophosphate and it is also described as the diphosphate-binding loop[48,62] (**Figure 1.6c**).
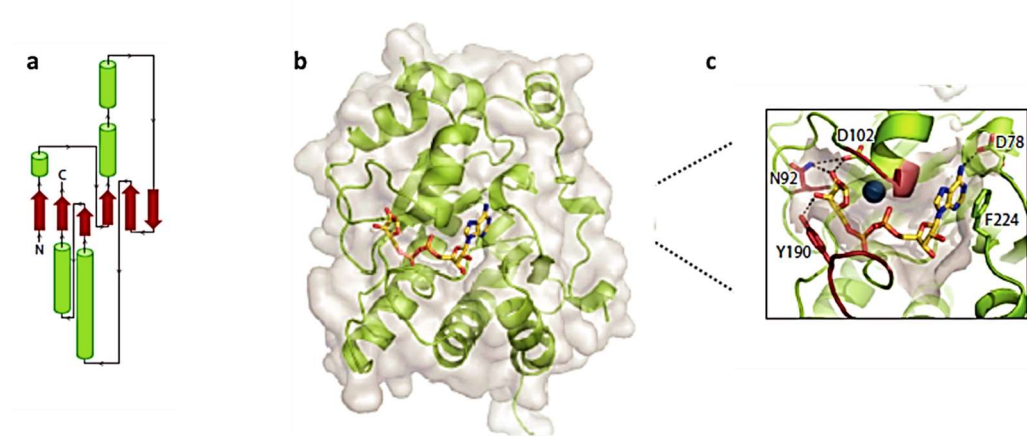
Figure 1.6 (a) *Topological representation of the macrodomain shows the organization of the central six-stranded β-sheet (red) flanked on both sides by five α-helices (green);* **(b)** *MacroD2, PDB 4IQY, (green) coordinates ADPr in a strained conformation owing to the presence of a structural water molecule (dark blue) and Tyr190 (loop 2). The catalytic residues Asn92 and Asp102 (loop 1) interact electrostatically with the distal ribose;* **(c)** *The magnification shows the coordination of the adenosine moiety by a conserved phenylalanine and/or asparagine residue as well as by the substrate-binding loops 1 and 2 (red)*

Macrodomain proteins are ubiquitously expressed in adult tissues, however, the physiological role of these proteins is not yet completely understood. Among the mammalian macrodomain proteins, only the potential role, in human embryogenesis, of macroH2A and the macroPARPs have been investigated. The role of macroH2A in fetal development is better characterized than that of other macrodomain proteins, actually because macroH2A was the first of these proteins to be described and the most intensively studied.[63] A driving factor for the role played by macrodomains in evolution may lie in the key role of NAD signaling/consumption processes, regulating DNA repair, redox defense, chromatin architecture, protein acylation, and response to viral infection, among others.[64,65] It has been well demonstrated that macrodomain proteins regulate PARylation, whereas it is emerging that other proteins control MARylation. PAR recognition is a well-established ability of several macrodomains. In particular, PARylation, in response to DNA damage, is sensed by several macrodomains which serve as recruitment modules for proteins involved in DNA repair. In contrast to the binding modules that have been well characterized for PAR, it remains to address

whether macrodomains are also involved in reading and processing MARylation.[66]

Macrodomains as readers of Protein ADP-Ribosylation

Macrodomains are key players in the complex network of NAD-dependent signaling. This is a consequence of their ability to interpret, not only protein ADP-ribosylation and PARP-dependent signaling, but also second messengers such as ADPr and its derivatives, which can be released apart from PARP activity (e.g., through sirtuin activation). According to their multiple activities, humans' *reader* macrodomains only occur in multidomain proteins combining, thus, signals recognition and effector domains in a single polypeptide, as discussed below. Among the macrodomain proteins that recognize and bind ADPr, there is macroH2A, ALC1 and MacroPARPS. Because a single ADPr fits into a macrodomain cleft, it has been suggested that macrodomains specifically bind MARylated proteins, even if they can also interact with the PARylated ones, and that the backbone sequence around the MARylation site may determine the substrate specificity of macrodomains, as in the case of bromodomains that interact with acetylated proteins.[67] Among the main readers of the ADPr pathway there are: macroH2A, that has been associated with several cellular processes, including cell differentiation and proliferation, transcription repression, and DNA repair. Moreover, a reduced macroH2A expression was observed in several cancer types, including breast and lung cancer, and has been associated with an increased tumor proliferation and metastatic potential. ALC1 is frequently amplified in certain cancer types like hepatocellular carcinoma and bladder cancer, as well as macroPARPs.[68] Three human members of the PARP family contain multiple macrodomains able to recognize ADPr, in addition to their PARP catalytic domain. A dysregulation of both PARP9 and PARP14 are often associated with cancer, as well as with lymphoma.[48]

Macrodomains as Erasers of Protein ADP-Ribosylation

Like other signal transduction pathways, ADPr-dependent signaling is a reversible modification, therefore it requires both recognition and removal of the mark. Basing on this point, it may not be surprising that macrodomains, in addition to their *reader*'s activity, have acquired the ability to reverse cellular ADP-ribosylation. The catalyzed signal termination reactions include the hydrolysis of mono- and poly-ADP-ribosylated substrates, as well as degradation of NAD^+- derived second messengers, such as O-acetyl-ADP-ribose (AAR).[53,69] PARGs (Poly-ADP-Ribosyl-Glycohydrolases) are enzymes able only to breakdown Poly-ADP-ribose chains, however, they are unable to remove the final ADP-ribose moiety from the protein. Few years ago, Jankevicius et al[51a] succeed to identify, through biochemical, structural and modeling analysis, some macrodomain proteins members able to reverse mono-ADP-rybosilation cellular glutamate. These two proteins, called MacroD1 and MacroD2, are orthologues of MacroD-type proteins and can be found in all living organisms. In vertebrates a duplication of the ancestral MacroD-type gene gave rise to MacroD1 and MacroD2 proteins.[51a] MacroD1 and MacroD2 act as mono-(ADP-ribosyl) hydrolases that reverse protein mono-(ADP-ribosylation) and catalyze the cleavage of the terminal ADPr moiety, e.g., from proteins after PARG-mediated polymer degradation.[51a] In addition, both enzymes can hydrolyze AAR[3]. Although their catalytic activities have been established in vitro, their exact protein targets and biological roles remain largely unknown. There is a high degree of sequence similarity between the catalytic domains of MacroD1 and MacroD2, however, their primary subcellular localizations are different (MacroD1 in mitochondria and MacroD2 in the cytoplasm), implying, thus, distinct functions.[51a]

MacroD1 and MacroD2 as Mono-ADP-Ribosyl-Hydrolases

To date, only two classes of macrodomains have been shown to contain mono-ADP-ribosyl-hydrolases activities: the MacroD-type class and the ALC1-like class. Biochemical and structural studies on MacroD1, MacroD2 and TARG1, the

members found in humans, revealed that these classes utilize different catalytic mechanisms.[20]

In MacroD1/2, the distal ribose is bound in a constrained conformation, oriented toward the α-phosphate group (**Figure 1.6b**). This orientation is maintained through the presence of a highly conserved aromatic residue that is part of the bipartite MacroD-type structure: two glycine-rich loops (loop 1, 97-GGGGV-101 and loop 2, 188-GIYG-191)[51a]. The major difference between the reading and erasing domains is the presence of a groove, in the pyrophosphate-binding site, in which there is a structural coordinated water molecule. Indeed, thanks to the analysis of site specific mutants of protein MacroD1 and MacroD2, it has been possible to disclose the high conserved amino acids that are crucial for the catalytic mechanism; in particular the key residues are: Asn-171, Asn-174, Asp-184 and His-188 for MacroD1, whereas Asn 92, Asp 102 and His 106 for MacroD2. Basing on these data, two models for the catalytic mechanism have been proposed. Even if the exact process is still unclear, according to a first hypothesis, a water molecule, located in the cleft between loop 1 and 2 and held by hydrogen bonds between the distal ribose and the neighboring ADPR α-phosphate, becomes activated through the α-phosphate group and carries out a nucleophilic attack on the protein-ADPr ester bond. In this frame, the constrained conformation of the substrate appears to be crucial for the catalysis, however, is still debated if the pKa of the α-phosphate is sufficient to activate the water molecule.[51a] Another hypothesis suggests that a conserved aspartate residue, in the active site, acts as a general base for the activation of a water molecule, which, in turn, carries out a nucleophilic attack on the C1 atom of the distal ribose (**Figure 1.7**).[51b] In contrast to the MacroD-type enzymes, the reaction catalyzed by TARG1 is triggered by a conserved lysine residue (Lys84 in human TARG1).
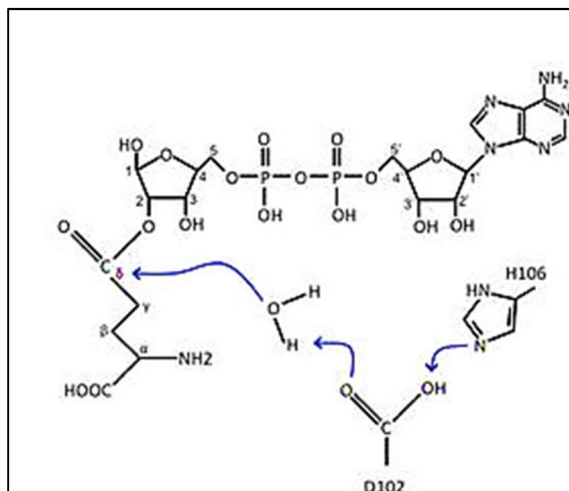
Figure 1.7 *Supposed catalytic mechanism of MacroD proteins*

1.7. Human MacroD1 and MacroD2 proteins

MacroD1 protein, also known as Leukemia-related protein 16 (LRP16), is a member of the macro domain superfamily characterized by only a single stand-alone macro module harbored at its C-terminal region.[70] Biochemical analysis revealed that MacroD1 can bind ADP-ribose metabolites, including both mono-ADP-ribose and PAR, by its macro domain module. Similarly to other macro domain proteins, MacroD1 can be recruited to the DNA damage sites thanks to its capacity to bind PAR.[48] The crystal structure of MacroD1 protein (PDB 2X47) was firstly solved in 2011 by Chen et al;[3] it shows a fairly simple structure of 325 amino acids with only one macrodomain at its C-terminus (amino acids 151-322) that exhibits the canonical macrodomain fold.

This core fold consists of a three-layered α-β-α sandwich, with a central six-stranded β-sheet. The N-terminal region (residues 91-136 in orange) is arranged in an elongated chain of helical segments and a short β-strand (**Figure 1.8a**).[71] It has been deeply investigated that this protein might harbor a catalytic activity toward AAR, the direct product of the NAD^+ dependent deacetylation reaction of sirtuins. The catalytic activity of MacroD1 was confirmed by mutation experiments where, the 270 conserved glycine residue, was mutated to glutamate, and the mutated MacroD1 lacked completely AAR deacetylation activity.

Moreover, ADPr docked in the putative binding site of human MacroD1 showed that ADPr may be tightly bound to MacroD1, in line with the observations on the activity of this enzyme. It should be noted that, in this model of ADPr bound to MacroD, a steric clash occurs between the adenine ring and the side chain of Phe-306 (**Figure 1.8b**). However, the homologous residues in other macrodomain proteins (e.g. Tyr-159 of E. coli YmdB) are rotated to a position that relieves the steric clash and provides a favorable stacking interaction with the adenine ring, therefore it is likely that Phe-306 of MacroD1 assumes a similar conformation in the ADPr-bound state. Moreover, MacroD1 has been demonstrated to remove ADP-ribose from glutamate residues in proteins bearing a single ADP-ribose moiety, and to be inactive towards proteins bearing poly-ADP-ribose.[72] Regarding its biological implications, it acts as a transcriptional co-activator of several nuclear hormone receptors, in particular the estrogen receptor (ER) and the androgen receptor (AR).[73] Although the precise mechanisms of its transcriptional cooperation are still unknown, it has been speculated that it involves remodeling of DNA structure.[74] On the other hand, transcription of MacroD1 itself is stimulated by estrogen and androgen, resulting in a feed-forward loop which may play a role in estrogen-responsive breast cancer cells.

Recent results also imply MacroD1 in invasion, metastasis and prognosis of gastric cancer.[75] Moreover, different expression degrees of this protein has been found in several tissues, including ovary, testicle, prostate, small intestine, spleen, thymus and stomach. Recently, MacroD1 has been identified as a novel interactor of NF-κB component p65 NF-κB-associated pathways, which have been widely implicated in oncogenesis and tumor progression by stimulating cell proliferation, inhibiting apoptosis, and promoting metastasis and angiogenesis.[1]
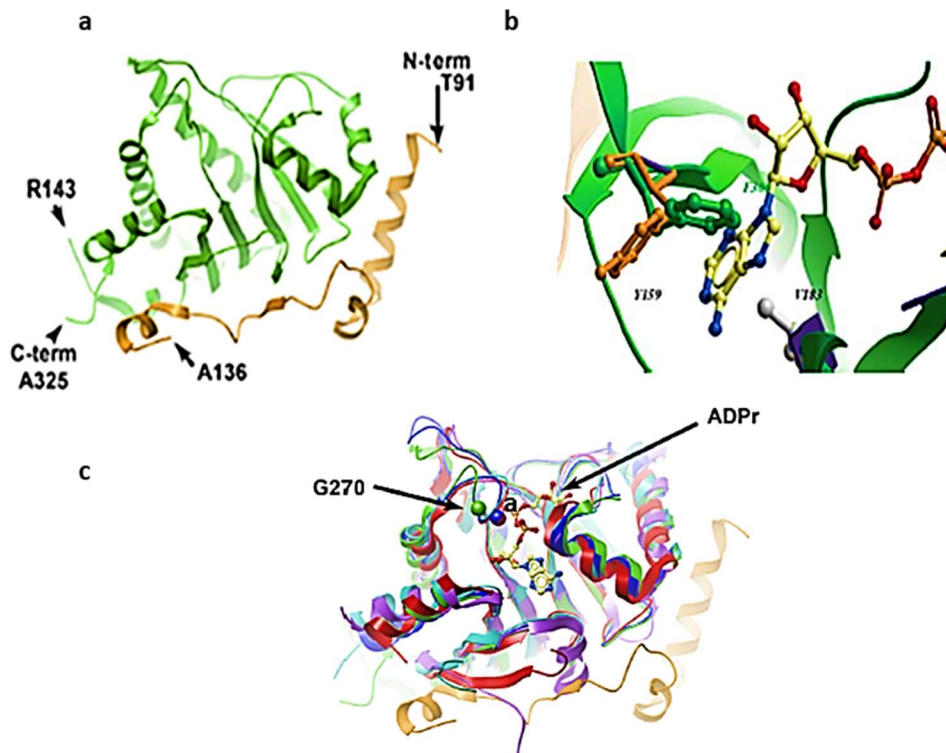
Figure 1.8 a) *MacroD1 conserved macrodomain is depicted in green, and the N-terminal is in orange. **b)** 2D and 3D modeling ADPr on the structure of MacroD1.*
c) overlay of MacroD1 (green/orange) on the structures of other macrodomains: Feline Sarcoma virus (purple), E. coli YmdB (blue), human PARP15 (cyan), and histone macroH2A1.1 (red)

MacroD2 is the paralog of MacroD1 protein hydrolase. Like its homologous, this protein is involved in removing ADP-ribose from mono-ADP-ribosylated proteins. The encoded protein has been shown to translocate from the nucleus to the cytoplasm, upon DNA damage, and to remove ADP-ribose from glutamate residues in proteins bearing a single ADP-ribose moiety. It has also been reported its inactivity towards proteins bearing poly-ADP-ribose. Indeed, because glutamate-linked proximal ADPr units, in mono-ADP-ribosylated proteins like PARP1, are chemically related to AAR, these MacroD proteins, able to reverse and antagonize cellular glutamate-linked mono-ADP-ribosylation, have been shown to be inactive towards lysine- and arginine-linked mono-ADP-ribose. In *vivo* studies showed also that MacroD2 recruitment to DNA-damage sites can interfere with PARP1-mediated functions. In particular, MacroD2 is able to reverse ADP-ribosylation on rybosilated-PARP1 protein, suggesting that it could suppress PARP1 activation by removing the related mono-ADP-ribosylated species at DNA level. For this reason,

inhibitors targeting macrodomain-like proteins might probably alter PARP1 signaling and could be therapeutically useful for cancer treatment.[6]

The three dimensional structure of MacroD2 (**Figure 1.9a**) was modeled by using the X-ray structure of MacroD1. Except for their flexible loops, the human MacroD1 and MacroD2 protein structures are highly similar. The crystal structure of MacroD2-ADPr complex (PDB 4IQY) was solved in 2013.[51a] This protein is expressed in the cytoplasm and catalyzes the same ADP-ribosyl hydrolysis reaction of MacroD1. It is composed by 448 amino acids and the macrodomain region, encompassing amino acids 60-240, exhibits the canonical macrodomain fold. Recent studies showed that MacroD2 binding sites become available through two different mechanisms during DNA damage. The first phase of recruitment is probably the result of the initial DNA damage-inducing-mono-ADP-rybosilation, whereas, the second phase, may represent the MacroD2's binding to mono-ADP-rybosilated species generated by PARG activity.[20]
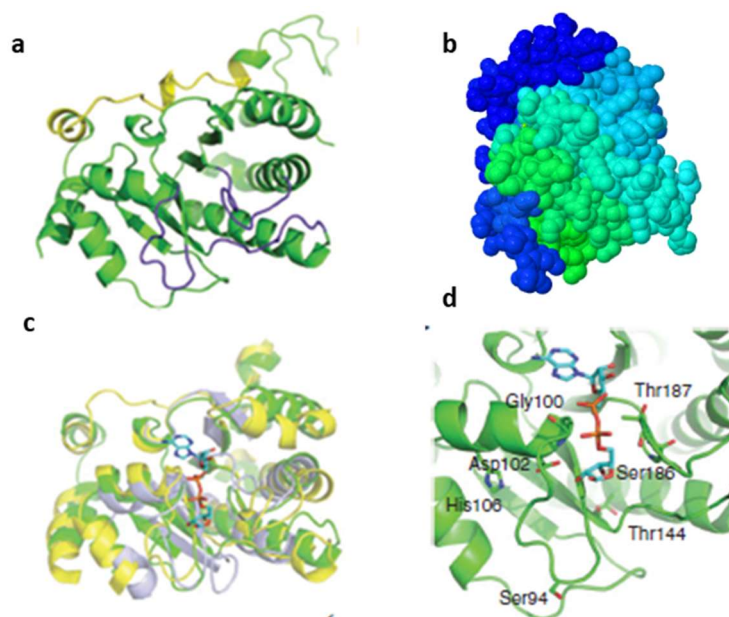
**Figure 1.9 a)** *Structure of MacroD2 modeled on the basis of the PDB 2X47 crystal structure of MacroD1. The primary macrodomain binding-site loops are marked in violet*
***b)** 3D Structure of the human MacroD2 (PDB: 4IQY)*
***c)** Overlay of the MacroD1 (yellow), MacroD2 (green) and C6orf130 (grey structures with the ADP-ribose product in the binding pocket).*
***d)** Structural model of MacroD2 with the mutated residues highlighted*

1.8. Macrodomains in Cancer

Several studies have well demonstrated that various members of the macrodomain protein family are overexpressed in a wide range of human tumors and, in addition, high levels of these proteins have shown to correlate with a poor prognosis and/or drug resistance. There are many examples testifying a direct link between macrodomain amplification and tumor biology; these include: ALC1, whose overexpression inhibits apoptosis; MacroD1, which is the family member most widely expressed in human cancers with particularly high level of expression in endometrial, gastric, colorectal and breast carcinoma;[76,74,77] MacroD2, inducing tamoxifen resistance in estrogen receptor–positive breast cancer cells [2], and, finally, PARP9, which can increase tumor cell migration.[78]

As already mentioned before, MacroD1 appears to be the family member most widely overexpressed in human cancers, with high levels of expression observed in endometrial carcinoma, gastric carcinoma, colorectal carcinoma, and breast carcinoma.[6] Moreover, its overexpression in endometrial cancer cell lines has been shown to increase the invasiveness of these cells in tissue cultures, whereas, on the other hand, MacroD1 knockdown in prostate cancer cell lines resulted in decreasing cell proliferation *in vitro.*[79] A recent study reported that MacroD1 acts as a cofactor, modulating estrogen and androgen receptor signaling, in particular, its expression is induced by estrogen/estrogen receptor alpha (ERα) signaling in ERα-positive breast cancer cell lines.[80,81] Overexpression of the estrogen receptor and an activated ERα signaling is observed in certain breast cancer subtypes where, a sustained activation of ERα signaling, stimulates proliferation of mammary cells which could lead to tumor formation. [82,74] MacroD1 has been shown to interact with ERα, acting in a positive feedback-loop as a co-activator of ERα-dependent transcription, enhancing the expression of several ERα target genes, and resulting, thus, in an increase of cell proliferation.[80,74] Similarly, MacroD1 stimulates the transcriptional activity of the androgen receptor in AR responsive prostate cancer cells, thereby it means that MacroD1 is needed for cell proliferation stimulated by testosterone.[74] Moreover, MacroD2, the related MacroD1 orthologue, has recently

been found to be amplified and overexpressed in a subset of breast cancers leading to tamoxifen resistance and estrogen independent growth. In particular, a high level of this protein has been detected in MCF-7 cell lines and its overexpression was even detected in samples of patients with breast cancer tamoxifen-resistant; as double check, it has been demonstrated that MacroD2 gene knockdown sensitizes tamoxifen resistant cells to tamoxifen treatment, and reduces tumor formation in a xenograft model.[2] This study shows that MacroD2, in the case of ER-positive breast cancers treated with tamoxifen, resulted amplified, so that drug resistant clones can emerge. Moreover, the metastatic sites of disease display a higher frequency of MacroD2 overexpression and, patients with primary breast cancers with overexpression/amplification of this enzyme, resulted to have a worse survival. All these data suggest that MacroD2 could become an important molecular target in this type of breast cancer and, hence, this enzyme may be considered as a new and relevant "druggable" protein for cancer treatment.

According to all the evidences collected on the important role played by macrodomain proteins in cancer development and progression, several new strategies can be explored in order to design new promising anticancer agents targeting these enzymes. Actually, this can be considered a challenging task owing to the many processes modulated by these protein family members and, overall, to the lack of clear structural requirements for an optimal interaction with the protein counterpart, since, to date, no inhibitor has been disclosed yet. Therefore, a starting point in terms of drug design can be offered by the several mutagenesis studies that have been accomplished on these proteins, indicating that the binding of ADPr to the macrodomain is due to a limited number of aminoacids. It is worth to consider that the availability of agents targeting the macrodomain proteins can be of great value in terms of anticancer therapy, and, moreover, they can represent molecular probes useful to interrogate the proteins and to investigate their related specific cellular processes.[83,84] In any case the increasing numbers of available macrodomain structures, together with advancements in structure-guided drug design approaches, may be considered as useful and potent tools to accelerate the

process and to be successful in discovering potential macrodomain proteins inhibitors as new attractive drug candidates.

CHAPTER 2

BAG3 (Bcl-2-associated athanogene 3)

antiapoptotic protein

2.1. BAG (Bcl-2 associated athanogene) proteins family

Bcl-2 is an oncogene and the most representative member of a whole family of genes. To date a total of 25 genes are included in the bcl-2 family, encoding for evolutionary conserved proapoptotic proteins (e.g., Bax, BAD, Bak, and Bok) and antiapoptotic proteins (including Bcl-2, Bcl-xL, and Bcl-w, and others).[85,86] In addition to the Bcl-2 gene family, also Bcl-2-associated athanogenes (BAGs) have been described so far. Initially, a novel Bcl-2 binding protein was cloned, called BAG1, which shared no significant homology with Bcl-2 or Bcl-2 family members. Later on, the research team of John Reed identified 'a family of BAG1-related proteins' from humans, the proteins: BAG2, BAG3, BAG4, and BAG5, and to date also another isoform, BAG6 has been identified.[87] The BAG (Bcl-2 associated athanogene) proteins are a family of chaperone regulators that interact with the ATPase domain of the heat shock protein Hsp70 and its constitutive isoform, Hsc70, through a common conserved region located near the C terminus, termed the BAG domain (BD) (110-124 amino acids).[88] Members of this protein family have been found throughout organisms evolution, in yeast (Saccharromyces cerevisiae, Schizosaccharromyces pombe)[88], invertebrates (Caenorhabditis elegans, Ciona intestinalis, Drosophila) amphibians (Xenopus laevis)[89], mammals (humans, mice)[90] and plants (Oryza sativa, Arabidopsis thaliana)[91], suggesting a fundamental biological role of these co-chaperones. Moreover, recently, seven BAG protein homologs in the *Arabidopsis thaliana* genome sequence have been identified, four of which have domain organization similar to their animal counterparts, underlining the fundamental biological role of these proteins.[92]

The human BAG protein family includes six family members (BAG1-6) that function as molecular chaperone regulators and all these proteins are constituted by a common domain, the BAG domain, which interacts with the molecular chaperone Hsp70.[93] BAG proteins showed to regulate both positively and negatively, the function of Hsp70/Hsc70, and to form complexes with a range of transcription factors, modulating various physiological processes such as apoptosis, tumorigenesis, neuronal differentiation, stress responses, and the cell cycle.[86] All these protein family members, in addition to the conserved BD, are characterized

by several other domains that are likely able to interfere with several other factors involved in prominent multiple signaling pathways.

2.2. Human BAG Proteins: BAG1, BAG2, BAG4, BAG5, and BAG6

The six human BAG proteins identified so far are BAG-1 (RAP46/HAP46), BAG-2, BAG-3 (CAIR stressed-1, CAIR-1/B), BAG-4 (SODD), BAG-5, and BAG-6 (BAT3/Scythe) (**Figure 2.1**).
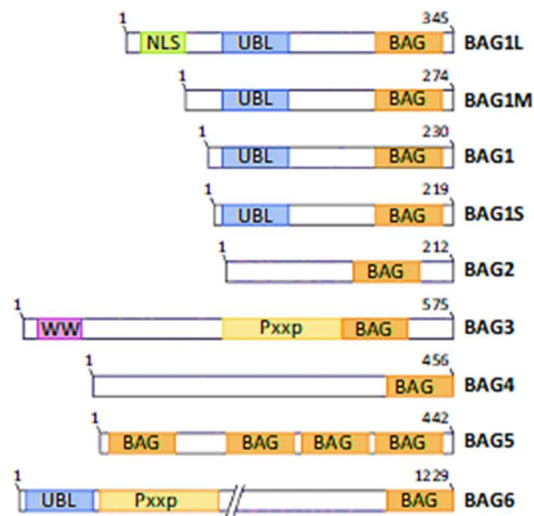
Figure2.1 *Human BAG protein family members*

All these proteins share the common architecture of the BAG Domain (BD) near the C-terminal end, with the exception of BAG 5, which contains four of such domains. Crystallography studies suggested that BAG domain contains 110 – 124 amino acids and consists of three anti-parallel helices of 30 –40 amino acids each.[94] The second and third helices represent the binding sites for the ATPase domain of Hsp70/Hsc70[7], whereas, their N terminus is the region that affects the specificity towards particular proteins and pathways. Very recently, depth studies, employing different deletion mutants and pull-down assays, showed that the human BAG domain (of BAG3 protein) is exactly composed by 78 amino acids, ranging from amino acids 421 to 498 (**Figure 2.2**). [95]
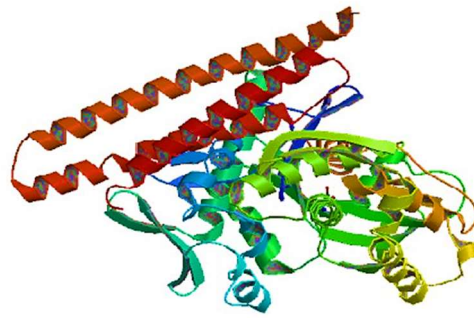
Figure2.2 *Crystal structure of a BAG domain in complex with the Hsc70 ATPase domain (PDB 1HX1)*

BAG1 is the first member of this family, occurring as four human isoforms structurally differing in their N-terminus, which are designated as BAG-1L p50, BAG-1M p46, BAG-1S p36, and p29, with molecular masses of 50, 46, 36, and 29 kDa, respectively (**Figure 2.1**).[93] The 36-kDa isoform is often referred to BAG-1 and it is generally the most abundant isoform expressed in cells, followed by BAG-1L and BAG-1M. The 29-kDa isoform is expressed at low levels and cannot be consistently detected.[96] In cellular studies showed that BAG1 exerts several functions and is able to bind to Hsc/Hsp70, driving the nucleotide exchange at the chaperone complex and stimulating the substrate release.[97,98] However, the exact molecular mechanism of BAG1 is still controversial, indeed, it was demonstrated that various BAG1 isoforms regulate Hsp70 in different ways. BAG-1M was found to inhibit the refolding of denatured substrates[98], while BAG-1S was shown to initially inhibit protein refolding [99], however in a recent study, this last showed to have a stimulating effect.[100] BAG1 protein is also a binding partner for a wide range of signaling molecules, such as, steroid hormone receptors[101,102] and the Raf-1 protein kinase.[103]

BAG2 protein was identified as a substrate for MAPK-activated protein (MAPKAP) kinase 2, which is known to mediate p38 MAPKdependent functions;[104] it carries a single BAG domain and it was identified as a specific inhibitor of the protein CHIP (C-terminus of the Hsc70-interacting protein).[105] Via CHIP inhibition, BAG2 can influence the balance of Hsc/Hsp70-controlled protein folding and degradation of substrate proteins. The effect of BAG2 on protein degradation, as part of cellular protein quality control, potentially links BAG2 to

those neurodegenerative disorders that are associated with misfolded and aggregated proteins.[106]

BAG4, also known as silencer of death domains (SODD), can bind to the so-called death domains that are found in members of the tumor necrosis factor (TNF) receptor family, including TNF receptor 1 and the death receptor. It has a similar domain organization as BAG2 and was also identified in a screen for Hsp70-interacting proteins.[88] Structurally, the helices in the BAG4 BAG domain (BD), are three to four turns shorter than in BAG1, and they likely constitute the minimal functional fragments able to bind and regulate Hsp70. While BAG4 has only one BAG domain, BAG5 is the only member of BAG proteins family having four putative BAG domains. The functions of BAG5 are not well known but, interestingly, it has been also implicated in the pathogenesis of Parkinson disease, and, in an *in vivo* study, BAG5 acts as driver of neuronal cell death by enhancing the degeneration of the dopaminergic neurons.[107] Finally, BAG6, also known as BAT3, is constituted by 1229 amino acids and represents the largest human BAG member. The inclusion of BAG6 into the BAG family is due to its sequence homology with the other BAG domains and its apparent Hsc70-regulating activity, however it is not very clear yet if this BAG domain is a real one. BAG6 has been also demonstrated to bind the protein Reaper, a central apoptotic regulator in *D. melanogaster* and to inhibit Hsp70-mediated protein refolding.[108]

2.3. BAG3 protein

BAG3 is a 74 kDa protein, originally identified by a screening on two-hybrid yeasts, using the ATPase domain of the heat shock protein Hsp70 as a bait.[109] BAG3 protein is evolutionarily highly conserved in mammals and BAG3 orthologues in mouse, rat and human show a significant homology not only at protein level, but also at gene level.[110] Two BAG3 isoforms have been described so far: one is the full-length product of the bag3 gene with an apparent mass of 74 kDa, the other one is a shorter BAG3 protein, 40kDa, and it is found to be mainly expressed in synaptosomes (**Figure 2.3**). The BAG3 full-length protein is localized in the cytoplasm, mainly concentrated in the rough endoplasmic reticulum; a nuclear

localization of a small BAG3 isoform could be observed in some cell types, such as glial cells or pancreatic carcinoma cells. Indeed, under acute stress or upon viral infection, BAG3 alters its subcellular distribution and the co-chaperone moves into the nucleus.[111]
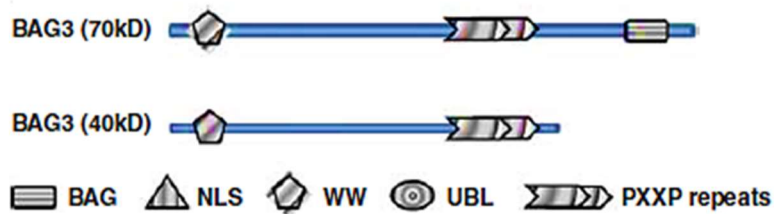

Figure 2.3 *Schematic representation of the full-length BAG3 protein and the shorter isoform, a 40kD BAG3 protein*

BAG3 is constitutively expressed in myocytes and in cancer cells derived from myeloid leukemias, neuroblastomas, prostate carcinomas, ovary and breast cancer, glioblastoma, and other tumor tissues.[7,112,113,114] In other non-transformed cells (e.g., epithelial and retinal cells) BAG3 expression can be induced by a variety of exogenous stressors, such as heavy metals, drugs or HIV infection.[95] Moreover, the bag3 gene promoter activity is regulated by the heat shock transcription factors HSFs[115,115b], suggesting again a role of this protein in tumor formation, since, as it has been established, the expression of stress-responsive genes is regulated by the heat shock transcription factors, including HSF1, that is required for tumor initiation and maintenance in a variety of cancer models. An increased cellular BAG3 level was found during cellular aging in neuronal cells as well as in lung fibroblasts.[116] Furthermore, in several types of cell lines, BAG3 protein expression can be induced by many chemotherapeutics, like fludarabine or etoposide, showing an important role of the protein in chemoresistance mechanisms. Indeed, silencing bag3 gene, allow to sensitize cancer cells to the drugs, leading cells to apoptosis.[117,118,119,120] In addition to the pathological role of BAG3, in rat and human cardiomyocytes it appears to be expressed during differentiation from cardiomyoblasts and to sustain myogenin expression.[121] These findings indicate an involvement of BAG3 protein in late heart development and are in line with the

described role of BAG3 in the survival and myofibrillar integrity in cardiocytes and, in general, in muscle cells.[122]

BAG3 domains structure

Like BAG1 and BAG2 proteins, BAG3 is characterized by a multi-modular domain structure that allows a wide range of protein–protein interactions in addition to the recognition of Bcl-2 protein.[123] Like the other members of the BAG protein family, BAG3 protein exhibits a highly conserved BAG domain in its C-terminal region.[88,124] Via this 78 aminoacids domain, BAG3 is able to bind the ATPase domain of the Hsc/Hsp70 chaperone, but also, as recently found, the heat shock factor HSF1. [94,125,126] For the human BAG3 protein (575 a.a), additional aminoacid sequence motifs and domains have been identified, including a WW domain, a PXXP region, and two conserved IPV (isoleucine–proline–valine) motifs, one located centrally in the protein structure, and the other one closer to the N-terminal domain (**Figure 2.4**).
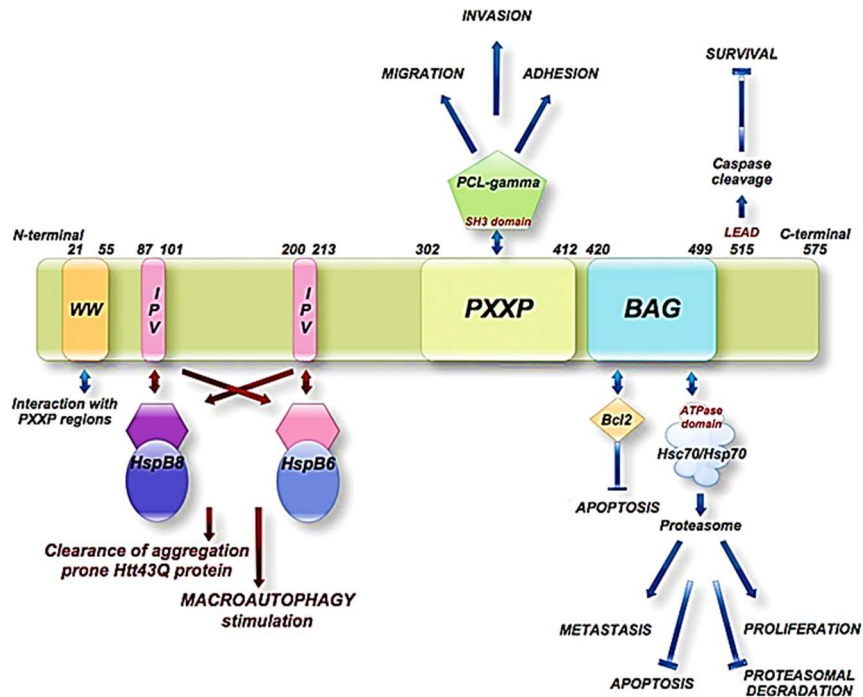

Figure 2.4 *Schematic representation of the BAG3 protein domains and their interactions*

The WW domain is able to interact with proline-rich repeats of proteins, such as the guanine nucleotide exchange factor 2 (PDZGEF2), the adenovirus (Ad) penton base protein, the synaptopodin-2 (SYNPO2), and the tuberous sclerosis 1 (TSC1) protein.[127,128,129] Two conserved IPV motifs were identified at N-terminus and in the middle of BAG3 and mediate the binding of the protein to the small heat shock proteins HspB8 (Hsp22), HspB6 (Hsp20) and, to some extent, also to HspB5 (aB-crystallin) and HspB1 (Hsp7).[130,131,132] The PXXP motif of BAG3 represents a binding site for proteins containing a SH3 (Src homology 3) domain, like phospholipase C gamma (PLC-g).[4,133] Between its two conserved IPV motifs, BAG3 possesses two phospho-serine-containing the 14-3-3 binding motifs (RSQS136 and RSQS173) which are crucial for its interaction with the 14-3-3 proteins.[134] Furthermore, a conserved caspase cleavage site is located in the PXXP region (344KEVD) of BAG3 and in its C-terminal region.[135] Besides these highly structured domains and motifs, BAG3 protein exhibits several disordered regions that, however, are not functionless, indeed, they were shown not only to be "linker" segments between structured protein domains, but also to be subjected to post-translational modifications and to mediate protein–protein interactions.[136] Due to its complex structural organization, BAG3 protein has a high number of already identified different interactors and this suggests its pivotal role in many key cellular processes, including apoptosis, cell proliferation, cytoskeleton arrangement, cell adhesion and motility, viral replication, and selective macroautophagy. Other functions of BAG-3 are related to Hsp70-dependent proteins degradation by means of the ubiquitin-mediated proteasome machinery.

2.4. BAG3 in normal cells

The BAG3 anti-apoptotic activity, in normal cells, was first disclosed in primary peripheral blood mononuclear cells (PBMC) treated with the glutathione depletor diethyl maleate (DEM). When PBMC were cultured with DEM, alone or in combination with bag3- directed phosphorothioate oligodeoxynucleotides (ODN), apoptosis induced by DEM was increased by the addition of oligo RNA interference (RNAi) that blocked BAG3 activity.[137] Recent studies have also demonstrated the

involvement of BAG3 in autophagy. Autophagy is the evolutionary conserved degradation process that targets cytoplasmic materials, including cytosol, macromolecules and organelles, and contributes to the cellular adaptation to stress; it plays a key role in several phases of cancer progression and in the metastatic process, and its deregulation is implicated in degenerative disorders of brain, muscle and other tissues. The role played by BAG3 in cytoskeleton remodeling and membrane trafficking suggests the possibility that it might be involved in autophagy. There is, indeed, a chaperone-mediated autophagy (CMA), selective for cytosolic proteins containing a pentapeptide motif: this motif is recognized by the chaperone heat shock cognate 70 (Hsc70), which transfers protein substrates to lysosomes. Since BAG3 is an Hsc/Hsp 70 co-chaperone, it is plausible to imagine its involvement in CMA[138], but it has been also speculated about a role in the other two types of autophagy. Indeed, BAG3 participates, along with HspB8, a member of the HspB family of molecular chaperones, in the degradation of misfolded and aggregated proteins via macroautophagy; in more details, protein binding to HspB8 is mediated by two conserved IPV (Ile-Pro-Val) motifs located between the WW- and the Pro-rich- domains of the co-chaperone (**Figure 2.5**).[139] Hence, BAG3 can be considered as an additional auxiliary factor and assistant protein, regulating the degradation of age-and disease-associated intracellular protein aggregates.
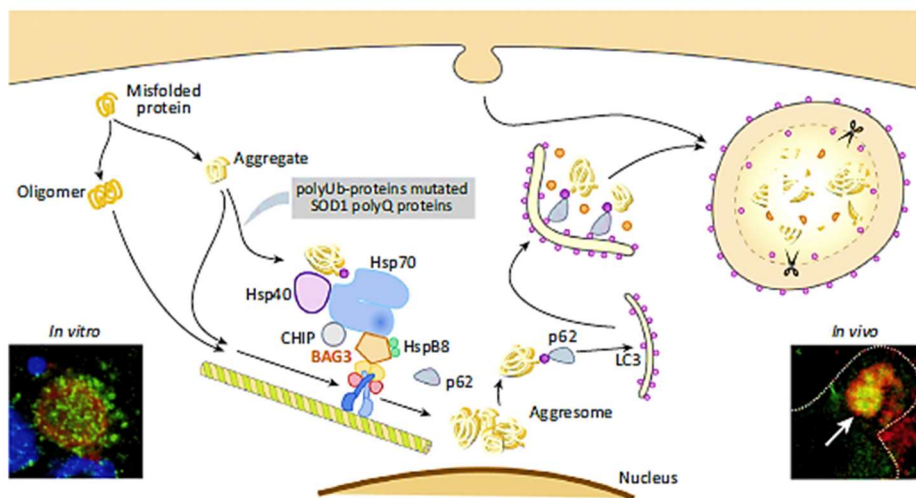

Figure 2.5 *Putative mechanism of Aggresome formation and induction of BAG3-mediated selective macro-autophagy*

Another physiological role of BAG3 is related to its constitutive expression in skeletal muscle and cardiac myocytes. Indeed, this protein appears in cardiomyoblasts during their differentiation and modulates the expression of the transcription factor myogenin, that coordinates myogenesis.[121] Moreover, BAG3 protein sustains myocyte homeostasis and myofibrillar integrity during mechanical, proteotoxic and other types of stress; such property is related both to BAG3 anti-apoptotic activity and its role in macroautophagy; moreover, BAG3 exerts also a structural role in myofibrils, where it maintains the structural integrity of the Z-disk by binding with CapZ.[140] As an additional mechanism, BAG3 may also have a regulatory effect on contractility and on calcium homeostasis, by directly interacting with β1 adrenergic receptors and with Ca^{2+} channels in ventricular myocytes.[141] In cardiac muscle, BAG3, through association with the sarcomeric Z-disk, maintains the integrity and contractility of heart muscle, on the contrary, a BAG3 defect can result in impairing myocyte survival, in inadeguate contractility and in heart and/or muscle myopathies.[142] Moreover**,** the expression of bag3 gene is detectable in neurons, where BAG3 protein appears to be involved in neuronal migration and differentiation;[143] synaptosomes selectively contain a smaller BAG3 of about 40 kDa, possibly reflecting a specialized activity in modulating synaptic response to stressful stimuli.[144] Recently, some neuropathies have been documented in patients with BAG3 mutations, in association with myopathies and cardiomyopathies, indicating a role for BAG3 also in neurophysiopathology.[145]

2.5. BAG3 in cancer cells

BAG3 in apoptosis

The first evidence of the anti-apoptotic role of BAG3 in tumor cells was obtained in primary acute and chronic leukemia, where, a down-modulation of BAG3 levels resulted in inducing spontaneous apoptosis. Another proof of evidence of its antiapoptotic mechanism is represented by the fact that, the increase of BAG3 binding to Hsp70 was shown to weaken Hsp70 interaction with some anti-apoptotic proteins whose delivery to proteasome resulted inhibited. As a consequence of the

increased levels of such anti-apoptotic factors, tumor cell survival and growth are promoted. These anti-apoptotic proteins include, in diverse tumor types, Akt[146], the gamma component of the IKK (IκB kinase) complex [114], BRAF[147], Mcl-1[148], Bcl-2 and Bcl-XL[149], and others. Moreover, many studies in tumor cell lines have demonstrated that bag3 silencing is related to an enhancement of spontaneous or drug induced apoptosis, whereas, conversely, an activation of BAG3 expression resulted in opposite effects.[94,118,150] BAG3 influences cell survival by its interaction with different molecular partners, through the activation of multiple pathways. The main mechanism of BAG3 anti-apoptotic activity is mediated by its role, as a co-chaperone, in proteins delivery to proteasome. Indeed, while BAG1 positively cooperates with Hsp70 and CHIP to direct, through its ubiquitin-like domain, client proteins to proteasome, BAG3 can interfere with this process by competing with BAG1.[151,152] For example, in osteosarcoma and melanoma cells BAG3 protects kinase IKKgamma from proteasome delivery and that results in a sustained NF-kB activation and in cell survival.[153] (**Figure 2.6**)
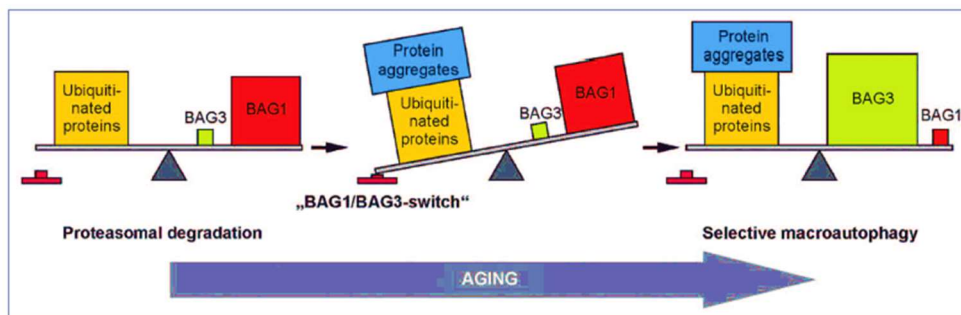
Figure 2.6 B*AG1-BAG3 switch in expression and function. The BAG1 and BAG3 expression levels are reciprocally regulated during cellular aging and under acute stress. Under physiological conditions, a high BAG1 expression, but a low BAG3 expression could be detected; under pathophysiological conditions, the BAG3 level is elevated and the BAG1 level is decreased*

In addition, a different mechanism has been observed in glioblastoma cells, where BAG3 retains BAX protein in the cytosol, preventing its mitochondrial translocation.[154] Actually, both these mechanisms rely on the interaction between BAG3 and Hsp70. It is also believed that, through its binding to Hsp70, BAG3 might also positively or negatively modulate the folding of other apoptosis-

regulating proteins, and for this reason, the scientific community is very interested in studying more deeply the very complex regulative mechanism mediated by this protein (**Figure 2.7.**). However, a BAG3 anti-apoptotic activity independent of Hsp70 interaction has been suggested; that can be due to the binding to other client proteins through its WW- or PXXP domain, directly influencing their stability, localization or activity.[155] Another mechanism related to the BAG3 anti-apoptotic activity, is its caspase-dependent cleavage. Notably, cellular decrease of BAG3 protein was associated with the appearance of a BAG3 fragment, of approximately 40 kDa, which appeared to be caspase-dependent and resulted in facilitating apoptosis in sensitive cells. Moreover, it has been recently demonstrated that BAG3 is also induced by proteasome inhibitors, at the transcriptional level, and, the consequent induction, of BAG3 levels, results in an antiapoptotic mechanism; indeed, the related increase of BAG3 protein caused cellular protection against Staurosporine (STS)-induced apoptosis and, in contrast, silencing BAG3 augmented STS-mediated apoptosis.[156] Together, these data confirm that BAG3 functions as a pro-survival protein, the presence of which is regulated by caspase cleavage followed by ubiquitination and proteasomal degradation and, impaired BAG3 degradation, is central in the protection of cancer cells against intrinsic apoptotic pathway stress.
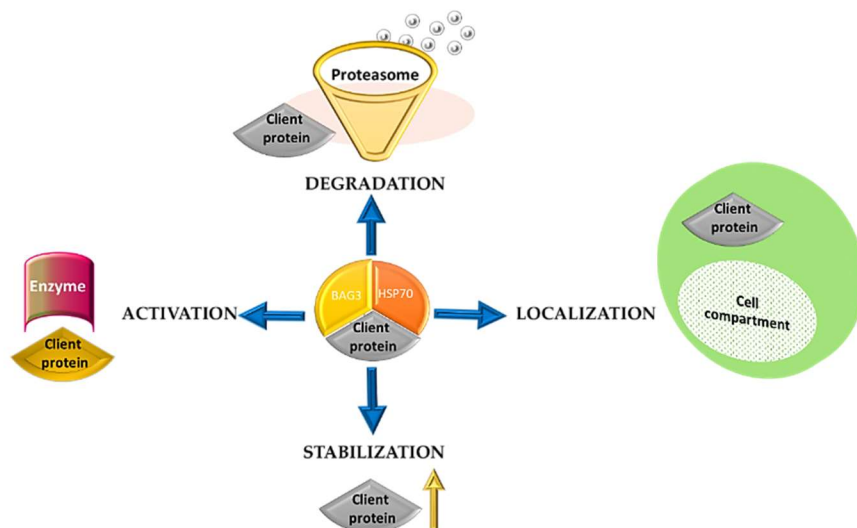

Figure 2.7. *Hsp70-BAG3 mediated pathways*

BAG3 in cell adhesion

BAG3 is also involved in the regulation of cell adhesion and motility, and this protein function is mediated by the different domains of the protein. Actually, bag3 gene silencing reduces adhesion and motility in epithelial (breast, prostate) tumor cell[157,158,159] and in MDA435 human breast cancer cells. Whereas, conversely, BAG3 protein over-expression resulted in an increasing of molecules migration and adhesion to the matrix, involving the BAG3 proline-rich (PXXP) domain through the interaction with a SH3 domain- containing protein.[160] In addition, BAG3 can regulate cell adhesion through the binding to guanine nucleotide exchange factor 2 (PDZGEF2); in more detail, the PDZ motif at the C-terminus of PDZGEF2 was shown to bind to the WW domain of BAG3 and to induce the activation of Rap 1 (Ras-proximate-1) a modulator of cell-cell junctions.[161] Moreover, recently, has been reported that BAG3, through its interaction with the cytosolic chaperonin CCT (Chaperonin Containing TCP-1), regulates actin folding and cytoskeleton organization, possibly influencing not only cell survival and migration, but also membrane trafficking and organelles dynamics.

BAG3 in human tumors

BAG3 overexpression has been detected in many human cancers of various origins for instance in pancreatic ductal adenocarcinomas (PDACs) [162,163], melanomas [164,165], hepatocellular carcinomas[166], lung cancers[167], colorectal carcinomas[168], astrocytomas and glioblastomas[154], leukemias[169], thyroid carcinomas[118], ovarian carcinomas [170], breast cancers [171], prostate cancers [172], endometrioid endometrial adenocarcinomas[173] (**Table 2.1**). BAG3 promotes the survival, the growth and the invasiveness of primary tumors and provides resistance to chemotherapy. As previously mentioned, its anti-apoptotic activity depends on its ability to bind numerous factors. For instance, in pancreatic adenocarcinoma it was recently found that BAG3 binds and activates macrophages, leading, thus, to the secretion of further cancer promoting factors. Macrophages activation occurs via its binding to the receptor IFITM-2 (interferon-induced transmembrane protein 2).[174] The BAG3-

mediated activation of macrophages occurs through the PI3K and the p38 MAPK signaling pathways and results in secretion of further cell proliferation stimulating factors, proposing a role of extracellular BAG3 in tumor development. In breast cancer cells an association of oxidative stress resistance with the expression of the estrogen receptor and BAG3 has been found;[171] in more details, CXCR4 receptor has been suggested to be a target of BAG3 protein and a crucial mediator of BAG3's role in promoting breast cancer. CXCR4 is the most common chemokine receptor detected in cell population of some tumors including breast cancer;[175] this study demonstrated that BAG3 stabilized CXCR4 transcription, acting at post-transcriptional level. A different mechanism operates in human glioblastoma cells where BAG3 binds to BAX in cell cytosol and prevents its translocation to mitochondria, thereby protecting cells from apoptosis in response to chemotherapeutic drugs. In prostate cancer (CaP) BAG3 has an essential role in promoting the emergence of metastatic castration-resistant growth.[176] In lung cancer cells BAG3 down-regulation induces cell apoptosis and impairs tumor growth also in small cell lung cancer (SCLC) cells. The molecular mechanisms and the proteins involved in BAG3 pro-survival function in SCLCs are still unknown and require further studies; however, recent reports indicate a relevant role for the tyrosine-protein kinase MET signaling pathway.[167] Resistance to chemotherapy is also the consequence of BAG3 over-expression in a subset of small cell lung cancer, moreover, high levels of the protein are responsible of resistance to apoptosis in therapy-induced senescent cells. In addition to its effects in sustaining tumor cells survival and resistance to therapy, BAG3 also promotes cancer invasiveness.[157, 177] This is accomplished by two distinct mechanisms: the first one includes direct or indirect effects of BAG3 activity on proteins involved in adhesion or in actin-cytoskeleton dynamics, such as FAK [160], Rac1[157] or the PDZGEF2 (PDZ domain-containing guanine nucleotide exchange factor 2);[128] the second one is related to the regulation of cell ability to degrade components of the extracellular matrix, through enhancement of metalloproteinases expression and activity.[178] Recent findings show that BAG3 protein can also support tumor neoangiogenesis, by inducing VEGF expression in cancer cells and by regulating ERK/DUSP6 interaction in cycling endothelial cells.[166]

Tumor	% positivity	Poor prognosis	Resistance to treatment	References
Acute lymphoblastic leukaemia (ALL)	ND	ND	ND	Romano,2003
B-cell chronic lymphocytic leukemia (B-CLL)	ND	ND	ND	Romano,2003, Chen 2010, Zhu 2014
Thyroid carcinomas	0,96	ND	ND	Chiappetta 2010
Prostate carcinomas	ND	ND	ND	Staibano 2010
Astrocytomas	20-50%	ND	ND	Festa 2011
Melanomas	67-70%	YES	ND	Franco 2012, Guerriero 2014
Colorectal carcinomas	ND	YES	ND	Yang, 2013
Ovarian carcinomas	ND	YES	ND	Aust, 2013, Sugio, 2014, Nymoen, 2015
Lung cancer	62-100%	ND	ND	Chiappetta, 2014
Liver cancer	1	YES	YES	Xiao, 2014
Breast cancer	ND	ND	ND	Nourashrafeddi, 2015
Endometrial cancer	1	ND	ND	Esposito, 2016
Pancreatic ductal carcinoma	1	YES	ND	Liao 2001, Rosati 2012

Table 2.1 *Human tumors showing BAG3 protein overexpression*

BAG3 in Melanoma

BAG3 protein has been deeply investigated for its antiapoptotic role in melanoma cells and, its expression in melanoma metastatic lymphnodes, was correlated to the aggressiveness of the tumor.[153] In melanoma cells, indeed, BAG3 acts as modulator of the Hsp70- mediated delivery of the IKKγ subunit of IKK complex to proteasome, thereby sustaining NF-κB activation and inhibiting cell apoptosis. IKK (IκB kinase) is an enzyme complex that is involved in propagating the cellular response to inflammation and is part of the upstream NF-κB signal transduction cascade. In particular, a double effect of BAG3 on IKKγ was investigated, indeed,

although BAG3 initially releases the kinase from the complex with Hsp70, increasing its availability in the cell, it also causes an increased IKKγ stabilization; this second effect is attributable to the inhibition of Hsp70-dependent delivery to the proteasome. In a melanoma *in vivo* study bag3 silencing resulted in a significant reduction of tumor growth with a subsequent prolonged animal's survival.[114] On the other hand, in this tumor BAG3 resulted overexpressed by comparing BAG3 levels in human melanomas from skin or eye. Another very recent study investigated BAG3 protein level in the human choroidal melanoma tissue, detecting an upregulation of the protein if compared to that in normal retinochoroidal tissue. Furthermore, in the same tumor also the expression levels of heat shock factor 1 (HSF1) and Hsp70 resulted upregulated; this data is in line with the previously reported results that linked BAG3-Hsp70 interaction with the anti-apoptotic function of BAG3 in melanoma cancer cells.[179] All together these results consolidate the eminent role, played by BAG3, in tumorigenesis and progression and provide a new attractive target for cancer therapy.

2.6. Targeting Hsp70-BAG3 interaction

As already mentioned in the previous paragraph, one of the principal mechanisms behind the antiapoptotic activity of BAG3 is the interaction, through its BAG domain, with the chaperone Hsp70. Even if this chaperone is known to collaborate with several co-chaperones, its interaction with BAG3 protein plays a key role in cancer pathologies since its expression resulted co-elevated with BAG3 in many tumor types.[180] Several findings point to the cytoprotective role of the complex Hsp70-BAG3 (HB), indeed, it has been shown to detect the building up of aberrant proteins due to proteasome decline and to activate several protective responses. In line with these observations, blocking the Hsp70-Bag3 interaction, by using mutations or gene knockdown, may result in a selective anti-proliferative activity in cancer cells[4], suggesting that the inhibition of Hsp70-BAG3 protein-protein interaction (PPI) might be one non-canonical way to interrupt Hsp70 or BAG3 mediated pathways. The Hsp70-Bag3 interaction occurs with relatively tight affinity (~30 nM) and involves a comparatively large surface of contact.[13,96] These

considerations, along with the difficulty of targeting directly the site of Hsp70, since it is located in a deep groove in its nucleotide binding domain, drove the scientific community to the identification of allosteric inhibitors of the protein, in order to weaken the Hsp70-Bag3 interaction in vitro and in cells. It is well known that the affinity of the Hsp70–Bag3 interaction is significantly weakened (13-fold) in the presence of ADP[181], suggesting that the ADP-bound state stabilization of Hsp70 might represent a way of blocking the Hsp70–Bag3 contact. Following this approach, two Hsp70 inhibitors have been identified so far, YM-01 and JG-98 (**Figure 2.8.**), that bind to Hsp70 and stabilizes it in the ADP-bound form.[182]
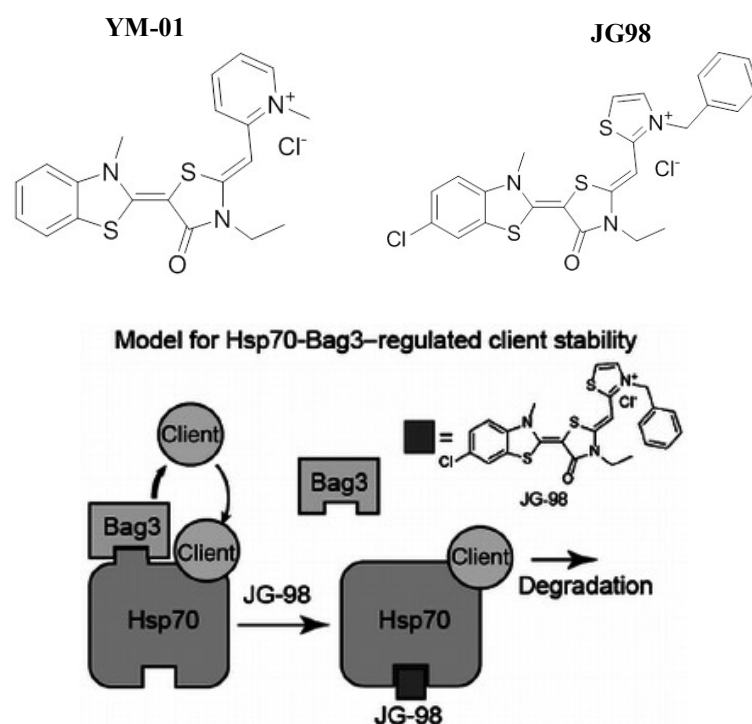
Figure 2.8 *Chemical structures of YM-01 and JG98 Hsp70 inhibitors and*
Supposed mechanism of action of JG-98

These molecules, thus, destabilizes Hsp70–Bag3 interaction; in particular, it was found that, inoculating YM-1 in *vivo* on a xenograft model, the tumor growth was strongly reduced. The structural related derivative JG98 showed a variable antiproliferative activity across a range of cancer cells ($EC_{50} \sim 0.3$ to 4 µmol/L) and resulted to be relatively less toxic in healthy mouse fibroblasts ($EC_{50} \sim 4.5$ µmol/L).

JG-98 also disrupted the FoxM1 cell-cycle pathway, according to the block of the Hsp70–Bag3 interaction. Although JG-98 was not orally bioavailable, it was well tolerated in mice when delivered intraperitoneally and it suppressed tumor growth in two xenograft models.[183] However, despite the many efforts so far invested in this research area, the development of strategies able to selectively inhibit the pathological role of Hsp70, without interfering with its important physiological activity, results to be quite challenging (**Figure 2.9**).[184]
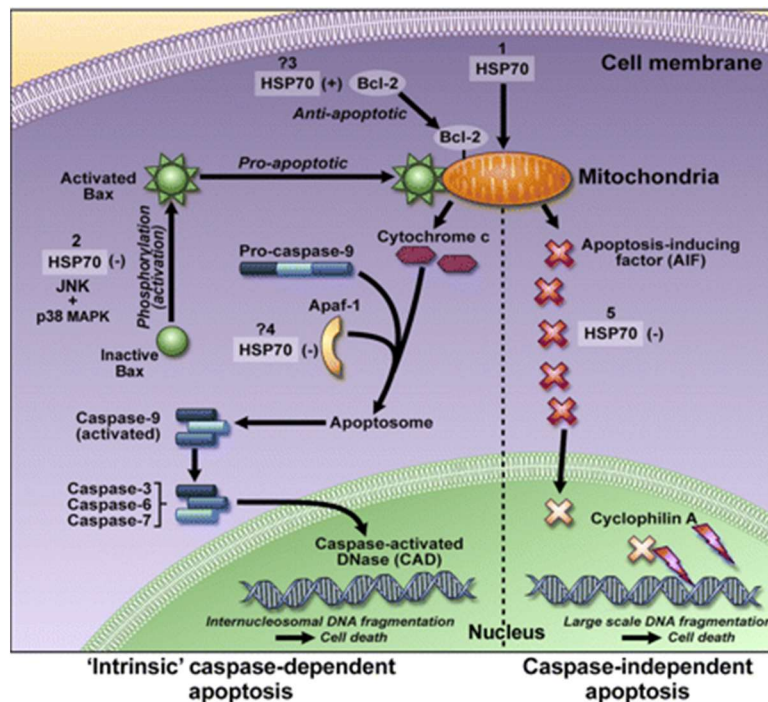

Figure 2.9 *Multiple effects of HSP70 on apoptosis control*

In addition to all these issues, Hsp70 has a relatively tight affinity (mid-nanomolar) for nucleotide 300-fold higher than Hsp90 and that makes even more difficult to target it.[185] Therefore, a feasible way may be to block the interactions between Hsp70 and its co-chaperone, selectively targeting BAG3 protein. Indeed, several findings suggest that disruption of the specific Hsp70-BAG protein contacts might be beneficial in disease. Basing on all these considerations, a part of my PhD project has been focused on targeting BAG3 protein and in particular its BD domain, with the aim of inhibiting its interaction with the co-chaperone Hsp70 and of reversing the related antiapoptic and proliferative effects. In more detail, basing on a

computational study, performed on a large library of commercially available compounds, we succeeded to identify a small collection of molecules that were screened against BAG3 full length protein and its isolated BD3 domain, by SPR technology. Thereby we discovered a potent and selective BAG3-Hsp70 complex modulator that represented our *lead* compound to design and synthesize a collection of structural analogues that have been subjected to a thorough biological screening. The details of this work will be deeply described in chapter 5.

2.7. The workflow of the projects

As above mentioned, the main focus of my PhD research program has been the design, synthesis, biochemical and biological evaluation of new promising anticancer agents targeting the proteins of interest. The general workflow followed for the investigation of these two targets can be described through these main steps:

1) In silico design of potential inhibitors of the target protein by means of fragment based design, structure-based design and ligand-based design approaches.

2) Chemical synthesis of the compounds selected by computational analysis.

3) Biochemical and biological evaluation and identification of possible hits or lead compounds.

4) Rationalization of ligand/protein interaction by crystallographic or computational methods.

5) Structural optimization of the identified lead compound in order to improve its biological profile.

- 50 -

- 51 -

RESULTS AND DISCUSSION

- 52 -

CHAPTER 3

Discovery of new modulators of the human Macrodomain protein MacroD2 by a structure-based-drug design approach

3.1. Targeting MacroD2 protein

Aim of the work

A part of my PhD project has been dedicated to the identification of potential modulators of the Macrodomain proteins MacroD1 and MacroD2. As mentioned in the introductive section, these two proteins are particularly hard to investigate; indeed, since they have recently emerged as epigenetic enzymes involved in the carcinogenesis process, so far no inhibitor has been yet disclosed. For this reason, lacking detailed information about the structural requirements for protein interaction, two different drug discovery approaches have been employed. In particular, in this section, a classic *structure based drug design* approach will be discussed. Starting from the deposited crystal structure of MacroD2 protein, in complex with its natural ligand (PDB: 4IQY)[51a], the ADP-ribose, a virtual screening has been performed, considering the key interactions of the natural ligand in the binding pocket of MacroD2 protein; this preliminary computational screening allowed to develop a collection of triazole molecules potentially able to bind the target enzyme. Concerning the other approach employed to study MacroD1 protein, it will be deeply described in the next section.

3.2. Structure based virtual screening

For the virtual screening campaign, the ZIN Click Database, a novel library containing over 16 million of 1,2,3- triazoles[186], which can be easily prepared starting from commercially available products, was selected. Moreover, most of the molecules in this database are new and patentable and should be rapidly prepared starting from commercially available azides and alkynes, enabling tests of the docking hypotheses.[187] The 1,2,3-triazole scaffold was chosen as template for the the rational design, since this five member heterocycle is well known to represent a privileged scaffold in medicinal chemistry due to its good pharmacological and pharmacokinetic properties and for its easy synthetic accessibility.

Indeed, a literature survey revealed that triazole derivatives possess a variety of biological properties including antimicrobial, antifungal, antileishmanial, antiviral, antitubercular, anticancer, antioxidant, anticholinesterase, anti-inflammatory, antidepressant, antianxiety and anticonvulsant activities.[188]

In this virtual screening campaign docking calculations were performed using Glide software (HTVS, SP and XP mode, according to the Glide Virtual Screening Workflow).[189] Docking experiments were performed generating a receptor grid focused on the MacroD2 protein binding site (considering the co-crystallized ligand ADP-ribose as reference structure, PDB code: 4IQY). In more details, a first round of docking experiments was performed setting the High-Throughput Virtual Screening (HTVS) precision mode of Glide. The 30% top-ranked poses, using docking score as selection parameter, were then saved and submitted to a second set of docking experiments, using the Standard Precision (SP) Glide mode. The selected poses were then submitted to a third docking round, setting in this case the Extra-Precision (XP) Glide mode that outperforms the SP mode for both sampling and scoring. Again, the 30% top-ranked poses were filtered and subsequently carefully analyzed for selecting new putative MacroD2 binders. Once the virtual screening process was completed, the binding mode of the selected compounds was carefully analyzed by selecting the docking poses establishing specific sets of interactions and showing a favorable accommodation in the binding sites after visual inspection. The analysis of the predicted *in silico* binding energies allowed us to select a first collection of the best molecules in terms of docking score and shape similarity (**Table 3.1**); in particular, only the triazoles which showed a shape similarity lower than 0.8 were chosen for the synthesis, hence the optimization of the synthetic strategy was accomplished.

Entry	Docking score (kcal/mol)	Entry	Docking score (kcal/mol)
SP1	-7.772	**SP7**	-9.408
SP2	-7.185	**SP8**	-9.777
SP3	-9.546	**SP9**	-8.876
SP4	-5.096	**SP10**	-7.066
SP5	-7.032	**SP11**	-10.062
SP6	-8.493	**SP12**	-8.493

Table 3.1 *Docking scores values of the in silico selected triazoles SP1-SP12*

3.3. Synthesis and biochemical evaluation

The compounds selected from the virtual screening protocol can be classified in two different groups: the first one composed of 1,2,3-1,4-disubstituted triazoles ((1-(benzo[d]thiazol-6-yl)-1H-1,2,3-triazol-4-yl)methyl esters) (**SP1-SP6**) and the second one of 1,2,3,-1,4,5-trisubstituted triazoles ((5-methyl-1-(thiazol-2-yl)-1H-1,2,3-triazol-4-yl)methyl esters) (**SP7-SP12**) (**Figure 3.1**).
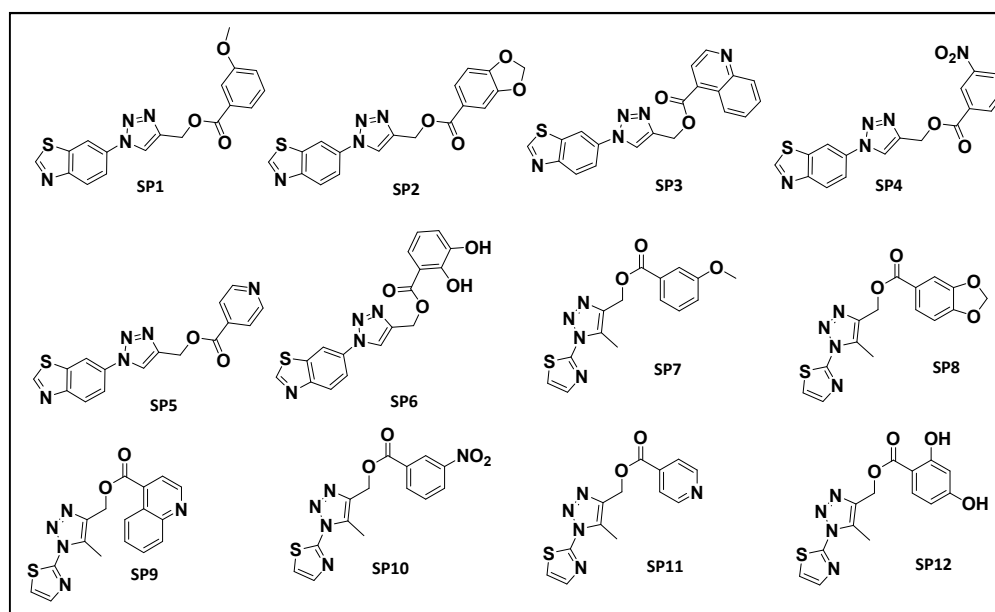

Figure 3.1 *Chemical structures of the triazoles **SP1-SP12***
selected from the virtual screening

All these molecules have been synthesized by a multi-steps protocol. In particular, the first step includes the synthesis of aryl or heteroaryl-azides in order to obtain the precursors for the Click chemistry reaction. The regioselective Cu-I-catalyzed azide/alkyne 1,4- cycloaddition (CuAAC) between the obtained azides and propargyl alcohol, as terminal alkyne, has been used to obtain the 1,2,3-1,4-disubstituted-triazole scaffold;[190] conversely, for the 1,4,5 trisubstituted triazoles a different strategy using ethyl acetoacetate in sodium methoxide, was selected.[191] Then, the desired final compounds were synthesized employing a Steglich

esterification procedure, a mild reaction which allows the conversion of sterically demanding and acid labile substrates in the respective esters.[192]

Synthesis of compounds SP1-SP12

The synthesis of compounds **SP1-SP6** was accomplished by means of two different steps. Concerning the first one, the 6-azidobenzo[d]thiazole (**1a**) was obtained from the corresponding benzo[d]thiazol-6-amine (**1**) with tert-butyl nitrite (t-BuONO) and azidotrimethylsilane (TMSN$_3$), under mild conditions. These azides, indeed, are commonly prepared from the corresponding amines via their respective diazonium salts, which may sometimes be problematic for the presence of incompatible functional groups. The one-pot procedure chosen consisted in a sequential procedure where, the amine, dissolved in acetonitrile, was treated with t-BuONO and TMSN$_3$ at 0 °C, and then warming to room temperature. The reaction proceeded smoothly and rapidly to afford, in high yields, the 6-azidobenzo[d]thiazole (**1a**). Then, after complete consumption of the starting material, a catalytic amount of CuSO$_4$, sodium ascorbate and propargyl alcohol were directly added, at room temperature, to the reaction mixture, without any workup procedure. The desired product (**2**) was obtained in excellent yields and without need for isolation of the intermediate azide, after an overnight time reaction (**Scheme 3.1**).[191]
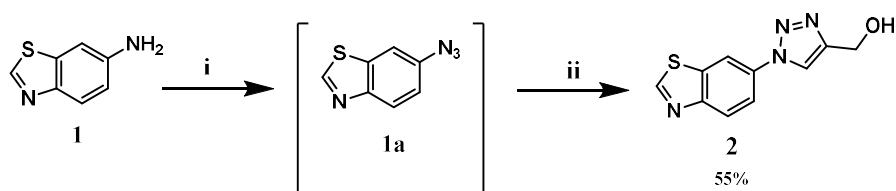

Scheme 3.1. *General procedure for the synthesis of compound* **2**:

Reagents and conditions: i) t-BuONO, TMSN$_3$

CH$_3$CN, 0°C, rt, 2h; ii) Propargyl alcohol, aq CuSO$_4$

sodium ascorbate, rt, 16h

The next step consisted in the functionalization of the hydroxymethyl group, in position -4 of the triazole scaffold, with different aromatic carboxylic acids (**Scheme 3.2**). The Steglich esterification was accomplished in presence of the Steglich catalyst, 4-dimethylaminopyridine (DMAP), and *N,N'*-Diisopropylcarbodiimide (DIC) as dehydrating agent.[192] Once the reaction was completed, soluble *N, N'*-diisopropylurea was removed through liquid-liquid extraction, and, the desired compounds (**SP1-SP6**), endowed with different aromatic ester moieties, were obtained (**Table 3.2**).
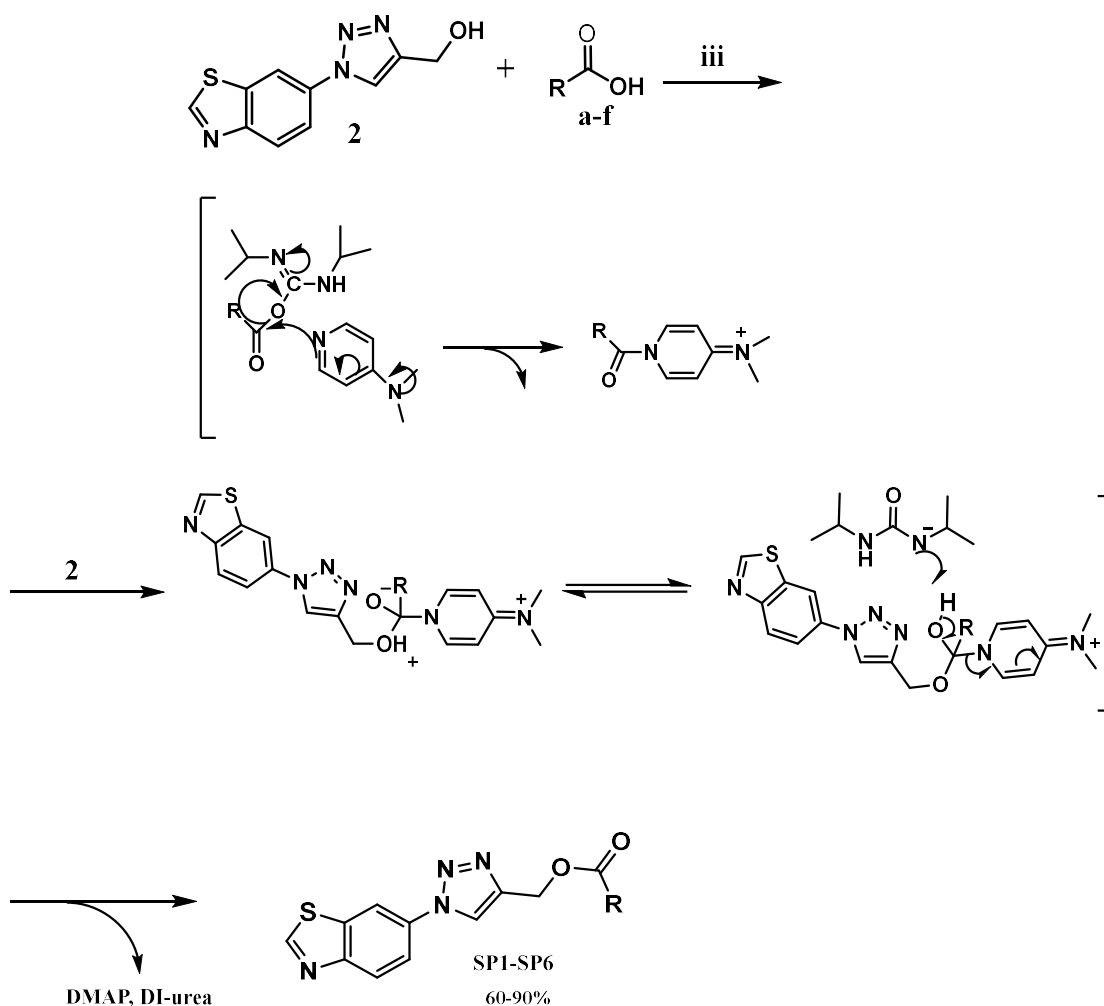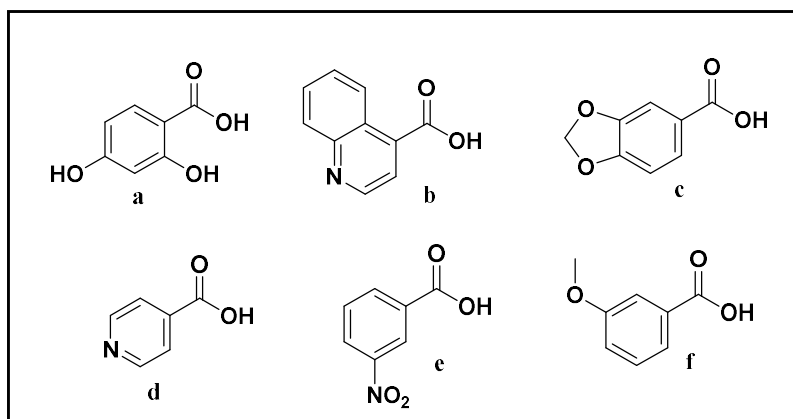
Scheme 3.2. *General procedure for the synthesis of compounds* **SP1-SP6**:

***Reagents and conditions***: iii) DIC, DMAP, DCM, room temperature overnight
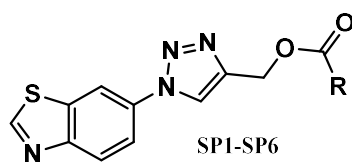
Compound	R	Yield (%)
SP1		63
SP2		62.5
SP3		60
SP4		90
SP5		60
SP6		87

Table 3.2 *Chemical structures of compounds* **SP1-SP6**

Concerning the second group of selected triazoles, compounds **SP7**- **SP12**, they have been synthesized through four consecutive steps. In more details, the intermediate azide (**5**) was obtained starting from the 2-amino-1,3-thiazole (**4**). Because of the structural peculiarities of 2-amino-1,3-thiazoles, there are not many examples of this class of compounds used in the diazotization reaction. Indeed, the availability of the amino group in 2-amino-1,3-thiazoles is linked to its tautomeric equilibrium (**Figure 3.2**). The data reported in literature shows that the predominance of the 2-(amino)-thiazoline tautomer depends, in solutions, on the nature of the solvent.[191]
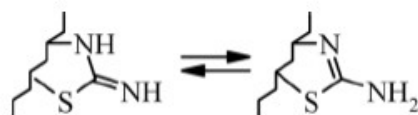

Figure 3.2. *2-amino-1,3-thiazoles tautomeric equilibrium*

For this reason, according to the procedure reported in literature, we performed the diazotization reaction of 2-aminothiazole (**4**) in concentrated HCl as solvent, which allowed to obtain the azide (**5**), with 36% yield (**Scheme 3.3A**);[191] unfortunately, despite the efforts lavished in the optimization of the reaction conditions, like exploring either different reaction times or different temperatures, some quantity of the aminothiazole remained always unreacted after the diazotization reaction. The second step consisted in the triazole core synthesis, however, using the classical Huisgen 1,3-dipolar cycloaddition, the reduction of the azido moiety to the amino group, instead of the triazole formation, took place (especially in the case of azides with electron-withdrawing substituents). For this reason to circumvent the problem we decided to carry out an alternative reaction with β-ketoesters in basic conditions.[191] The reaction was accomplished by the use of the azido thiazole and ethyl acetoacetate at room temperature. Using this strategy, the 2-azidothiazole rapidly reacted and was converted into the product (**7**), in good yields, after the addition *in situ* of sodium hydroxide, to hydrolyze the ethyl ester group (**Scheme 3.3B**).
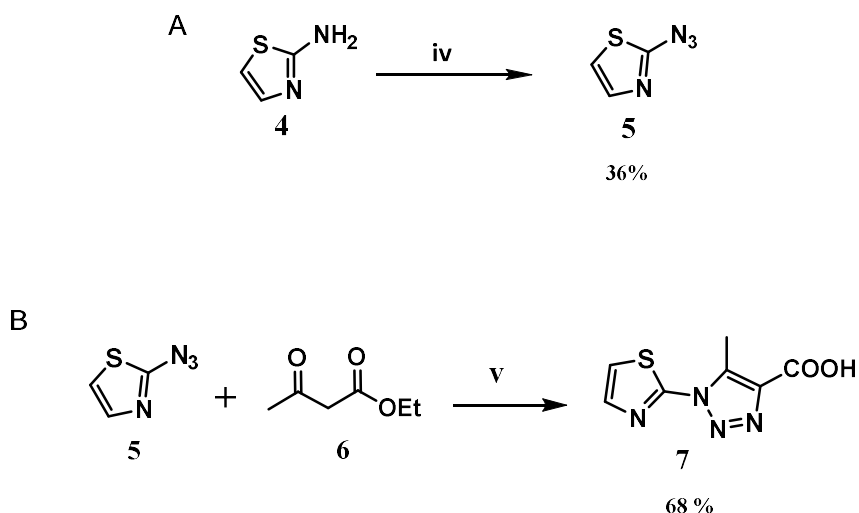
Scheme 3.3. *General procedure for the synthesis of compounds* **5** *and* **7**:

Reagents and conditions: *iv) NaN$_3$, NaNO$_2$, HCl conc.*

2h, 0° then room temperature; v) MeO$^-$ Na$^+$, 2h, 0°

then NaOH 2 N, 1 hour, reflux

Afterwards, the reduction of the carboxylic group in position -4 of the triazole scaffold to hydroxymethyl group was accomplished. For this aim 1-hydroxybenzotriazole (HOBt)/carbodiimide, as coupling agents were used, to furnish a highly reactive benzotriazole ester that could be reduced under mild reaction conditions[193] in presence of sodiumborohydride (NaBH$_4$) and THF as solvent, at 0° for 30 minutes (**Scheme 3.4.A**). This step allowed to obtain compound **8** in good yields; this last was finally subjected to Steglich esterification reaction with different carboxylic acids (**a-g**) (**Scheme 3.4.B**) in order to obtain the desired products **SP7-SP12** (**Table 3.3**) (see also **Scheme 3.2)**.
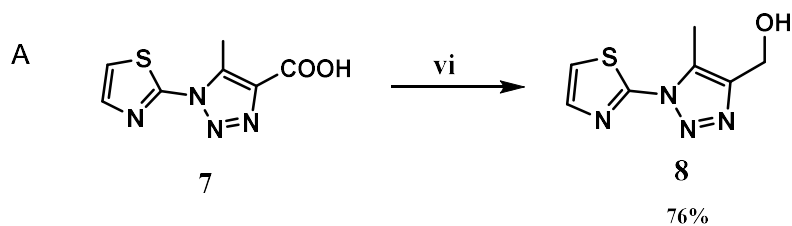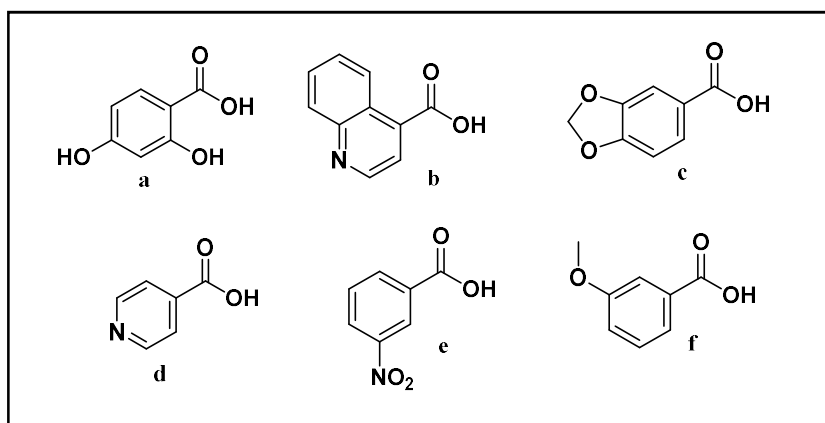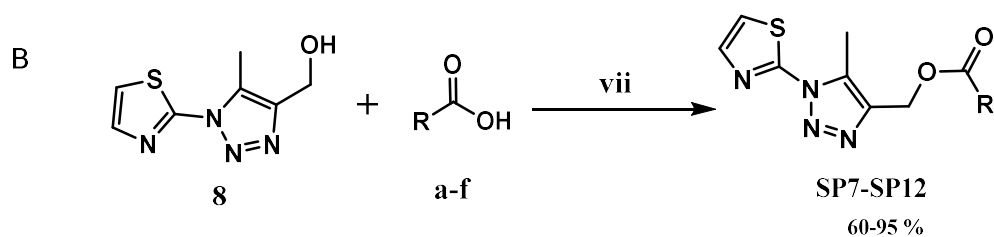
Scheme 3.4. *General procedure for the synthesis of compounds **SP7-SP12**:*

***Reagents and conditions**: vi) HOBt, DIC, DCM,*

30 min, room temperature; then NaBH₄, THF, 30 min, 0°;

vii) DIC, DMAP, DCM, room temperature overnight
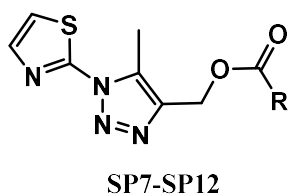
SP7-SP12

Compound	R	Yield (%)
SP7		60.3
SP8		75.3
SP9		56
SP10		93.3
SP11		86.4
SP12		95.5

Table 3.3 *Chemical structures of compounds SP7-SP12*

Biochemical evaluation

All the synthesized compounds have been screened with *AlphaScreen* technology, in collaboration with Dr. Jon Elkins of the *Structural Genomics Consortium* (Oxford University), against a small panel of different macrodomain containing proteins, in order to evaluate their potential inhibition toward the enzymes. AlphaScreen technology is routinely utilized in high throughput screening assays, to quantify analyte accumulation or depletion, biomolecular interactions, and post-

translational modifications. In the epigenetic field this approach has recently been described as a useful tool that makes use of peptides with dissociation constants in the low micromolar range.[194] In the current case the AlphaScreen peptide binds, via its biotinylated lysine, to streptavidin coated donor beads, whereas, the macrodomain protein binds to Ni^{2+}- chelated acceptor beads, by its hexahistidine tag. The use of donor beads coated with streptavidin allowed the conjugation to terminally-biotinylated peptide, while, the acceptor beads coated with a nickel chelator, allowed the conjugation to His-tagged macrodomain proteins (**Figure 3.3**). Laser excitation (680 nm) of a photosensitizer within the donor bead converts ambient oxygen to singlet oxygen. The binding of the macrodomain to the ADP-ribose of the fragment peptide enables an energy transfer from the donor to the acceptor bead, which results in a measurable AlphaScreen signal; ADP-ribose was used as positive control. If the beads are brought within ~200 nm apart, by a binding interaction between the macrodomain and histone peptide, the singlet oxygen initiates a chemiluminescent reaction in the acceptor bead, which emits light in the 520 to 620 nm range. If there is no interaction between the proteins and histone peptide, the singlet oxygen returns to its ground state and no signal is detected. Due to the multiplicity of binding sites on the AlphaScreen beads, binding partners appear to have a higher affinity for each other, amplifying the signal and, thereby, making the technology suitable for screening assays with binding partners that interact in the low micromolar range.
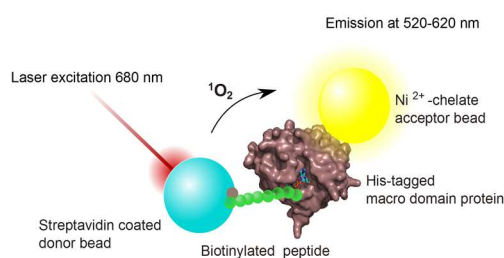

Figure 3.3. *AlphaScreen protocol set up for macrodomain proteins*

All the compounds have been tested at 12 different concentrations, with two-fold dilutions, spanning from 0.02 μM to 50 μM as top concentration. As showed in **Table 3.4** all the synthesized compounds have been evaluated against the Macrodomain proteins MacroD1, MacroD2 and PARP14, whereas "hypothetical protein" LOC221443A[56] was used as counterscreen. These data showed a good percentage of inhibition of the protein MacroD2, binded to the ADPr, for five compounds **SP2**, **SP3**, **SP7, SP10** and **SP12** highlighted in red in the **Table 3.4**.

Percentage of Inhibition at 50μM

Compound	LOC221443A	MACROD1A	MACROD2A	PARP14A
SP1	n.d.	25	30.2	n.d.
SP2	38.26	14.34	80.02	-3.8
SP3	92.54	65.55	99.5	43.58
SP4	-5.06	-6.63	32.59	-9.45
SP5	n.d.	n.d.	n.d.	n.d.
SP6	n.d.	n.d.	n.d.	n.d.
SP7	16.19	3.54	85.63	6.05
SP8	38.75	11.76	41.09	53.95
SP9	5.39	4.67	55.61	-1.88
SP10	22.6	2.52	79.61	-6.48
SP11	61.84	20.8	66.05	87.8
SP12	3.67	6.69	80.08	-2.11

Table 3.4 *Percentages of inhibition calculated for compounds **SP1-SP12**
by AlphaScreen technology against a panel of Macrodomain proteins*

In particular, all these molecules showed a good percentage of protein inhibition, in the range of 80-99%, and at the same time, a good selectivity, except from compound **SP3** which showed to interfere with the ADPr recognition of the other tested proteins, in different percentages (**Table 3.4**). The IC$_{50}$ values of these five compounds were then calculated. In more detail, compounds **SP2** and **SP10** showed the lowest IC$_{50}$ values, (**SP2**: 10.58 ± 0.02 μM and, **SP10**: 32.27 ± 0.1 μM), whereas, for compounds **SP7** and **SP12**, higher values of IC$_{50}$ were measured (**SP7**:

70.98 ± 0.06 μM, **SP12**: 88.39 ± 0.09 μM). Finally, for compound **SP3**, which showed to inhibit MacroD2, PARP14A protein and the counterscreen LOC221443a, an IC_{50} of 6.27 ± 0.05μM for MacroD2, an IC_{50} of 14.31 ± 0.03μM for PARP14A and an IC_{50} of 21.43 ± 0.03 μM for LOC221443A, respectively, were calculated, showing, thus, an aspecific activity on the tested proteins (**Table 3.5)**.

IC_{50}± SD Values

Compound	LOC221443A	MACROD1A	MACROD2A	PARP14A
SP2	n.d	n.d	10.58 ± 0.02 μM	n.d
SP3	21.43±0.03μM	n.d	6.27 ± 0.05μM	14.31 ± 0.03μM
SP7	n.d	n.d	70.98 ± 0.06 μM	n.d
SP10	n.d	n.d	32.27 ± 0.1 μM	n.d
SP12	n.d	n.d	88.39 ± 0.09 μM	n.d

Table 3.5. *IC_{50} values calculated for compounds **SP2, SP3, SP7, SP10** and **SP12** by AlphaScreen technology, against a panel of Macrodomain proteins*

Basing on these preliminary results we decided to design a new collection of 1,2,3-triazoles, combining the ester moieties in position -4 of the triazole core of the most promising compounds, **SP2** and **SP10**, with different benzyl halides, in position-1, in order to explore a larger chemical space. In particular, the piperonylic function of compound **SP2** and the 3-nitro benzoic moiety of compound **SP10** were combined with several benzyl-halides; the new collection of compounds thereby obtained (**Figure 3.4**) has been submitted to the same virtual screening protocol previously described.

Figure 3.4 *Chemical structures of the triazoles designed on the basis of the AlphaScreen results*

The analysis of the binding mode of these new compounds and the related docking score values allowed us to select a new group of variously substituted triazoles that have been successfully synthesized (**Figure 3.5**).
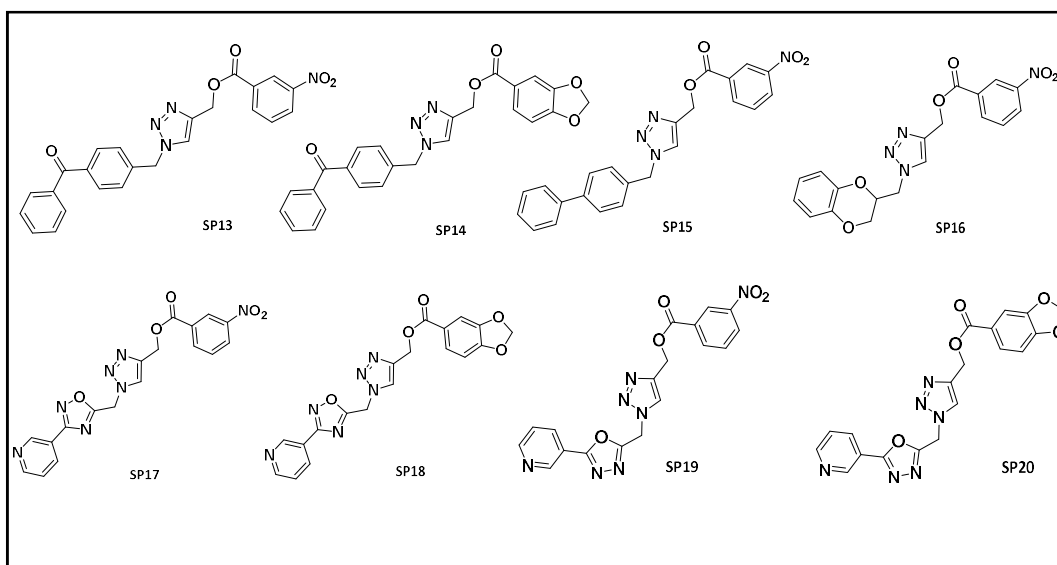
Figure 3.5 *Chemical structures of the selected compounds SP13-SP20*

Synthesis of compounds SP13-SP20

These 1,2,3-triazol-4-yl-methyl esters (**SP13-SP20**) have been obtained through a three steps synthetic approach. The synthesis of the different benzyl azides was realized through the classic nucleophilic substitution reaction of alkyl halides with inorganic azides. Water was used as reaction medium, as a safer experimental procedure, in order to prevent the potential explosion danger of azidation in an halogenated solvent.[195] In more details the benzyl halides and the sodium azide were dissolved in a mixture of water/acetone and the reaction was conducted at reflux; after 3 hours compounds (**11h-n**) have been obtained in good yields. (**Scheme 3.5.A**). The second step consisted of a *click reaction* between the benzyl-azides (**11h-n**) and the propargyl alcohol as terminal alkyne. This regioselective 1,4 Huigsen cycloaddition allowed to obtain the 1,4-disubstituted 1,2,3-triazoles.[196] The reaction was accomplished in the presence of sodium ascorbate, as reducing agent, and copper (II) sulfate, as catalyst, in a mixture of water and tert-butyl alcohol. This step afforded the 1,4-disubstituted triazoles (**13h-13n**) (**Table 3.6**), in high yields, after stirring overnight at room temperature (**Scheme 3.5.B**).
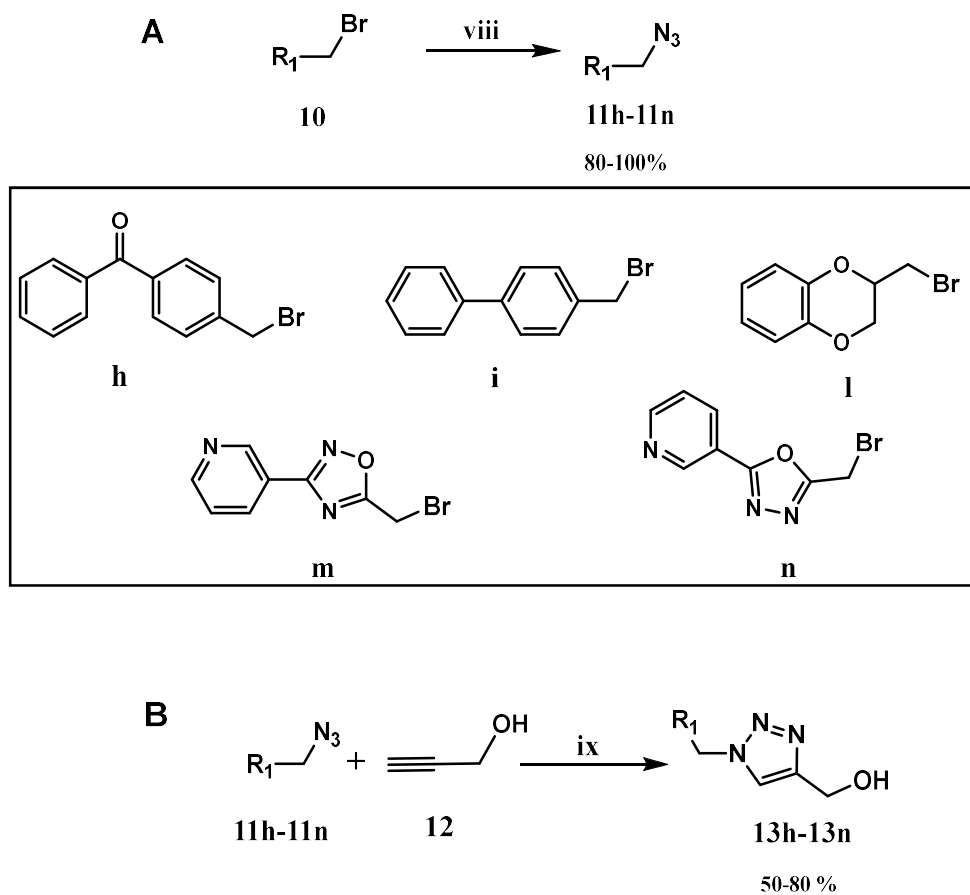
Scheme 3.5. *General procedure for the synthesis of compounds 11h-n and 13h-n*:

Reagents and conditions: viii) NaN₃, H₂O/CH₃COCH₃, reflux, 3h;

ix) CuSO₄·5H₂O, sodium ascorbate, H₂O/TBA, r.t., overnight
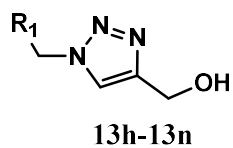
13h-13n

Compound	R₁	Yield (%)
13h		*50*
13i		*72*
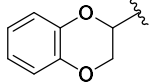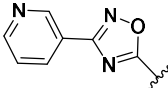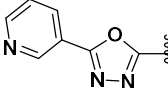
13l		*65.2*
13m		*54*
13n		*70*

Table 3.6 *Chemical structures of compounds 13h-13n*

The last step was the esterification reaction in position -4 of the triazole scaffold (**Scheme 3.7**) that afforded the desired products **SP13-SP20** (**Table 3.6**), in good yields (see also **Scheme 3.2**).
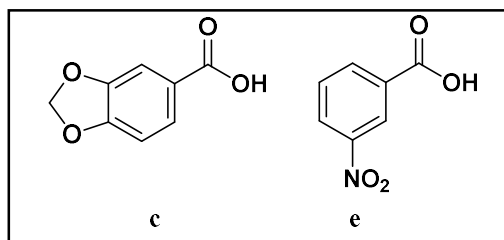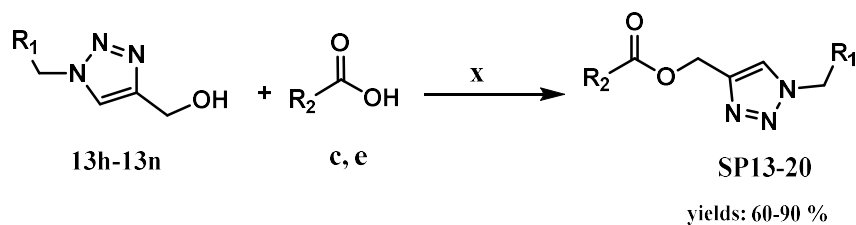
Scheme 3.6. *General procedure for the synthesis of compounds* **SP13-20**:

Reagents and conditions: x) DIC, DMAP, DCM,

room temperature overnight
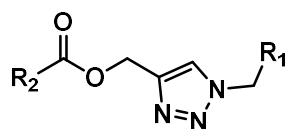
SP13-20

Compound	R_1	R_2	Yield (%)
SP13			*45*
SP14			*40*
SP15			*60*
SP16			*87.2*
SP17			*70.2*
SP18			*82.2*
SP19			*89.1*
SP20			*75.1*

Table 3.7 *Chemical structures of compounds* **SP13-SP20**

Biological evaluation

All these new synthesized compounds have been tested, similarly to the previous ones, by means of Alpha Screen technology. Compounds **SP13-SP20** have been screened against the same panel of macrodomain proteins, at 12 different concentrations ranging from 0.02 to 50 μM (**Table 3.8**).

Percentage of Inhibition at 50μM

| Compound	LOC221443A	MACROD1A	MACROD2A	PARP14A
SP13	n.d	n.d	n.d	n.d
SP14	n.d	n.d	91.62	58.85
SP15	-11.54	24.08	-3.95	-2.3
SP16	n.d.	n.d.	-5.92	-9.39
SP17	n.d	n.d	99.76	7.05
SP18	n.d	n.d	99.49	-0.37
SP19	n.d	n.d	99.61	0.81
SP20	n.d	n.d	84.46	60.26

Table 3.8 *Percentages of inhibition against a panel of Macrodomain proteins, calculated for compounds **SP13-SP20**, by AlphaScreen technology*

These new results allowed to disclose compounds **SP17-SP20**, with a good percentage of protein inhibition, in the range of 84-99 %, as shown in **Table 3.8**. These compounds showed also a good selectivity against the MacroD2 protein, indeed, no inhibition was detected for the other tested proteins. At this point, for the best compounds the IC$_{50}$ values have been calculated (**Table 3.9**).

IC$_{50}$± SD Values

Compound	LOC221443A	MACROD1A	MACROD2A	PARP14A
SP14	n.d	n.d	73.33 ± 0.03 μM	12.5±2.1
SP17	n.d	n.d	6.16 ± 0.02 μM	n.d
SP18	n.d	n.d	11.99 ± 0.05 μM	n.d
SP19	n.d	n.d	11.22 ± 0.02 μM	n.d
SP20	n.d	n.d	17.1 ± 0.02 μM	40.47 ± 3.2 μM

Table 3.9 *IC$_{50}$ values calculated for compounds **SP14**, **SP17**, **SP18**, **SP19** and **SP20** By AlphaScreen technology, against a panel of Macrodomain proteins*

Compounds **SP17**, **SP18** and **SP19**, which showed the lowest IC$_{50}$ values and the best selectivity, have been subjected, together with **SP2**, disclosed in the previous Alpha Screen assay, to a further binding affinity evaluation.

Basing on these results, in order to better investigate the potential binding to the target protein MacroD2, compounds **SP2**, **SP17, SP18** and **SP19** have been tested, in collaboration with the *Structural Genomics Consortium*, using the Biolayer interferometry technology (BLI). BLI method, based on the optical interferometry principle, is an optical technique that represents a useful tool for measuring macromolecular interactions, by analyzing interference patterns of white light reflected from the surface of a biosensor tip. BLI experiments are used to determine the kinetics and the affinity of molecular interactions; in more details, in a BLI experiment one molecule is immobilized to a *Dip* and *Read* Biosensor and the binding to a second molecule is measured. A change in the number of molecules, bound to the end of the biosensor tip, causes a shift in the interference pattern that is measured in real-time (**Figure 3.6.**).
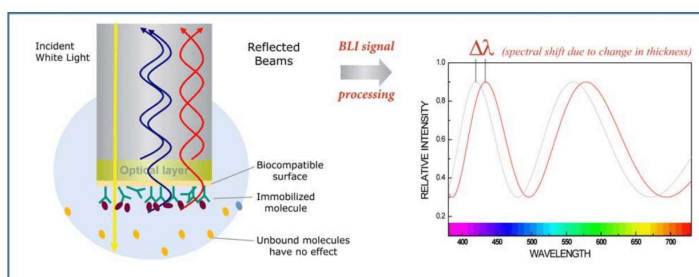

Figure 3.6. *BioLayer Interferometry (BLI) technology assay principle*

The experiment was carried out on MacroD2 protein bound to superstreptavidin (SSA) sensors. Compound **SP2, SP17, SP18** and **SP19** were dissolved at different concentrations, 100μM, 50μM, 25μM, 12.50μM, 6.25μM, 3.12μM, 1.56μM and various solutions of the samples were dispensed in the wells of a black microtiter plate. As shown in the sensorgrams (**Figures 3.7-3.10**), compounds **SP2** and **SP18** showed a good binding affinity against the protein with a measured dissociation constant K_D of 4.2 ± 1.1 μM, for compound **SP2**, and of 14.5 ± 2.8 μM for compound **SP18**, respectively. Unfortunately, for compounds **SP17** and **SP19** a real K_D value was not possible to measure for technical problems. Indeed, these molecules showed to stick on the BLI sensor tips of the instrument, also in the absence of the protein, probably due to an aggregation occurring at higher concentrations or to the presence of nitro groups in both the molecules.
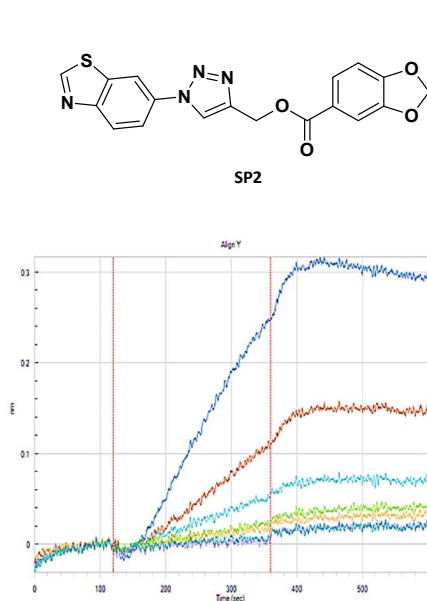
Figure 3.7. *BLI sensorgram acquired for compound* **SP2** *interacting with MacroD2 protein*
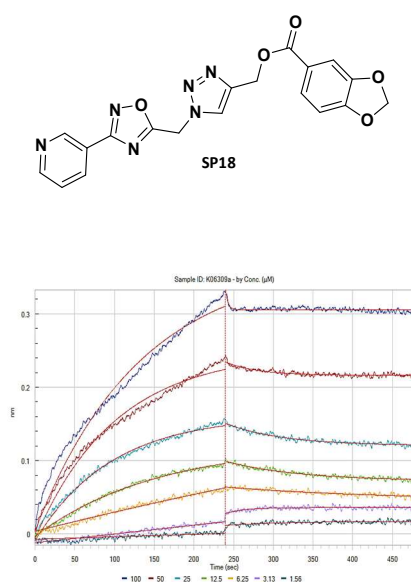
Figure 3.8. *BLI sensorgram acquired for compound* **SP18** *interacting with MacroD2 protein*
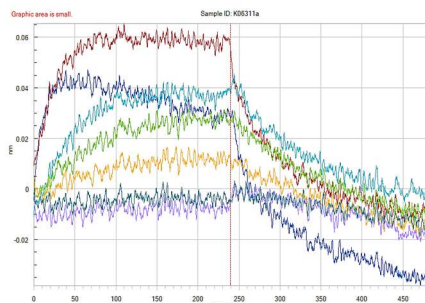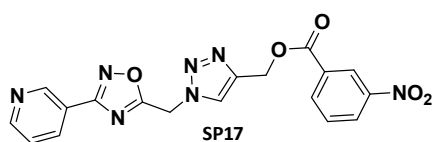
Figure 3.9. *BLI sensorgram acquired for compound **SP17** interacting with MacroD2 protein*
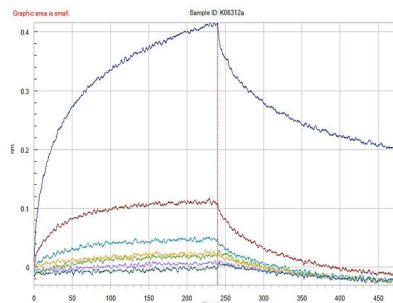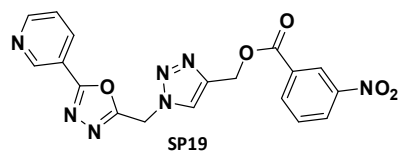
Figure 3.10. *BLI sensorgram acquired for compound **SP19** interacting with MacroD2 protein*

Basing on these new outcomes, we decided to stand on compound **SP2** which showed a good value of IC$_{50}$ (10.58 ± 0.02 μM), in the AlphaScreen experiment, and at the same time, the best value of the dissociation constant in the BLI experiment. In particular, an isothermal titration calorimetry experiment (ITC) was performed to definitely confirm the binding of this molecule to the target protein MacroD2. This label-free method measures the binding between any pair of molecules that release or absorb heat upon binding. ITC technique allows to measure the thermodynamic parameters of biomolecular interactions, including affinity (Ka), enthalpy (ΔH), entropy (ΔS), and stoichiometry (n) (**Figure 3.11**).
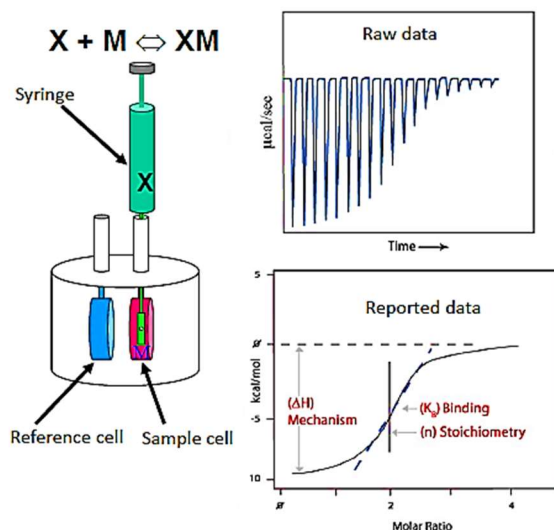
Figure 3.11. *Isothermal titration calorimetry (ITC) assay principle.*

To perform the experiment, the sample cell is filled with the protein and the injection syringe is loaded with the ligand. The syringe is inserted into the sample cell and series of small aliquots of ligand are injected into the sample solution, while stirring. If there is a binding of the ligand to the sample, heat changes of a few millionths of Celsius degree are detected and measured. This method, endowed with a very high accuracy, allows to record protein–ligand complex formation, ranging approximately from low-micromolar to double-digit nanomolar of binders concentration. The experiment was carried out on a MicroCal VP-ITCVP-ITC instrument, titrations were carried out in 50 mM of HEPES pH 7.5, 300 mM NaCl, 0.5 mM TCEP (at 4°C). The protein was in the syringe with a final concentration of 400 µM, whereas compound **SP2** was in the cell in a concentration of 40 µM. The first 2 µL injection was then followed by 27 x 10 µL injections. The resulted curve revealed a binding affinity (**K**) of 3.94×10^5 M^{-1}, a dissociation constant (**K$_D$**) of 2.54± 1.1 µM, an enthalpy (**ΔH**) of binding of 408 cal/mol and a stoichiometry of binding (**N**) of 2.0±0.05 (**Figure 3.12**). Interestingly, the measured dissociation constant in the low micromolar range definitively confirmed, for compound **SP2**, the high binding affinity for MacroD2 protein.

SP2
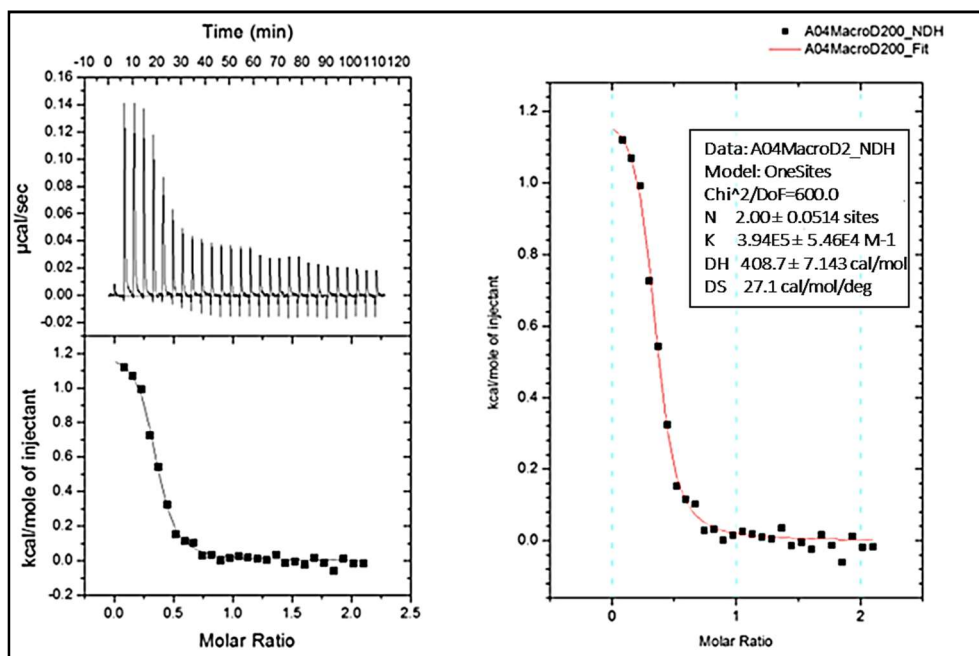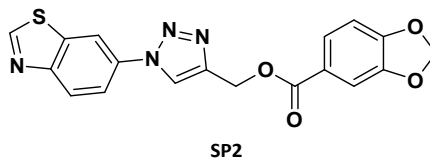
Figure 3.12. *Isothermal titration calorimetry (ITC) experiment*

*performed on compound **SP-2** showing raw injection heats for titrations of protein into compound*

Finally, to gather more information about the binding mode of this very promising molecule, **SP2** was docked on the crystal structure of MacroD2, in complex with the ADP-ribose (PDB code: 4IQY1).[51a] Like other macrodomains, MacroD2 binds ADPr in a deep cleft, but the distal ribose unit, lined by two glycine-rich loops (loop 1, 97-GGGGV-101 and loop 2, 188-GIYG-191), is especially tightly coordinated. Besides forming van der Waals contacts, mediated by Ile189 and Tyr190, this ribose unit establishes hydrogen-bonds with several residues, maintaining an orientation in which the 1″- and 3″-OH groups point toward solvent, while the 2″-OH is shielded, forming hydrogen bonds with Asn92 and Asn102. The 1″-OH is positioned to accommodate mono-ADP-ribosyl-protein substrates (**Figure 3.13A**). In line with our experimental results, **SP2** compound showed to occupy the same region of the ADP-ribose, establishing a similar pattern of H-bonds between the

nitrogens of the triazole scaffold and Ile 189 and Ser186, while the piperonylic moiety is involved in a π-π stacking interaction with Phe 224 and a cation-π interaction with Cyt222. Moreover, the benzothiazole establishes H-bond contacts with Gly99, whereas the methyl-acetate group is involved in several hydrogen bonds with the receptor counterpart, including Tyr187, Val223 and Asp102 (**Figure 3.13B**). The analysis of this set of interactions, by means of molecular docking, allow to rationalize the results obtained from the different biophysical techniques employed. These promising outcomes led us to the identification of compound **SP2**, the most promising of the series, as the first disclosed real binder of MacroD2 protein.
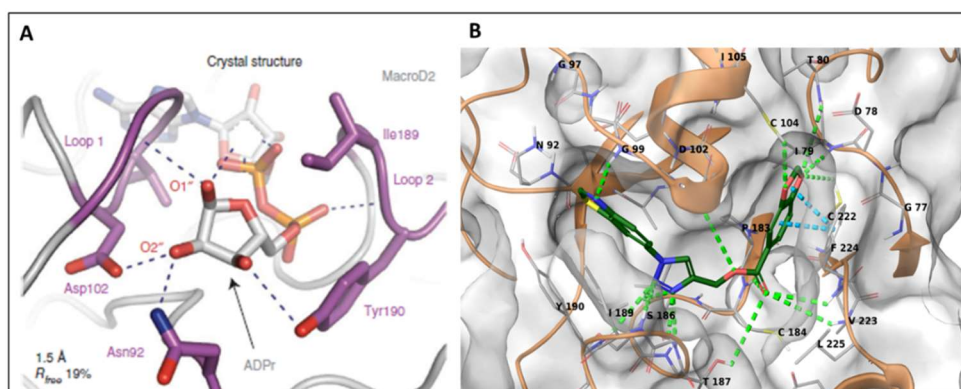
Figure 3.13 *A) Close-up view of the 1.5-Å-resolution X-ray structure of the MacroD2 macrodomain in complex with ADPr (gray), focusing on the distal ribose unit of ADPr. Residues in the vicinity of the distal ribose are shown in stick representation (purple). Hydrogen bonds between protein and ligand are indicated by dashed lines (blue*); **B)** Binding mode of compound **SP2** in the MacroD2 binding pocket; the π-π stacking interactions are indicated as light blue dotted lines, and H-bonds are reported as dotted green lines*

To expand the current project and to be able to assess the potential antitumor activity of this interesting molecule, further biological investigations have been planned, including a cell-viability assay on MCF7, breast cancer cell lines, since these cells have been shown to overexpress MacroD2 protein; this condition has been proved to lead to a worst prognosis of patients and, at the same time, to the induction to Tamoxifen resistance.[2]

- 80 -

CHAPTER 4

Discovery of new modulators of human

Macrodomain protein MacroD1 by a fragment

screening X-ray crystallography based approach

4.1. Targeting MacroD1 protein

Aim of the work

In this section I will deeply describe a new and high-throughput method, the Fragment screening based on X-ray crystallography, which I had the chance to learn and perform during the research period I spent at the *Structural Genomics Consortium (SGC)*, University of Oxford, under the supervision of Dr. Jon Elkins. This approach exploits a great number of crystals of the target protein to soak them with libraries of hundreds of fragments. Libraries containing hundreds of thousands of compounds achieve similar coverage of chemical space as the millions required for traditional high throughput screening (HTS) campaigns. As a result, this method is considerably more affordable as a hit-finding method and has gained a widespread success in both academia and industry. Thanks to this advanced approach, we succeeded to identify a fragment *hit* compound, bound to the protein, which represents our starting point for the design and development of more potent compounds able to bind MacroD1 protein.

4.2. MacroD1 overexpression in E. coli

The expression of MacroD1 protein has been optimized at *SGC* and it was carried out in order to obtain a huge amount of purified protein for the crystallization process. The His$_6$ tagged human MacroD1 (His6-MACROD1A) has been overexpressed in BL21(DE3) competent cells[197], transformed with His$_6$-MACROD1A pNH-TrxTC-terminal His vector, a pET expression vector with His6–Trx (E. coli thioredoxin) in a 128- a.a. N-terminal fusion peptide, with TEV protease cleavage site (**Figure 4.1**).
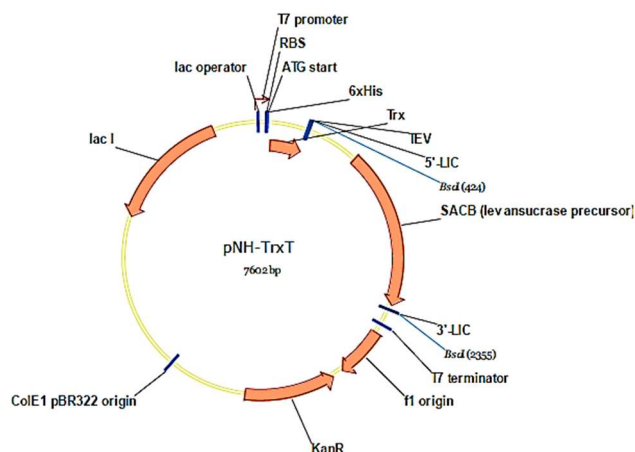
Figure 4.1 *Full Sequence Map for pNH-TrxT expression vector*

BL21-(DE3)-R3-pRARE (a phage-resistant derivative of Rosetta2) competent cells were transformed with the vector, and an initial expression screening was carried out by inoculating a glycerol stock in 10mL starter culture containing Terrific broth (TB) media and growing it overnight at 37°C, then MacroD1 overexpression was scaled-up in 1L TB/Kanamycin inoculated with 3 ml of the starter culture. Cells were grown at 37°C until an appropriate value of optical density was reached (OD_{600}= 0.6-0.8), afterwards temperature was cooled to 18 °C and protein expression was induced with the addition of β-D-1-thiogalactopyranoside (IPTG). Cells continued to grow overnight and were subsequently harvested by centrifugation and lysed by sonication. His_6-MacroD1 protein was purified from the whole cell extract through an immobilized metal ion affinity chromatography on a chelating Sepharose column charged with Ni^{2+}. The supernatant following centrifugation was loaded on the nickel column and all the His_6-MacroD1 was retained on the column, while the unspecifically bound proteins were removed by a wash step of imidazole 60 mM. The pure MacroD1 protein was then eluted by the addition of imidazole 250 mM and, all fractions containing the protein, were then pooled togheter and treated with (*Tobacco Etch Virus nuclear-inclusion-endopeptidase)* TEV protease, for the His-tag cleavage. After an overnight dialysis, fractions were loaded on a Ni-sepharose column and pure protein was then eluted by Gel Filtration buffer; finally the flow -through fraction was purified through a size exclusion chromatography on a Superdex S75 column, and the pure protein

was analyzed by Comassie-staining SDS-PAGE gels (**Figure 4.2a**). A 26,000 kDa purified protein was identified, and its molecular weight was calculated from its electrophoretic mobility relative to standards used for SDS-PAGE gel. The purified protein was identified as MacroD1 by mass spectrometry which revealed a peak at 26535.9, corresponding to the molecular weight of the desired construct (**Figure 4.2 b**). The mass of the protein, following cleavage of the tag by TEV, indicated that the protein was lacking in 25 a.a. downstream of the TEV protease cleavage site, resulting in a fragment encompassing a.a. 82-325 of MacroD1 (**Figure 4.2c**). The obtained yield was of 34 mg/ml of purified protein per 1 liter of expression culture.
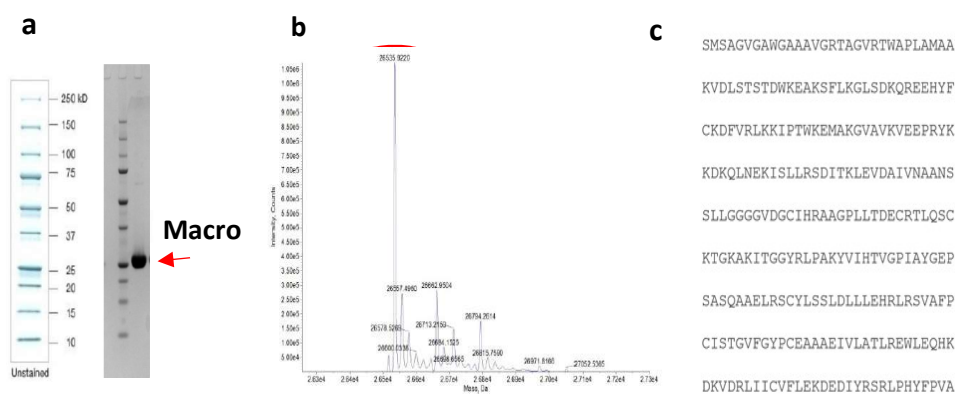
Figure 4.2 a) *SDS-PAGE from large scale purification of MacroD1a.* **b)** *Mass reconstruction of +TOF MS from purified MacroD1a.* **c)** *Protein sequence without TAG*

4.3. MacroD1 protein crystallization

MacroD1 crystals were grown using the sitting drop method; the fresh protein 37 mg/ml in GF buffer was mixed with different ratios of a reservoir solution containing malic acid (DL-) and PEG3350; 96- well sitting drop plates were set up, pipetting 20 μL of the screen into the sitting-drop crystallization plates (SWISSCI 3-drop plates). Then, with the help of the Mosquito robot, (**Figure 4.3a**) the sitting drops were set up with different ratios: 2:1, 1:1, 1:2, with a total drop volume of 150 nL. The plates were sealed and stored in the Minstrel HT UV, an ultraviolet and visible crystal imaging and protein crystal monitoring system, at 4 °C and 20 °C (**Figure 4.3b**).

Crystals appeared overnight from sitting drop plates at 4°C and MacroD1 crystallized in a P212121 space group with typical unit cell dimensions of a=60Å, b=92Å, c=24Å, corresponding to one MacroD1 molecule in the asymmetric unit, with a X-ray diffraction of 2.1 Å (**Figure 4.3b-c**). MacroD1 protein crystallization experiments were repeated several times until one hundred crystals, for each crystallization plate, were approximately obtained.
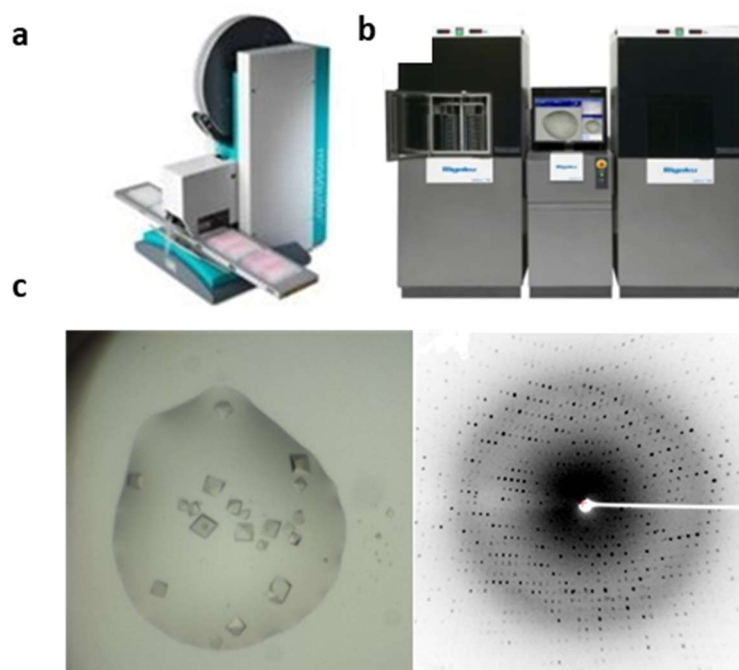
Figure 4.3 a) *TTP Labtech Mosquito liquid handler; Minstrel HT UV imaging system* **b**) *MacroD1a crystals*; **c**) *2.1 Å spots seen in the corner of MACROD1*

4.4. X-ray crystallography based fragment screening on MacroD1 protein

Fragment-based screening is now well-established as a powerful approach to drug discovery. Among the many suitable biophysical techniques, X-ray crystallography was one of the first to be used and is the most directly informative;[198] however, the experimental overheads have historically been too high for it to be widely used for primary screening. At the beamline I04-1 of the Diamond Light Source (Didcot) the full X-ray screening experiment has now been implemented as a highly streamlined process, allowing to screen up to 1000 compounds individually in less

than a week. The process covers soaking, harvesting, automatic data collection and data analysis; the fragment libraries are available, even though the users can bring their own.

The workflow of an ideal experiment is characterized by four steps (**Figure 4.4**) that are iterative and require a few dozen crystals, and in difficult cases even several Lab Visits. The final "Full run" soaking and harvesting will be scheduled once the soaking protocol is confirmed. The data analysis is realized on the existing automatic data processing, and with the help of innovative tools, to streamline density interpretation and refinement (PanDDA and XChemExplorer).
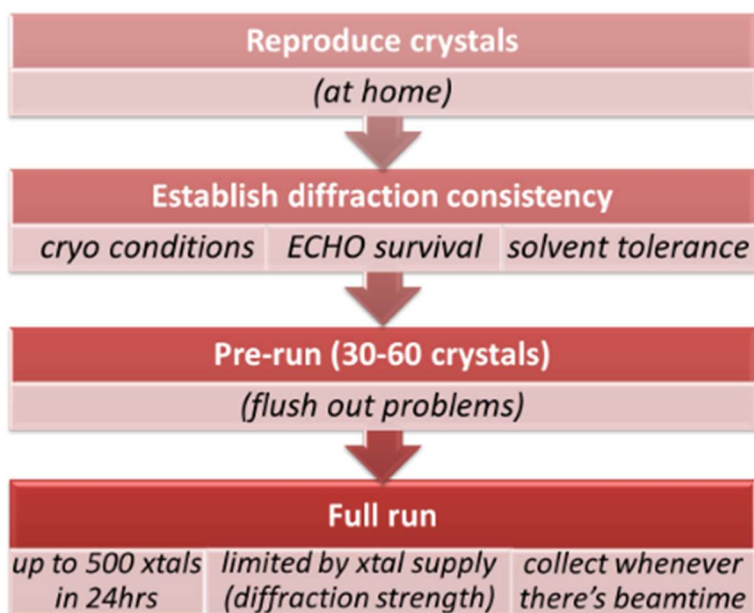
Figure 4.4 *Overview of a fragment screening experiment*

MacroD1 crystallization experiments were repeated several times, until we obtained approximately one hundred crystals for each crystallization plate. The solvent characterization and the crystal soaking were performed through the XChem user program at the synchrotron of the Diamond Light Source. Crystal soaking is the process of taking pre-grown crystals and soaking them with the small molecules of interest. The potential ligand can access the binding sites by diffusing through solvent channels within the crystal lattice, as long as the sites are not involved in crystal packing or otherwise obscured.[199] A common obstacle is the low

solubility of many compounds in aqueous solutions, requiring organic solvents such as dimethylsulfoxide (DMSO) for solubilization[199], which, however, alter the chemistry of the crystal drop and tend to affect the integrity of the crystal. Thus, one of the basic challenge of crystal soaking is how to introduce the compound to the crystal without destroying the crystal. Acoustic droplet ejection is a recent liquid-handling approach that relies on ultrasound pulses focused towards the surface of a liquid, thereby ejecting nanolitre or smaller volume droplets.[200] The precision and volume scales of acoustic transfer have enabled new developments in protein crystallography, such as crystal-based fragment screening. Fragment-based methods involve the screening of a protein target against a library of small molecules typically under 300 Da in size. The Echo operates by moving a transducer below the stationary compound-library plate (source plate) and focusing sound pulses at the meniscus of the solution in the requested well, resulting in solvent droplets being ejected upwards (red dots in **Figure 4.5a**). The fixed-frequency sound pulse, from the transducer in the Echo 550, (**Figure 4.5b**) produces a fixed-sized 2.5 nl droplet, and larger transfer volumes, are achieved by dispensing multiple drops of 2.5 nl at a rate of 200 Hz. The inverted sitting-drop crystallization plate (destination plate) is moved above the compound-library plate (origin plate), to position the requested target above the stream of the solvent droplets; the relevant wells need to be uncovered during this process.
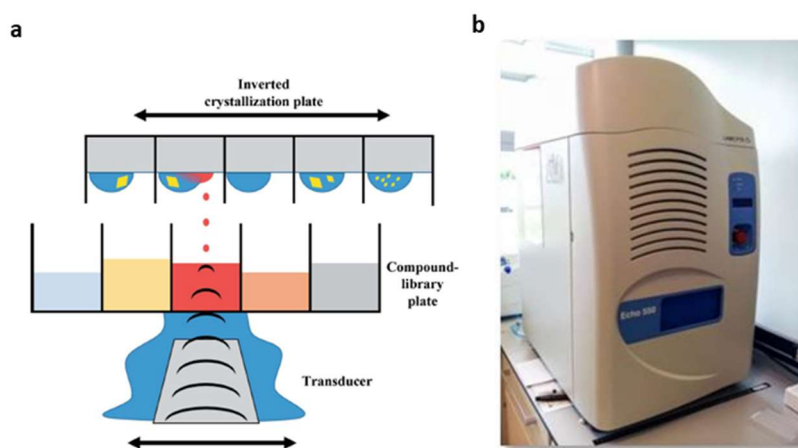

Figure 4.5 *a)* *Schematic representation of acoustic droplet ejection for crystal soaking using the Labcyte Echo;* ***b)*** *ECHO (Labcyte) acoustic liquid handler*

In order to build a list of targeted locations, the crystallization plates were imaged during incubation(Rigaku Minstrel) and the images were analysed with TeXRank.[201] TeXRank is a useful tool to rank drops by the likelihood of containing a crystal, which greatly facilitates drop selection by ranking the most interesting drops at the beginning of the inspection list; additionally, TeXRank identifies the center of each drop, providing the precise physical location of the well to be targeted by the Echo dispensing. The pixel-to-micrometer scale is also calibrated for the plate imager. All the information related to each plate can be easily exported from TeXRank (**Figure 4.6**).
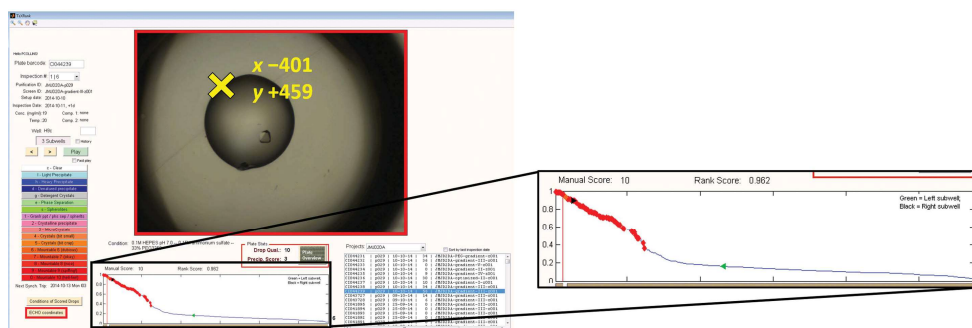
Figure 4.6 *TeXRank interface showing a crystallization drop containing a single protein crystal. Clicking a location, records the acoustic dispensing target for compound-containing solvents. The yellow 'X' and xy coordinates have been added for clarity. The expanded section shows the ranked plot of crystal images.*

To test our crystals tolerance in organic solvents we performed a solvent characterization by soaking, with Echo Liquid Handler, a small amount of MacroD1 protein crystals with different percentages of DMSO and Ethylen glycol (EG) since the fragment libraries we were going to use were dissolved in these solvents. The 52 crystals were soaked for 2 hours with different percentage of DMSO and EG: 0%, 5%, 10%, 15%, 20%, 25%, 30%. Then we mounted them with Shifter, a microscope x-y stage that also handles the unsealing and the resealing processes as well as the automatic samples tracking (**Figure 4.7**); afterwards the crystals were stored in a Robot Dewar in the beamline I04-1 at the Diamond Light Source for the next data collection. The diffraction data, luckily, showed that our crystals survived

quite well after 1 hour soaking in 25% DMSO, with good diffraction resolutions (2-4 Å).

Figure 4.7 *The Shifter: a microscope x-y stage that also handles the unsealing and the resealing as well as the automatically samples tracking*

Concerning the compounds soaking, for the fragments screening, we used the Diamond and SGC Poised Fragment Library 1.0 (DSPL1) composed by a subset of 406 compounds, ensuring diversity, of chemotype and poised classification.[202] The compounds used were dissolved in DMSO at 200 mM concentration and placed in Labcyte 1536-well source plates, the supernatant of compounds, which did not fully dissolve, was used as a saturated solution. The solutions were soaked into protein crystals in crystal buffer in a 1:1 volume ratio to give an approximate final compound concentration of 100 mM. All the 406 fragments in DSPL1 were soaked into MacroD1 crystals and the plates were resealed and incubated for at least 1 hour at 4°C, before the crystals were mounted in nylon loops and immediately flash frozen in liquid nitrogen. In this phase, almost 700 crystals were mounted, which led to the analysis of 276 workable data sets (**Table 4.1**).

All datasets were collected on beamline I04-1 at the Diamond Light Source. Data were integrated and scaled with Xia2[203], which is part of the Diamond Light Source autoprocessing pipeline. Electron-density maps were generated using XChemExplorer[204] via DIMPLE. Ligand restraints were generated with AceDRG

[205] and ligand binding was detected with PanDDA[204], with ligands built into PanDDA event maps. Once a hit was identified, further rounds of refinement and manual model correction was performed using REFMAC[206] and manual rebuilding with Coot[207] were carried out. The quality of the final models was validated with MOLPROBITY.

Mounted Crystal ID	XDS Domain	XDS Resolution (Scaled)	XDS Type	XDS Outcome	Mounted Crystal ID	XDS Domain	XDS Resolution (Scaled)	XDS Type-XDS Outcome	
MACROD1A-x0083		10,42	3dii-runP212121	Success - model created	MACROD1A-x0222		6,57	3d-runP212121	Success - model created
MACROD1A-x0085		14,85	fast_dp	Success - model created	MACROD1A-x0223		9,57	dials-runP212121	Success - model created
MACROD1A-x0086		11	dials-runP212121	Success - model created	MACROD1A-x0226		10,42	dials-runP212121	Success - model created
MACROD1A-x0087		10,69	3dii-run	Success - model created	MACROD1A-x0230		7,16	3d-runP212121	Success - model created
MACROD1A-x0088		8,81	3dii-runP212121	Success - model created	MACROD1A-x0231		5,05	dials-runP212121	Success - model created
MACROD1A-x0089		7,39	autoPROC	Success - model created	MACROD1A-x0233		7,56	3dii-runP212121	Success - model created
MACROD1A-x0092		9,79	3dii-runP212121	Success - model created	MACROD1A-x0234		16,99	3dii-runP212121	Success - model created
MACROD1A-x0095		6,02	autoPROC	Success - model created	MACROD1A-x0235		6,8	3d-run	Success - model created
MACROD1A-x0099		12,38	fast_dp	Success - model created	MACROD1A-x0236		9,62	3dii-runP212121	Success - model created
MACROD1A-x0100		12,57	3d-runP212121	Success - model created	MACROD1A-x0237		6,98	3d-runP212121	Success - model created
MACROD1A-x0102		11,31	3dii-runP212121	Success - model created	MACROD1A-x0239		10,51	dials-run	Success - model created
MACROD1A-x0104		7,51	3d-run	Success - model created	MACROD1A-x0241		8,36	3dii-run	Success - model created
MACROD1A-x0108		9,21	dials-runP212121	Success - model created	MACROD1A-x0243		9,62	3d-runP212121	Success - model created
MACROD1A-x0110		10,51	3dii-runP212121	Success - model created	MACROD1A-x0244		7,71	autoPROC	Success - model created
MACROD1A-x0114		10,1	autoPROC	Success - model created	MACROD1A-x0245		6,98	dials-runP212121	Success - model created
MACROD1A-x0115		8,32	3dii-runP212121	Success - model created	MACROD1A-x0246		11	3dii-runP212121	Success - model created
MACROD1A-x0118		5,68	autoPROC	Success - model created	MACROD1A-x0247		7,56	dials-run	Success - model created
MACROD1A-x0121		6,21	autoPROC	Success - model created	MACROD1A-x0248		14,62	dials-runP212121	Success - model created
MACROD1A-x0122		8,86	3d-run	Success - model created	MACROD1A-x0249		10,02	3dii-runP212121	Success - model created
MACROD1A-x0125		8,94	3dii-runP212121	Success - model created	MACROD1A-x0250		9,3	3d-run	Success - model created
MACROD1A-x0126		8,03	autoPROC	Success - model created	MACROD1A-x0252		8,01	3d-runP212121	Success - model created
MACROD1A-x0127		10,33	3dii-run	Success - model created	MACROD1A-x0254		6,88	autoPROC	Success - model created
MACROD1A-x0130		7,47	3d-runP212121	Success - model created	MACROD1A-x0255		8,36	3d-runP212121	Success - model created
MACROD1A-x0132		7,38	3d-runP212121	Success - model created	MACROD1A-x0257		9,08	3d-run	Success - model created
MACROD1A-x0138		11,78	fast_dp	Success - model created	MACROD1A-x0261		9,39	3dii-runP212121	Success - model created
MACROD1A-x0139		11,18	3dii-runP212121	Success - model created	MACROD1A-x0262		6,89	3d-run	Success - model created
MACROD1A-x0140		7,5	autoPROC	Success - model created	MACROD1A-x0264		7,16	3d-run	Success - model created
MACROD1A-x0143		7,24	3d-run	Success - model created	MACROD1A-x0266		11,09	3dii-runP212121	Success - model created
MACROD1A-x0144		6,53	3d-run	Success - model created	MACROD1A-x0268		7,16	3d-run	Success - model created
MACROD1A-x0145		5,84	autoPROC	Success - model created	MACROD1A-x0269		5,99	3d-run	Success - model created
MACROD1A-x0146		9,48	dials-run	Success - model created	MACROD1A-x0271		9,84	3dii-runP212121	Success - model created
MACROD1A-x0151		10,11	3dii-runP212121	Success - model created	MACROD1A-x0272		8,63	dials-runP212121	Success - model created
MACROD1A-x0154		9,3	dials-run	Success - model created	MACROD1A-x0273		7,96	3dii-runP212121	Success - model created
MACROD1A-x0155		16,73	dials-runP212121	Success - model created	MACROD1A-x0274		9,62	3dii-runP212121	Success - model created
MACROD1A-x0156		5,43	3dii-runP212121	Success - model created	MACROD1A-x0275		6,8	3d-runP212121	Success - model created
MACROD1A-x0160		8,01	dials-run	Success - model created	MACROD1A-x0276		6,75	3d-run	Success - model created
MACROD1A-x0161		9,3	3dii-runP212121	Success - model created	MACROD1A-x0279		6,62	3d-runP212121	Success - model created
MACROD1A-x0164		6,89	3dii-runP212121	Success - model created	MACROD1A-x0280		8,01	3dii-runP212121	Success - model created
MACROD1A-x0165		7,74	dials-runP212121	Success - model created	MACROD1A-x0281		7,38	3dii-run	Success - model created
MACROD1A-x0166		8,94	3dii-runP212121	Success - model created	MACROD1A-x0282		6,13	3d-runP212121	Success - model created
MACROD1A-x0167		8,99	3d-run	Success - model created	MACROD1A-x0283		10,47	3dii-runP212121	Success - model created
MACROD1A-x0168		7,16	3dii-run	Success - model created	MACROD1A-x0284		6,98	3d-run	Success - model created
MACROD1A-x0170		11,28	fast_dp	Success - model created	MACROD1A-x0285		6,98	3dii-run	Success - model created
MACROD1A-x0172		6,27	autoPROC	Success - model created	MACROD1A-x0286		11,94	dials-runP212121	Success - model created
MACROD1A-x0173		14,85	3dii-runP212121	Success - model created	MACROD1A-x0287		8,14	3d-runP212121	Success - model created
MACROD1A-x0175		13,37	3dii-runP212121	Success - model created	MACROD1A-x0288		9,62	dials-runP212121	Success - model created
MACROD1A-x0177		6,26	3d-run	Success - model created	MACROD1A-x0289		7,16	3d-runP212121	Success - model created
MACROD1A-x0178		6,31	3dii-runP212121	Success - model created	MACROD1A-x0290		7,96	3d-run	Success - model created
MACROD1A-x0184		12,88	3dii-runP212121	Success - model created	MACROD1A-x0291		7,47	3d-run	Success - model created
MACROD1A-x0187		5,12	autoPROC	Success - model created	MACROD1A-x0292		6,75	3d-runP212121	Success - model created
MACROD1A-x0188		6,4	3dii-run	Success - model created	MACROD1A-x0295		7,74	3dii-run	Success - model created
MACROD1A-x0190		8,45	3dii-run	Success - model created	MACROD1A-x0297		7,92	3d-run	Success - model created
MACROD1A-x0194		8,14	3dii-run	Success - model created	MACROD1A-x0298		13,46	3d-runP212121	Success - model created
MACROD1A-x0197		14,18	dials-runP212121	Success - model created	MACROD1A-x0299		7,25	3dii-runP212121	Success - model created
MACROD1A-x0204		8,85	dials-run	Success - model created	MACROD1A-x0301		8,45	3dii-runP212121	Success - model created
MACROD1A-x0206		6,4	3dii-runP212121	Success - model created	MACROD1A-x0302		7,65	3dii-run	Success - model created
MACROD1A-x0207		7,92	dials-runP212121	Success - model created	MACROD1A-x0303		6,22	dials-runP212121	Success - model created
MACROD1A-x0209		9,62	3d-runP212121	Success - model created	MACROD1A-x0304		11,25	fast_dp	Success - model created
MACROD1A-x0210		12,82	fast_dp	Success - model created	MACROD1A-x0305		6,62	3d-runP212121	Success - model created
MACROD1A-x0211		7,92	dials-runP212121	Success - model created	MACROD1A-x0306		8,5	3dii-run	Success - model created
MACROD1A-x0213		8,14	fast_dp	Success - model created	MACROD1A-x0307		8,77	3dii-run	Success - model created
MACROD1A-x0214		9,7	3dii-runP212121	Success - model created	MACROD1A-x0308		10,87	3dii-runP212121	Success - model created
MACROD1A-x0215		7,51	dials-run	Success - model created	MACROD1A-x0310		13,24	dials-run	Success - model created
MACROD1A-x0219		**6,75**	**3d-run**	**Success - model created**	MACROD1A-x0312		8,32	3dii-run	Success - model created
MACROD1A-x0221		6,29	autoPROC	Success - model created	MACROD1A-x0314		12,2	fast_dp	Success - model created

Mounted Crystal ID	XDS Domain	XDS Resolution (Scaled)	XDS Type- XDS Outcome	Mounted Crystal ID	XDS Domain	XDS Resolution (Scaled)	XDS Type- XDS Outcome
MACROD1A-x0316	10,15	3dii-runP212121	Success - model created	MACROD1A-x0495	8,86	3dii-runP212121	Success - model created
MACROD1A-x0317	7,74	3dii-runP212121	Success - model created	MACROD1A-x0497	9,26	dials-runP212121	Success - model created
MACROD1A-x0318	12,92	3dii-runP212121	Success - model created	MACROD1A-x0499	13,69	3dii-runP212121	Success - model created
MACROD1A-x0319	11,9	3dii-run	Success - model created	MACROD1A-x0503	11,18	fast_dp	Success - model created
MACROD1A-x0320	14,81	dials-runP212121	Success - model created	MACROD1A-x0505	13,42	dials-run	Success - model created
MACROD1A-x0321	9,48	dials-runP212121	Success - model created	MACROD1A-x0506	11,23	dials-runP212121	Success - model created
MACROD1A-x0322	8,14	3dii-runP212121	Success - model created	MACROD1A-x0508	7,24	3dii-run	Success - model created
MACROD1A-x0324	8,94	3dii-runP212121	Success - model created	MACROD1A-x0512	9,97	3dii-run	Success - model created
MACROD1A-x0326	8,86	dials-run	Success - model created	MACROD1A-x0516	8,41	3dii-runP212121	Success - model created
MACROD1A-x0327	10,38	3dii-runP212121	Success - model created	MACROD1A-x0517	10,29	dials-run	Success - model created
MACROD1A-x0328	11,4	3dii-run	Success - model created	MACROD1A-x0523	6,89	3d-runP212121	Success - model created
MACROD1A-x0329	7,65	3dii-run	Success - model created	MACROD1A-x0524	11	dials-runP212121	Success - model created
MACROD1A-x0335	9,66	dials-runP212121	Success - model created	MACROD1A-x0545	7,94	autoPROC	Success - model created
MACROD1A-x0336	7,24	dials-run	Success - model created	MACROD1A-x0555	12,08	dials-runP212121	Success - model created
MACROD1A-x0337	7,69	3dii-run	Success - model created	MACROD1A-x0560	11,72	3dii-runP212121	Success - model created
MACROD1A-x0338	6,53	3dii-run	Success - model created	MACROD1A-x0561	11,52	fast_dp	Success - model created
MACROD1A-x0339	11,9	dials-runP212121	Success - model created	MACROD1A-x0575	13,78	3dii-runP212121	Success - model created
MACROD1A-x0340	16,32	dials-runP212121	Success - model created	MACROD1A-x0581	9,62	3dii-runP212121	Success - model created
MACROD1A-x0341	15,47	dials-runP212121	Success - model created	MACROD1A-x0582	8,54	3dii-run	Success - model created
MACROD1A-x0343	8,9	3d-runP212121	Success - model created	MACROD1A-x0600	7,07	3dii-runP212121	Success - model created
MACROD1A-x0344	16,82	dials-runP212121	Success - model created	MACROD1A-x0601	5,99	autoPROC	Success - model created
MACROD1A-x0352	7,56	3dii-runP212121	Success - model created	MACROD1A-x0602	7,87	3d-runP212121	Success - model created
MACROD1A-x0353	7,2	autoPROC	Success - model created	MACROD1A-x0604	6,44	3dii-run	Success - model created
MACROD1A-x0357	10,46	dials-run	Success - model created	MACROD1A-x0605	7,69	3d-runP212121	Success - model created
MACROD1A-x0361	7,07	3dii-runP212121	Success - model created	MACROD1A-x0606	5,64	3dii-run	Success - model created
MACROD1A-x0366	7,51	3d-run	Success - model created	MACROD1A-x0608	7,87	3dii-runP212121	Success - model created
MACROD1A-x0369	5,24	autoPROC	Success - model created	MACROD1A-x0609	7,24	3d-run	Success - model created
MACROD1A-x0373	8,5	3dii-run	Success - model created	MACROD1A-x0611	8,54	3dii-runP212121	Success - model created
MACROD1A-x0374	7,02	3dii-run	Success - model created	MACROD1A-x0613	6,93	3d-runP212121	Success - model created
MACROD1A-x0375	11,32	3dii-runP212121	Success - model created	**MACROD1A-x0614**	6,08	dials-runP212121	Success - model created
MACROD1A-x0377	6,98	autoPROC	Success - model created	MACROD1A-x0615	7,87	3dii-runP212121	Success - model created
MACROD1A-x0385	8,5	fast_dp	Success - model created	MACROD1A-x0669	15,34	3dii-runP212121	Success - model created
MACROD1A-x0392	10,5	fast_dp	Success - model created	MACROD1A-x0672	6,04	dials-run	Success - model created
MACROD1A-x0398	9,53	dials-runP212121	Success - model created	MACROD1A-x0673	10,69	dials-runP212121	Success - model created
MACROD1A-x0407	8,05	3dii-run	Success - model created	MACROD1A-x0679	6,17	3dii-runP212121	Success - model created
MACROD1A-x0411	9,75	3d-run	Success - model created	MACROD1A-x0680	16,01	dials-runP212121	Success - model created
MACROD1A-x0418	6,78	autoPROC	Success - model created	MACROD1A-x0681	6,13	3dii-run	Success - model created
MACROD1A-x0424	10,78	3dii-runP212121	Success - model created	MACROD1A-x0682	9,66	3dii-runP212121	Success - model created
MACROD1A-x0426	6,53	3dii-runP212121	Success - model created	MACROD1A-x0683	7,47	3d-run	Success - model created
MACROD1A-x0427	6,44	3dii-runP212121	Success - model created	MACROD1A-x0684	8,32	3dii-runP212121	Success - model created
MACROD1A-x0428	6,53	3d-runP212121	Success - model created	MACROD1A-x0685	5,14	autoPROC	Success - model created
MACROD1A-x0431	6,04	3d-run	Success - model created	MACROD1A-x0686	12,79	3dii-runP212121	Success - model created
MACROD1A-x0432	7,63	autoPROC	Success - model created	MACROD1A-x0687	8,68	3d-run	Success - model created
MACROD1A-x0434	13,33	3dii-runP212121	Success - model created	MACROD1A-x0688	7,47	3d-run	Success - model created
MACROD1A-x0435	6,17	3d-runP212121	Success - model created	MACROD1A-x0691	10,73	3dii-runP212121	Success - model created
MACROD1A-x0437	4,63	autoPROC	Success - model created	MACROD1A-x0692	8,05	3dii-runP212121	Success - model created
MACROD1A-x0438	6,62	3d-run	Success - model created	MACROD1A-x0694	8,68	3dii-run	Success - model created
MACROD1A-x0439	7,65	3dii-runP212121	Success - model created	MACROD1A-x0695	9,3	3d-run	Success - model created
MACROD1A-x0440	6,75	3d-runP212121	Success - model created	MACROD1A-x0696	8,68	3dii-runP212121	Success - model created
MACROD1A-x0444	5,81	autoPROC	Success - model created	MACROD1A-x0697	7,74	3dii-runP212121	Success - model created
MACROD1A-x0456	9,3	dials-runP212121	Success - model created	MACROD1A-x0698	11,63	3dii-runP212121	Success - model created
MACROD1A-x0457	10,56	3dii-runP212121	Success - model created	MACROD1A-x0702	11	dials-run	Success - model created
MACROD1A-x0459	9,17	3d-run	Success - model created	MACROD1A-x0704	5,94	autoPROC	Success - model created
MACROD1A-x0463	12,97	3dii-runP212121	Success - model created	MACROD1A-x0705	6,89	dials-runP212121	Success - model created
MACROD1A-x0469	6,01	autoPROC	Success - model created	MACROD1A-x0706	6,4	3d-runP212121	Success - model created
MACROD1A-x0470	10,42	dials-run	Success - model created	MACROD1A-x0707	7,2	3dii-runP212121	Success - model created
MACROD1A-x0476	16,01	3dii-runP212121	Success - model created	MACROD1A-x0708	8,02	autoPROC	Success - model created
MACROD1A-x0478	13,96	fast_dp	Success - model created	MACROD1A-x0709	5,99	3dii-runP212121	Success - model created
MACROD1A-x0480	7,47	3dii-run	Success - model created	MACROD1A-x0710	9,21	dials-runP212121	Success - model created
MACROD1A-x0483	10,06	3dii-runP212121	Success - model created	MACROD1A-x0712	12,18	autoPROC	Success - model created
MACROD1A-x0484	6,22	3dii-runP212121	Success - model created	MACROD1A-x0713	16,42	3dii-runP212121	Success - model created
MACROD1A-x0486	9,17	3dii-runP212121	Success - model created	MACROD1A-x0714	7,16	3dii-runP212121	Success - model created
MACROD1A-x0487	9,48	dials-runP212121	Success - model created				
MACROD1A-x0488	11,55	fast_dp	Success - model created				
MACROD1A-x0494	10,69	dials-runP212121	Success - model created				

Table 4.1 *Summary of X-ray diffraction data processing statistics for MacroD1 crystals soaked at various DMSO concentrations (final DMSO % (v/v)), after acoustic transfer of solvent.*
In yellow are highlighted the three identified crystals co-crystallized with the fragment hits

After the long refinement process the structures were solved and the crystals **MACROD1A-x0219**, **MACROD1A-x0484**, and **MACROD1A-x0619** were found to be bound to compounds **1**–**3** (1.2% hit rate). In particular, the analysis of the crystal structures showed that one promising fragment, compound **3**, was bound in a macrodomain pocket very proximate to the kinase binding site. In addition, two

other fragments, compounds **1** and **2**, were found bound at the kinase surface but close to crystal contacts of two molecules of the same crystal (**Figure 4.8**).


Compound 1- FMOPL000485a   Compound 2-FMOPL000314a   Compound 3 - FMOPL000074a

FMOPL000485a binding site in x484
(binding site near crystal contact)

FMOPL000314a binding site in x219
(binding site near crystal contact)

FMOPL000074a binding site in x614
(putative allosteric site)
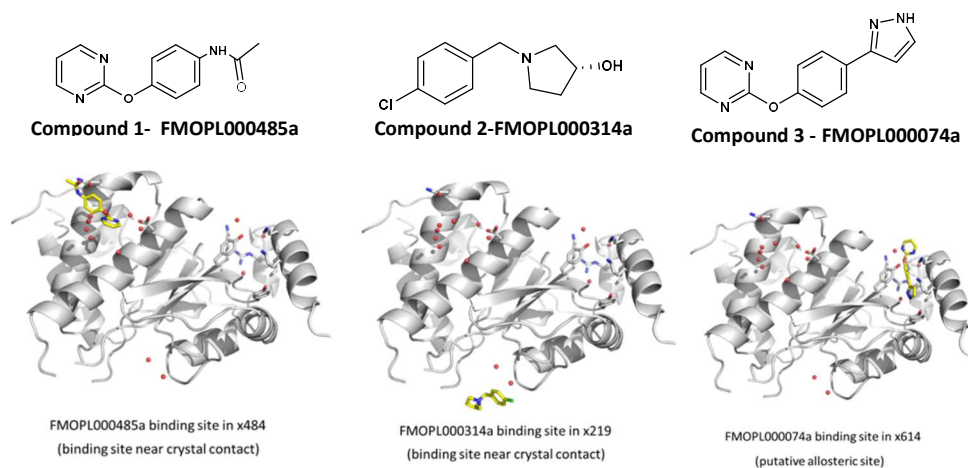
Figure 4.8 *Chemical structures of the fragment hits, co-crystallized in different sites of the target protein MacroD1*

Starting from these promising results, we decided to confirm the binding to the protein by means of Surface Plasmon Resonance (SPR) spectroscopy and Alpha Screen assay.

Biochemical evaluation

SPR has been proven to be one of the most powerful technologies to determine specificity, affinity and kinetic parameters during binding of macromolecules or small compounds.[208] This optical technique measures the refractive index changes in the vicinity of thin metal layers (i.e., gold, silver, or aluminum films) in response to biomolecular interactions. While a sample solution flows across the SPR surface, capturing agents, such as antibodies, enzymes, peptides and DNAs are immobilized on the surface. The changes in the SPR angle, which is the angle of minimum reflectivity, can be determined by varying the incidence angle and recording the reflected light intensity during the biological binding reactions between various biomolecules (**Figure 4.9**).
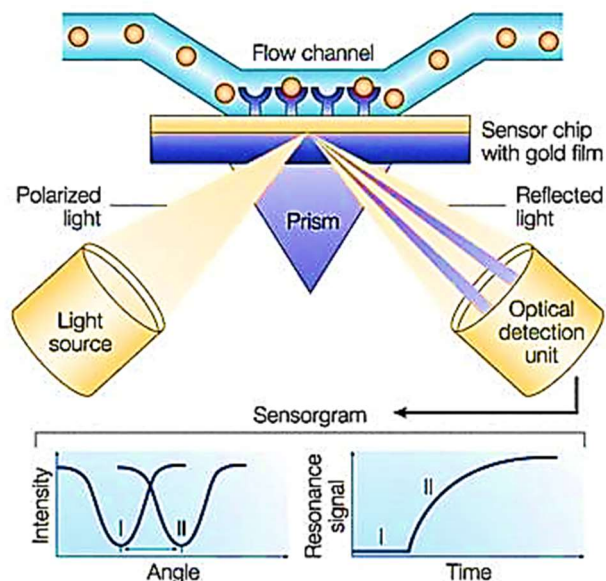
Figure 4.9 *SPR analysis principle*:
the changes in the refractive index in the immediate vicinity of
the surface layer of a sensor chip can be detected by SPR

For the SPR analysis I expressed the biotinylated protein that was then easily immobilized on Streptavidin chips (SA chips), exploiting the strong streptavidin-biotin bond, the strongest known non-covalent interaction between a protein and a ligand (K_D = 10-15M). Indeed, since the basal isoelectric point of the MacroD1 protein is 9.58 and the immobilization on the CM5 chips requires that the protein is dissolved in a buffer with a lower pH, in order to obtain a net positive charge of the protein, we tried to dissolve MacroD1 in different buffers, such as sodium acetate pH 8.5, 7.5, 6.5, 5.5 and 4.5. Unfortunately none of these buffers allowed us to immobilize the protein on the chip and we thought this was due to the protein precipitation in these conditions.

The expression of biotinylated MacroD1 was performed, as previously mentioned. In more details, BL21-(DE3)-R3-pRARE competent cells were transformed with the vector pCDF-BIRA, an expression vector for E.coli biotin ligase (BIR), and an initial expression screening was carried out by inoculating a glycerol stock in 10ml starter culture containing Luria-Bertani (LB) media; the cells were let growing overnight at 37°C. Then Biotinyl-His6-MacroD1 overexpression was scaled-up in

1L of LB/Kanamycin inoculated with 3 ml of the starter culture. Cells were grown at 37°C, until an appropriate value of optical density was reached (OD_{600}= 0.6-0.8), afterwards, temperature was cooled to 18 °C and protein expression was induced with the addition of IPTG; moreover, biotin was added for the BirA cultures. Cells continued to grow overnight and were subsequently harvested by centrifugation and lysed by sonication. Biotinyl-His_6-MacroD1 protein was purified from the whole cell extract by an immobilized metal ion affinity chromatography, on a chelating Sepharose column charged with Ni^{2+}. The supernatant, following centrifugation, was loaded on the nickel column and all the protein was retained on the column; the unspecifically bound proteins were removed by a wash step of imidazole 60 mM. The protein was then eluted by the addition of 250 mM imidazole, and all fractions containing the protein were then pooled together and treated with TEV protease, for the His-tag cleavage. After an overnight dialysis, fractions were loaded on a Ni-sepharose column and pure protein was then eluted by Gel Filtration buffer; finally, the flow through fraction was purified by size exclusion chromatography on a Superdex S75 column, and the pure protein was analyzed by Comassie-staining SDS-PAGE gels (**Figure 4.10a**). A 29000 kDa purified protein was identified, and its molecular weight was calculated in electrophoresis in comparison with the standards used for SDS-PAGE gel. The purified protein was identified as Biotinyl-MacroD1 by mass spectrometry which revealed a peak at 29153.6 (**Figure 4.10b**). The yield obtained, was of 36 mg/ml of purified protein per 1 liter of expression culture.
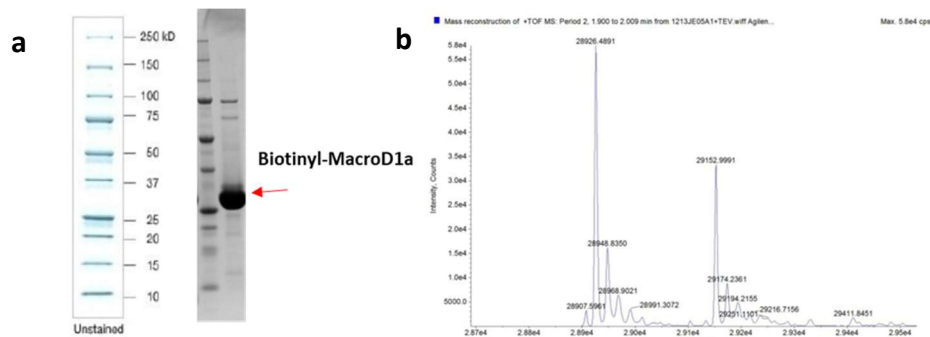

Figure 4.10 a) *SDS-PAGE from large scale purification of Biotinyl-MacroD1; **b)** Mass reconstruction of +TOF MS from purified Biotyinil-MacroD1*

The surface plasmon resonance analysis was performed using a Biacore 3000 optical biosensor equipped with research-grade SA sensor chips. Protein was coupled to the surface of a SA sensor chip using the standard immobilization method. Since fragments are usually of low potency but of high quality, and the nominal concentration reached during the crystallization process was 100 mM, for each molecule five concentrations, including $0 - 0.31 - 0.625 - 1.25 - 2.5$ mM, were set up, and for each sample the complete binding study was performed using triplicate aliquots. On the basis of this preliminary screening, two of the three tested compounds were found to bind, with a dose-response affinity, to the target protein. In particular, for compound **1** a K_D of 0.0116 ± 0.002 mM and for compound **3** a K_D of 0.012 ± 0.0015 mM were detected (**Figure 4.11**), whereas for compound **2**, no binding could be detected; actually these data were perfectly in line with the lower resolution of the related crystal electron-density map found for this compound.

Compound 1   **Compound 3**
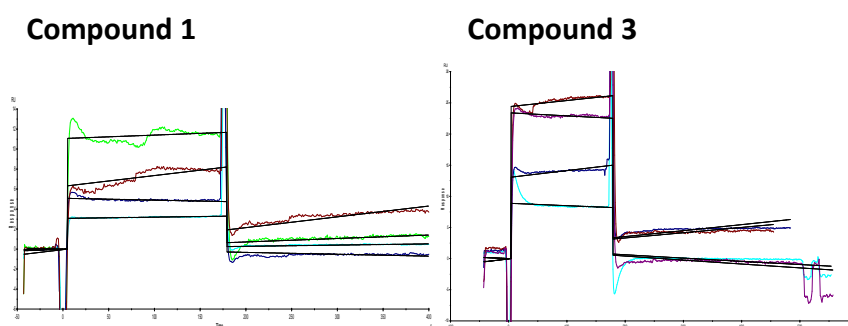
Figure 4.11 *Surface Plasmon resonance sensorgrams acquired for compounds 1 and 3 interacting with Biotinyl-MacroD1*

Basing on these promising results, the AlphaScreen analysis was performed to evaluate the potential inhibition of the two identified compounds of the MacroD1 protein; twelve final compound concentrations were used, with two fold dilutions, spanning from 1000 to 0.25 μM. As result, compound **1**, which showed to bind to MacroD1 surface at crystals contact, showed a 25% inhibition at 500 μM, whereas for compound **3**, found to bind to MacroD1 into a binding pocket near to the natural ligand binding site, no inhibition was measured (**Figure 4.12**). This negative result could be due to two different reasons: the AlphaScreen signal

couldn't be detected or because the compound had a very low target affinity, or because the compound binding did not displace ADP-ribose. However, comparing this data to the SPR measurement, this result is more probably due to the weak binding affinity of the fragment. Concerning compound **1**, even if it seemed to have a better inhibition in the AlphaScreen experiment, the fact that it did not locate in a binding pocket, on the protein, did not allow to define a binding mode profile for this molecule. Basing on these considerations we decided to investigate compound **3** starting from the study of its binding mode in the MacroD1 binding site.

Compound 1
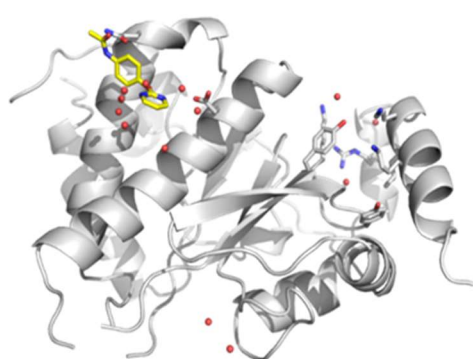
FMOPL000485a binding site in x484
(binding site near crystal contact)
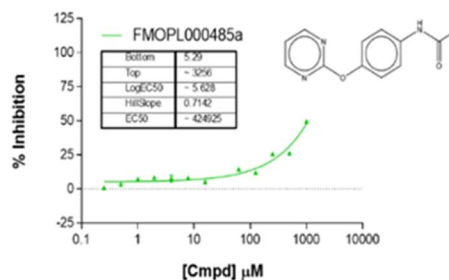
AlphaScreen assay with FMOPL000485a

Compound 3
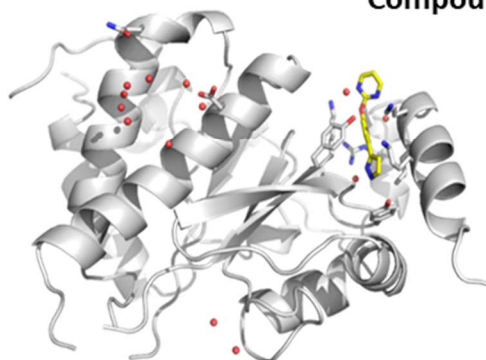
FMOPL000074a binding site in x614
(putative allosteric site)
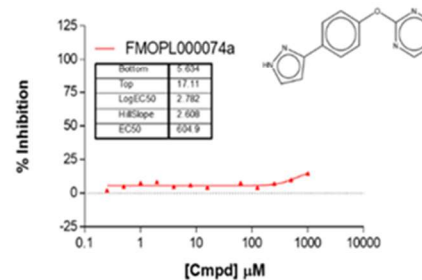
AlphaScreen assay with FMOPL000074a

Figure 4.12 *AlphaScreen curves related to the experiment performed with compound 1 and 3 against MacroD1 protein*

4.5. Compound 3 chemical exploration

Basing on these preliminary results, we decided to analyze the binding mode of compound **3** in order to possibly identify the key amino acidic residues for the interaction. This fragment has also been selected due to the higher resolution of the PDB file related to the crystal obtained (3.2 Å). The in *silico* study was realized through a computational modeling aimed at the optimization of compound **3**. In particular, from the analysis of the PDB file of the protein, co-crystallized with this fragment, a pharmacophore model has been proposed and three main structural requirements have been identified (**Figure 4.13**):

- An H-bond between the nitrogen on the pyrazole ring and the phenolic moiety of the Tyr216.
- A π stacking interactions between the aromatic ring, in position -5 of the pyrazole ring, and the Tyr 222, and cation- π interactions between the aromatic ring with the Arg110.
- An H-bond between the oxygen and the nitrogen of the phenoxy-pirimidine group and the Lys 221.
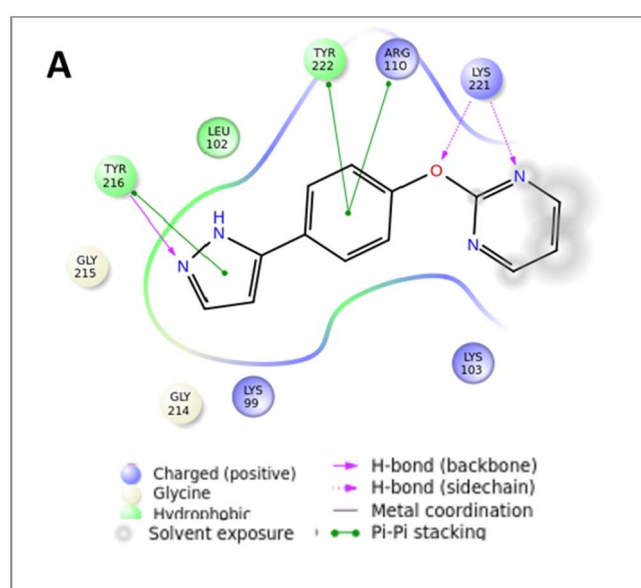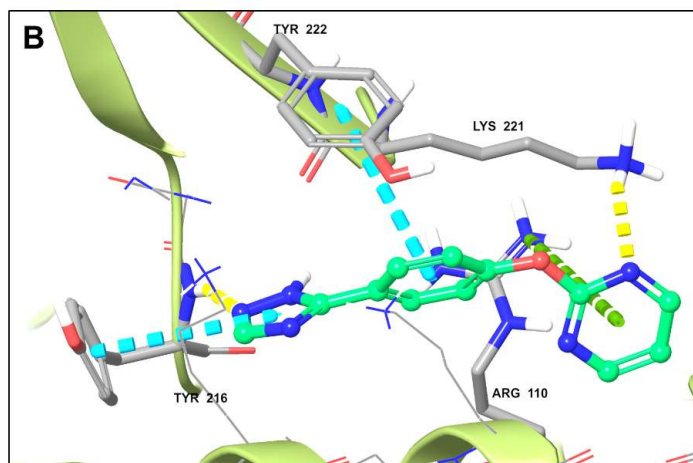
Figure 4.13 (A) *Compound 3 (FMOPL000074a) 2D interaction diagram in the putative allosteric binding site; (B) Compound 3 binding mode: the protein is depicted with green ribbons. The compound is represented with aquamarine tubes. The yellow, green and light blue dotted lines represent the H-bonds, cation-π and π-stacking interactions respectively.*

Keeping in mind these features, a series of derivatives of compound **3** has been designed and tested *in silico*; the binding affinity of the most promising compounds has been predicted by means of molecular docking calculations (**Table 4.2**). In Figure **4.14** the structures of the best molecules are reported.

Entry	Docking score (kcal/mol)
LA-1	-6.899
LA-2	-7.487
LA-3	-7.539
LA-4	-7.487
LA-5	-7.675
LA-6	-7.622
LA-7	-7.370

Table 4.2 *Docking scores values of the in silico selected compounds **LA1-LA7***
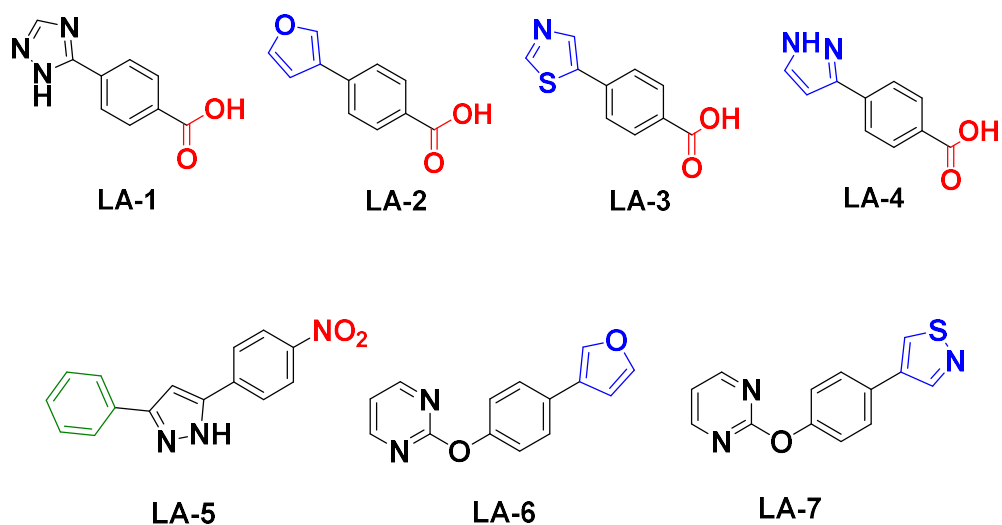
Figure 4.14 *Chemical structures of compounds LA1-7;*
the chemical modifications realized according to the computational studies
are highlighted in red, blue and green colors

The synthesis of compounds **LA1-7** was accomplished under classic heating or under microwave irradiation; in more detail, the synthesis of compounds **LA1-4** was performed starting from the 4-carboxyphenylboronic acid (**1**) reacting with four different heterocyclic bromides (**a-d**), by using Pd(OAc)$_2$ and triphenylphosphine-3,3',3''-trisulfonic acid trisodium salt, as the catalytic system, with Cs$_2$CO$_3$ as base, in a water-acetonitrile reaction solvent. This approach allowed the synthesis of the desired compounds with very short reaction times (5-15 min), and with high yields and purity (**Scheme 4.1**).
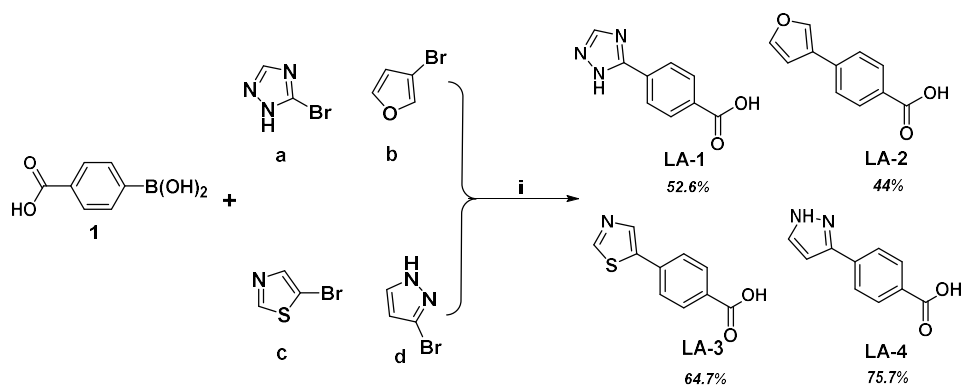
Scheme 4.1. *General procedure for the synthesis of compounds* **LA1-4**:

Reagents and conditions: i) Pd(OAc)$_2$, P(C$_6$H$_4$SO$_3$Na)$_3$, Cs$_2$CO$_3$, H$_2$O/CH$_3$CN, MW,150°,5 min

Concerning the synthesis of compounds **LA5-7** (**Figure 4.14**), compound **LA-5** was synthesized starting from 5-bromo-3-phenyl-1H-pyrazole (**2**) reacting with the the 4-(nitrophenyl)-boronic acid (**3**) by using Pd(OAc)$_2$ and triphenylphosphine-3,3',3''-trisulfonic acid trisodium salt, as the catalytic system, with Cs$_2$CO$_3$ as base, in a water-acetonitrile reaction solvent. This approach allowed the synthesis of the desired compound with very short reaction times (5-15 min), and with high yields and purity (**Scheme 4.2A**). Whereas, compounds **LA6-7** were obtained according to a procedure by Tofi *et al*[209], through the coupling between the 2-(4-bromophenoxy)pyrimidine (**4**) with the furan-3-ylboronic acid (**e**) or the thiazol-4-ylboronic acid (**f**) to obtain the desired compounds (**Scheme 4.2B**). The coupling step, for **LA-5**, was realized as described for the previous compounds whereas, for compounds **LA-6** and **LA-7**, the coupling was performed at 80 °C for 16 h by using tetrakis(triphenylphosphine)palladium(0) as catalyst, sodium carbonate as base and a mixture toluene/water (2:1) as the reaction solvent. All the products were obtained in high yields.
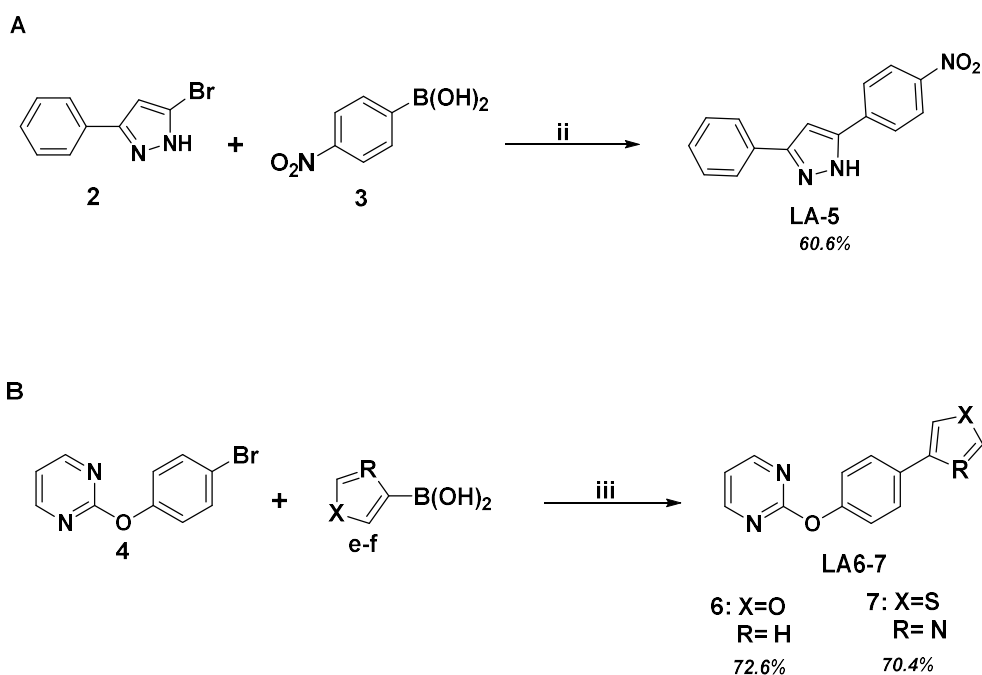
Scheme 4.2. *General procedure for the synthesis of compounds* **LA5-7**:

Reagents and conditions: ii) Pd(OAc)$_2$, P(C$_6$H$_4$SO$_3$Na)$_3$, Cs$_2$CO$_3$, H$_2$O/CH$_3$CN, MW,150°,5 min; iii) Pd(PPh$_3$)$_4$, Na$_2$CO$_3$, H$_2$O/toluene, 80°C,16h

Biochemical evaluation

In order to verify the binding affinity of the new synthesized derivatives of compound **3** all the compounds have been screened by SPR analysis, as previously described for the fragments **1-3**, to assess their potential affinity against the Biotinyl-MacroD1. In this new experiment each molecule was evaluated at five concentrations, 0–6–12–25–and 50 μM. For each sample the complete binding study was performed using triplicate aliquots. The analysis of the sensorgrams curves related to these compounds (**Figure 4.15**) revealed that four of them, in particular compound **LA1-4**, showed a very high binding affinity against the protein with K_D calculated in the low micromolar range and with a dose response profile (**Table 4.3**).
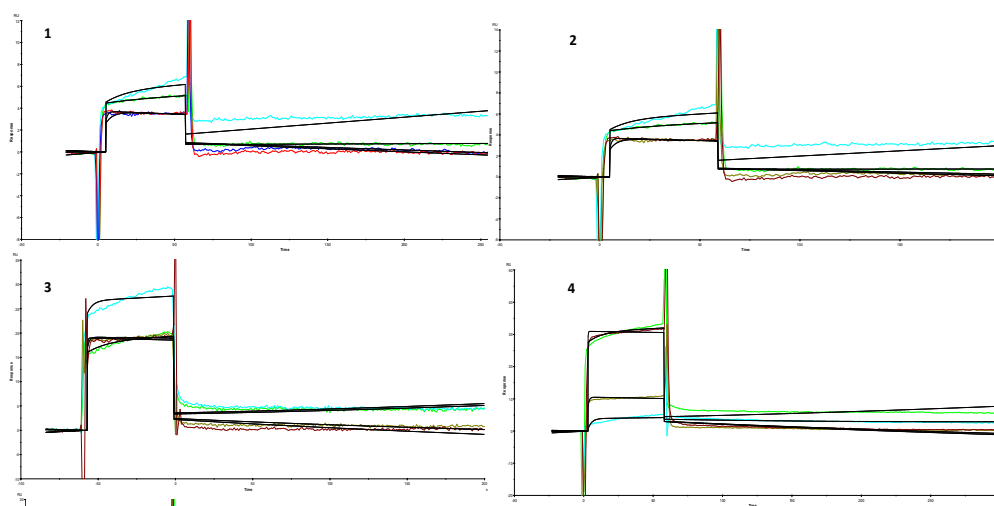
Figure 4.15 *SPR sensorgrams documenting the interaction*

between compounds LA1-4 and MacroD1 protein

Compound	K_D (μM)
LA-1	0.3 ±0.01
LA-2	17 ±0.01
LA-3	1.9 ±0.05
LA-4	1.17 ±0.08
LA-5	N.B.
LA-6	80 ±3.4
LA-7	N.B.

Table 4.3 *Thermodynamic constants measured by SPR for the interaction between the tested compounds and the immobilized MacroD1*

Hence, these preliminary data are in accordance with the computational predicted results showing an increased binding affinity against the target protein. For this reason the selected molecules have been sent to the *SGC* in order to perform additional experiments to confirm the real binding site on the MacroD1 protein and, at the same time, to further explore the potential activity of these molecules as new promising potential modulators of MacroD1 protein.

CHAPTER 5

Design, synthesis and biological evaluation of the first BAG3 modulator as an attractive candidate for the development of a new class of chemotherapeutics

5.1. Targeting BAG3-Hsp70 protein protein interaction

Aim of the work

BAG3 protein is a molecular co-chaperone that regulates many important physiological and pathological cellular processes, including cell survival and apoptosis. Moreover, its overexpression has been demonstrated in many human cancers and, high levels of the protein, have been correlated with the aggressiveness of the tumor type. Although BAG3 biological role has been mostly disclosed, to date, no selective BAG3 modulator has been yet identified. Considering its potential value as a biological tool for future antitumor therapeutics, I decided to embark on the identification of possible BAG3 modulators, focusing in particular on its BAG domain. This project has been carried out exploiting a combined approach of structure-based drug design and biophysical analysis which provided a fast and cost-efficient lead identification. In particular, we succeeded to disclose **LK-4** compound, as the first synthetic BAG3 modulator able to interfere with the BAG3-Hsp70 protein-protein interaction.

5.2. Structure based drug design

With the aim of identifying new chemical platforms able to bind BAG3 protein, as attractive drug candidates, a *structure based drug discovery strategy* has been employed. This research project started from a structure-based Virtual Screening performed on a large library of commercially available compounds from Otava, Ltd. (~ 3.1×10^5 compounds).

BAG3- protein 3D-structure, used for the molecular modeling experiments, was retrieved from the Protein Data Bank (PDB), (PDB code: 4HWF)[92], and refers to AtBAG3 from *Arabidopsis thaliana*. Indeed, even if the human BAG3 protein crystal structure has not been deposited yet, recently, seven BAG protein homologs in the *A. thaliana* genome sequence, have been identified, four of which have domain organization highly similar to their animal counterparts.[91] In particular, two putative binding sites were identified, on the AtBAG3 protein, with the SiteMap

software, that were subsequently used for the molecular docking calculations (Glide software).[189]

The Virtual Screening campaign performed, by using the "Virtual Screening Workflow", has been implemented in Schrodinger Suite, following this scheme (**Figure 5.1**):[189]

- High-Throughput Virtual Screening scoring and sampling (HTVS) (input: $\sim 3.1 \times 10^5$ compounds), saved first 30% of ranked compounds (output: 9.0×10^4 compounds);

- Standard Precision scoring and sampling phase (SP) (input: 9.0×10^4 compounds), saved first 30% of ranked compounds (output: 2.7×10^4 compounds);

- Extra Precision scoring and sampling phase (XP) (input: 2.7×10^4 compounds), saved first 10% of ranked compounds as final output (2.7×10^3 compounds). Furthermore, the obtained compounds were also re-scored using the MMGBSA method.
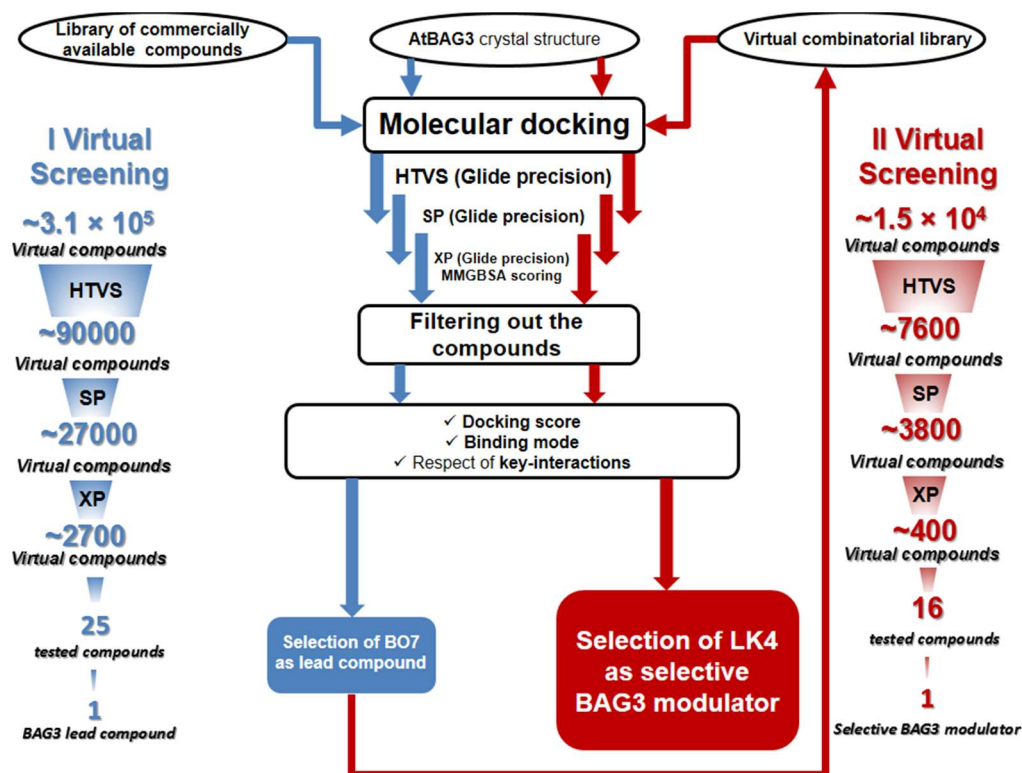
Figure 5.1 *The Virtual Screening workflow for the identification of BAG3 inhibitors*

Once the screening process was completed, the binding mode of the selected compounds was carefully analyzed by selecting docking poses, establishing specific sets of interactions and showing a favorable accommodation in the binding sites after visual inspection. In particular, two different sets of interactions were considered for the two different identified binding sites:

- *Grid A*: residues involved in the binding of BAG proteins with

  HSP70/HSC70:

  Glu176 – Asp186 – Arg198 – Lys199 – Gln206 – Asp213.

- *Grid B*: Lys165 – Glu167 – Glu168 – Asp191 (polar interactions).

In this way, concerning *Grid A*, 56 compounds were filtered out (MMGBSA energetic range: 20 kcal/mol, between -46.648 kcal/mol and -26.018 kcal/mol), whereas, for *Grid B*, only 2 compounds were selected (MMGBSA energetic range:

20 kcal/mol, between -60.414 kcal/mol and -40.000 kcal/mol). The analysis of the predicted *in silico* binding energies (obtained by our Virtual Screening exploration) allowed us to select the 24 top-scoring compounds, featuring an high variability of chemical frameworks; in the same time, other two molecules **25** and **26**, which did not show any significant binding affinity for the target protein, were selected as negative controls (**Figure 5.2**). All these above compounds have been purchased from Otava Chemicals and have been subjected to the post-processing phase in order to verify their ability to physically bind to the target protein.
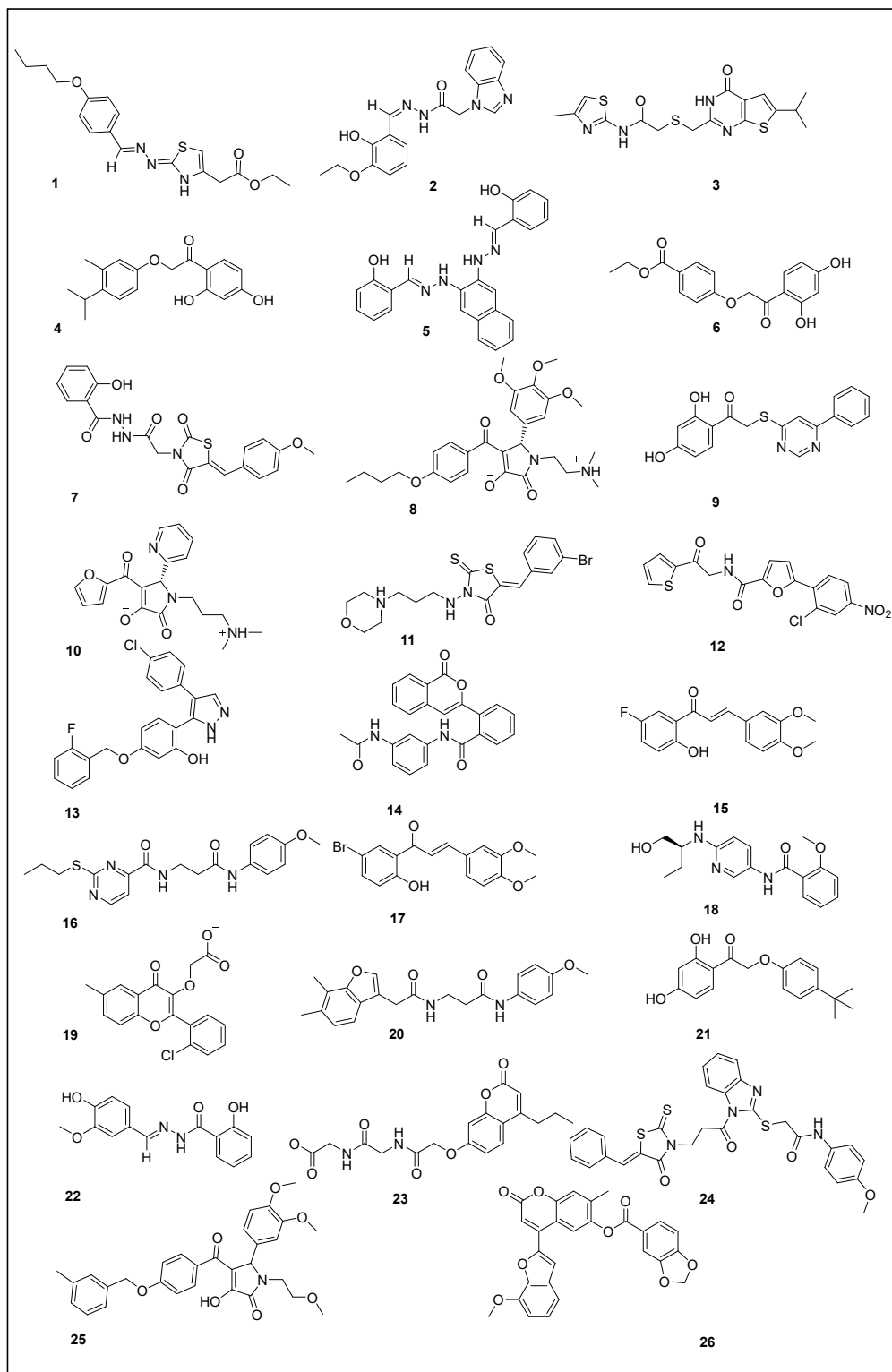
Figure 5.2 *Chemical structures of commercially available compounds 1-26*

5.3. Biological evaluation of the selected compounds 1-26

For this purpose we decided to perform, on the purchased molecules, a Surface Plasmon Resonance (SPR) assay, using a recombinant rBAG3 protein. SPR analyses were performed using a Biacore 3000 optical biosensor equipped with research-grade CM5 sensor chips. Using this platform, a recombinant BAG3 surface, a BSA surface and one unmodified reference surface were prepared for simultaneous analyses. Proteins were immobilized on individual sensor chip surfaces at a flow rate of 5 µL min^{-1}, using standard amine-coupling protocols to obtain densities of 8–12 kRU (**Table 5.1**).

Compound	K_D nM±SD	Compound	K_D nM±SD
1	No Binding	14	No Binding
2	No Binding	15	No Binding
3	No Binding	16	No Binding
4	No Binding	17	No Binding
5	No Binding	18	No Binding
6	No Binding	19	No Binding
7	5.2±3.8	20	No Binding
8	No Binding	21	No Binding
9	No Binding	22	No Binding
10	No Binding	23	No Binding
11	No Binding	24	5.99±0.4
12	No Binding	25	38.0 ±4.6
13	No Binding	26	19.8 ±1.49

Table 5.1 *SPR assays of compounds (1-26) on rBAG3 protein full length*

Based on this assay, two compounds (**7** and **24**) have been identified as high affinity leads for the target protein with very low K_D values (compound **7** K_D**:** 5.2±3.8 nM, and compound **24** K_D**:** 5.99±0.4 nM, respectively) while compounds **25** and **26**,

showed a lower ligand affinity (compound **25** K_D**:** 38.0 ±4.6 nM and compound **26** K_D**:** 19.8 ±1.49 nM). Basing on the obtained results, we focused our attention on compounds **7**, **24**, **25**, and **26**. In order to explore the potential selectivity of these molecules, we performed a further SPR analysis on other members of BAG family, in particular, we selected both BAG4, as the most closely BAG3 related among human BDs, and BAG1 which contains a structurally and evolutionarily distinct BD. Moreover, since as stated before the target protein contains several functional additional domains, in order to gather more information about the binding site of our molecules, we decided also to test their ability to bind the isolated BAG3 domain (BAG3BD) (**Table 5.2**).

Compound	BAG3 (full- length) K_D (nM) ±SD	BAG4 (full- length) K_D (nM) ± SD	BAG1 (full- length) K_D (nM) ± SD	BAG3 domain (BAG3BD) K_D (nM) ± SD
7	5.2±3.8	3240±90	No Binding	3.51±2.7
24	5.99±0.4	No Binding	No Binding	287.0±13.2
25	38.0 ±4.6	No Binding	No Binding	No Binding
26	19.8 ±1.5	No Binding	No Binding	No Binding

Table 5.2 *SPR assays of compounds (**7**, **24**, **25** and **26**) on BAG3, BAG4,*

BAG1 proteins and on BAG3 domain

The SPR analysis showed the best results for compounds **7** and **24**, indeed they displayed a high binding affinity for the isolated BAG3BD, without any binding for the other two BAG protein isoforms tested. Concerning compounds **25** and **26**, SPR analysis allowed to rule them out**,** indeed, they did not show to bind BAG3 domain, as expected; taking together these results enabled to disclose two interesting molecules, **7** and **24** that, actually, showed a relevant binding affinity for the BAG3 domain that has been established to be involved in key biological functions, including the interaction with the molecular chaperone Hsp70 (**Table 5.2**, see column IV); moreover, the identified compounds, showed a good selectivity for the protein of interest (**Table 5.2**, see column III, IV).

At this point we decided to perform, on the disclosed molecules, a preliminary cytotoxic assay in order to verify the agreement between virtual screening results, SPR binding analysis and biological outcomes. Since BAG3 protein has been reported to be overexpressed in melanoma cells (A375) and its down-modulation, mediated by specific small RNA interfering, showed to reduce M14 tumor growth in vivo by suppressing its anti-apoptotic activity[153], we verified the antiproliferative effect of the most promising compounds on this kind of cells. The cell viability assay, performed on human melanoma cancer cell line (A375), showed that compound **7** was the most active one, with an IC_{50} value of 25±1.5 μM. While, compound **24** with an IC_{50} of 41.6±1.9 μM, was less active (probably due either to its limited solubility, or, to its lower binding affinity to BAG3 domain, as reported in Table 5.2). Compounds **25** and **26**, tested as negative controls, were totally inactive in the same antiproliferative experiment, according to our *in silico* predictions. Having disclosed this interesting hit, compound **7** was chosen for further investigations in order to define in more details its structural interaction with the molecular target.

In particular, with the aim of identifying in more detail the BAG3 region involved in the binding with compound **7**, a limited proteolysis mass spectrometry based experiment was used for the structural analysis of the BAG3/ compound **7** complex. The efficiency of this approach relies on the evidence that the exposed, weakly structured and flexible regions of a target protein can be recognized by a proteolytic enzyme and, therefore, the observed differences in the proteolytic patterns, in the presence or in the absence of a putative protein ligand, can be useful to identify the protein regions involved in the molecular interactions.[210]

Limited proteolysis experiments were performed both on BAG3 and on BAG3/ compound **7** complex. The proteolytic patterns obtained both, on BAG3 and on BAG3/ compound **7** complex, using trypsin or chymotrypsin as proteolytic agents, identified on the basis of MALDI analysis of the respective digestion mixtures, are summarized in **Figure 5.3**. A comparison of the results achieved in these experiments suggests a direct interaction between **7** and the BAG3 domain of the protein. Indeed, it was observed that amino-acidic residues Arg331, Arg380,

Lys425, Lys455, Lys483 and Lys534 were protected from the enzymatic hydrolysis, in the complex BAG3/ compound **7**. Conversely, the new preferential cleavage sites of the BAG3/ compound **7** complex, located at the level of Lys97, Arg176, Lys284, Arg304 and Arg346 amino-acidic residues, became susceptible to enzymatic hydrolysis.

Hence, these data suggest that, the binding of compound **7** to BAG3 protein, induced significant conformational changes of its three-dimensional structure. Specifically, the protection from proteolysis, of the PXXP and BAG domains of BAG3 indicated that these are the protein domains mainly involved in interaction with the tested compound.[211 -212]
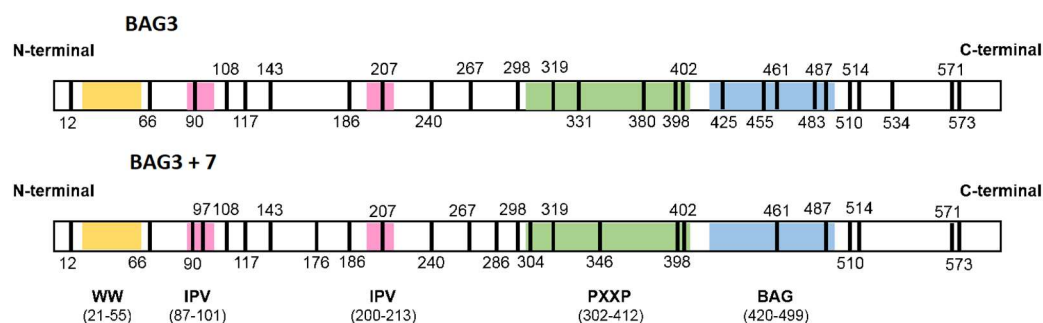
Figure 5.3 *Schematic representation of limited proteolysis experiments. The preferential cleavage sites detected on recombinant BAG3 and BAG3/7 complex are indicated in black. The WW domain is highlighted in yellow, the IPV domains are highlighted in pink, the PXXP domain in highlighted in grey and the BAG domain is highlighted in light blue*

Basing on these encouraging results, and considering the synthetic tractability of the disclosed hit, we selected compound **7** (**Figure 5.4**) as the parent molecule to expand the chemical diversity around the 2,4-thiazolidinedione scaffold and to generate a small collection of synthetic compounds which, if possible, could retain and even increase the biological profile of the identified *lead*.
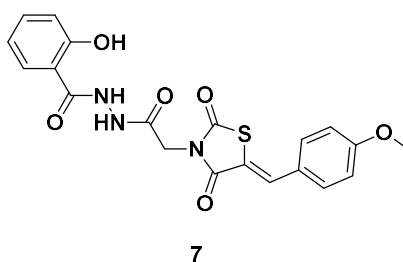
Figure 5.4 *Chemical structure of compound 7 identified as lead*

In this aim a CombiGlide virtual screening approach was used in order to generate, starting from the 2,4-thiazolidindione core of the parent molecule, a collection of structurally related compounds. The CombiGlide software, based on an accurate ligand-receptor scoring and coupled with intelligent and efficient combinatorial docking and core-hopping methods, can accelerate the lead optimization process and aid in designing the optimal focused compound library. In more details, Schrödinger's CombiGlide can flexibly vary the core or side-chain substitutions, creating virtual combinatorial libraries that may be screened for identifying novel scaffolds, or generate focused collections in support of lead optimization efforts. According to the chemical route we built *in silico* a new set of screening compounds featuring the 2,4-thiazolidindione chemical core and differently substituted in 3 and 5 positions basing on the related commercially available synthons (~2.3 × 104 items). The **23331** molecules built (considering all stereoisomers, tautomers and protonation states) were screened, with Glide HTVS, SP, and XP precision modes filters, as described above for the first virtual screening. From this *in silico* analysis, the **17** top scoring molecules have been selected (filters: predicted binding energy, observance of the key-interactions) for the chemical synthesis and biological evaluation (**Figure 5.5**).
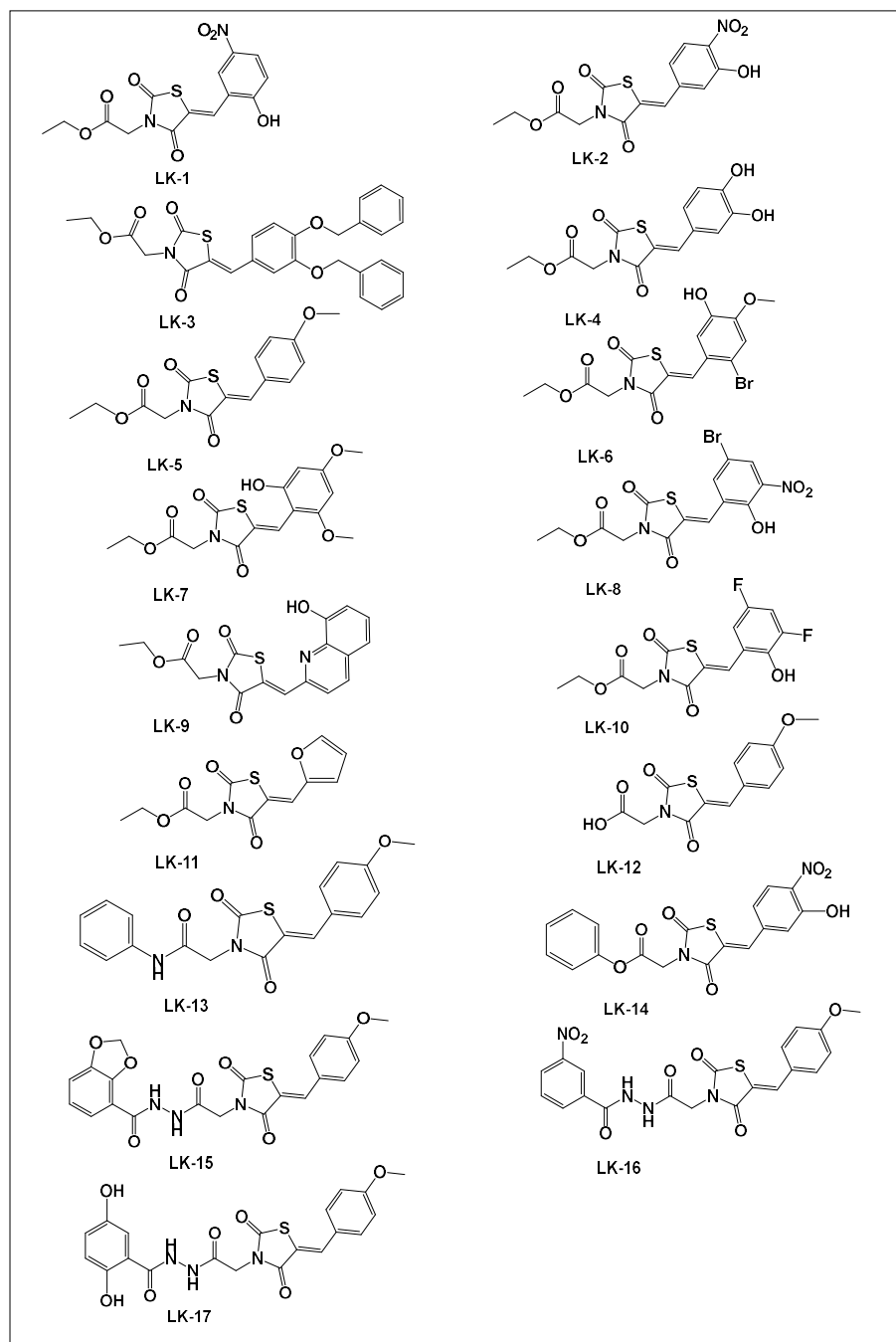
Figure 5.5 *Chemical structures of the compounds selected by virtual screening*

5.4. Synthesis of compounds LK1-LK17

The synthesis of the selected compounds, starting from a stereoselective Knoevenagel condensation between the commercially available 2,4-thiazolidindione **1** with different aromatic aldehydes (**a-m**), chosen in accordance

with the docking results, in basic conditions for piperidine, under refluxing ethanol, allowed us to obtain the (Z)-5-arylidene-2,4-thiazolidinediones **2a-m** in high yields (**Scheme 5.1A**). The structure of compounds was assigned on the basis of ^{1}H and ^{13}C NMR data, in particular the *Z* configuration of the exocyclic double bond was determined basing on the comparison of our spectral data with those reported for other (Z)-5-arylidene-2,4-thiazolidinediones reported in literature.[213] The treatment of **2a-m** with ethyl bromoacetate, in presence of NaH and THF dry as solvent, provided the desired compounds **LK1-LK11** (**Scheme 5.1B**). Moreover, the reaction of **2d** and **2m** with bromoacetic acid afforded the intermediate **3d** and compound **LK-12** (**Scheme 5.1B**). In order to obtain compound **LK-13**, **LK-12** was further coupled with phenylamine, whereas compound **3d** was esterified with phenol, affording compound **LK-14**; both the reactions were performed in presence of hydroxybenzotriazole (HOBt) and *N,N* diisopropylcarbodiimide (DIC) as coupling agents (**Scheme 5.2A**). Concerning the synthesis of compounds **LK15-17**, the most structurally related to the parent molecule **7**, they have been obtained starting from **LK-12**. In particular, **LK-12** was coupled with hydrazine-hydrate to afford the compound ((Z)-2-(5-(4-methoxybenzylidene)-2,4-dioxothiazolidin-3-yl)acetohydrazide) **4m**. Then, the treatment of **4m** with three different aromatic carboxylic acids (piperonylic acid, 2,4-dihydroxybenzoic acid and 3-nitrobenzoic acid respectively) afforded the desired products **LK15**, **LK16** and **LK-17** (**Scheme 5.2B**).
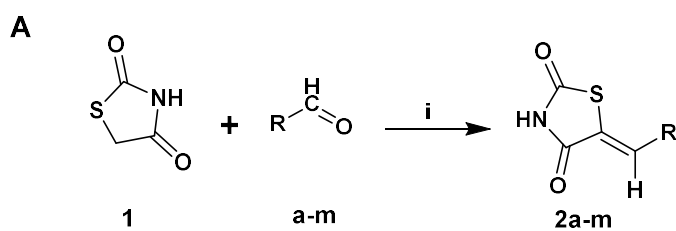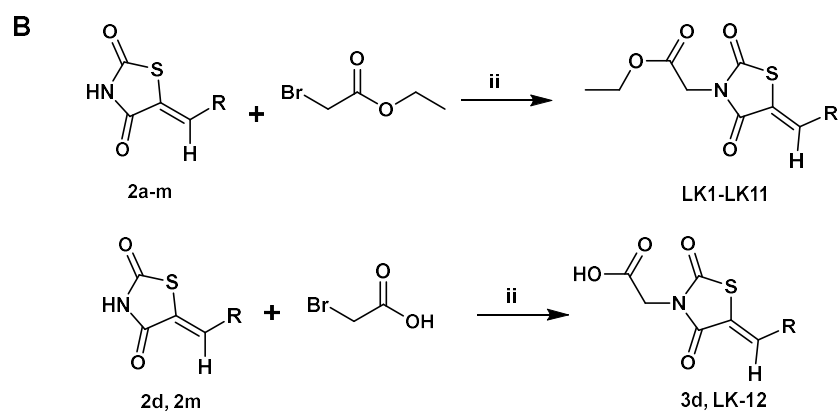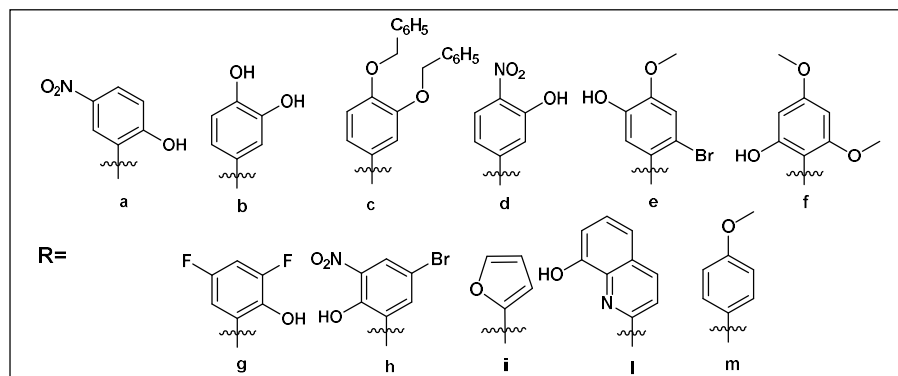
Scheme 5.1. *General procedure for the synthesis of compounds **LK1-LK12**, **3d** and **3m**;*

***Reagents and conditions**: (A) i) Pyperidine, EtOH, reflux, 16-24 h;*

(B) ii) NaH, THF dry. 0 °C, then reflux, 3h
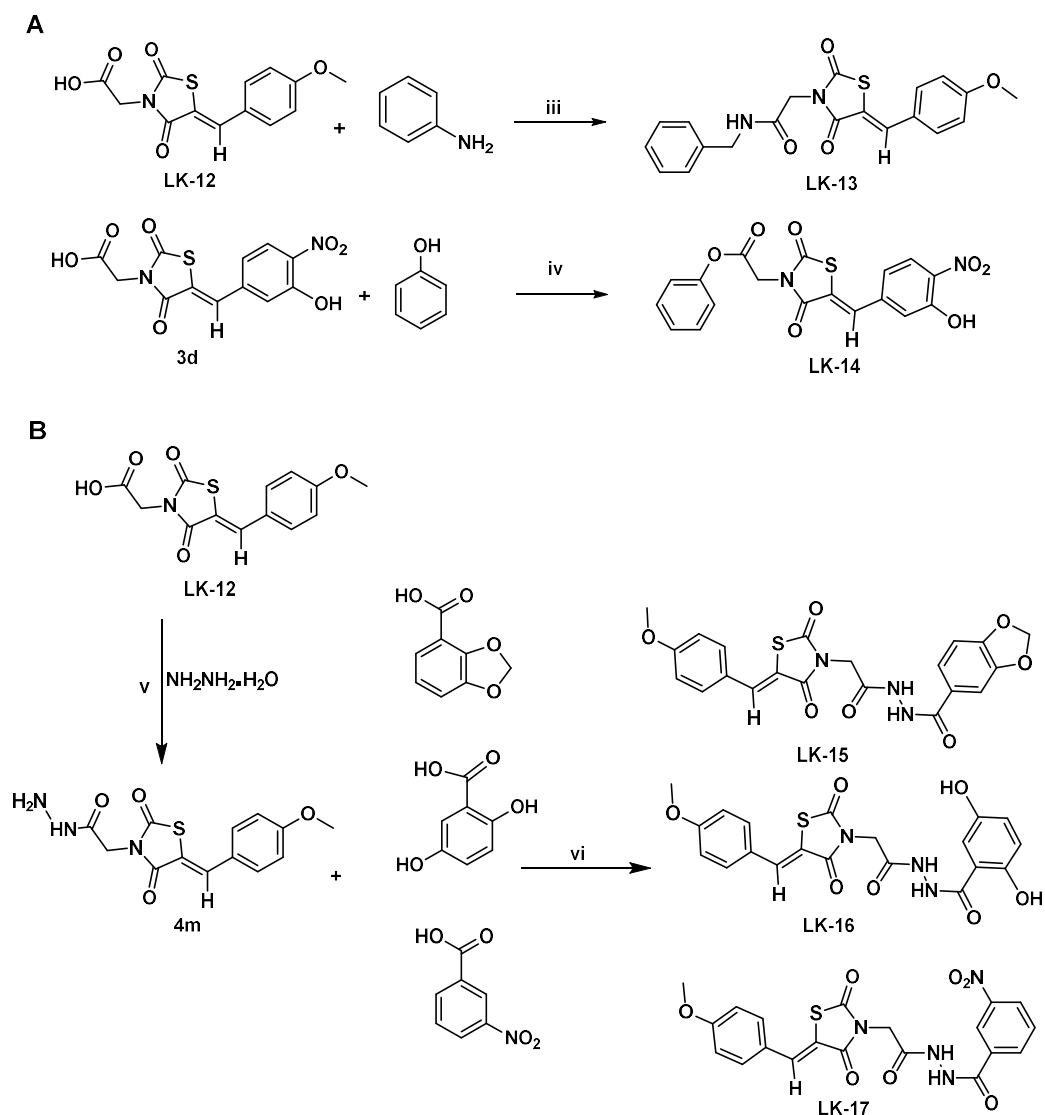
Scheme 5.2. *General procedure for the synthesis of compounds **LK13-17**;*

***Reagents and conditions**: (A) iii) HOBt, DIC, DCM, rt, overnight;*

iv) DMAP, DIC, DCM, rt, overnight;

***(B)** v) HOBt, DIC, DCM, rt, overnight; vi) HOBt, DIC, DMF, rt, overnight*

5.5. Biological evaluation

All the synthetized molecules have been subjected to the same screening procedure used for the previous compound disclosed by virtual screening exploration, in order to verify their binding affinity for the full-length protein, the affinity for the isolated BAG domain and finally their potential cytotoxic effects (**Table 5.3**).

Entry	BAG3 (full- length) K_D (nM) ±SD	BAG3 domain (BAG3BD) K_D (nM) ±SD	Entry	BAG3 (full- length) K_D (nM) ±SD	BAG3 domain (BAG3BD) K_D (nM) ±SD
LK-1	No Binding	_	LK-10	No Binding	_
LK-2	27.5±8.8	No Binding	LK-11	No Binding	
LK-3	6.0 ±2.9	13.5±1.1	LK-12	14.0±2.6	8.2± 1.1
LK-4	11.1±3.9	6.4±2.2	LK-13	7.2±4.7	9.8±4.4
LK-5	No Binding	_	LK-14	30.2 ±9.8	No Binding
LK-6	No Binding	_	LK-15	No Binding	_
LK-7	179.0 ±10.4	No Binding	LK-16	10.8 ±2.2	34.2 ±12.3
LK-8	42.5 ±3.2	43.3 ±4.0	LK-17	32.8 ±6.1	67.6 ±11.3
LK-9	200.0 ±21.7	No Binding			

Table 5.3 *SPR assays results of compounds (**LK1-LK17**) on BAG3 full protein and BAG3 domain*

Following this approach we found that, among compounds **LK15-17**, showing an high level of structural similarity with the parent molecule **7**, **LK-16** and **LK-17** were able to bind in SPR analysis both the full protein and the isolated BAG3BD, while **LK-15** did not show any affinity for the target protein (**Table 5.3**). Concerning the other molecules, nine of them, (**LK-2, LK-3,LK4, LK-7, LK-8, LK-9, LK-12, LK-13, LK-14**) were able to bind the full length protein, however among these compounds only **LK-3**, **LK-4**, **LK-8**, **LK-12** and **LK-13** showed to efficiently interact with the BAG3BD (**Table 5.3**). These last molecules, together with **LK-16** and **LK-17**, have been finally subjected to biological evaluation in order to assess their antiproliferative potency. In more detail, all compounds have been tested on A375 cells by a MTT cell viability assay, using different concentrations (5-50 μM), and the IC_{50} have been calculated after 72 hours of treatment (**Table 5.4**).

Compound	IC$_{50}$ ± SD (μM) 72h
LK-3	>50
LK-4	16.0 ± 1.5
LK-8	>50
LK-12	NA
LK-13	NA
LK-16	50 ± 2.0
LK-17	NA

Table 5.4 *IC$_{50}$ values of the antiproliferative activity of compounds **LK-3, LK-4, LK-8, LK-12, LK-13, LK-16** and **LK-17** on A375 cancer cell lines after 72 h treatment*

The obtained results allowed to disclose compound **LK-4**, endowed with a relevant cytotoxic activity (IC$_{50}$: 16.0 ±1.5μM), as the most attractive candidate for a further biological evaluation (**Table 5.4**). For this reason, we decided to evaluate the cytotoxic activity of this promising compound on a small panel of cancer cell lines: pancreatic carcinoma (Panc-1), breast cancer (MCF7), prostate cancer (PC3) and lung cancer cells (A549), that are known to be able to overexpress BAG3 protein.[214] Moreover, compound **LK-4** was tested, at the same conditions, also on PHA-stimulated proliferating non-tumor human cell line (PBMC). The analysis of the results showed that **LK-4** displays an anti-proliferative activity in all the tested cancer cell lines (**Table 5.5**), even though it resulted to be less active compared to the results obtained on A375 cells. Moreover, no cytotoxic activity was detected in PBMC non-tumor cell line after 72h of exposure and at increasing concentrations of the compound (10-50 μM).

Cell line	IC$_{50}\pm$ SD(μM) 72h
A375	16.6 ± 1.5
MCF7	> 50
PC3	48.1 ± 1.5
Panc-1	> 50
A549	32.3 ± 0.9
PBMC	NA

Table 5.5 *IC$_{50}$ values of the antiproliferative activity of compounds **LK-4** on human cell lines after 72 h of treatment*

At this point, in order to definitely clarify the binding selectivity of compound **LK-4**, it was screened by SPR assay against the other two BAG isoforms, BAG1 and BAG4, as well as against the molecular chaperone Hsp70. Interestingly, **LK-4** did not interact with any of the tested protein isoforms, either with Hsp70, confirming its role of selective binder of BAG3 protein.

Having identified this promising molecule, we decided to study, in more detail, its mechanism of action in the attempt to clarify how BAG3 activity was functionally modulated. Since several studies reported that down-modulation of BAG3 protein levels does not affect the basal cell survival but instead it modifies the cellular response to pro-apoptotic stimuli, we analyzed the effect of compound **LK-4** on A375 cell cycle distribution, by flow cytometry analysis. The cells were incubated for 72 h with **LK-4**, at concentrations of 10 and 20 μM; the cell cycle analysis showed that the tested compound affected the cell cycle progression by arresting the cells in G$_2$/M without any significant increase of subG$_1$ cell fraction (**Figure 5.6A**). These results are perfectly in line with the modulation of BAG3 protein activity, which determines a cytostatic effect mediated by **LK-4** compound, without any increase of the percentage of cell death.

Conversely, the treatment of A375 cells with **LK-4** produced an increased cell death, detected as sub-G1 peak of propidium iodide-stained cells, in response to serum deprivation or the proapoptotic antibiotic Staurosporine. This experiment

definitively confirmed the BAG3 down-modulation mediated by our molecule (**Figure 5.6B**).
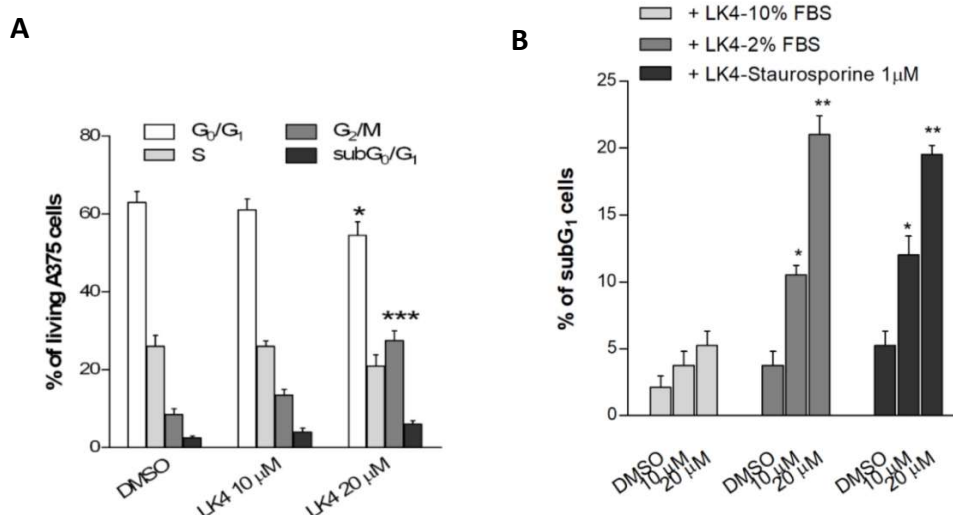
Figure 5.6 *LK-4 affected A375 cell-cycle progression and increased the starvation (low serum condition) or Staurosporine-induced apoptosis in A375 cells:*

*(A) Cell cycle analysis of DNA content, with propidium iodide staining, by flow cytometric evaluation. The A375 cells were treated with DMSO or **LK-4** (10 or 20 μM) for 72 h. Results are expressed as means ±SD of three experiment performed in duplicate. (***P≤0.001, *P≤0.05).*

*(B) Percentage of A375 cells in sub-G$_1$ for DNA content, with PI staining, analyzed by flow cytometry. The cells were incubated in complete medium with DMSO or **LK-4** (10 or 20 μM) for 72 h; in low medium (2% FBS) condition with DMSO or **LK-4** (10 or 20 μM) for 72 h; in complete medium with DMSO or **LK-4** (10 or 20 μM) for 72 h and in presence of Staurosporine (1 μM) for an additional 6 h.*

Moreover, since as reported in literature, the effect of BAG3 on cell survival is partially mediated by the interaction with Hsp70[7], we decided to verify if **LK-4** was able to influence the BAG3-Hsp70 protein-protein interaction. For this purpose a co-immunoprecipitation experiment was performed and BAG protein was immunoprecipitated from A375 cell lysate in the presence of **LK-4** (70 μM) or DMSO vehicle control, and immunoblotted for BAG protein. Interestingly, **LK-4** showed to reduce the BAG3-Hsp70 complex by a percentage of 60% as indicated by densitometric analysis (**Figure 5.7**). This result confirms that **LK-4** binds to BAG domain of the protein disrupting, thus, BAG3-Hsp70 interaction.
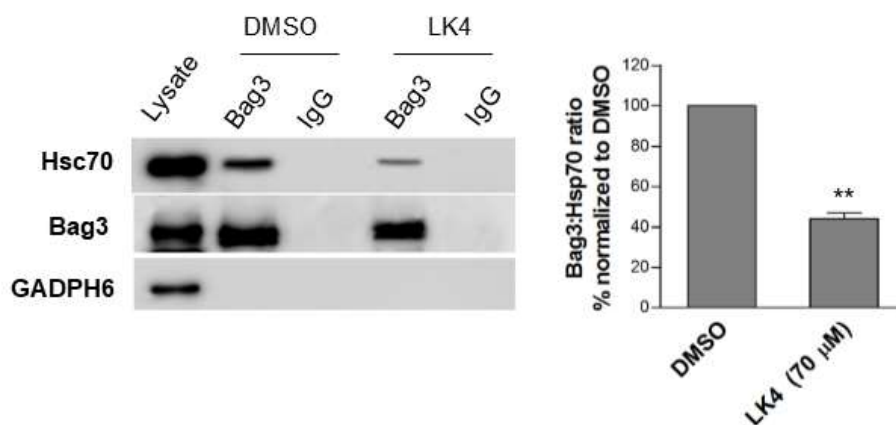
Figure 5.7 *LK-4 inhibits the Bag3-Hsp70 protein-protein interaction:*
*Co-immunoprecipitation cell free assay of A375 cell lysate with **LK-4**;*
***LK-4** inhibits the Bag3-Hsp70 protein-protein interaction in melanoma cells.*
BAG3 was immuno-precipitated with
***LK-4** (70 μM) or DMSO and blotted for bound Hsp70*

Finally, in order to assess that BAG3-Hsp70 interaction was also inhibited inside the cells, in a time dependent manner, A375 cells were exposed for 24, 48 and 72 hours to **LK-4** compound, with a concentration of 20 μM, close to the calculated IC_{50} value. Endogenous BAG3-Hsp70 complex was co-immunoprecipitated from cell lysates and analyzed by western blotting; the densitometric analysis revealed, once again, that the BAG3-Hsp70 interaction was inhibited by a percentage of 40% after 24 h, while a percentage of 80% of inhibition was reached after 72h of treatment (**Figure 5.8**).
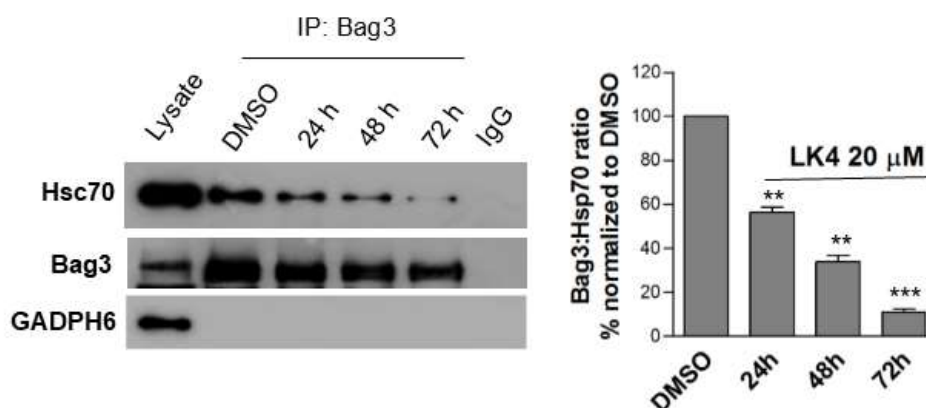
Figure 5.8. *LK-4 inhibits the Bag3-Hsp70 protein-protein interaction in melanoma cells:*

Co-immunoprecipitation assay of cell extract from A375 treated with LK-4 (20 μM) for 24, 48 or 72 h; BAG3 was immuno-precipitated and analyzed by immunoblotting with anti-Hsp70. The blots are representative of two different experiments with similar results and the amount of co-immunoprecipitated Hsp70, quantified by densitometry, was normalized to the amount of BAG3 and was expressed as means ± SD of these experiments.GADPH6 was used as a negative control. The significance between the two groups was calculated by the Student's t test (**P 0.005, *P ≤ 0.05)

Taking together, all these data point out the important role of **LK-4** in disrupting Hsp70-BAG3 protein protein interaction, emerging thus as an attractive candidate for drug development and representing also a useful tool for further biological investigations of the multifaceted role of the molecular co-chaperone BAG3.

Hence, by using a combined approach of virtual screening, biophysical techniques and biological assays, the 2,4-thiazolidindione scaffold was successfully identified as a promising chemical platform able to selectively bind and inhibit BAG3-Hsp70 protein-protein interaction.

CONCLUSIONS

Conclusions

The research work carried out in the frame of my PhD project has been devoted to the study of new and attractive biological targets involved in cancer progression. Among these, the epigenetic Macrodomain proteins and the BAG3 chaperone-regulator are of great interest, as they are mainly involved, with different mechanisms, in cancer processes. In virtue of their biological importance and their potential for therapeutic applications, this research project has been mainly addressed to the discovery of modulators of these two biological targets, exploiting the use of advanced technologies, both for lead identification process and for biophysical profile evaluation of the disclosed molecules. In order to identify new MacroD1 and MacroD2 modulators, basing on two different drug discovery approaches, I succeeded to identify different chemical platforms able to bind these two target proteins. In particular, compound **SP2** has been identified as a high affinity binder of MacroD2 protein, through the application of a virtual screening approach and biophysical techniques. The interaction between this new emerged 1,2,3 triazole-1,4-disubstituted binder and the macrodomain cavity of MacroD2 has been analyzed by biophysical and docking experiments; its activity in cancer cells is currently under evaluation, in order to better clarify the biological consequences of its protein modulation. These outcomes will be of great value because they can pave the way for the development of new and more potent modulators of MacroD2 epigenetic protein. At the same time, a fragment screening approach, based on X-ray crystallography was pursued for discovering new chemical entities able to interact with the MacroD1 protein. This strategy, that I had the opportunity to carry out during my research period at the Structural Genomics Consortium of Oxford, allowed to identify compound **3**, endowed with a pyrazol-3-yl-phenoxy-pyrimidine core, as a promising lead compound to develop a small collection of higher affinity compounds. Crystallography studies, combined with SPR technology, confirmed the real binding ability of this compound in the macrodomain pocket of MacroD1. Afterwards, the *in silico* analysis of the binding mode of the disclosed hit offered new insights to develop a small collection of derivatives, four of which showed to bind with higher affinities the target protein. Further experiments are still in

progress to definitely assess their potentiality as attractive candidates for drug development. Concerning the other target of interest, BAG3 protein, the use of a combined approach of a *structure-based drug design* and SPR spectroscopy allowed to identify the 2,4-thiazolidindione scaffold as a new molecular platform for BAG3 domain interaction, yielding compound **7**, which showed a nanomolar dissociation constant against the full length protein and a good cytotoxicity against melanoma cancer cell lines. Basing on this promising hit, we designed and synthesized a collection of differently decorated compounds, as potential modulators of the BAG3 BD domain. After an extensive biological evaluation, we disclosed compound **LK-4** as a new promising cytostatic and antiproliferative agent, which exerts its activity interfering with BAG3-Hsp70 complex formation. These promising results may stimulate further research toward the identification of more potent and selective inhibitors of this protein-protein interaction, that, beyond their potentiality in drug development, represent chemical probes to deepen the biological functions of this multifaceted protein.

EXPERIMENTAL SECTION

CHAPTER 6

Discovery of new modulators of the human Macrodomain protein MacroD2 by a structure-based-drug design approach: Experimental procedures

6.1. General synthetic methods

All commercially available starting materials were purchased from Sigma- Aldrich and were used as received. Solvents used for the synthesis were of HPLC grade and were purchased from Sigma-Aldrich or VWR. NMR spectra were recorded on Bruker Advance 400 or 300 MHz instruments. Compounds were dissolved in 0.5 ml of CD_3OD, or $CDCl_3$.Coupling constants (J) are reported in Hertz, and chemical shifts are expressed in parts per million (ppm) on the delta (δ) scale relative to the solvent peak as internal reference. Multiplicities are reported as follows: s, singlet; d, doublet; t, triplet; m, multiplet; dd, doublet of doublets. Electrospray mass spectrometry (ESI-MS) was performed on a LCQ DECA TermoQuest (San Josè, California, USA) mass spectrometer. Chemical reactions were monitored on silica gel 60 F254 plates (Merck) and spots were visualized under UV light. Analytical and semi-preparative reversed-phase HPLC were performed on an Agilent Technologies 1200 Series high performance liquid chromatography system using a Fusion-RP, C18 reversed-phase column (100 x 2mm, 4µM, 80 Å, flow rate = 1 mL/min; 250 x 10.00mm, 4µM, 80 Å, flow rate = 4 mL/min respectively, Phenomenex ®). The binary solvent system (A/B) was as follows: 0.1% TFA in water (A) and 0.1% TFA in CH_3CN (B). Absorbance was detected at 240 nm. The purity of all tested compound (> 95%) was determined by HPLC analysis.

6.2. Methods and materials

Scheme 1. General method for the Synthesis of compounds SP1-SP6

A) *Synthesis of (1-(benzo[d]thiazol-6-yl)-1H-1,2,3-triazol-4-yl)methanol (2)*
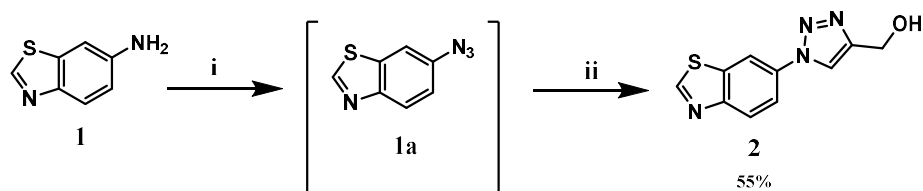
A mixture of benzo[d]thiazol-6-amine (**1**) (1 eq., 100mg) in acetonitrile (4 mL) was placed in a 25 ml bottom flask and cooled to 0 °C. Then, tert-butyl nitrite (t-BuONO) (1.5 eq) and azidotrimethylsilane (TMSN₃) (1.2 eq.) were added dropwise and the reaction mixture was stirred, for 2 hours, at room temperature. The course of the reaction was monitored by TLC. Once the the diazotization reaction was completed, to the reaction mixture were added Propargyl alcohol (1 eq.), an aqueous solution of $CuSO_4 \cdot 5H_2O$ (0.05 eq.) and sodium ascorbate (0.2 eq.). The reaction mixture was stirred overnight, at room temperature and monitored by TLC. The reaction solvent was evaporated under vacuum and the mixture was poured into methanol. The resulting precipitate was filtered off to give the product (**2**). HPLC purification was performed by semi-preparative reversed-phase HPLC (Fusion-RP, C18 reversed-phase column: 250 x 10.00mm, 4μM, 80 Å, flow rate = 4 mL/min) using the gradient conditions reported below and the final products were characterized by ESI-MS (High purity> 97% detected by HPLC analysis).

## B) Synthesis of ((1-(benzo[d]thiazol-6-yl)-1H-1,2,3-triazol-4-yl)methyl esters (SP1-SP6)
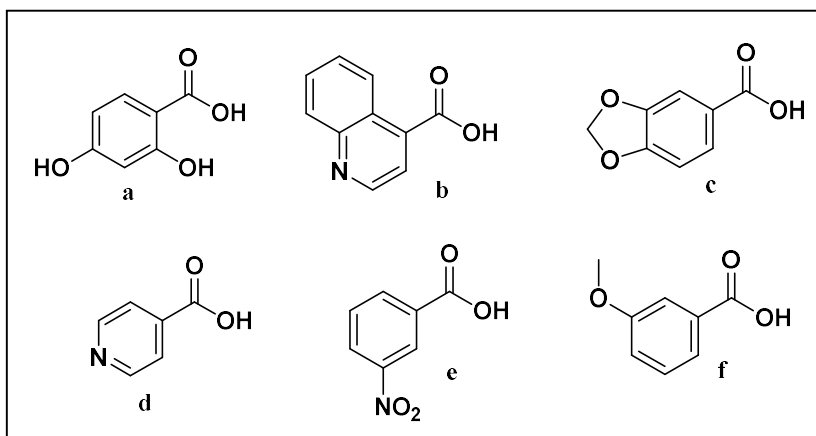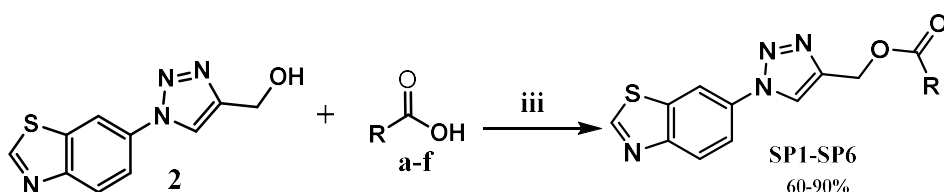

A mixture of (**2**) (2 eq.), aromatic carboxylic acids (**a-f**) (1 eq.), *N,N'*-Diisopropylcarbodiimide (1.2 eq.), 4-Dimethylaminopyridine (DMAP) (0.12 eq.) and dichloromethane, were placed in a 25 ml bottom flask. The reaction mixture was stirred for a period of 16 h, at room temperature. The course of the reaction was monitored by TLC. Then, the mixture was extracted with ethyl acetate, followed by washing the organic phase with citric acid (10%). The organic phase was evaporated under vacuum to give the products (**SP1**–**SP6**). HPLC purification was performed by semi-preparative reversed-phase HPLC (Fusion-RP, C18 reversed-phase column: 250 x 10.00mm, 4μM, 80 Å, flow rate = 4 mL/min) using

the gradient conditions reported below and the final products were characterized by ESI-MS and NMR spectra (High purity> 97% detected by HPLC analysis).

Scheme 2 General method for the Synthesis of compounds *SP7-SP12*

A) *Synthesis of 2-azidothiazole (5)*
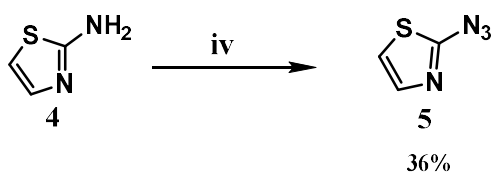
To a mixture of 2-amino-thiazole (**4**) (2 eq.) in HCl conc. (1 mL), cooled to 0°C, sodium nitrite (NaNO$_2$) (1 eq.) and sodium azide (NaN$_3$) (1 eq.) were added dropwise. After ten minutes, the mixture was left at room temperature and stirred for 2 hours. The course of the reaction was monitored by TLC and after extraction with diethyl ether, the organic phase was evaporated under vacuum to give 2-azido-thiazole (**5**). HPLC purification was performed by semi-preparative reversed-phase HPLC (Fusion-RP, C18 reversed-phase column: 250 x 10.00mm, 4μM, 80 Å, flow rate = 4 mL/min) using the gradient conditions reported below and the final products were characterized by ESI-MS (High purity> 97% detected by HPLC analysis).

B) Synthesis of 5-methyl-1-(thiazol-2-yl)-1H-1,2,3-triazole-4-carboxylic acid (7)

A mixture of (**5**) (1 eq.), ethyl acetoacetate (1 eq.) and sodium methoxide (CH₃ONa) (2 mL) were placed in a 25 ml bottom flask and cooled in an ice bath, stirring for 30 minutes. Then, the reaction mixture was heated under reflux (60°C) and continuously stirred for 1 h, then, hot water was added to dissolve the observed precipitate. The course of the reaction was monitored by TLC and, after 1 hour, to the reaction mixture was added an aqueous solution of NaOH (1M) to hydrolyze *in situ* the ethyl ester and stirred under reflux for one more hour. Once the reaction was completed, the mixture was poured into HCl conc. and the resulting precipitate was filtered off and recrystallized to give compound (**7**). HPLC purification was performed by semi-preparative reversed-phase HPLC (Fusion-RP, C18 reversed-phase column: 250 x 10.00mm, 4μM, 80 Å, flow rate = 4 mL/min) using the gradient conditions reported below and the final products were characterized by ESI-MS (High purity> 97% detected by HPLC analysis).

### C) Synthesis of (5-methyl-1-(thiazol-2-yl)-1H-1,2,3-triazol-4-yl)methanol (8)

A mixture of (**7**) (1 eq.), Hydroxybenzotriazole (HOBt) (1 eq.), *N,N'*-Diisopropylcarbodiimide (1 eq.) and dichloromethane (2 mL) were placed in a 25 ml bottom flask and stirred for 30 minutes, at room temperature. After this time, the solvent was evaporated, the organic layer dissolved in THF, and water and Sodium borohydride (NaBH$_4$) (2 eq.) were added to the reaction mixture, which was stirred for 30 minutes at 0°C. The course of the reaction was monitored by TLC and after completion, the reaction mixture was quenched with methanol, extracted with ethylacetate, then washing the organic phase with citric acid (10%), NaHCO$_3$ and Brine, achieved the product (**8**). HPLC purification was performed by semi-preparative reversed-phase HPLC (Fusion-RP, C18 reversed-phase column: 250 x 10.00mm, 4μM, 80 Å, flow rate = 4 mL/min) using the gradient conditions reported below and the final products were characterized by ESI-MS (High purity> 97% detected by HPLC analysis).

### D) Synthesis of (5-methyl-1-(thiazol-2-yl)-1H-1,2,3-triazol-4-yl)methyl esters (SP7-SP12)
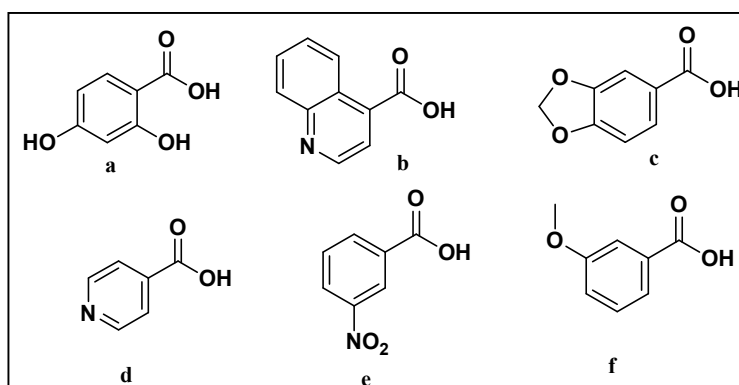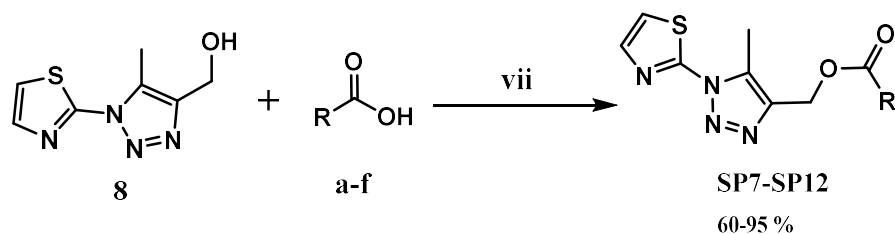
A mixture of (**8**) (2 eq.), aromatic carboxylic acids (**a-f**) (1 eq.), *N,N'*-Diisopropylcarbodiimide (1.2 eq.), 4-Dimethylaminopyridine (DMAP) (0.12 eq.) and dichloromethane, were placed in a 25 ml bottom flask. The reaction mixture was stirred for a period of 16 h, at room temperature. The course of the reaction was monitored by TLC. Then, the mixture was extracted with ethyl acetate, followed by washing the organic phase with citric acid (10%). The organic phase was evaporated under vacuum to give the products (**SP7**–**SP12**). HPLC purification was performed by semi-preparative reversed-phase HPLC (Fusion-RP, C18 reversed-phase column: 250 x 10.00mm, 4μM, 80 Å, flow rate = 4 mL/min) using

the gradient conditions reported below and the final products were characterized by

ESI-MS and NMR spectra (High purity> 97% detected by HPLC analysis).

Scheme 3. General method for the Synthesis of SP13-SP20

### A) *Synthesis of various substituted aryl-azides (11h-11n)*

A

R_1—CH$_2$—Br $\xrightarrow{\text{viii}}$ R_1—CH$_2$—N$_3$

10h-n   11h-11n

80-100 %

h   i   l

m   n

Compound	R_1	Yield (%)
11h		*80*
11i		*82*
11l		*95.2*

11m		*94*
11n		*100*
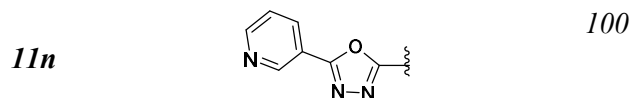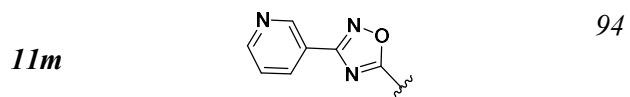
A mixture of different aryl-halides (**10h-n**) (1 eq.), sodium azide (1.5 eq.), and a solution of water/acetone (1:4), were placed in a 25 ml bottom flask. The reaction mixture was heated under reflux and continuously stirred for a period of 3 h. The course of the reaction was monitored by TLC. The reaction mixture was extracted with dichloromethane and the organic phase was then evaporated under vacuum to achieve the products (**11h**–**n**). HPLC purification was performed by semi-preparative reversed-phase HPLC (Fusion-RP, C18 reversed-phase column: 250 x 10.00mm, 4μM, 80 Å, flow rate = 4 mL/min) using the gradient conditions reported below and the final products were characterized by ESI-MS (High purity> 97% detected by HPLC analysis).

B) Synthesis of various substituted 1,4 disubstituted triazoles (13h-13n)
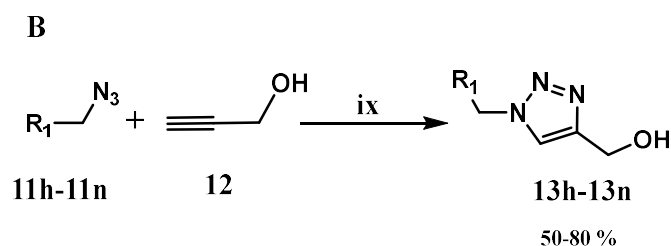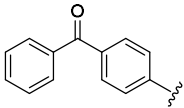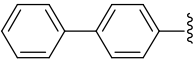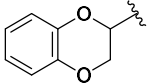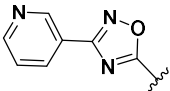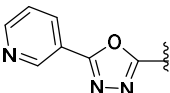
Compound	R₁	Yield (%)
13h		*50*
13i		*72*
13l		*65.2*
13m		*54*
13n		*70*

A mixture of (**11h-n**) (1 eq.), propargyl alcohol (1 eq.), an aqueous solution of CuSO₄·5H₂O (0.033 eq.) and sodium ascorbate (0.07 eq.), and water/tert-butanol (TBA) (1:1) were placed in a 25 ml bottom flask. The reaction mixture was stirred, overnight, at room temperature. The course of the reaction was monitored by TLC, and after completion, the reaction mixture was extracted with dichloromethane and the organic phase was evaporated under vacuum, to give the triazoles (1**3h-13n**). HPLC purification was performed by semi-preparative reversed-phase HPLC (Fusion-RP, C18 reversed-phase column: 250 x 10.00mm, 4μM, 80 Å, flow rate = 4 mL/min) using the gradient conditions reported below and the final products were characterized by ESI-MS (High purity> 97% detected by HPLC analysis).

## C) Synthesis of (1-aryl)-1H-1,2,3-triazol-4-yl)methyl esters (SP13-SP20)
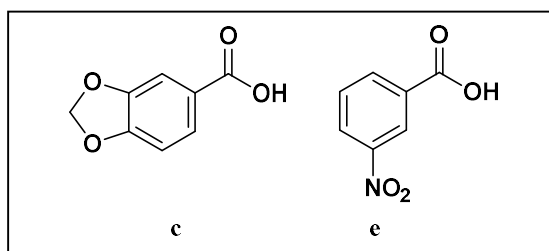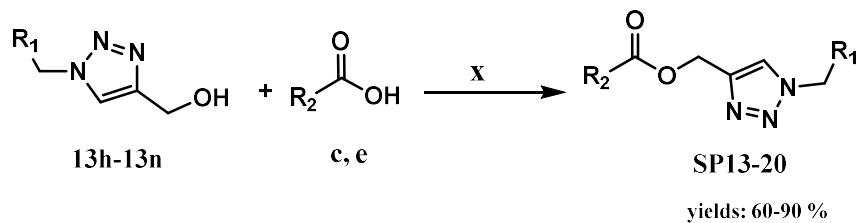
13h-13n   c, e   x   SP13-20

yields: 60-90 %

c   e

Compound	R_1	R_2	Yield (%)
SP13			45
SP14			40
SP15			60
SP16			87.2
SP17			70.2
SP18			82.2
SP19			89.1
SP20			75.1

A mixture of (**13h-13n**) (2 eq.), piperonylic acid (**a**) and 3-nitro benzoic acid (**b**) (1 eq.), *N,N′*-Diisopropylcarbodiimide (1.2 eq.), 4-Dimethylaminopyridine (DMAP) (0.12 eq.) and dichloromethane, were placed in a 25 ml bottom flask. The reaction mixture was stirred for a period of 16 h, at room temperature. The course of the reaction was monitored by TLC. Then, the mixture was extracted with ethyl acetate, followed by washing the organic phase with citric acid (10%). The organic phase was evaporated under vacuum to give the products (**SP13**–**SP20**).

1.1 (1-(benzo[d]thiazol-6-yl)-1H-1,2,3-triazol-4-yl)methyl 3-methoxybenzoate (SP-1)
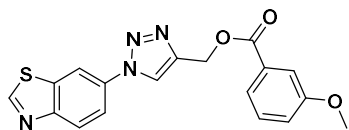
 was obtained by following the general procedure as a pale

yellow powdery solid (80 mg, 62% yield after HPLC purification); RP-HPLC t_R = 32.06

min, gradient condition: from 5% B ending to 100 % B over 50 min, flow rate of 4 mL/min,

λ = 254 nm. ^{1}H NMR (300 MHz, Chloroform-*d*): δ 9.18 (s, 1H), 8.44 (s, 1H), 8.26 (s, 2H),

7.8 (d, J = 2.1 Hz, 2H), 7.88 (d, J = 1.6 Hz, 1H), 6.87 (d, J = 2.1 Hz, 2H), 5.50 (s, 2H), 3.80

(s, 3H). ^{13}C NMR (101 MHz, Chloroform-*d*): δ 166.28, 158.23, 157.04, 156.03, 148.10,

137.70, 132.32, 131.88, 131.63, 128.39, 124.65, 122.78, 119.62, 119.38, 114.34, 113.72,

57.67, 55.47. ESI-MS, calcd for $C_{18}H_{14}N_4O_3S$ 366.39; found m/z = 367.3 [M+ H]$^+$

1.2 (1-(benzo[d]thiazol-6-yl)-1H-1,2,3-triazol-4-yl)methylbenzo[d][1,3]dioxole-5-carboxylate (SP-2)
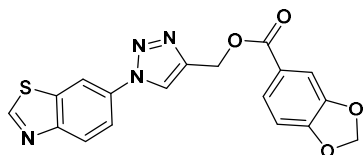
 was obtained by following the general procedure as a white

powdery solid (153,7 mg, 63% yield after HPLC purification); RP-HPLC t_R = 26.87 min,

gradient condition: from 5% B ending to 100% B over 50 min, flow rate of 4 mL/min, λ =

254 nm. ^{1}H NMR (400 MHz, Methanol-*d₄*): δ 9.19 (s, 1H), 8.77 (s, 1H), 8.67 (d, J = 2.2

Hz, 1H), 8.29 (d, J = 8.8 Hz, 1H), 8.11 (d, J = 8.8 Hz, 1H), 7.71 (d, J = 8.2 Hz, 1H), 7.49

(s, 1H), 6.92 (d, J = 8.2 Hz, 1H), 6.07 (s, 2H), 5.54 (s, 2H).^{13}C NMR (125 MHz, Methanol-

d₄): δ 167.36, 152.36, 151.82, 149.46, 148.76, 138.74, 133.24, 131.63, 127.44, 124.28,

121.09 , 119.14, 115.50, 111.98, 110.27, 108.80, 101.50, 56.23. ESI-MS, calcd for

$C_{18}H_{12}N_4O_4S$ 380.38; found m/z = 381.3 [M + H]$^+$.

1.3 (1-(benzo[d]thiazol-6-yl)-1H-1,2,3-triazol-4-yl)methylquinoline-4-carboxylate(SP-3)
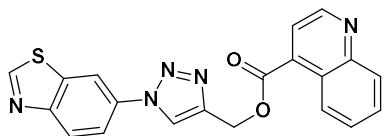
 was obtained by following the general procedure as a pale yellow solid (91,8 mg, 60% yield after HPLC purification); RP-HPLC t_R = 26.51 min, gradient condition: from 5% B ending to 100% B over 50 min, flow rate of 4 mL/min, λ = 254 nm. ^{1}H NMR (300 MHz, Methanol-d_4): δ 9.09 (s, 1H), 8.88 (d, J = 6.9 Hz, 2H), 8.69 (d, J = 2.1 Hz, 1H), 8.29 (d, J = 8.8 Hz, 1H), 8.21 – 8.11 (m, 3H), 7.94 (t, J = 7.7 Hz, 2H), 7.81 (t, J = 7.8 Hz, 1H), 5.75 (s, 2H). ^{13}C NMR (125 MHz, Methanol-d_4): δ 168.22 ,157.04, 152.36, 149.41 (2C), 147.72 , 146.82 , 138.74, 134.48, 132.92, 130.69, 128.74, 127.74, 125.81, 123.57, 123.53, 122.49, 119.35, 114.36, 58.43. ESI-MS, calcd for $C_{20}H_{13}N_5O_2S$ 387.42; found m/z = 388.4 $[M + H]^+$.

1.4 (1-(benzo[d]thiazol-6-yl)-1H-1,2,3-triazol-4-yl)methyl 3-nitrobenzoate (SP-4)
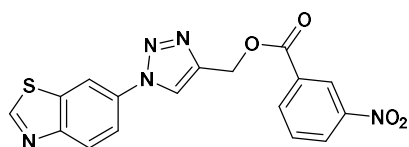
 was obtained by following the general procedure as a pale yellow solid (50,9 mg, 90% yield after HPLC purification); RP-HPLC t_R = 24.38 min, gradient condition: from 5% B ending to 100 % B over 50 min, flow rate of 4 mL/min, λ = 254 nm. ^{1}H NMR (400 MHz, Chloroform-d):δ 9.32 (s, 1H), 8.49-8.32 (m, 5H), 8.36 (s, 1H), 8.01 (dt, J = 7.5, 2.0 Hz, 1H), 7.31 (t, J = 7.5 Hz, 1H), 5.51 (s, 2H). ^{13}C NMR (125 MHz, Chloroform-d): δ 167.28, 158.23, 157.04, 156.03, 148.10, 137.70, 132.32, 131.88, 131.63, 128.39, 124.65, 122.78, 119.62, 119.38, 114.34, 113.72, 56.11. ESI-MS, calcd for $C_{17}H_{11}N_5O_4S$ 381.37; found m/z = 382.3 $[M + H]^+$.

1.5 (1-(benzo[d]thiazol-6-yl)-1H-1,2,3-triazol-4-yl)methyl isonicotinate (SP-5)
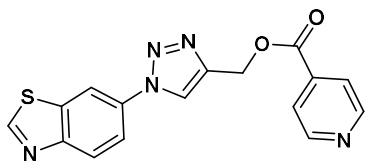

was obtained by following the general procedure as pale yellow solid (60,6 mg, 80% yield after HPLC purification); RP-HPLC t_R = 23.9 min, gradient condition: from 5% B ending to 100 % B over 50 min, flow rate of 4 mL/min, λ = 240 nm. ^{1}H NMR (400 MHz, Chloroform-*d*): δ 9.32 (s, 1H), 8.90 (d, J = 5.1 Hz, 2H), 8.34 (s, 1H), 7.97 – 7.89 (m, 4H), 7.31 (dd, J = 7.5, 1.5 Hz, 1H), 5.51 (s, 2H). ^{13}C NMR (125 MHz, Chloroform-*d*): δ 167.43, 152.36, 150.87 (2C), 149.46, 146.82, 139.05, 138.74, 133.24, 127.44, 122.72 (2C), 121.09, 119.14, 111.98, 56.23. ESI-MS, calcd for $C_{16}H_{11}N_5O_2S$ 337,36; found m/z = 338.3 [M + H]$^+$.

1.6 (1-(benzo[d]thiazol-6-yl)-1H-1,2,3-triazol-4-yl)methyl 2,4-dihydroxybenzoate (SP-6)
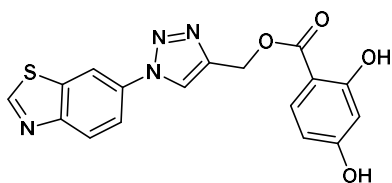
was obtained by following the general procedure as a white solid (48.5 mg, 85% yield after HPLC purification); RP-HPLC t_R= 35.42 min, gradient condition: from 5% B to ending to 100 % B over 40 min, flow rate of 4 mL/min, λ = 254 nm. ^{1}H NMR (400 MHz, Chloroform-*d*): δ 9.32 (s, 1H), 8.35 (s, 1H), 7.98 – 7.89 (m, 1H), 7.64 (d, J = 7.5 Hz, 1H), 7.31 (dd, J = 7.5, 1.5 Hz, 1H), 7.00 (s, 1H), 6.45 (dd, J = 7.5, 2.0 Hz, 1H), 6.31 (d, J = 2.0 Hz, 1H), 5.51 (s, 2H). ^{13}C NMR (125 MHz, Chloroform-*d*): δ 168.41, 164.60, 163.58 , 152.36 , 149.46 , 146.82 , 138.74 , 133.23 (2C), 127.44 , 121.09 , 119.14 , 112.03 (2C), 108.67, 103.19, 56.49. ESI-MS, calcd for $C_{17}H_{12}N_4O_4S$ 368.37; found m/z = 369.3 [M + H]$^+$.

1.7 (5-methyl-1-(thiazol-2-yl)-1H-1,2,3-triazol-4-yl)methyl 3-methoxybenzoate (SP-7)
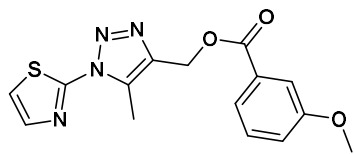
was obtained by following the general procedure as a pale yellow solid (122 mg, 60% yield after HPLC purification); RP-HPLC t_R = 33.09 min, gradient condition: from 5% B ending to 100 % B over 50 min, flow rate of 4 mL/min, λ = 254 nm. ^{1}H NMR (400 MHz, Chloroform-*d*): δ 8.04 (d, J = 3.5 Hz, 1H), 7.75 (d, J = 3.5 Hz, 2H), 7.33 (d, J = 3.5 Hz, 2H), 6.94 (d, J = 3.5 Hz, 1H). 5.51 (s, 2H), 3.89 (s, 3H), 2.81 (s, 3H). ^{13}C NMR (125 MHz, Chloroform-*d*): δ 167.36, 159.50, 153.58, 138.07, 137.81, 131.47, 129.40, 128.12, 122.10, 118.99, 114.20, 112.91, 55.49, 53.46, 10.88. ESI-MS, calcd for $C_{15}H_{14}N_4O_3S$ 330.36; found m/z = 331.3 [M + H]$^+$.

1.8 (5-methyl-1-(thiazol-2-yl)-1H-1,2,3-triazol-4-yl)methylbenzo[d][1,3]dioxole-5-carboxylate (SP-8)
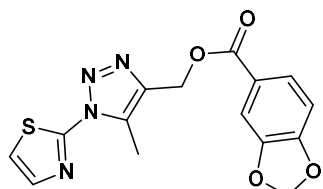
was obtained by following the general procedure as a yellow solid (63.7 mg, 75% yield after HPLC purification); RP-HPLC t_R = 32.6 min, gradient condition: from 5% B ending to 100 % B over 50 min, flow rate of 4 mL/min, λ = 254 nm. ^{1}H NMR (400 MHz, Chloroform-*d*) δ 7.75 (d, J = 3.4 Hz, 1H), 7.69 (ddd, J = 8.2, 2.6, 1.4 Hz, 1H), 7.50 (d, J = 1.7 Hz, 1H), 7.33 (d, J = 3.4 Hz, 1H), 6.85 (d, J = 8.2, 2.0 Hz, 1H), 6.06 (s, 2H), 5.49 (s, 2H), 2.83 (s, 3H). ^{13}C NMR (125 MHz, Chloroform-*d*): δ 167.36, 153.58, 149.10, 148.76, 138.07, 137.81, 128.12 , 124.28 (2C) , 112.91 , 110.27, 108.80, 101.50, 53.46, 10.88. ESI-MS, calcd for $C_{15}H_{12}N_4O_4S$ 344.36; found m/z = 345.3 [M + H]$^+$.

1.9 (5-methyl-1-(thiazol-2-yl)-1H-1,2,3-triazol-4-yl)methyl isonicotinate (SP-9)
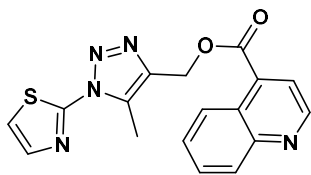

was obtained by following the general procedure as a yellow solid (116 mg, 56% yield after HPLC purification); RP-HPLC t_R = 26.62, gradient condition: from 5% B ending to 100 % B over 50 min, flow rate of 4 mL/min, λ = 254 nm. ^{1}H NMR (400 MHz, Chloroform-*d*): δ 9.29 (d, J = 4.9 Hz, 1H), 8.97 (d, J = 8.7 Hz, 1H), 8.53 (d, J = 8.6 Hz, 1H), 8.28 (d, J = 4.8 Hz, 1H), 8.05 (t, J = 7.8 Hz, 1H), 7.93 (t, J = 7.9 Hz, 1H), 7.78 (d, J = 3.7 Hz, 1H), 7.36 (dd, J = 3.5, 1.5 Hz, 1H), 5.71 (s, 2H), 2.90 (s, 3H). ^{13}C NMR (125 MHz, Chloroform-*d*): δ 168.22, 153.58, 149.37, 147.72, 138.07, 137.81, 132.94, 130.02, 129.73, 128.52, 128.17, 128.10, 125.68, 123.80, 112.91, 53.46, 10.88. ESI-MS, calcd for $C_{17}H_{13}N_5O_2S$ 351.38; found m/z = 352.3 [M + H]$^+$.

1.10 (5-methyl-1-(thiazol-2-yl)-1H-1,2,3-triazol-4-yl)methyl 3-nitrobenzoate (SP-10)
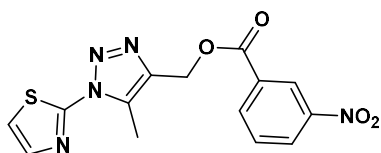
was obtained by following the general procedure as a pale yellow solid (63.7 mg, 86.4% yield after HPLC purification); RP-HPLC t_R = 34.3 min, gradient condition: from 5% B ending to 100 % B over 50 min, flow rate of 4 mL/min, λ = 240 nm. ^{1}H NMR (400 MHz, Chloroform-*d*): δ 8.95 – 8.90 (m, 2H), 8.49 – 8.40 (m, 3H), 7.69 (t, J = 8.0 Hz, 1H), 5.60 (s, 2H), 2.88 (s, 3H).^{13}C NMR (125 MHz, Chloroform-*d)*: δ 167.36, 153.58, 147.92, 138.07, 137.81, 130.92, 129.76, 128.99, 128.12, 127.25, 123.87, 112.91, 53.46, 10.88. ESI-MS, calcd for $C_{14}H_{11}N_5O_4S$ 345.33; found m/z = 346.3 [M + H]$^+$.

1.11 (5-methyl-1-(thiazol-2-yl)-1H-1,2,3-triazol-4-yl)methyl isonicotinate (SP-11)
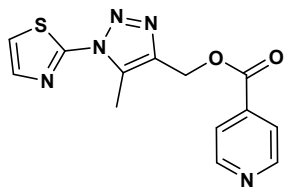
 was obtained by following the general procedure as a white solid (116 mg, 93.3% yield after HPLC purification); RP-HPLC t_R = 18.8 min, gradient condition: from 5% B ending to 100 % B over 50 min, flow rate of 4 mL/min, λ = 254 nm. ^{1}H NMR (400 MHz, Chloroform-*d*): δ 8.98 (s, 2H), 8.39 (s, 2H), 7.78 (d, J = 3.5 Hz, 1H), 7.37 (d, J = 3.5 Hz, 1H), 5.65 (s, 2H), 2.87 (s, 3H). ^{13}C NMR (125 MHz, Chloroform-*d*): δ 167.43, 153.58, 150.87 (2C), 139.05, 138.07, 137.81, 128.12, 122.7 (2C), 112.91, 53.46, 10.88. ESI-MS, calcd for $C_{13}H_{11}N_5O_2S$ 301.32; found m/z = 302.3 [M + H]$^+$.

### 1.12 (5-methyl-1-(thiazol-2-yl)-1H-1,2,3-triazol-4-yl)methyl 2,5-dihydroxybenzoate (SP-12)
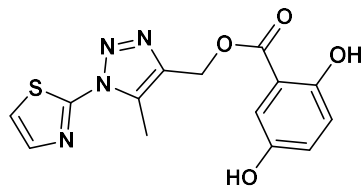
 was obtained by following the general procedure as a yellow solid (116 mg, 87% yield after HPLC purification); RP-HPLC t_R = 31.9 min, gradient condition: from 5% B ending to 100 % B over 50 min, flow rate of 4 mL/min, λ = 254 nm. ^{1}H NMR (400 MHz, Chloroform-*d*): δ 7.78 – 7.74 (m, 1H), 7.34 (t, J = 2.9 Hz, 1H), 6.64 (s, 1H), 6.44 – 6.34 (m, 2H), 5.53 (s, 2H), 2.84 (s, 3H). ^{13}C NMR (125 MHz, Chloroform-*d*): δ 169.45, 156.70, 153.58, 150.32, 138.07, 137.81, 128.12, 121.30, 116.20, 115.50, 112.89, 103.15, 53.46, 10.88. ESI-MS, calcd for $C_{14}H_{12}N_4O_4S$, 332.33; found m/z= 333.33 [M + H]$^+$.

1.13 (1-(4-benzoylbenzyl)-1H-1,2,3-triazol-4-yl)methyl 3-nitrobenzoate (SP-13)
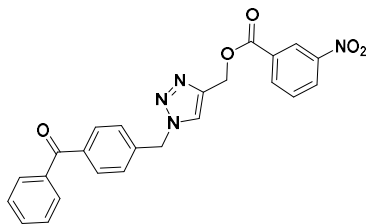

was obtained by following the general procedure as a grey solid (80 mg, 45% yield after HPLC purification); RP-HPLC t_R = 34.6 min, gradient condition: from 5% B ending to 100 % B over 50 min, flow rate of 4 mL/min, λ = 254 nm. ^{1}H NMR (300 MHz, Chloroform-*d*): δ 8.87 (d, J = 2.2 Hz, 1H), 8.47 – 8.34 (m, 1H), 7.88 – 7.73 (m, 6H), 7.71 – 7.58 (m, 2H), 7.50 (t, J = 8.0 Hz, 3H), 7.41 (d, J = 7.9 Hz, 1H), 5.66 (s, 2H), 5.55 (s, 2H). ^{13}C NMR (125 MHz, Chloroform-*d*): δ 196.60, 164.14, 148.32, 139.90, 137.48, 137.14, 134.89, 132.53, 131.38, 130.20, 130.06, 129.87, 129.55 (2C), 128.76, 128.73, 128.13 (2C), 127.75, 127.31, 125.13, 123.87, 58.03, 53.09. ESI-MS, calcd for $C_{24}H_{18}N_4O_5$ 442.13; found m/z = 443.3 [M+H]$^+$.

1.14 (1-(4-benzoylbenzyl)-1H-1,2,3-triazol-4-yl)methyl benzo[d][1,3]dioxole-5-carboxylate (SP-14)
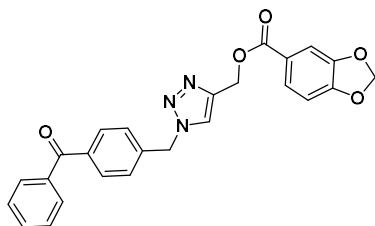

was obtained by following the general procedure as a yellow solid (70 mg, 40.0% yield after HPLC purification); RP-HPLC t_R = 33.54 min, gradient condition: from 5% B ending to 100 % B over 50 min, flow rate of 4 mL/min, λ = 254 nm. ^{1}H NMR (300 MHz, Chloroform-*d*): δ 7.87 – 7.74 (m, 3H), 7.70 – 7.57 (m, 3H), 7.55 – 7.45 (m, 3H), 7.39 (d, J = 7.9 Hz, 2H), 6.84 (d, J = 8.1 Hz, 2H), 6.05 (s, 2H), 5.64 (s, 2H), 5.46 (s, 2H).^{13}C NMR (125 MHz, Chloroform-*d*): δ 195.84, 167.36, 149.10, 148.76, 142.00, 138.04, 136.23, 134.96, 132.42, 129.58 (2C), 128.75 (2C), 128.73 (2C),

128.07 (2C) , 127.64, 124.28 (2C), 110.27, 108.80, 101.50, 56.46, 53.30. ESI-MS, calcd for $C_{25}H_{19}N_3O_5$ 441.44; found m/z = 442.4[M+ H]$^+$.

1.15 (1-([1,1'-biphenyl]-4-ylmethyl)-1H-1,2,3-triazol-4-yl)methyl 3-nitrobenzoate (SP-15)
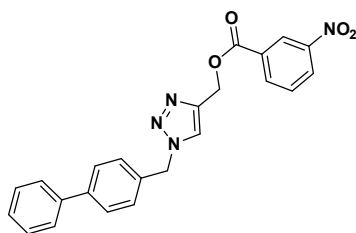
was obtained by following the general procedure as a yellow solid (97.2 mg, 60.0% yield after HPLC purification); RP-HPLC t_R = 37.03 min, gradient condition: from 5% B ending to 100 % B over 50 min, flow rate of 4 mL/min, λ = 254 nm. ^{1}H NMR (300 MHz, Chloroform-*d*): δ 8.86 (s, 1H), 8.48 – 8.32 (m, 2H), 7.75 – 7.54 (m, 7H), 7.50 – 7.37 (m, 4H), 5.61 (s, 2H), 5.53 (s, 2H).^{13}C NMR (125 MHz, Chloroform-*d*): δ 167.36, 149.75, 142.05, 141.94, 140.72, 135.92, 133.16, 130.93, 129.72, 128.81 (2C), 128.64 (2C) , 127.71 , 127.65 , 127.55 (2C) , 127.25, 126.98 (2C), 123.85, 56.46, 53.35. ESI-MS, calcd for $C_{23}H_{18}N_4O_4$ 414.42; found m/z = 415.4 [M+H]$^+$.

1.16 (1-((2,3-dihydrobenzo[b][1,4]dioxin-2-yl)methyl)1H-1,2,3-triazol-4-yl)methyl-3-nitrobenzoate (SP-16)
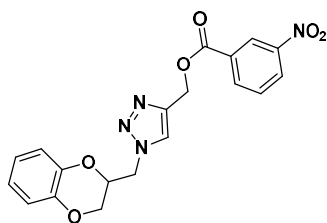
was obtained by following the general procedure as a yellow solid (120 mg, 87.2% yield after HPLC purification); RP-HPLC t_R = 32.09 min, gradient condition: from 5% B ending to 100 % B over 50 min, flow rate of 4 mL/min, λ = 240 nm. ^{1}H NMR (300 MHz, Chloroform-*d*): δ 8.88 (s, 1H), 8.41 (dd, J = 13.9, 7.8 Hz, 2H), 7.88 (s, 1H), 7.67 (t, J = 8.0 Hz, 1H), 6.91 (s, 4H), 5.56 (s, 2H), 4.78 – 4.67 (m, 2H), 4.65 (s,

1H), 4.37 (d, J = 11.4 Hz, 1H), 3.94 (dd, J = 11.6, 5.7 Hz, 1H).^{13}C NMR (125 MHz, Chloroform-*d*): δ 167.36, 147.92, 145.38, 144.08, 142.03, 130.92, 129.76, 128.99, 127.25, 123.92 (2C), 121.55 (2C), 117.39 , 117.20, 71.96, 66.11, 56.46, 49.15. ESI-MS, calcd for $C_{19}H_{16}N_4O_6$ 396.36; found m/z = 397.3 [M+H]$^+$.

1.17 (1-((3-(pyridin-3-yl)1,2,4-oxadiazol-5-yl)methyl)-1H-1,2,3-triazol-4-yl)methyl-3-nitrobenzoate (SP-17)
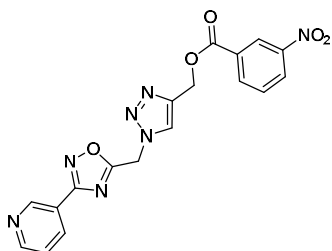

was obtained by following the general procedure as a yellow solid (100mg, 70.2% yield after HPLC purification); RP-HPLC t_R 24.03 min, gradient condition: from 5% B ending to 100 % B over 50 min, flow rate of 4 mL/min, λ = 254nm. ^{1}H NMR (300 MHz, Chloroform-*d*): δ 8.88 (s, 1H), 8.64 (s, 1H), 8.43 (dt, J = 11.8, 4.7 Hz, 4H), 8.09 (s, 1H), 7.68 (t, J = 7.9 Hz, 2H), 5.97 (s, 2H), 5.60 (s, 2H).^{13}C NMR (125 MHz, Chloroform-*d*): δ 167.50, 164.27, 158.52, 152.96 , 147.97, 147.89 , 143.47, 135.42, 134.58, 131.32, 129.77, 127.82 , 124.63, 124.05, 123.60, 119.63, 58.37, 44.28. ESI-MS, calcd for $C_{18}H_{13}N_7O_5$ 407.35; found m/z = 408.3 [M+H]$^+$.

1.18 (1-((3-(pyridin-3-yl)-1,2,4-oxadiazol-5-yl)methyl)-1H-1,2,3-triazol-4yl)methylbenzo[d][1,3]dioxole-5 carboxylate (SP-18)
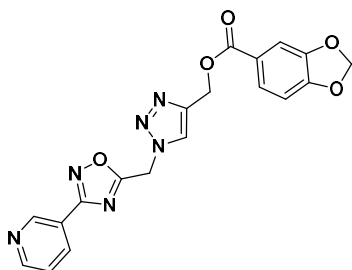

was obtained by following the general procedure as a yellow solid (68.2 mg, 82.2% yield after HPLC purification); RP-HPLC t_R = 32.33 min, gradient

condition: from 5% B ending to 100 % B over 50 min, flow rate of 4 mL/min, $\lambda = 254$nm. ^{1}H NMR (300 MHz, Chloroform-*d*): 9.31 (s, 1H), δ 8.59 (d, J = 8.2 Hz, 1H), 8.03 (s, 1H), 7.67 (d, J = 8.2 Hz, 2H), 7.47 (s, 1H), 7.28 (s, 1H), 6.84 (d, J = 8.2 Hz, 1H), 6.05 (s, 2H), 5.95 (s, 2H), 5.50 (s, 2H).^{13}C NMR (125 MHz, Chloroform-*d*): δ 172.56, 167.36, 167.01, 152.24, 149.40, 149.10, 148.76, 141.64, 136.36, 126.87, 124.38, 124.28 (2C), 124.16, 110.27, 108.80, 101.50, 56.46, 41.10. ESI-MS, calcd for $C_{19}H_{14}N_6O_5$ 406.36; found m/z = 407.3 [M + H]$^+$.

1.19((1-((5-(pyridin-3-yl)-1,3,4-oxadiazol-2-yl)methyl)1H-1,2,3-triazol-4-yl)methyl-3-nitrobenzoate(SP-19)
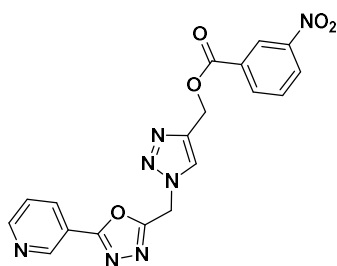
was obtained by following the general procedure as a pale yellow solid (68.2 mg, 82.2% yield after HPLC purification); RP-HPLC t_R = 23.4 min, gradient condition: from 5% B ending to 100 % B over 50 min, flow rate of 4 mL/min, λ = 254nm. ^{1}H NMR (300 MHz, Chloroform-*d*): δ 8.94 – 8.78 (m, 2H), 8.52 (d, J = 7.9 Hz, 1H), 8.48 – 8.34 (m, 2H), 8.03 (s, 1H), 7.66 (s, 2H), 5.95 (s, 2H), 5.50 (s, 2H). ^{13}C NMR (125 MHz, Chloroform-*d*): δ 167.50, 164.27, 158.52, 152.96, 147.97, 147.89, 143.47, 135.42, 134.58, 131.32, 129.77, 127.82, 124.63, 124.05, 123.60, 119.63, 58.37, 44.28. ESI-MS, calcd for $C_{18}H_{13}N_7O_5$ 407.35; found m/z = 408.3 [M + H]$^+$.

1.20 (1-((5-(pyridin-3-yl)-1,3,4-oxadiazol-2-yl)methyl)-1H-1,2,3-triazol-4-

yl)methylbenzo[d][1,3]dioxole-5-carboxylate (SP-20)
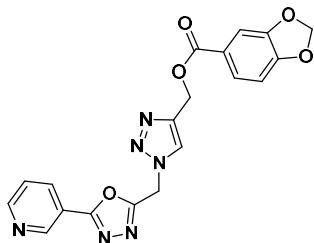
was obtained by following the general procedure as a yellow

solid (70.1 mg, 75.5% yield after HPLC purification); RP-HPLC t_R = 22.38 min, gradient

condition: from 5% B ending to 100 % B over 50 min, flow rate of 4 mL/min, λ = 254nm.

^{1}H NMR (500 MHz, Chloroform-*d*): δ 8.59 (d, J = 7.9 Hz, 2H), 7.99 (s, 1H), 7.66 (dd, J =

8.2, 1.7 Hz, 1H), 7.46 (d, J = 1.7 Hz, 1H), 6.84 (d, J = 8.2 Hz, 1H), 6.04 (s, 2H), 5.95 (s,

2H), 5.48 (s, 2H).^{13}C NMR (125 MHz, Chloroform-*d*): δ 172.56, 167.36, 167.01 , 152.24,

149.40, 149.10, 148.76, 141.64, 136.36, 126.87, 124.38, 124.28 (2C), 124.16, 110.27,

108.80, 101.50, 56.46, 41.10. ESI-MS, calcd for $C_{19}H_{14}N_6O_5$ 406.36; found m/z = 407.3

$[M + H]^+$.

CHAPTER 7

Discovery of new modulators of human Macrodomain protein MacroD1 by a fragment screening X-ray crystallography based approach: Experimental procedures

7.1.General methods

BL21 (DE3)-R3-pRARE (a phage-resistant derivative of Rosetta2) competent *E. coli* cells were purchased from Novagen. Ni-NTA sepharose gravity flow columns and size Exclusion Chromatography – S75 HiLoad 16/60 Superdex columns were from GE Healthcare Life Sciences and run on ÄKTA-Express system. SDS page was performed on ready made 18% polyacrylamide gels from Bio-Rad. Gelcode Blue stain and BCA Protein Assay Reducing Agent Compatible were from Pierce. All other chemicals were of reagent grade and obtained from common commercial sources.

Bacterial overexpression of Human MACROD1A

The His_6 tagged human MACROD1A (His_6-MACROD1A) was expressed from His_6-MACROD1A pNH-TrxTC-terminal His vector in E. coli BL21 (DE3) competent cells. A glycerol stock was used to inoculate a 10ml starter culture containing LB media with 50µg/ml Kanamycin + 34 µg/ml Chloramphenicol. The starter culture was grown overnight at 37°C with shaking at 200 rpm. The following morning, flasks containing 1L TB/Kanamycin were each inoculated with 3 ml of the starter culture. Cultures were incubated at 37°C with shaking at 170 rpm until an OD600nm ≥ 1.4 was reached. The flasks were then cooled down to 18°C and 0.4 mM Isopropyl β-D-1 thiogalactopyranoside (IPTG) added to induce protein expression overnight at OD600nm ≥ 2.0. Cells were harvested by centrifugation at 5000 rpm at 4°C for 15 min. Cell pellets from each flask were resuspended in 15ml Binding buffer (50mM HEPES, pH 7.5; 500mM NaCl; 5% Glycerol; 5mM Imidazole; 0.5mM TCEP; 1:2000 Protease Inhibitor Cocktail) and frozen at -20°C.

Preparation of whole cell extract

The frozen cells were thawed. The cells were lysed by ultrasonication over 15 min with the sonicator pulsing ON for 5 sec and OFF for 10. A final concentration of 0.15% polyethylenimine (PEI) was added to the lysate. The cell lysate was spun

down by centrifugation at 22 K rpm at 4°C for 1 h. The supernatant was recovered for purification.

IMAC (Immobilized metal affinity chromatography)

Recombinant Human His$_6$-MACROD1A was purified first by Immobilized metal ion affinity chromatography (IMAC) carried out in a cold room: 5 ml of 50 % Ni-sepharose slurry was applied onto a 1.5 x 10 cm column. The column was equilibrated with binding buffer (50 mM Hepes, pH 7.5; 500 mM NaCl; 5% Glycerol; 5 mM imidazole; 0.5mM Tris-(2-chloroethyl)-phosphate (TCEP). The supernatant following centrifugation was applied by gravity flow onto the Ni-sepharose column. The bound protein was then washed with 50ml binding buffer and subsequently with 30 ml wash buffer (50 mM Hepes, pH 7.5; 500 mM NaCl; 5% Glycerol; 30 mM imidazole 0.5mM TCEP). MACROD1A protein was then eluted by applying a step gradient of imidazole – using 5 ml portions of elution buffer (50 mM HEPES, pH 7.5; 500 mM NaCl; 5% Glycerol; 50, 100, 150 and 250 mM imidazole 0.5mM TCEP) with increasing concentration of imidazole (1 x 50 mM, 1 x 100 mM, 1 x 150 mM and 2 x 250 mM). Fractions were analyzed by SDS PAGE and the first, second, third & fourth elution fractions were kept and pooled.

Enzymatic treatment: TEV protease cleavage

The elute fractions containing MACROD1A were treated with *Tobacco Etch Virus nuclear-inclusion-a endopeptidase* TEV protease and dialyzed against GF buffer (300 mM NaCl, 50 mM HEPES pH 7.5, 0.5 mM TCEP, pH 7.5, 5% glycerol) overnight at 4°C.

Nickel rebinding chromatography

Ni-Affinity Chromatography: 1 ml of 50 % Ni-sepharose slurry was applied onto a 1.0 x 10 cm column. The column was equilibrated with binding buffer (15ml). Carried out at room temperature, with fractions stored on ice immediately following

collection. The pooled fractions from gel filtration were applied by gravity flow onto the Ni-sepharose column and flow-through collected. The column was then washed with 4ml wash buffer and subsequently with 5ml elution buffer. Fractions were analyzed by SDS PAGE and the flow-through containing MacroD1A was stored.

Size-exclusion chromatography (SEC)

Size Exclusion Chromatography – S75 HiLoad 16/60 Superdex run on ÄKTA-Express. Column stored in a cold room. The Superdex S75 column was first equilibrated with Gel Filtration buffer. The protein fraction from above step was concentrated to <5ml using a centrifugal filter with a 30kDa cut-off, before being syringe injected onto the column through 0.2µM pore filter and eluted with Gel Filtration buffer. Fractions containing the target protein were pooled together.

Fractions Pooling, Mass Spec and Concentration

The fractions containing the target protein from gel filtration were pooled together. A Mass spectrometry was run on Agilent 6530 QTOFmass spectrometer for the pooled sample concentrated in a 10 KD MW cutoff spin concentrator. The concentrated samples were aliquoted in PCR tubes and kept in -80°C.

Gel Electrophoresis and Western Blotting

SDS-PAGE was performed in 18% polyacrylamide gels. Protein bands were detected by Gelcode Blue Coomassie stain.High Resolution Clear Native Electrophoresis (hrCNE) was performed on 4-16% Bis-Tris Glycine gels using sodium deoxycholate (0.05%) and Triton X-100 (0.05%) in place of Comassie Brilliant Blue G-250 in cathode buffers.

Expressed protein sequence

AMAAKVDLSTSTDWKEAKSFLKGLSDKQREEHYFCKDFVRLKKIPTWKE
MAKGVAVKVEEPRYKKDKQLNEKISLLRSDITKLEVDAIVNAANSSLLGG
GGVDGCIHRAAGPLLTDECRTLQSCKTGKAKITGGYRLPAKYVIHTVGPI
AYGEPSASQAAELRSCYLSSLDLLLEHRLRSVAFPCISTGVFGYPCEAAAEI
VLATLREWLEQHKDKVDRLIICVFLEKDEDIYRSRLPHYFPVA.

MacroD1 Crystallization

The protein was concentrated to 22mg/mL. We pipetted 20 uL screen into 2 x CI plates. The plates were then sealed and refrigerated until use. We used Mosquito Crystal robots (http://www.ttplabtech.com) (3-drop CI method) to set up sitting drops: 2:1, 1:1, 1:2 ratios. Total drop volume was 150 nL. The plates were sealed and incubated at, 4 °C and 20°C, with drops automatically imaged at fixed time intervals by Minstrel HT(http://www.rigaku.com) systems and at at room temperature. Crystals grew under multiple conditions using freshly prepared protein. The best-diffracting crystals of the MACROD1A were obtained using a reservoir solution containing 0.1M malic acid (DL-), 21% PEG3350 1:1 with MACROD1A. Crystals were then flash frozen in liquid nitrogen.

7.2. Fragment screening general methods

Compounds Soaking

All compounds of DSPL1 (Diamond-SGC Poised Fragment Library v1.0) were dissolved in DMSO at a nominal concentration of 200mM. It should be noted that not all compounds could be dissolved at such high concentrations, but in this case we assumed that the solution was saturated; 600nl of each compound was mixed with 600nl of reservoir solution and the mixture was added to the crystals by using a Mosquito® crystallization robot (TTP Labtech). The plates were resealed and incubated for at least 12 hours at 4°C before the crystals were mounted in nylon loops and immediately flash frozen in liquid nitrogen.

Data Collection and Structure Solution

X-ray diffraction data were collected on beamline I04-1 at Diamond Light Source using monochromatic radiation at wavelength 0.9795 Å. Crystals belonged to spacegroup P212121 with unit cell parameters a=61.8 Å b=55.05 Å c=86.57 Å, α=90° β= 104.44 γ= 90° a and were processed using the Diamond autoprocessing pipeline, which utilizes xia2, DIALS, XDS, POINTLESS and CCP4. Electron-density maps were generated using XChemExplorer via DIMPLE. Ligand restraints were generated with AceDRG and ligand binding was detected with PanDDA with ligands built into PanDDA event maps. Three molecules were present in the asymmetric unit. Once a hit was identified, further rounds of refinement with REFMAC24 and manual rebuilding with COOT were carried out. ACEDRG22 was used to generate compound coordinates and restraint files. The quality of the final models was validated with MOLPROBITY.

Bacterial overexpression of MacroD1A biotinylated protein.

The His$_6$ tagged human MACROD1A (His$_6$-MACROD1A) was expressed from His$_6$-MACROD1A pNH-TrxTC-terminal His vector in E. coli BL21 (DE3) competent cells. A glycerol stock was used to inoculate a 10ml starter culture containing LB media with 50μg/ml Kanamycin + 34 μg/ml Chloramphenicol and 50μg/ml Streptomycin. The starter culture was grown overnight at 37°C with shaking at 200 rpm. The following morning, flasks containing 1L TB/Kanamycin were each inoculated with 3 ml of the starter culture. Cultures were incubated at 37°C with shaking at 170 rpm until an OD 600nm ≥ 1.4 was reached. The flasks were then cooled down to 18°C and 0.4 mM Isopropyl β-D-1 thiogalactopyranoside (IPTG) and 0.2 mM biotin added for the BirA cultures. (Added 20 ml of 10 mM biotin in 10 mM bicine pH 8.3 to each 1L culture) added to induce protein expression overnight at OD 600nm ≥ 2.0. Cells were harvested by centrifugation at 5000 rpm at 4°C for 15 min. Cell pellets from each flask were resuspended in 15ml Binding buffer (50mM HEPES, pH 7.5; 500mM NaCl; 5% Glycerol; 5mM Imidazole; 0.5mM TCEP; 1:2000 Protease Inhibitor Cocktail) and frozen at -20°C.

Preparation of whole cell extract

The frozen cells were thawed. The cells were lysed by ultrasonication over 15 min with the sonicator pulsing ON for 5 sec and OFF for 10. A final concentration of 0.15% polyethylenimine (PEI) was added to the lysate. The cell lysate was spun down by centrifugation at 22 K rpm at 4°C for 1 h. The supernatant was recovered for purification.

IMAC (Immobilized metal affinity chromatography)

Recombinant Human His_6-biotinyl-MACROD1A was purified first by Immobilized metal ion affinity chromatography (IMAC) carried out in a cold room: 5 ml of 50 % Ni-sepharose slurry was applied onto a 1.5 x 10 cm column. The column was equilibrated with binding buffer (50 mM Hepes, pH 7.5; 500 mM NaCl; 5% Glycerol; 5 mM imidazole; 0.5mM Tris-(2-chloroethyl)-phosphate (TCEP). The supernatant following centrifugation was applied by gravity flow onto the Ni-sepharose column. The bound protein was then washed with 50ml binding buffer and subsequently with 30 ml wash buffer (50 mM Hepes, pH 7.5; 500 mM NaCl; 5% Glycerol; 30 mM imidazole 0.5mM TCEP). MACROD1A protein was then eluted by applying a step gradient of imidazole – using 5 ml portions of elution buffer (50 mM HEPES, pH 7.5; 500 mM NaCl; 5% Glycerol; 50, 100, 150 and 250 mM imidazole 0.5mM TCEP) with increasing concentration of imidazole (1 x 50 mM, 1 x 100 mM, 1 x 150 mM and 2 x 250 mM). Fractions were analyzed by SDS PAGE and the first, second, third & fourth elution fractions were kept and pooled.

Enzymatic treatment: TEV protease cleavage

The elute fractions containing MACROD1A were treated with Tobacco Etch Virus nuclear-inclusion- endopeptidase TEV protease and dialysed against GF buffer (300 mM NaCl, 50 mM HEPES pH 7.5, 0.5 mM TCEP, pH 7.5, 5% glycerol) overnight at 4°C.

Nickel rebinding chromatography

Ni-Affinity Chromatography: 1 ml of 50 % Ni-sepharose slurry was applied onto a 1.0 x 10 cm column. The column was equilibrated with binding buffer (15ml). Carried out at room temperature, with fractions stored on ice immediately following collection. The pooled fractions from gel filtration were applied by gravity flow onto the Ni-sepharose column and flow-through collected. The column was then washed with 4ml wash buffer and subsequently with 5ml elution buffer. Fractions were analyzed by SDS PAGE and the flow-through containing MacroD1A was stored.

Size-exclusion chromatography (SEC)

Size Exclusion Chromatography – S75 HiLoad 16/60 Superdex run on ÄKTA-Express. Column stored in a cold room. The Superdex S75 column was first equilibrated with Gel Filtration buffer. The protein fraction from above step was concentrated to <5ml using a centrifugal filter with a 30kDa cut-off, before being syringe injected onto the column through 0.2µM pore filter and eluted with Gel Filtration buffer. Fractions containing the target protein were pooled together.

Fractions Pooling, Mass Spec and Concentration

The fractions containing the target protein from gel filtration were pooled together. A Mass spectrometry was run on Agilent 6530 QTOF mass spectrometer for the pooled sample concentrated in a 10 KD MW cutoff spin concentrator. The concentrated samples were aliquoted in PCR tubes and kept in -80°C. MACROD1A-construct protein mass is 28927.3, and the observed mass was 29153.6 (=+226.3).4.

Gel Electrophoresis and Western Blotting

SDS-PAGE was performed in 18% polyacrylamide gels. Protein bands were detected by Gelcode Blue Coomassie stain.High Resolution Clear Native Electrophoresis (hrCNE) was performed on 4-16% Bis-Tris Glycine gels using sodium deoxycholate (0.05%) and Triton X-100 (0.05%) in place of Comassie Brilliant Blue G-250 in cathode buffers.

7.3. SPR General methods

Recombinant human biotinyl-MacroD1 was previously expressed and SPR analyses were carried out according to our previously SPR published data.[210] Surface Plasmon Resonance Spectroscopy (SPR) analyses were performed to determine binding of various molecules to MacroD1 protein using a Biacore 3000 optical biosensor equipped with research-grade SA sensor chips (GE Healthcare). Biotnyl-MacroD1 was coupled to the surface of a SA sensor chip using standard biotinylated ligand-coupling protocols, according to the manufacturer's instructions. Biotinylated ligand is immobilized on Sensor Chip SA by non-covalent capture (binding to streptavidin). The protein (100 µg mL−1 in 10 mM PBS, pH 7.4) was immobilized on individual sensor chip surfaces at a flow rate of 10 µL min−1 to obtain densities of 8–12 kRU, with 1 minute of contact time. For the experiments a recombinant biotinyl-MacroD1 surface, a BSA surface and one unmodified reference surface were prepared for simultaneous analyses. Compounds **1-3** were dissolved, to obtain 500 mM solutions, in 100% DMSO and diluted 1:200 (v/v) in PBS (10 mM NaH_2PO_4, 150 mM NaCl, pH 7.4) to a final DMSO concentration of 5%. For each molecule a six-point concentration series were set up, spanning 0 – 0.31 – 0.625 – 1.25 – 2.5 mM, and for each sample the complete binding study was performed using triplicate aliquots. Whereas compounds **LA1-LA7** were dissolved, to obtain 50 mM solutions, in 100% DMSO and diluted 1:1000 (v/v) in PBS (10 mM NaH_2PO_4, 150 mM NaCl, pH 7.4) to a final DMSO concentration of 0.1%. For each molecule a five-point concentration series were set up, spanning 0–6–12–25–and 50 µM. Changes in mass, due to the binding response,

were recorded as resonance units (RU). To obtain the dissociation constant (K_D) these responses were fit to a 1:1 Langmuir binding model by nonlinear regression using the BiaEvaluation software program provided by GE Healthcare. Simple interactions were suitably fitted to a single-site bimolecular interaction model (A + B = AB), yielding a single K_D. SPR experiments were performed at 25 °C, using a flow rate of 15 µL min−1, with 60 s monitoring of association and 300 s monitoring of dissociation.

7.4. General synthetic methods

All commercially available starting materials were purchased from Sigma- Aldrich and were used as received. Solvents used for the synthesis were of HPLC grade and were purchased from Sigma-Aldrich or VWR. NMR spectra were recorded on Bruker Advance 400 or 300 MHz instruments. Compounds were dissolved in 0.5 ml of CD_3OD, or $CDCl_3$.Coupling constants (J) are reported in Hertz, and chemical shifts are expressed in parts per million (ppm) on the delta (δ) scale relative to the solvent peak as internal reference. Multiplicities are reported as follows: s, singlet; d, doublet; t, triplet; m, multiplet; dd, doublet of doublets. Electrospray mass spectrometry (ESI-MS) was performed on a LCQ DECA TermoQuest (San Josè, California, USA) mass spectrometer. Chemical reactions were monitored on silica gel 60 F254 plates (Merck) and spots were visualized under UV light. Analytical and semi-preparative reversed-phase HPLC were performed on an Agilent Technologies 1200 Series high performance liquid chromatography system using a Nucleodur, C8 reversed-phase column (100 x 2mm, 4µM, 80 Å, flow rate = 1 mL/min; 250 x 10.00mm, 4µM, 80 Å, flow rate = 4 mL/min respectively, Phenomenex ®). The binary solvent system (A/B) was as follows: 0.1% TFA in water (A) and 0.1% TFA in CH_3CN (B). Absorbance was detected at 240 nm. The purity of all tested compound (> 95%) was determined by HPLC analysis. All microwave irradiation experiments were carried out in a dedicated CEM-Discover® Focused Microwave Synthesis apparatus, operating with continuous irradiation power from 0 to 300 W utilizing the standard absorbance level of 300 W maximum power. The reactions were carried out in 10 mL sealed microwave glass vials. The DiscoverTM system also offers controllable ramp time, hold time

(reaction time) and uniform stirring. The temperature was monitored using the CEM-Discover built-in-vertically focused IR temperature sensor. After the irradiation period, the reaction vessel was cooled rapidly (60-120 s) to ambient temperature by air jet cooling.

7.5. Methods and materials

Scheme 1. General method for the Synthesis of compounds LA1-LA5

A) *Suzuki-Miyaura cross-coupling for the synthesis of LA1-LA4*
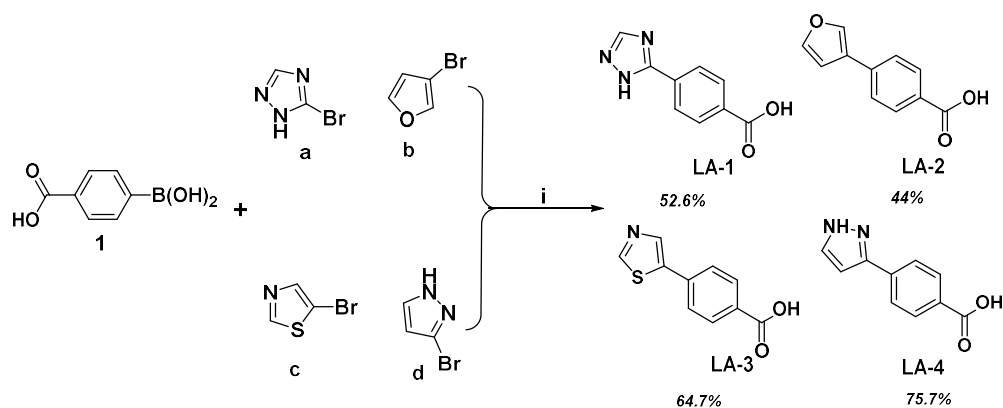
Carboxy-phenyl boronic acid (**1**) (50.0 mg, 1 eq.), commercially available heteroaryl-bromides (**a-d**, 0.8 eq), Pd(OAc)$_2$ (0.04 eq.), P(C$_6$H$_4$SO$_3$Na)$_3$ (0.2 eq.) and Cs$_2$CO$_3$ (2.4 eq.) were added to a 10 ml microwave vial equipped with a magnetic stirrer. The vial was evacuated and backfilled with nitrogen three times. Degassed acetonitrile (0.5 ml) and degassed water (1.0 ml) were added by means of an air-tight syringe. The mixture was heated under microwave irradiation at 150 ºC for 5-15 min. After irradiation, the vial was cooled to ambient temperature by air jet cooling and a mixture of cold water and 1.5 M HCl were added (5.0 and 2.0 ml, respectively). The mixture was subsequently poured into crushed ice and then left at 4 ºC overnight. The resulting precipitate was filtered and purified by HPLC

to give the desired product in good yields (52-75%). HPLC purification was performed by semi-preparative reversed-phase HPLC using the gradient conditions reported below for each compound.

B) Suzuki-Miyaura cross-coupling for the synthesis of LA-5
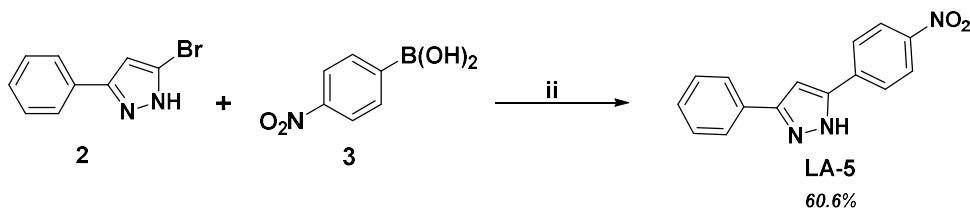
5-bromo-3-phenyl-1H-pyrazole (**2**) (50.0 mg, 0.8 eq.) and commercially available 4-nitrophenylboronic acid (**3**) (1 eq.), Pd(OAc)$_2$ (0.04 eq.), P(C$_6$H$_4$SO$_3$Na)$_3$ (0.2 eq.) and Cs$_2$CO$_3$ (2.4 eq.) were added to a 10 ml microwave vial equipped with a magnetic stirrer. The vial was evacuated and backfilled with nitrogen three times. Degassed acetonitrile (0.5 ml) and degassed water (1.0 ml) were added by means of an air-tight syringe. The mixture was heated under microwave irradiation at 150 ºC for 5 min. After irradiation, the vial was cooled to ambient temperature by air jet cooling and a mixture of cold water and 1.5 M HCl were added (5.0 and 2.0 ml, respectively). The mixture was subsequently poured into crushed ice and then left at 4 ºC overnight. The resulting precipitate was filtered and purified by HPLC to give the desired product in good yields (60.6%). HPLC purification was performed by semi-preparative reversed-phase HPLC using the gradient conditions reported below for each compound.

Scheme 2. General method for the Synthesis of compounds LA6-LA7

Suzuki-Miyaura cross-coupling
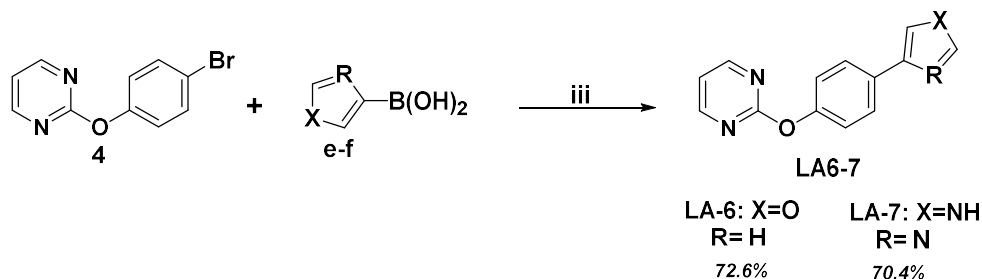
A solution of furan-3 boronic acid (**e**) (1.2 eq.) and thiazol-4-ylboronic acid (**f**) (1.2 eq) in methanol (0.6 mL) was added to a solution of 2-(4-bromophenoxy) pyrimidine (**4**) (1 eq.), Pd(PPh₃)₄ (4 mol%) and sodium carbonate (2.2 eq.) in a toluene/water-mixture (2:1). The reaction mixture was stirred for 16 h at 80 °C. The reaction course was monitored by TLC and, once it was completed, the mixture was diluted with dichloromethane and the aqueous layer was washed with brine, dried over Na₂SO₄, filtered and concentrated under reduced pressure. The resulting crude product was purified by HPLC to give the desired product in good yields (70-72%). HPLC purification was performed by semi-preparative reversed-phase HPLC using the gradient conditions reported below for each compound.

1.1 *4-(1H-1,2,4-triazol-5-yl)benzoic acid (LA-1)*
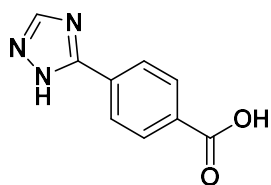
was obtained by following the general procedure as a white powdery solid (30 mg, 55.6% yield after HPLC purification); RP-HPLC t_R = 22.03 min,

gradient condition: from 5% B ending to 100 % B over 54 min, flow rate of 4 mL/min, λ = 240 nm. ^{1}H NMR (300 MHz, Methanol-d_4): δ 8.43 (s, 1H), 7.89 (d, J = 4.0 Hz, 2H), 6.83 (d, J = 5.5 Hz, 2H).^{13}C NMR (101 MHz, Methanol-d_4): δ 168.14, 151.62, 149.30, 130.96 (2C), 128.61 (2C), 127.61, 126.71. ESI-MS, calcd for $C_9H_7N_3O_2$ 189.17; found m/z = 188.1 [M-H]$^{\cdot}$

1.2 *4-(furan-3-yl) benzoic acid (LA-2)*
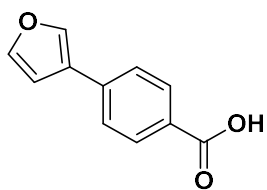

was obtained by following the general procedure as a white powdery solid (153,7 mg, 63% yield after HPLC purification); RP-HPLC t_R = 29.58 min, gradient condition: from 5% B ending to 100% B over 40 min, flow rate of 4 mL/min, λ = 240 nm. ^{1}H NMR (300 MHz, Methanol-d_4): δ 8.04 (d, J = 8.4 Hz, 1H), 7.72 – 7.59 (m, 3H), 7.61 (d, J = 1.9 Hz, 2H), 6.90 (d, J = 1.9 Hz, 1H).^{13}C NMR (125 MHz, Methanol-d_4): δ 168.10, 145.13, 142.53, 141.08, 131.20 (2C), 128.98, 126.07, 123.93, 108.93, 106.8. ESI-MS, calcd for $C_{11}H_8O_3$ 188.18; found m/z = 187.1 [M - H].

1.3. *4-(thiazol-5-yl)benzoic ac**id** (LA-3)*
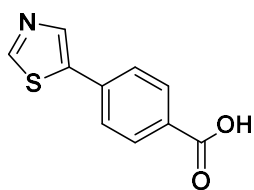
was obtained by following the general procedure as a pale yellow solid (91,8 mg, 60% yield after HPLC purification); RP-HPLC t_R = 21.44 min, gradient condition: from 5% B ending to 100% B over 40 min, flow rate of 4 mL/min, λ = 240nm. ^{1}H NMR (300 MHz, Methanol-d_4): δ 8.92 (s, 1H), 8.18 (s, 1H), 7.97 (d, J = 8.1 Hz, 2H), 7.65 (d, J = 7.9 Hz, 2H).^{13}C NMR (125 MHz, Methanol-d_4): δ 168.14, 152.00, 140.88,

137.49, 135.46, 131.15, 130.3 (2C), 125.10 (2C). ESI-MS, calcd for $C_{10}H_7NO_2S$ 205.23; found m/z = 204.5 [M-H].

1.4 *4-(1H-pyrazol-3-yl) benzoic acid (LA-4)*
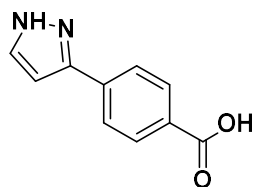
 was obtained by following the general procedure as a white powdery solid (85.9 mg, 75.7% yield after HPLC purification); RP-HPLC t_R = 16.63 min, gradient condition: from 5% B ending to 100 % B 4 min, flow rate of 4 mL/min, λ = 240 nm. ^{1}H NMR (500 MHz, Methanol-d_4): δ 8.20 (d, J = 7.9 Hz, 2H), 7.66 (d, J = 7.5 Hz, 2H), 7.30 (d, J = 7.5 Hz, 1H), 6.71 (d, J = 7.5 Hz, 1H); ^{13}C NMR (125 MHz, Methanol-d_4): δ 168.14, 147.63, 133.65, 131.28, 129.89 (2C), 127.35, 126.45 (2C), 101.95. ESI-MS, calcd for $C_{10}H_8N_2O_2$ 188.19; found m/z = 187.1 [M - H].

1.5 *5-(4-nitrophenyl)-3-phenyl-1H-pyrazole (LA-5)*
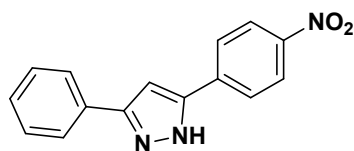
 was obtained by following the general procedure as white solid (86 mg, 70% yield after HPLC purification); RP-HPLC t_R = 25.9 min, gradient condition: from 5% B ending to 100 % B over 50 min, flow rate of 4 mL/min, λ = 240 nm. ^{1}H NMR (400 MHz, Chloroform-d): δ 8.32 (d, 2H), 8.17 – 8.11 (m, 2H), 7.83 (d, J = 7.3 Hz, 2H), 7.53 – 7.47 (m, 3H), 7.41 (s, 1H); ^{13}C NMR (125 MHz, Chloroform-d): δ 148.05, 147.78, 146.89, 135.16, 131.89, 129.48, 128.25 (2C), 127.58 (2C), 125.55 (2C), 124.29 (2C), 99.96. ESI-MS, calcd for $C_{15}H_{11}N_3O_2$ 265.27; found m/z = 266.2 [M + H]$^+$.

1.6 (2-(4-(furan-3-yl)phenoxy)pyrimidine (LA-6)
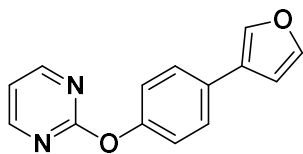
was obtained by following the general procedure as a white solid (50.2 mg, 45% yield after silica chromatography column purification);. ^{1}H NMR (300 MHz, Chloroform-*d*): δ 8.42 (d, J = 4.9 Hz, 2H), 7.76 (s, 1H), 7.52 (d, J = 7.7 Hz, 3H), 7.40 (t, J = 6.8 Hz, 2H), 7.29 (t, J = 6.8 Hz 1H), 6.73 (t, J = 6.8 Hz, 1H); ^{13}C NMR (125 MHz, Chloroform-*d*): δ 166.31, 160.60 (2C), 149.59, 144.70, 140.30, 135.02, 127.99 (2C), 127.58 , 121.82 (2C), 117.40, 109.00. ESI-MS, calcd for $C_{14}H_{10}N_2O_2$ 238.07; found m/z = 239.1 $[M+H]^+$.

1.7 *4-(4-(pyrimidin-2-yloxy)phenyl)isothiazole* (LA-7)
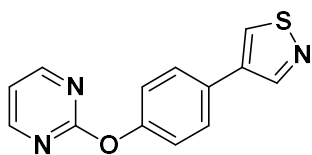
was obtained by following the general procedure as a brown solid (100 mg, 60% yield after silica chromatography column purification) .^{1}H NMR (400 MHz, Chloroform-*d*): δ 8.65 (d, J = 4.8 Hz, 2H), 7.91 – 7.76 (m, 3H), 7.30 – 7.19 (m, 3H), 6.71 (t, J = 6.8 Hz, 1H); ^{13}C NMR (125 MHz, Chloroform-*d*): δ 166.31, 160.60 (2C), 157.18, 149.53, 143.89, 141.59, 131.21, 128.43 (2C), 120.74 (2C), 117.40. ESI-MS, calcd for $C_{13}H_9N_3OS$; 255.09.; found m/z = 256.0 $[M+H]^+$.

CHAPTER 8

Design, synthesis and biological evaluation of the first BAG3 modulator as an attractive candidate for the development of a new class of chemotherapeutics: Experimental procedures

8.1 General synthetic methods

All commercially available starting materials were purchased from Sigma- Aldrich and were used as received. Solvents used for the synthesis were of HPLC grade and were purchased from Sigma-Aldrich or VWR. NMR spectra were recorded on Bruker Advance 400 or 300 MHz instruments. Compounds were dissolved in 0.5 ml of CD3OD or CDCl$_3$. Coupling constants (*J*) are reported in Hertz, and chemical shifts are expressed in parts per million (ppm) on the delta (δ) scale relative to the solvent peak as internal reference. Multiplicities are reported as follows: s, singlet; d, doublet; t, triplet; m, multiplet; dd, doublet of doublets. Electrospray mass spectrometry (ESI-MS) was performed on a LCQ DECA TermoQuest (San Josè, California, USA) mass spectrometer. Chemical reactions were monitored on silica gel 60 F254 plates (Merck) and spots were visualized under UV light. Analytical and semi-preparative reversed-phase HPLC were performed on an Agilent Technologies 1200 Series high performance liquid chromatography system using a Fusion-RP, C18 reversed-phase column (100 x 2mm, 4μM, 80 Å, flow rate = 1 mL/min; 250 x 10.00mm, 4μM, 80 Å, flow rate = 4 mL/min respectively, Phenomenex ®). The binary solvent system (A/B) was as follows: 0.1% TFA in water (A) and 0.1% TFA in CH$_3$CN (B). Absorbance was detected at 240 nm. The purity of all tested compound (> 95%) was determined by HPLC analysis.

8.2 Methods and materials

Scheme 1. General method for the Synthesis of compounds LK1-LK12

A) *Synthesis of 5-arylidene-thiazolidine-2,4-diones (2a-m) (Knoevenagel condensation)*
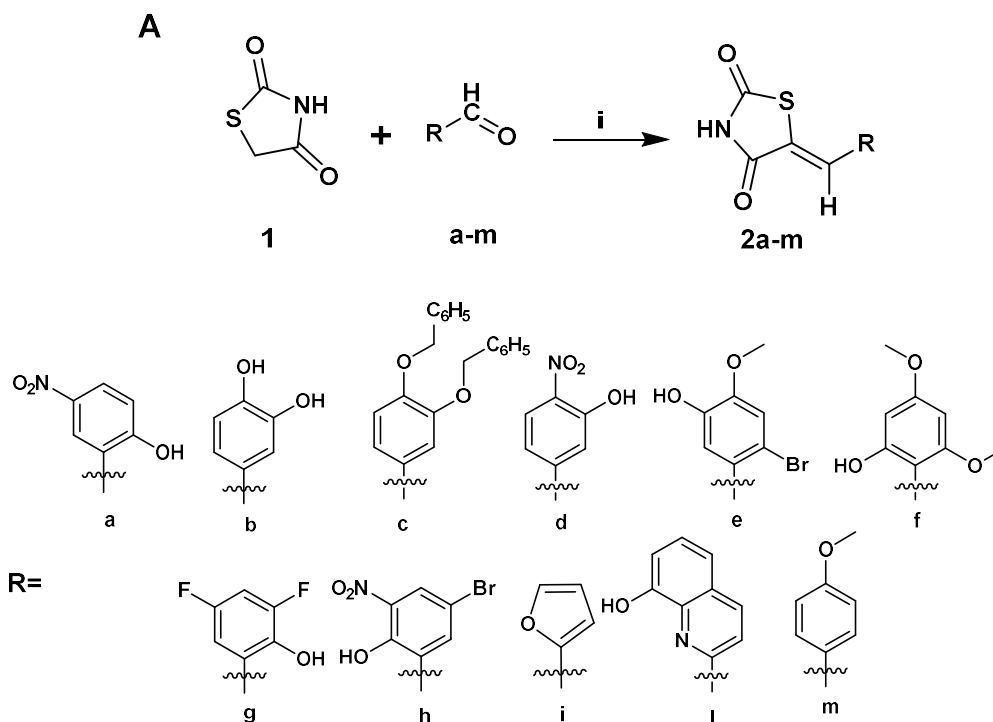
A mixture of thiazolidine-2,4-dione (**1**) (2.5 g, 1 eq.), aldehydes **a-m** (1 eq.), piperidine (0.5 eq.), and ethanol (150 mL) were placed in a 25 ml bottom flask. The reaction mixture was heated under reflux and continuously stirred for a period of 8-9 h. The course of the reaction was monitored by TLC. The reaction mixture was poured into water and acidified with acetic acid. The resulting precipitate was filtered off and recrystallized from acetic acid to give **2a–m**. HPLC purification was performed by semi-preparative reversed-phase HPLC (Fusion-RP, C18 reversed-phase column: 250 x 10.00mm, 4µM, 80 Å, flow rate = 4 mL/min) using the

gradient conditions reported below and the final products were characterized by ESI-MS and NMR spectra. (High purity> 97% detected by HPLC analysis)

B) *Synthesis of compounds LK1-LK12 and 3d*
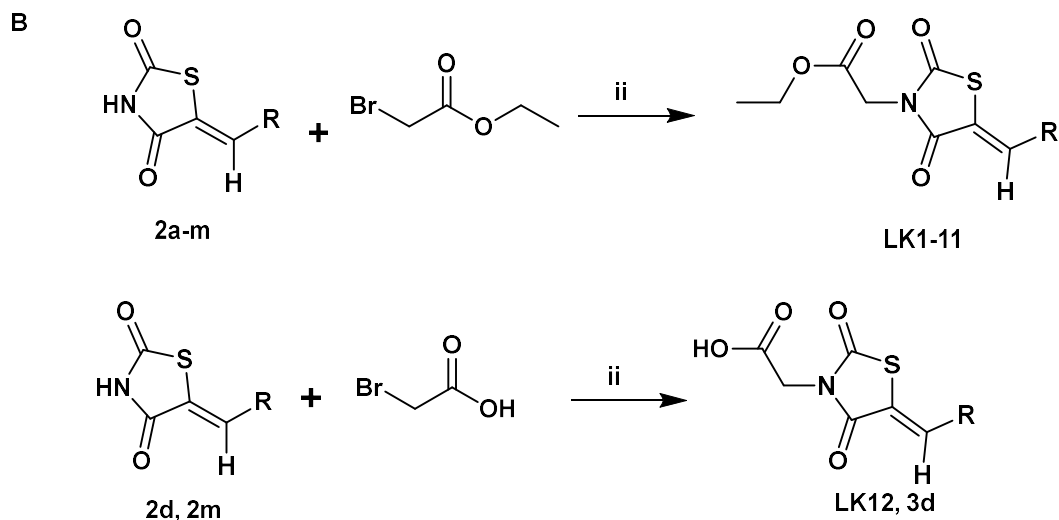
A 1 mmol (1 eq.) of **2a-m** was dissolved in DMF (3.5 mL), and fine disperse anhydrous sodium hydride (1.5 eq.) was added on ice. The mixture was stirred for 30 min and to the resulting suspension were added ethyl bromoacetate (1.1 eq.) or bromoacetic acid (1.1 eq.). The mixture was stirred at 80°C for 3 h. The reaction was monitored by TLC. After completion of the reaction, the reaction mass was poured into ice-cold water. The resulted precipitate was filtered, washed with water, dried, and then recrystallized from absolute methanol to give compounds **LK1-LK11** and **LK12**, **3d**. HPLC purification was performed by semi-preparative reversed-phase HPLC (Fusion-RP, C18 reversed-phase column: 250 x 10.00mm, 4μM, 80 Å, flow rate = 4 mL/min) using the gradient conditions reported below and

the final products were characterized by ESI-MS and NMR spectra (High purity> 97% detected by HPLC analysis).

Scheme 2. General method for the Synthesis of compounds LK13-LK17

A) Synthesis of compound LK-13
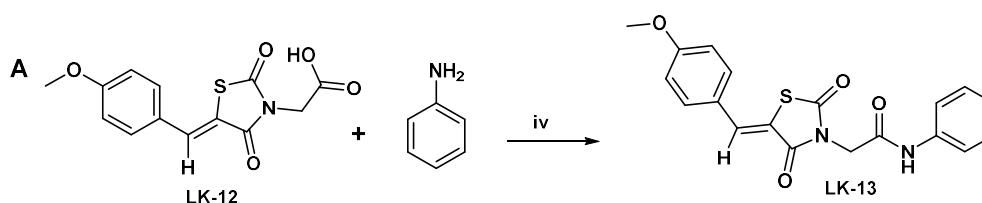
1 eq. (70 mg) of **LK-12** was dissolved in DCM (4 mL), and fine disperse phenylamine (2 eq.), hydroxybenzotriazole (1 eq.) and liquid *N,N'*-Diisopropylcarbodiimide (1.5 eq.) were added. The mixture was stirred overnight at room temperature to give the desired product. The reaction was monitored by TLC. After completation the reaction mixture was extracted with EtOAc and the organic phase was anhydrified with Sodium sulphate anhydrous and then evaporated under vacuum to give the crude product **LK-13**. HPLC purification was performed by semi-preparative reversed-phase HPLC (Fusion-RP, C18 reversed-phase column: 250 x 10.00mm, 4μM, 80 Å, flow rate = 4 mL/min) using the gradient conditions reported below and the final products were characterized by ESI-MS and NMR spectra (High purity> 97% detected by HPLC analysis).

B) Synthesis of compound LK-14
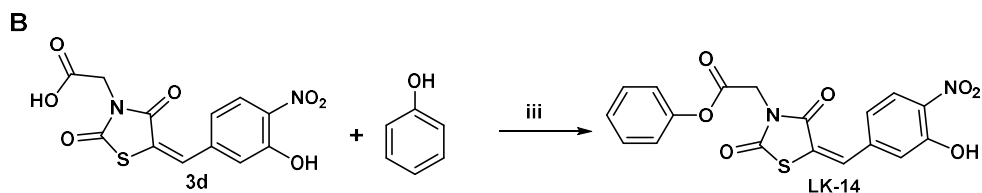
1 eq. (70mg) of **3d** was dissolved in DCM (4 mL), and fine disperse 4-dimethylaminopyridine (1 eq.), liquid phenol (1 eq.) and liquid *N,N'*-Diisopropylcarbodiimide (1 eq.) were added. The mixture was stirred overnight at room temperature to give the desired product. The reaction was monitored by TLC. After completion of the reaction, the mixture was filtered off in order to remove the precipitated *N,N'*-Dicyclohexylurea and the reaction mixture was extracted with EtOAc; the organic phase was anhydrified with Sodium sulphate anhydrous and then evaporated under vacuum to give the crude product **LK-14**. HPLC purification was performed by semi-preparative reversed-phase HPLC (Fusion-RP, C18 reversed-phase column: 250 x 10.00mm, 4μM, 80 Å, flow rate = 4 mL/min) using the gradient conditions reported below and the final products were characterized by ESI-MS and NMR spectra (High purity> 97% detected by HPLC analysis).

C) Synthesis of compounds LK15-LK17
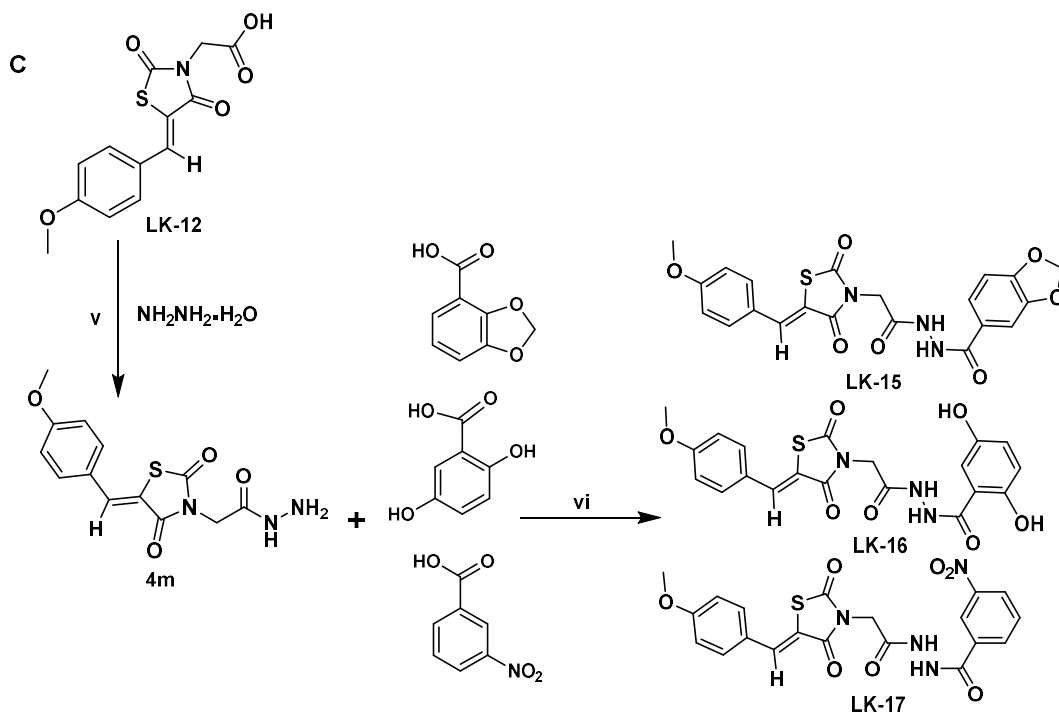
1 eq. (70 mg) of **LK-12** was dissolved in DCM (4 mL) and liquid Hydrazine hydrate (2 eq.), hydroxybenzotriazole (1 eq.) and liquid *N,N'*-Diisopropylcarbodiimide (1.5 eq.) were added. The mixture was stirred overnight at room temperature to give the desired product **4m**. The reaction was monitored by TLC. After completation the reaction mixture was extracted with EtOAc and the organic phase was anhydrified with Sodium sulphate anhydrous and then evaporated under vacuum. HPLC purification was performed by semi-preparative reversed-phase HPLC (Fusion-RP, C18 reversed-phase column: 250 x 10.00mm, 4μM, 80 Å, flow rate = 4 mL/min) using the gradient conditions reported below and the final products were characterized by ESI-MS and NMR spectra (High purity> 97% detected by HPLC

analysis). Then, 1 eq. (50mg) of **4m** was dissolved in DCM (4 mL), and fine disperse 4-dimethylaminopyridine (1 eq.), 1,3-benzodioxole-4-carboxylic acid (2 eq.); 2,5-Dihydroxybenzoic acid (2 eq.) or 3-nitrobenzoic acid (2 eq.) and liquid *N,N'*-Diisopropylcarbodiimide (1 eq.) were added. The mixture was stirred overnight at room temperature to give the desired products **LK15-LK17**. The reaction was monitored by TLC. After completion of the reaction, the mixture was filtered off in order to remove the precipitated *N,N'*-Dicyclohexylurea and the reaction mixture was extracted with EtOAc and the organic phase was anhydrified with Sodium sulphate anhydrous and evaporated under vacuum. HPLC purification was performed by semi-preparative reversed-phase HPLC (Fusion-RP, C18 reversed-phase column: 250 x 10.00mm, 4μM, 80 Å, flow rate = 4 mL/min) using the gradient conditions reported below and the final products were characterized by ESI-MS and NMR spectra (High purity> 97% detected by HPLC analysis).

1.1 Ethyl (Z)-2-(5-(5-hydroxy-2-nitrobenzylidene)-2,4-dioxothiazolidin-3-yl)acetate(LK-1)
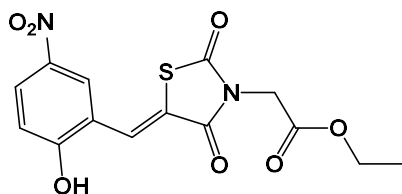
was obtained by following the general procedure as a pale brown powdery solid (75 mg, 44% yield after HPLC purification); RP-HPLC t_R = 32.6 min, gradient condition: from 5% B ending to 100 % B over 50 min, flow rate of 4 mL/min, λ = 240 nm. ^{1}H NMR (400 MHz, Chloroform-*d*): δ 8.24 (s, 1H), 8.10 (dd, *J* = 9.0, 2.6 Hz, 1H), 7.84 (s, 1H), 6.95 (d, *J* = 9.0 Hz, 1H), 4.44 (s, 2H), 4.21 (q, J = 7.1 Hz, 2H), 1.25 (t, J = 7.1 Hz, 3H).^{13}C NMR (101 MHz, Chloroform-*d*): δ 171.81, 166.86, 165.41, 162.81, 140.49, 127.73, 124.63, 124.18, 122.73, 120.82, 115.62, 61.89, 41.58, 13.08. ESI-MS, calcd for $C_{14}H_{12}N_2O_7S$ 352.32; found m/z = 351.2 [M -H]

1.2 Ethyl-(Z)-2-(5-(3-hydroxy-4-nitrobenzylidene)-2,4-dioxothiazolidin-3-yl)acetate (LK-2)
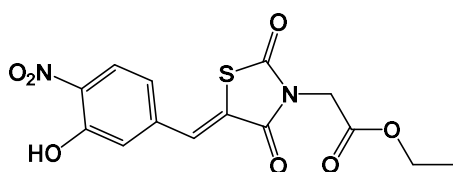
was obtained by following the general procedure as a pale yellow powdery solid (109.8 mg, 63.3% yield after HPLC purification); RP-HPLC t_R = 32.6 min, gradient condition: from 5% B ending to 100 % B over 50 min, flow rate of 4 mL/min, λ = 240 nm. ^{1}H NMR (400 MHz, Chloroform-*d*): δ 8.14 (d, J = 8.8 Hz, 1H), 7.77 (s, 1H), 7.22 (s, 1H), 7.05 (dd, J 8.8, 1.9, 1H), 4.42 (s, 2H), 4.19 (q, J = 7.1 Hz, 2H), 1.24 (t, J = 7.1 Hz, 3H). ^{13}C NMR (101 MHz, Chloroform-*d*): δ 171.81, 166.86, 165.41, 162.81, 140.49, 127.73, 124.63, 124.18, 122.73, 120.82, 115.62, 61.89, 41.58, 13.08. ESI-MS, calcd for $C_{14}H_{12}N_2O_7S$ 352.32; found m/z = 351.2 [M -H].

1.3 Ethyl-(Z)-2-(5-(3,4-bis(benzyloxy)benzylidene)-2,4-dioxothiazolidin-3-yl)acetate (LK-3)
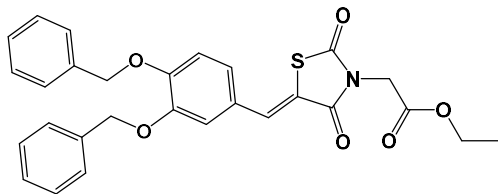
was obtained by following the general procedure as a grey solid (106.6 mg, 44% yield after HPLC purification); RP-HPLC t_R = 41.4 min, gradient condition: from 5% B ending to 100% B over 50 min, flow rate of 4 mL/min, λ = 240 nm. ^{1}H NMR (400 MHz, Chloroform-*d*): δ 7.72 (s, 1H), 7.40 – 7.34 (m, 3H), 7.34 – 7.23 (m, 7H), 7.02 – 6.97 (m, 2H), 6.92 (d, J = 8.4 Hz, 1H), 5.17 (d, J = 7.0 Hz, 4H), 4.38 (s, 2H), 4.17 (q, J = 7.1 Hz, 2H), 1.22 (t, J = 7.2 Hz, 3H). ^{13}C NMR (101 MHz, Chloroform-*d*): δ 171.79, 169.25, 169.13, 152.13, 148.91, 138.00, 135.19, 130.44, 128.53 (4C), 127.87 (2C), 127.20 (4C), 125.38, 115.98, 114.57, 114.28, 71.32 (2C), 62.15, 41.93, 29.69, 14.09. ESI-MS, calcd for $C_{28}H_{25}NO_6S$ 503.5; found m/z = 504.3 [M + H]$^+$.

1.4 Ethyl (Z)-2-(5-(3,4-dihydroxybenzylidene)-2,4-dioxothiazolidin-3-yl)acetate (LK-4)
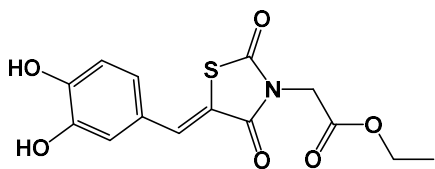
was obtained by following the general procedure as a bright yellow powdery solid (70 mg, 47% yield after HPLC purification); RP-HPLC t_R = 25.66 min, gradient condition: from 5% B ending to 100% B over 50 min, flow rate of 4 mL/min, λ = 240 nm. ^{1}H NMR (400 MHz, Chloroform-*d*): δ 7.81 (s, 1H), 7.06 (s, 1H), 7.02 (d, J = 8.1 Hz, 1 H), 6.90 (d, J=8.21 Hz, 1H), 4.41 (s, 2H), 4.19 (q, J = 7.1 Hz, 2H), 1.24 (t, J = 7.1 Hz, 3H). ^{13}C NMR (101 MHz, Chloroform-*d*): δ 170.32, 169.31, 169.11, 148.08, 145.97, 134.71, 125.12, 121.98, 119.89, 116.63, 116.34, 62.27, 29.69, 14.07. ESI-MS, calcd for $C_{14}H_{13}NO_6S$ 323.32; found m/z = 322.3 [M- H].

1.5 Ethyl (Z)-2-(5-(3-methoxybenzylidene)-2,4-dioxothiazolidin-3-yl)acetate (LK-5)
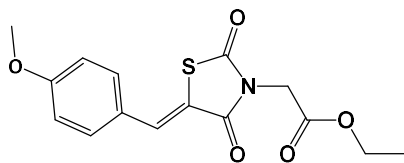
 was obtained by following the general procedure as

pale yellow solid (173.6 mg, 80% yield after HPLC purification); RP-HPLC t_R = 36.93

min, gradient condition: from 5% B ending to 100 % B over 50 min, flow rate of 4 mL/min,

λ = 240 nm. ^{1}H NMR (300 MHz, Chloroform-*d*): δ 7.96 (1 H, s), 7.62 (d, J= 9.5 Hz, 2H),

7.12 (d, J = 9.6 Hz, 2H), 4.17 (q, J = 7.1 Hz, 2H), 3.85 (s, 3H), 1.21 (t, J = 7.1 Hz, 3H). [13]C

NMR (125 MHz, Chloroform-*d*): δ 171.79, 169.25, 169.13, 159.84, 131.93, 130.90 (2C),

127.47, 122.27, 115.61(2C), 61.54, 55.35, 42.80, 14.13. ESI-MS, calcd for $C_{15}H_{15}NO_5S$

321.35; found m/z = 322.35 [M +H]$^+$;

1.6 Ethyl-(Z)-2-(5-(2-bromo-5-hydroxy-4-methoxybenzylidene)-2,4-dioxothiazolidin-3-yl)acetate (LK-6)
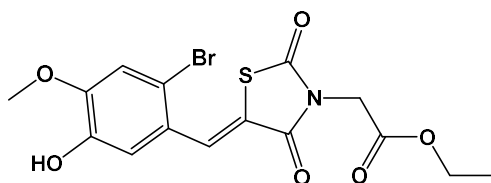
 was obtained by following the general

procedure as a pale yellow solid (124 mg, 60.5% yield after HPLC purification); RP-HPLC

t_R = 31.1 min, gradient condition: from 5% B ending to 100 % B over 50 min, flow rate of

4 mL/min, λ = 240 nm. ^{1}H NMR (300 MHz, Chloroform-*d*): δ 8.02 (s, 1H), 7.20 (s, 1H),

7.01 (s, 1H), 4.50 (s, 2H), 4.27 (q, J = 9.1 Hz, 2H), 3.98 (s, 3H), 1.32 (t, J = 7.1 Hz, 3H).

^{13}C NMR (125 MHz, Chloroform-*d*): δ 167.08, 166.70, 165.30, 150.40, 145.51, 132.41,

124.99, 120.91, 116.31, 116.03, 114.54, 61.69, 55.43, 41.61, 12.88. ESI-MS, calcd for

$C_{15}H_{14}BrNO_6S$ 416.24; found m/z = 415.2 [M -H].

1.7 *Ethyl-(Z)-2-(5-(5-hydroxy-2,4-dimethoxybenzylidene)-2,4-dioxothiazolidin-3-yl)acetate (LK-7)*
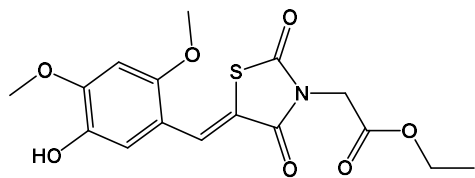
was obtained by following the general procedure as pale yellow solid (138.6 mg, 77% yield after HPLC purification); RP-HPLC t_R = 29.1 min, gradient condition: from 5% B ending to 100 % B over 50 min, flow rate of 4 mL/min, λ = 240 nm. ^{1}H NMR (300 MHz, Chloroform-*d*): δ 7.90 (s, 1H), 6.07 (s, 1H), 5.99 (s, 1H), 4.48 (s, 2H), 4.26 (q, J = 7.1 Hz, 2H), 3.88 (s, 3H), 3.84 (s, 3H), 1.31 (t, J = 7.2 Hz, 3H). ^{13}C NMR (125 MHz, Chloroform-*d*): δ 171.79, 169.25, 169.13, 166.30, 160.64, 158.66, 129.80, 125.53, 110.26, 97.44, 89.53, 61.54, 56.31, 55.87, 42.86, 14.13. ESI-MS, calcd for $C_{16}H_{17}NO_7S$ 367.37; found m/z = 366.3 [M–H].

1.8 *Ethyl-(Z)-2-(5-(5-bromo-2-hydroxy-3-nitrobenzylidene)-2,4-dioxothiazolidin-3-yl)acetate (LK-8)*
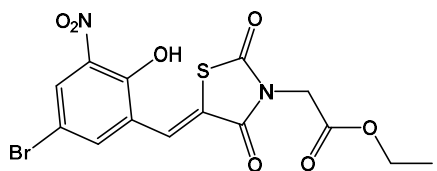
was obtained by following the general procedure as a pale grey solid (218.6 mg, 67% yield after HPLC purification); RP-HPLC t_R = 38.5 min, gradient condition: from 5% B ending to 100 % B over 50 min, flow rate of 4 mL/min, λ = 240 nm. ^{1}H NMR (300 MHz, Chloroform-*d*): δ 8.35 (d, J = 2.3 Hz, 1H), 7.99 (s, 1H), 7.85 (d, J = 2.3 Hz, 1H), 4.52 (s, 2H), 4.28 (q, J = 7.1 Hz, 2H), 1.33 (t, J = 7.1 Hz, 3H). ^{13}C NMR (125 MHz, Chloroform-*d*): δ 171.79, 169.25, 169.13, 158.74, 137.19, 135.17, 127.04, 124.55, 123.41, 122.03, 114.50, 61.54, 42.86, 14.13. ESI-MS, calcd for $C_{14}H_{11}BrN_2O_7S$ 431.21; found m/z = 454.2 [M + Na]$^+$.

1.9 Ethyl (Z)-2-(5-((8-hydroxyquinolin-2-yl)methylene)-2,4-dioxothiazolidin-3-yl)acetate (LK-9)
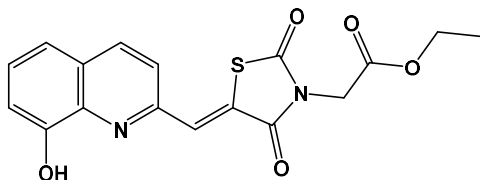
was obtained by following the general procedure as a yellow solid (135.2 mg, 77% yield after HPLC purification); RP-HPLC t_R = 30.5 min, gradient condition: from 5% B ending to 100 % B over 50 min, flow rate of 4 mL/min, λ = 240 nm. ^{1}H NMR (400 MHz, DMSO-d_6): δ 8.42 (d, J= 8.8, 4.7, 1H), 8.17 (s, 1H), 7.95 (d , J = 8.4, 4.6 Hz, 1H), 7.51 (t, J = 7.1 Hz, 1H), 7.43 (d, J = 2.3 Hz, 1H), 7.23 (d, J = 3.8 Hz, 1H), 4.51 (s, 2H), 4.18 (q, J= 7.1 Hz, 2H), 1.22 (t, J = 7.1 Hz, 3 H). ^{13}C NMR (125 MHz, DMSO-d_6): δ 167.46, 165.46, 154.37, 151.06, 138.21, 137.53, 129.71, 129.11 129.03, 126.81, 124.25, 122.24, 118.04, 111.66, 61.54, 42.86, 14.13. ESI-MS, calcd for $C_{17}H_{14}N_2O_5S$ 358.37; found m/z = 381.4 [M+Na]$^+$.

### 1.10 Ethyl (Z)-2-(5-(3,5-difluoro-2-hydroxybenzylidene)-2,4-dioxothiazolidin-3-yl)acetate (LK-10)
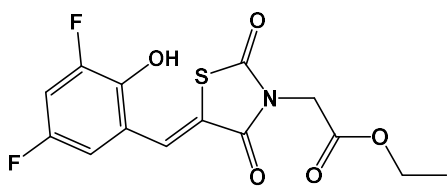
was obtained by following the general procedure as a white solid (63.3 mg 37.5% yield after HPLC purification); RP-HPLC t_R = 34.75 min, gradient condition: from 5% B to ending to 100 % B over 40 min, flow rate of 4 mL/min, λ = 240 nm. ^{1}H NMR (300 MHz, Acetone-d_6) δ 8.25 (s, 1H), 7.02 (s, 1H), 6.98(s, 1H), 4.51 (s, 2H), 4.28 (q, J = 7.1 Hz, 2H), 1.33 (t, J = 7.1 Hz, 3H). ^{13}C NMR (125 MHz, Acetone-d_6): δ 171.79, 169.25, 169.13, 158.74, 137.19, 135.17, 127.04, 124.55, 123.41, 122.03,

114.50, 61.54, 42.86, 14.13; ESI-MS, calcd for $C_{14}H_{11}F_2NO_5S$ 343.30; found m/z = 342.3 [M - H].

1.11 Ethyl (Z)-2-(5-(furan-2-ylmethylene)-2,4-dioxothiazolidin-3-yl)acetate (LK-11)
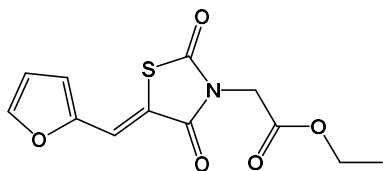

was obtained by following the general procedure as a white solid (74 mg, 53.3% yield after HPLC purification); RP-HPLC t_R = 28.9 min, gradient condition: from 5% B ending to 100 % B over 50 min, flow rate of 4 mL/min, λ = 240 nm. ^{1}H NMR (300 MHz, Acetone-d_6): δ 7.61 (d, J = 3.6 Hz, 1H), 7.22 (s, 1H), 6.74 (d, J = 3.6 Hz, 1H), 6.52 (t, J = 3.0, 1.4 Hz, 1H), 4.39 (s, 2H), 4.17 (q, J = 7.1, 1.1 Hz, 2H), 1.21 (t, J = 7.1 Hz, 3H). ^{13}C NMR (125 MHz, Acetone-d_6): δ 170.12, 169.25, 169.13, 149.56, 142.28, 124.45, 116.02, 111.23, 110.53, 61.54, 42.86, 14.13. ESI-MS calcd for $C_{12}H_{11}NO_5S$ 281.28; found m/z = 304.30 [M + Na]$^+$.

1.12 (Z)-2-(5-(3-methoxybenzylidene)-2,4-dioxothiazolidin-3-yl)acetic acid (LK-12)
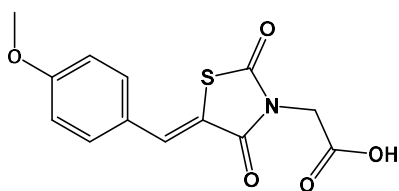
was obtained by following the general procedure as a yellow solid (38.6 mg, 35.6% yield after HPLC purification); RP-HPLC t_R = 28.10 min, gradient condition: from 5% B ending to 100 % B over 50 min, flow rate of 4 mL/min, λ = 240 nm. ^{1}H (300 MHz, Chloroform-d): δ 7.96 (1 H, s), 7.62 (d, J= 9.5 Hz, 2H), 7.12 (d, J = 9.6 Hz, 2H), 4.17 (s, 2H), 3.91 (s, 3H). ^{13}C NMR (125 MHz, Chloroform-d): δ 171.79, 170.00, 169.13, 159.84, 131.93, 130.90 (2C), 127.47, 122.27, 115.61 (2C), 55.35, 41.76. ESI-MS, calcd for $C_{13}H_{11}NO_5S$ 293.29; found m/z = 292.29 [M -H].

1.13 (Z)-N-benzyl-2-(5-(3-methoxybenzylidene)-2,4-dioxothiazolidin-3-yl)acetamide (LK-13)
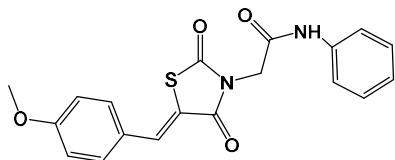
was obtained by following the general procedure as a light grey solid (108.7 mg, 83.3% yield after HPLC purification); RP-HPLC t_R = 42.3 min, gradient condition: from 5% B ending to 100 % B over 50 min, flow rate of 4 mL/min, λ = 240 nm. ^{1}H NMR (400 MHz, Chloroform-*d*): δ 7.76 (s, 1H), 7.55 – 7.48 (m, 4H), 7.31 (d, J = 9.5 Hz, 2H), 7.16–7.13(m, 1H), 7.00 (d, J = 8.4 Hz, 2H), 5.17 (s, 2H), 3.88 (s, 3H). ^{13}C NMR (101 MHz, Chloroform-*d*) δ 172.81, 171.79, 169.13, 168.99, 159.84, 138.94, 132.06 (2C), 129.12, 128.46, 123.49, 127.94 (2C), 119.81 (2C), 114.75 (2C), 55.50, 46.54. ESI-MS, calcd for $C_{19}H_{16}N_2O_4S$ 368.41; found m/z = 367.4 [M - H];

1.14 phenyl (Z)-2-(5-(3-hydroxy-4-nitrobenzylidene)-2,4-dioxothiazolidin-3-yl)acetate (LK-14)
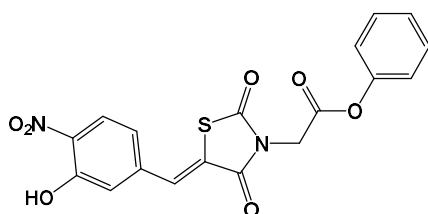
was obtained by following the general procedure as a yellow solid (123.2 mg, 99.7% yield after HPLC purification); RP-HPLC t_R = 34.44 min, gradient condition: from 5% B ending to 100 % B over 50 min, flow rate of 4 mL/min, λ = 240 nm. ^{1}H NMR (400 MHz, Chloroform-*d*): δ 8.10 (d, J = 8.8 Hz, 1H), 7.44 (s, 1H), 7.35 (d, J = 7.9 Hz, 1H), 7.28 (d, J = 1.9 Hz, 1H), 7.23 (t, J = 3.0, 1.4 Hz, 2H), 7.15 – 7.07 (m, 1H), 6.67 (d, J = 8.1 Hz, 2H), 4.34 (s, 2H). ^{13}C NMR (125 MHz, Chloroform-*d*): δ 171.79, 169.13, 168.84, 152.20, 150.66, 138.83, 136.03, 135.24, 130.44, 129.44, 125.12,

125.05, 124.49, 121.98 (2C), 119.87, 115.67, 43.39. ESI-MS, calcd for $C_{18}H_{12}N_2O_7S$ 400.36; found m/z = 423.4 [M + Na]$^+$.

1.15(Z)-N'-(2-(5-(3-methoxybenzylidene)-2,4-dioxothiazolidin-3-yl)etyl)benzo[d][1,3]dioxole-4-carbohydrazide (LK-15)
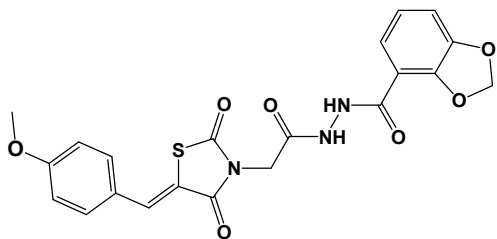
was obtained by following the general procedure as a white solid (110 mg, 74.2% yield after HPLC purification); RP-HPLC t_R = 32.1 min, gradient condition: from 5% B ending to 100 % B over 50 min, flow rate of 4 mL/min, λ = 240 nm. ^{1}H NMR (400 MHz, Methanol-d_4): δ 7.46 – 7.41 (m, 3H), 7.38 (d, J = 7.3 Hz, 1H), 7.27(s, 1H), 6.98 (d, J = 8.8 Hz, 2H), 6.91 (dd, J = 8.3, 4.1 Hz, 1H), 6.06 (d, J = 2.4 Hz, 2H), 4.45 (s, 2H), 3.81 (s, 3H). ^{13}C NMR (125 MHz, Methanol-d_4): δ 171.79 , 169.13, 167.79, 166.13, 159.84, 148.78, 148.56, 131.93, 130.90, 130.43 (2C), 127.47, 124.56, 120.72, 115.61, 114.78, 109.82, 107.72, 101.50, 55.35, 42.84. ESI-MS, calcd for $C_{21}H_{17}N_3O_7S$ 455.44; found m/z = 456.4 [M + H]$^+$.

1.16 (Z)-N'-(2-(5-(3-methoxybenzylidene)-2,4-dioxothiazolidin-3-yl)acetyl)-3-nitrobenzohy drazide (LK-16)
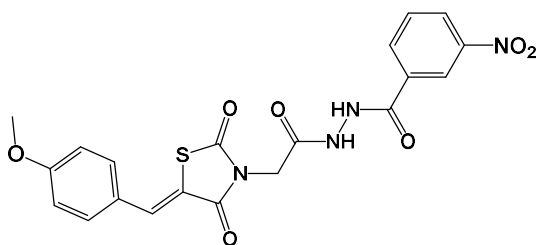
was obtained by following the general procedure as a yellow solid (69.4 mg, 46% yield after HPLC purification); RP-HPLC t_R = 29.9 min, gradient condition: from 5% B ending to 100 % B over 50 min, flow rate of 4

mL/min, λ = 240 nm. ^{1}H NMR (400 MHz, Methanol-d_4): δ 7.94 (s, 1H), 7.86 (d, J = 8.0, 1.7 Hz, 1H), 7.63 (d, J = 8.8 Hz, 2H), 7.44 (t, J = 8.31 Hz, 1H), 7.13 (d, J = 8.7 Hz, 2H), 6.96 (t, J = 7.5 Hz, 2H), 4.44 (s, 2H), 3.84 (s, 3H). ^{13}C NMR (125 MHz, Methanol-d_4): δ 171.79, 169.13, 167.79, 166.13, 159.84, 147.81, 134.05, 131.93, 130.90, 129.65, 129.33, 127.47, 125.58, 122.93, 120.72, 115.61 (2C), 114.78, 55.35, 42.84. ESI-MS, calcd for $C_{20}H_{16}N_4O_7S$ 456.43; found m/z = 457.43 $[M + H]^+$.

1.17 (Z)-2,5-dihydroxy-N'-(2-(5-(3-methoxybenzylidene)-2,4-dioxothiazolidin-3-yl)acetyl) benzohydrazide (LK-17)
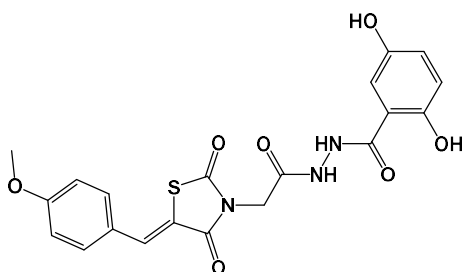

was obtained by following the general procedure as a pale grey solid (108 mg, 74.8% yield after HPLC purification); RP-HPLC t_R = 31.2 min, gradient condition: from 5% B ending to 100 % B over 50 min, flow rate of 4 mL/min, λ = 240 nm. ^{1}H (400 MHz, Methanol-d_4): δ 7.73 (s, 1H), 7.44 (dd, J = 6.3, 3.0 Hz, 2H), 7.24 (d, J = 3.1 Hz, 1H), 7.12 – 7.05 (m, 2H), 7.00 (dd, J = 8.9, 3.1 Hz, 1H), 6.89 (d, J = 8.9 Hz, 1H), 4.48 (s, 2H), 3.77 (s, 3H).^{13}C NMR (125 MHz, Methanol-d_4): δ 171.79, 169.13, 167.79, 163.78, 159.84, 156.62, 151.84, 131.93, 130.90, 129.65, 127.47, 121.00, 120.72, 118.97, 115.67, 115.61 (2C), 114.87, 55.35, 42.84. ESI-MS, calcd for $C_{20}H_{17}N_3O_7S$ 443.43; found m/z = 442.43 [M -H].

8.3 SPR General methods

Recombinant human r-BAG3 protein was previously expressed, r-BAG3 domain was purchased from ARETA International S.r.l., BAG1 and BAG4 human recombinant proteins were purchased from Abnova. SPR analyses were performed using a Biacore 3000 optical biosensor equipped with research-grade CM5 sensor chips (GE Healthcare). Using this platform, two separate recombinant rBAG proteins surfaces, a BSA surface and one unmodified reference surface were prepared for simultaneous analyses. Proteins (BAG3 and BAG3 domain 100 µg mL-1 in 10 mM CH_3COONa, pH 4.5, BAG1 100 µg mL-1 in 10 mM CH_3COONa, pH 7.2 and BAG4 100 µg mL-1 in 10 mM CH_3COONa, pH 4.5) were immobilized on individual sensor chip surfaces at a flow rate of 5 µL min-1 using standard amine-coupling protocols to obtain densities of 8–12 kRU. Commercially available compounds **1-26** were purchased from Otava Chemicals.

Commercially available compounds **1-26**, as well as synthetic compounds **LK1-LK17**, were dissolved in 100% DMSO to obtain 4 mM solutions, and diluted 1:200 (v/v) in PBS (10 mM NaH_2PO_4, 150 mM NaCl, pH 7.4) to a final DMSO concentration of 0.5%. Compounds concentration series were prepared as two-fold dilutions into running buffer: for each sample, the complete binding study was performed using a six-point concentration series, typically spanning 0.025–20 µM, and triplicate aliquots of each compound concentration were dispensed into disposable vials. Binding experiments were performed at 25°C, using a flow rate of 50 µL min-1, with 60 s monitoring of association and 300 s monitoring of dissociation. Simple interactions were suitably fitted to a single-site bimolecular

interaction model (A+B = AB), yielding a single K_D (Table 1). Sensorgram

elaborations were performed using the BIA evaluation software provided by GE

Healthcare.

APPENDIX

Based on:

New dihydropyrimidin-2(1H)-one based Hsp90 C-terminal inhibitors

S. Terracciano, A. Foglia, M. G. Chini, M. C. Vaccaro, **A. Russo**, F. Dal Piaz, C. Saturnino, R. Riccio, G. Bifulco and I. Bruno

RSC Advances, **2016**, **6**, 82330-82340.

Discovery of new molecular entities able to strongly interfere with Hsp90 C-terminal domain

Stefania Terracciano, **Alessandra Russo**, Maria G. Chini, Maria C. Vaccaro, Marianna Potenza, Antonio Vassallo, Raffaele Riccio, Giuseppe Bifulco, and Ines Bruno

Scientific Reports, **2018**, **8**, *1709,* 1-11*;*

Targeting Hsp90 C-terminal domain

Besides the main projects developed in the frame of my PhD research experience, I had the opportunity to participate to an ongoing study focused on the development of Hsp90 C-terminal domain inhibitors, carried out by the research group of Organic Chemistry. Heat shock protein 90 (Hsp90) is a molecular chaperone involved in the control of a wide range of cellular processes through directing the folding and conformational maturation of many client proteins under both normal and stress conditions. The amplified expression of Hsp proteins is a common feature in human cancers and is associated with increased tumor growth, metastatic potential of tumor cells and resistance to chemotherapy.[215] Among Hsp90's clients there are different oncoproteins (Her2, Bcr-Abl, Akt, etc) that are linked to the six hallmarks of cancer. The depletion of these clients oncoproteins and the simultaneous suppression of multiple oncogenic pathways highlights the strategic approach of targeting Hsp90 machinery in cancer therapy.[216] In the last decades many effective and selective Hsp90 inhibitors (Hsp90-I), targeting the N-terminal domain, have been identified. However, despite their efficacy, these classical inhibitors have not yet achieved the expected success because they also stimulate a cytoprotective mechanism in cancer cells due to the heat shock response (HSR), leading to an increase in the expression of heat shock proteins (mainly Hsp70 and Hsp27), which may limit their clinical potential.[215] In contrast to these modulators, molecules that interfere with Hsp90 C-terminus have been shown to not produce the deleterious HSR emerging, thus, as a promising alternative and a more effective therapeutic anti-cancer strategy.[217] So far, for this less-targeted C-terminal domain only few inhibitors have been disclosed, including both natural products and their synthetic derivatives[217], owing to both the structural complexity of the protein domain and the absence of the crystal structures of C-terminal Hsp90-inhibitor complexes. In the frame of this project, I had the opportunity to perform some experimental procedures that allowed the identification of new interesting modulators of the Hsp90 C-terminal domain.

In more details, starting from the previous identification of a 3,4-dihydropyrimidin-2-(1H)-one (DHPM) based compound 1[218], disclosed as the first non natural

inspired C-terminal Hsp90 inhibitor, a new set of synthetic derivatives (Figure A.1) was explored by means of SPR analysis, followed by biological screening.
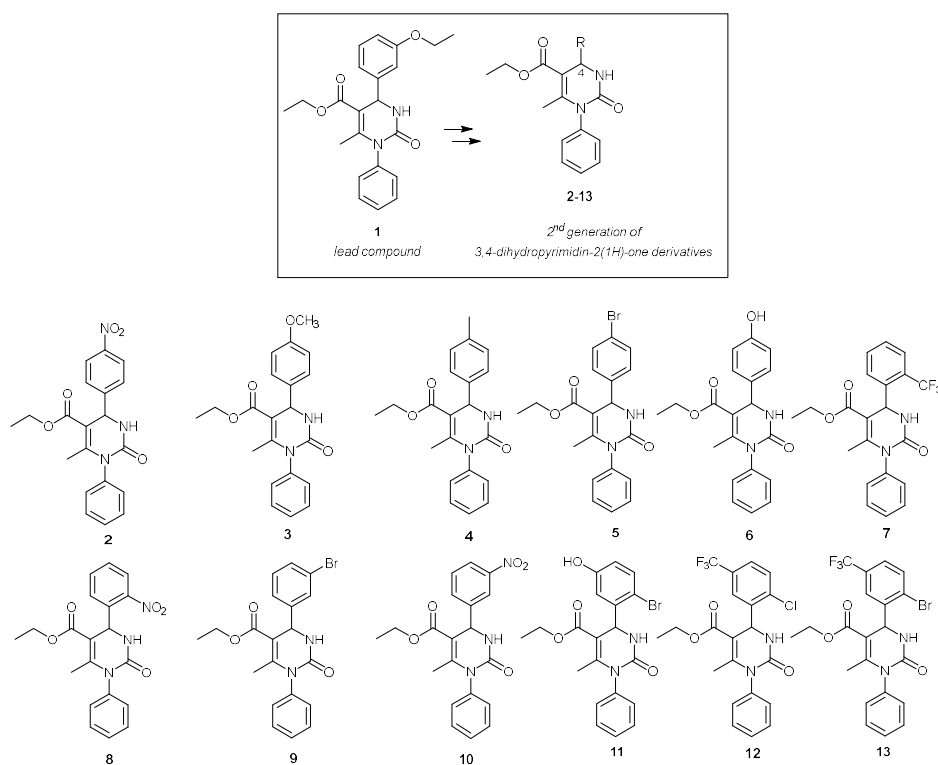
Figure A.1. *Chemical structures of the lead compound **1** and new DHPM-based compounds **2-13***

In particular, I was involved in the optimization of some steps of the synthetic procedure and in the SPR analysis of the synthesized molecules. In the table A.1 the KD constants, measured in the SPR assay, have been reported; the lead compound 1 and the known Hsp90 inhibitor 17-N-allylamino-17-demethoxygeldanamycin (17-AAG)[219] were used as positive controls.

Compound	K_D (nM)	Compound	K_D (nM)
1	76 ± 7	**8**	2.9 ± 0.8
2	76.2 ± 1.9	**9**	NB
3	17.6 ± 4.9	**10**	NB
4	13.0 ± 4.9	**11**	23.6 ± 0.7
5	12.0 ± 1.9	**12**	NB
6	3.7 ± 0.9	**13**	NB
7	NB	**17-AAG**[a]	388 ± 89

[a]17-N-allylamino-17-demethoxygeldanamycin

Table A.1. *Thermodynamic constants measured by SPR for the interaction between the tested compounds and the immobilized Hsp90*

The seven best DHPM binders 2-6 and 8, 11 have been further investigated for their anti-proliferative activity against two cancer cell lines: A375 (human melanoma) and Jurkat (human leukemic) (Table A.2).

Compound	IC_{50} (µM) 24h *Jurkat cell line*	IC_{50} (µM) 48h *Jurkat cell line*	IC_{50} (µM) 24h *A375 cell line*	IC_{50} (µM) 48h *A375 cell line*
2	-	-	-	-
3	-	-	-	86.1 ± 0.9
4	-	-	51.2 ± 0.8	40.3 ± 0.6
5	85.1 ± 0.8	74.2 ± 1.1	55.0 ± 0.6	43.5 ± 1.0
6	-	-	-	-
8	-	-	-	-
11	81.0 ± 1.2	70.5 ± 1.4	21.3 ± 0.9	15.2 ± 1.1
Novobiocin	550.3 ± 1.3	460.5 ± 0.9	170.6 ± 1.1	150.5 ± 0.7

Table A.2. *IC_{50} values of compounds **2-6, 8, 11** and Novobiocin, from cells viability assay, on human T lymphocyte cell line Jurkat and on human melanoma cancer cell line A375*

The obtained data allowed the identification of compounds **4**, **5** and **11** displaying a biological profile better than Novobiocin, a known C-terminal Hsp90 inhibitor, and similar to the lead compound **1**. These findings have been reported in a recent paper, entitled: "*New dihydropyrimidin-2(1H)-one based Hsp90 C-terminal inhibitors*", published on *RSC Advances*, **2016**, 6, 82330-82340.

Continuing this research line I took part in another project focused on the biophysical screening of a collection of commercially available compounds. The details of this research work that afforded the discovery of two new chemical entities **7** and **10** (see **Figure A.2**), able to target the C-terminal Hsp90 domain, have been reported in the last published paper on *Scientific Reports* entitled: "*Discovery of new molecular entities able to strongly interfere with Hsp90 C-terminal domain*".
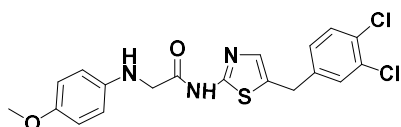
Compound 7

K_D: 5.2±3.8 nM [a]

IC$_{50}$ (on U937 cancer cell lines) 24 h[b]

51.0±0.7 μM

IC$_{50}$ (on Jurkat cancer cell lines) 24 h[b]

25.1± 0.4 μM
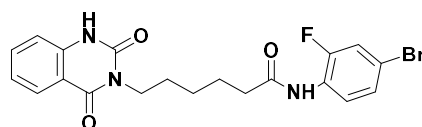
Compound 10

K_D: 20.8±8.7 nM [a]

IC$_{50}$ (on U937 cancer cell lines) 24h[b]

50.0± 0.7 μM

IC$_{50}$ (on Jurkat cancer cell lines) 24 h[b]

26.1± 0.7 μM

Figure A.2. Chemical structures of the compounds 7, 10

[a]*Termodynamic constants measured by SPR for the interaction between the tested compounds and the immobilized Hsp90α;* [b] *IC$_{50}$ values of compounds 7, 10, from cells viability assay on human monocytic cell line U397, from histiocytic lymphoma, and human leukemik T lymphocyte cell line Jurkat*

- 196 -

References

1. Shao, Y.; Li, X.; Lu, Y.; Liu, L.; Zhao, P., Aberrant LRP16 protein expression in primary neuroendocrine lung tumors. *Int J Clin Exp Pathol* **2015,** *8* (6), 6560-5.

2. Mohseni, M.; Cidado, J.; Croessmann, S.; Cravero, K.; Cimino-Mathews, A.; Wong, H. Y.; Scharpf, R.; Zabransky, D. J.; Abukhdeir, A. M.; Garay, J. P.; Wang, G. M.; Beaver, J. A.; Cochran, R. L.; Blair, B. G.; Rosen, D. M.; Erlanger, B.; Argani, P.; Hurley, P. J.; Lauring, J.; Park, B. H., MACROD2 overexpression mediates estrogen independent growth and tamoxifen resistance in breast cancers. *Proc Natl Acad Sci U S A* **2014,** *111* (49), 17606-11.

3. Chen, D.; Vollmar, M.; Rossi, M. N.; Phillips, C.; Kraehenbuehl, R.; Slade, D.; Mehrotra, P. V.; von Delft, F.; Crosthwaite, S. K.; Gileadi, O.; Denu, J. M.; Ahel, I., Identification of macrodomain proteins as novel O-acetyl-ADP-ribose deacetylases. *J Biol Chem* **2011,** *286* (15), 13261-71.

4. Colvin, T. A.; Gabai, V. L.; Gong, J.; Calderwood, S. K.; Li, H.; Gummuluru, S.; Matchuk, O. N.; Smirnova, S. G.; Orlova, N. V.; Zamulaeva, I. A.; Garcia-Marcos, M.; Li, X.; Young, Z. T.; Rauch, J. N.; Gestwicki, J. E.; Takayama, S.; Sherman, M. Y., Hsp70-Bag3 interactions regulate cancer-related signaling networks. *Cancer Research* **2014,** *74* (17), 4731-4740.

5. Zhu, H.; Liu, P.; Li, J., BAG3: A new therapeutic target of human cancers? *Histology and Histopathology* **2012,** *27* (3), 257-261.

6. Han, W.; Li, X.; Fu, X., The macro domain protein family: structure, functions, and their potential therapeutic implications. *Mutat Res* **2011,** *727* (3), 86-103.

7. Rosati, A.; Ammirante, M.; Gentilella, A.; Basile, A.; Festa, M.; Pascale, M.; Marzullo, L.; Belisario, M. A.; Tosco, A.; Franceschelli, S.; Moltedo, O.; Pagliuca, G.; Lerose, R.; Turco, M. C., Apoptosis inhibition in cancer cells: a novel molecular pathway that involves BAG3 protein. *Int J Biochem Cell Biol* **2007,** *39* (7-8), 1337-42.

8. van der Lee, M. M.; Groothuis, P. G.; Ubink, R.; van der Vleuten, M. A.; van Achterberg, T. A.; Loosveld, E. M.; Damming, D.; Jacobs, D. C.; Rouwette, M.; Egging, D. F.; van den Dobbelsteen, D.; Beusker, P. H.; Goedings, P.; Verheijden, G. F.; Lemmens, J. M.; Timmers, M.; Dokter, W. H., The Preclinical Profile of the Duocarmycin-Based HER2-Targeting ADC SYD985 Predicts for Clinical Benefit in Low HER2-Expressing Breast Cancers. *Mol Cancer Ther* **2015,** *14* (3), 692-703.

9. Chen, Q. W.; Zhu, X. Y.; Li, Y. Y.; Meng, Z. Q., Epigenetic regulation and cancer (review). *Oncol Rep* **2014,** *31* (2), 523-32.

10. Baylin, S. B.; Jones, P. A., A decade of exploring the cancer epigenome - biological and translational implications. *Nat Rev Cancer* **2011,** *11* (10), 726-34.

11. Kouzarides, T., Chromatin modifications and their function. *Cell* **2007,** *128* (4), 693-705.

12. Dawson, M. A.; Kouzarides, T., Cancer epigenetics: from mechanism to therapy. *Cell* **2012,** *150* (1), 12-27.

13. Minucci, S.; Pelicci, P. G., Histone deacetylase inhibitors and the promise of epigenetic (and more) treatments for cancer. *Nat Rev Cancer* **2006,** *6* (1), 38-51.

14.   Ehrlich, M., DNA methylation in cancer: too much, but also too little. *Oncogene* **2002,** *21* (35), 5400-13.

15.   Watt, F.; Molloy, P. L., Cytosine methylation prevents binding to DNA of a HeLa cell transcription factor required for optimal expression of the adenovirus major late promoter. *Genes Dev* **1988,** *2* (9), 1136-43.

16.   Nan, X.; Ng, H. H.; Johnson, C. A.; Laherty, C. D.; Turner, B. M.; Eisenman, R. N.; Bird, A., Transcriptional repression by the methyl-CpG-binding protein MeCP2 involves a histone deacetylase complex. *Nature* **1998,** *393* (6683), 386-9.

17.   Silverman, L. R.; Demakos, E. P.; Peterson, B. L.; Kornblith, A. B.; Holland, J. C.; Odchimar-Reissig, R.; Stone, R. M.; Nelson, D.; Powell, B. L.; DeCastro, C. M.; Ellerton, J.; Larson, R. A.; Schiffer, C. A.; Holland, J. F., Randomized controlled trial of azacitidine in patients with the myelodysplastic syndrome: a study of the cancer and leukemia group B. *J Clin Oncol* **2002,** *20* (10), 2429-40.

18.   Adamietz, P.; Rudolph, A., ADP-ribosylation of nuclear proteins in vivo. Identification of histone H2B as a major acceptor for mono- and poly(ADP-ribose) in dimethyl sulfate-treated hepatoma AH 7974 cells. *J Biol Chem* **1984,** *259* (11), 6841-6.

19.   (a) Adriouch, S.; Ohlrogge, W.; Haag, F.; Koch-Nolte, F.; Seman, M., Rapid induction of naive T cell apoptosis by ecto-nicotinamide adenine dinucleotide: requirement for mono(ADP-ribosyl)transferase 2 and a downstream effector. *J Immunol* **2001,** *167* (1), 196-203; (b) Adolph, K. W.; Song, M. K., Variations in ADP-ribosylation of nuclear scaffold proteins during the HeLa cell cycle. *Biochem Biophys Res Commun* **1985,** *126* (2), 840-7.

20.   Hassa, P. O.; Haenni, S. S.; Elser, M.; Hottiger, M. O., Nuclear ADP-ribosylation reactions in mammalian cells: where are we today and where are we going? *Microbiol Mol Biol Rev* **2006,** *70* (3), 789-829.

21.   Greer, E. L.; Shi, Y., Histone methylation: a dynamic mark in health, disease and inheritance. *Nat Rev Genet* **2012,** *13* (5), 343-57.

22.   Kahn, T. G.; Schwartz, Y. B.; Dellino, G. I.; Pirrotta, V., Polycomb complexes and the propagation of the methylation mark at the Drosophila ubx gene. *J Biol Chem* **2006,** *281* (39), 29064-75.

23.   Roth, S. Y.; Denu, J. M.; Allis, C. D., Histone acetyltransferases. *Annu Rev Biochem* **2001,** *70*, 81-120.

24.   Lowndes, N. F.; Toh, G. W., DNA repair: the importance of phosphorylating histone H2AX. *Curr Biol* **2005,** *15* (3), R99-R102.

25.   Fullgrabe, J.; Hajji, N.; Joseph, B., Cracking the death code: apoptosis-related histone modifications. *Cell Death Differ* **2010,** *17* (8), 1238-43.

26.   Gibson, B. A.; Kraus, W. L., New insights into the molecular and cellular functions of poly(ADP-ribose) and PARPs. *Nat Rev Mol Cell Biol* **2012,** *13* (7), 411-24.

27.   Okazaki, I. J.; Moss, J., Characterization of glycosylphosphatidylinositiol-anchored, secreted, and intracellular vertebrate mono-ADP-ribosyltransferases. *Annu Rev Nutr* **1999,** *19*, 485-509.

28.   Okazaki, I. J.; Moss, J., Mono-ADP-ribosylation: a reversible posttranslational modification of proteins. *Adv Pharmacol* **1996,** *35*, 247-80.

29.   Okazaki, I. J.; Kim, H. J.; Moss, J., Cloning and characterization of a novel membrane-associated lymphocyte NAD:arginine ADP-ribosyltransferase. *J Biol Chem* **1996,** *271* (36), 22052-7.

30.   Asher, G.; Reinke, H.; Altmeyer, M.; Gutierrez-Arcelus, M.; Hottiger, M. O.; Schibler, U., Poly(ADP-ribose) polymerase 1 participates in the phase entrainment of circadian clocks to feeding. *Cell* **2010,** *142* (6), 943-53.

31.   von Lukowicz, T.; Hassa, P. O.; Lohmann, C.; Boren, J.; Braunersreuther, V.; Mach, F.; Odermatt, B.; Gersbach, M.; Camici, G. G.; Stahli, B. E.; Tanner, F. C.; Hottiger, M. O.; Luscher, T. F.; Matter, C. M., PARP1 is required for adhesion molecule expression in atherogenesis. *Cardiovasc Res* **2008,** *78* (1), 158-66.

32.   Forst, A. H.; Karlberg, T.; Herzog, N.; Thorsell, A. G.; Gross, A.; Feijs, K. L.; Verheugd, P.; Kursula, P.; Nijmeijer, B.; Kremmer, E.; Kleine, H.; Ladurner, A. G.; Schuler, H.; Luscher, B., Recognition of mono-ADP-ribosylated ARTD10 substrates by ARTD8 macrodomains. *Structure* **2013,** *21* (3), 462-75.

33.   Huang, H.; Sabari, B. R.; Garcia, B. A.; Allis, C. D.; Zhao, Y., SnapShot: histone modifications. *Cell* **2014,** *159* (2), 458-458 e1.

34.   Corda, D.; Di Girolamo, M., Functional aspects of protein mono-ADP-ribosylation. *EMBO J* **2003,** *22* (9), 1953-8.

35.   Ord, M. G.; Stocken, L. A., Adenosine diphosphate ribosylated histones. *The Biochemical journal* **1977,** *161* (3), 583-92.

36.   Koch-Nolte, F.; Haag, F., Mono(ADP-ribosyl)transferases and related enzymes in animal tissues. Emerging gene families. *Adv Exp Med Biol* **1997,** *419*, 1-13.

37.   Kreimeyer, A.; Adamietz, P.; Hilz, H., Alkylation-induced mono(ADP-ribosyl)-histones H1 and H2B. Hydroxylamine-resistant linkage in hepatoma cells. *Biol Chem Hoppe Seyler* **1985,** *366* (6), 537-44.

38.   Kreimeyer, A.; Wielckens, K.; Adamietz, P.; Hilz, H., DNA repair-associated ADP-ribosylation in vivo. Modification of histone H1 differs from that of the principal acceptor proteins. *J Biol Chem* **1984,** *259* (2), 890-6.

39.   Golderer, G.; Grobner, P., ADP-ribosylation of core histones and their acetylated subspecies. *The Biochemical journal* **1991,** *277 (Pt 3),* 607-10.

40.   Corda, D.; Di Girolamo, M., Mono-ADP-ribosylation: a tool for modulating immune response and cell signaling. *Sci STKE* **2002,** *2002* (163), pe53.

41.   Cervantes-Laurean, D.; Jacobson, E. L.; Jacobson, M. K., Glycation and glycoxidation of histones by ADP-ribose. *J Biol Chem* **1996,** *271* (18), 10461-9.

42.   Cervantes-Laurean, D.; Minter, D. E.; Jacobson, E. L.; Jacobson, M. K., Protein glycation by ADP-ribose: studies of model conjugates. *Biochemistry* **1993,** *32* (6), 1528-34.

43.   Chambon, P.; Weill, J. D.; Mandel, P., Nicotinamide mononucleotide activation of new DNA-dependent polyadenylic acid synthesizing nuclear enzyme. *Biochem Biophys Res Commun* **1963,** *11*, 39-43.

44.   Aubin, J. E.; Heersche, J. N.; Merrilees, M. J.; Sodek, J., Isolation of bone cell clones with differences in growth, hormone responses, and extracellular matrix production. *J Cell Biol* **1982,** *92* (2), 452-61.

45.   Sims, N. R.; Bowen, D. M.; Allen, S. J.; Smith, C. C.; Neary, D.; Thomas, D. J.; Davison, A. N., Presynaptic cholinergic dysfunction in patients with dementia. *J Neurochem* **1983,** *40* (2), 503-9.

46.   Slattery, E.; Dignam, J. D.; Matsui, T.; Roeder, R. G., Purification and analysis of a factor which suppresses nick-induced transcription by RNA polymerase II and its identity with poly(ADP-ribose) polymerase. *J Biol Chem* **1983,** *258* (9), 5955-9.

47.   Ogata, N.; Ueda, K.; Kagamiyama, H.; Hayaishi, O., ADP-ribosylation of histone H1. Identification of glutamic acid residues 2, 14, and the COOH-terminal lysine residue as modification sites. *J Biol Chem* **1980,** *255* (16), 7616-20.

48.   Timinszky, G.; Till, S.; Hassa, P. O.; Hothorn, M.; Kustatscher, G.; Nijmeijer, B.; Colombelli, J.; Altmeyer, M.; Stelzer, E. H.; Scheffzek, K.; Hottiger, M. O.; Ladurner, A. G., A macrodomain-containing histone rearranges chromatin upon sensing PARP1 activation. *Nat Struct Mol Biol* **2009,** *16* (9), 923-9.

49.   Tulin, A.; Spradling, A., Chromatin loosening by poly(ADP)-ribose polymerase (PARP) at Drosophila puff loci. *Science* **2003,** *299* (5606), 560-2.

50.   Slade, D.; Dunstan, M. S.; Barkauskaite, E.; Weston, R.; Lafite, P.; Dixon, N.; Ahel, M.; Leys, D.; Ahel, I., The structure and catalytic mechanism of a poly(ADP-ribose) glycohydrolase. *Nature* **2011,** *477* (7366), 616-20.

51.   (a) Jankevicius, G.; Hassler, M.; Golia, B.; Rybin, V.; Zacharias, M.; Timinszky, G.; Ladurner, A. G., A family of macrodomain proteins reverses cellular mono-ADP-ribosylation. *Nat Struct Mol Biol* **2013,** *20* (4), 508-14; (b) Rosenthal, F.; Feijs, K. L.; Frugier, E.; Bonalli, M.; Forst, A. H.; Imhof, R.; Winkler, H. C.; Fischer, D.; Caflisch, A.; Hassa, P. O.; Luscher, B.; Hottiger, M. O., Macrodomain-containing proteins are new mono-ADP-ribosylhydrolases. *Nat Struct Mol Biol* **2013,** *20* (4), 502-7.

52.   Daniels, C. M.; Thirawatananond, P.; Ong, S. E.; Gabelli, S. B.; Leung, A. K., Nudix hydrolases degrade protein-conjugated ADP-ribose. *Sci Rep* **2015,** *5*, 18271.

53.   Feijs, K. L.; Forst, A. H.; Verheugd, P.; Luscher, B., Macrodomain-containing proteins: regulating new intracellular functions of mono(ADP-ribosyl)ation. *Nat Rev Mol Cell Biol* **2013,** *14* (7), 443-51.

54.   Lee, H. J.; Shieh, C. K.; Gorbalenya, A. E.; Koonin, E. V.; La Monica, N.; Tuler, J.; Bagdzhadzhyan, A.; Lai, M. M., The complete sequence (22 kilobases) of murine coronavirus gene 1 encoding the putative proteases and RNA polymerase. *Virology* **1991,** *180* (2), 567-82.

55.   Pehrson, J. R.; Fried, V. A., MacroH2A, a core histone containing a large nonhistone region. *Science* **1992,** *257* (5075), 1398-400.

56.   Ahel, D.; Horejsi, Z.; Wiechens, N.; Polo, S. E.; Garcia-Wilson, E.; Ahel, I.; Flynn, H.; Skehel, M.; West, S. C.; Jackson, S. P.; Owen-Hughes, T.; Boulton, S. J., Poly(ADP-ribose)-dependent regulation of DNA repair by the chromatin remodeling enzyme ALC1. *Science* **2009,** *325* (5945), 1240-3.

57.   Borges, H. L.; Linden, R.; Wang, J. Y., DNA damage-induced cell death: lessons from the central nervous system. *Cell Res* **2008,** *18* (1), 17-26.

58.   Allen, M. D.; Buckle, A. M.; Cordell, S. C.; Lowe, J.; Bycroft, M., The crystal structure of AF1521 a protein from Archaeoglobus fulgidus with homology to the non-histone domain of macroH2A. *J Mol Biol* **2003,** *330* (3), 503-11.

59.   Tallis, M.; Morra, R.; Barkauskaite, E.; Ahel, I., Poly(ADP-ribosyl)ation in regulation of chromatin structure and the DNA damage response. *Chromosoma* **2014,** *123* (1-2), 79-90.

60.   Rack, J. G.; Perina, D.; Ahel, I., Macrodomains: Structure, Function, Evolution, and Catalytic Activities. *Annu Rev Biochem* **2016,** *85*, 431-54.

61.   Karras, G. I.; Kustatscher, G.; Buhecha, H. R.; Allen, M. D.; Pugieux, C.; Sait, F.; Bycroft, M.; Ladurner, A. G., The macro domain is an ADP-ribose binding module. *EMBO J* **2005,** *24* (11), 1911-20.

62.   Zaja, R.; Mikoc, A.; Barkauskaite, E.; Ahel, I., Molecular Insights into Poly(ADP-ribose) Recognition and Processing. *Biomolecules* **2012,** *3* (1), 1-17.

63.   Pasque, V.; Radzisheuskaya, A.; Gillich, A.; Halley-Stott, R. P.; Panamarova, M.; Zernicka-Goetz, M.; Surani, M. A.; Silva, J. C., Histone variant macroH2A marks embryonic differentiation in vivo and acts as an epigenetic barrier to induced pluripotency. *J Cell Sci* **2012,** *125* (Pt 24), 6094-104.

64.   Daugherty, M. D.; Young, J. M.; Kerns, J. A.; Malik, H. S., Rapid evolution of PARP genes suggests a broad role for ADP-ribosylation in host-virus conflicts. *PLoS Genet* **2014,** *10* (5), e1004403.

65.   de Souza, R. F.; Aravind, L., Identification of novel components of NAD-utilizing metabolic pathways and prediction of their biochemical functions. *Mol Biosyst* **2012,** *8* (6), 1661-77.

66.   Dani, N.; Stilla, A.; Marchegiani, A.; Tamburro, A.; Till, S.; Ladurner, A. G.; Corda, D.; Di Girolamo, M., Combining affinity purification by ADP-ribose-binding macro domains with mass spectrometry to define the mammalian ADP-ribosyl proteome. *Proc Natl Acad Sci U S A* **2009,** *106* (11), 4243-8.

67.   Filippakopoulos, P.; Picaud, S.; Mangos, M.; Keates, T.; Lambert, J. P.; Barsyte-Lovejoy, D.; Felletar, I.; Volkmer, R.; Muller, S.; Pawson, T.; Gingras, A. C.; Arrowsmith, C. H.; Knapp, S., Histone recognition and large-scale structural analysis of the human bromodomain family. *Cell* **2012,** *149* (1), 214-31.

68.   Cheng, W.; Su, Y.; Xu, F., CHD1L: a novel oncogene. *Mol Cancer* **2013,** *12* (1), 170.

69.   Barkauskaite, E.; Jankevicius, G.; Ladurner, A. G.; Ahel, I.; Timinszky, G., The recognition and removal of cellular poly(ADP-ribose) signals. *FEBS J* **2013,** *280* (15), 3491-507.

70.   Aguiar, R. C.; Takeyama, K.; He, C.; Kreinbrink, K.; Shipp, M. A., B-aggressive lymphoma family proteins have unique domains that modulate transcription and exhibit poly(ADP-ribose) polymerase activity. *J Biol Chem* **2005,** *280* (40), 33756-65.

71.   Chen, D.; Vollmar, M.; Rossi, M. N.; Phillips, C.; Kraehenbuehl, R.; Slade, D.; Mehrotra, P. V.; Von Delft, F.; Crosthwaite, S. K.; Gileadi, O.; Denu, J. M.; Ahel, I., Identification of macrodomain proteins as novel O-acetyl-ADP-ribose deacetylases. *J. Biol. Chem.* **2011,** *286* (15), 13261-13271.

72.   Wu, Z.; Li, Y.; Li, X.; Ti, D.; Zhao, Y.; Si, Y.; Mei, Q.; Zhao, P.; Fu, X.; Han, W., LRP16 integrates into NF-kappaB transcriptional complex and is required for its functional activation. *PLoS one* **2011,** *6* (3), e18157.

73.   Han, W. D.; Zhao, Y. L.; Meng, Y. G.; Zang, L.; Wu, Z. Q.; Li, Q.; Si, Y. L.; Huang, K.; Ba, J. M.; Morinaga, H.; Nomura, M.; Mu, Y. M., Estrogenically regulated LRP16 interacts with estrogen receptor alpha and enhances the receptor's transcriptional activity. *Endocr Relat Cancer* **2007,** *14* (3), 741-53.

74.   Meng, Y. G.; Han, W. D.; Zhao, Y. L.; Huang, K.; Si, Y. L.; Wu, Z. Q.; Mu, Y. M., Induction of the LRP16 gene by estrogen promotes the invasive growth of

Ishikawa human endometrial cancer cells through the downregulation of E-cadherin. *Cell Res* **2007,** *17* (10), 869-80.

75.   Li, Y. Z.; Zhao, P.; Han, W. D., Clinicopathological significance of LRP16 protein in 336 gastric carcinoma patients. *World J Gastroenterol* **2009,** *15* (38), 4833-7.

76.   Liao, D. X.; Han, W. D.; Zhao, Y. L.; Pu, Y. D.; Mu, Y. M.; Luo, C. H.; Li, X. H., [Expression and clinical significance of LRP16 gene in human breast cancer]. *Ai Zheng* **2006,** *25* (7), 866-70.

77.   Xi, H. Q.; Zhao, P.; Han, W. D., Clinicopathological significance and prognostic value of LRP16 expression in colorectal carcinoma. *World J Gastroenterol* **2010,** *16* (13), 1644-8.

78.   Juszczynski, P.; Kutok, J. L.; Li, C.; Mitra, J.; Aguiar, R. C.; Shipp, M. A., BAL1 and BBAP are regulated by a gamma interferon-responsive bidirectional promoter and are overexpressed in diffuse large B-cell lymphomas with a prominent inflammatory infiltrate. *Mol Cell Biol* **2006,** *26* (14), 5348-59.

79.   Butepage, M.; Eckei, L.; Verheugd, P.; Luscher, B., Intracellular Mono-ADP-Ribosylation in Signaling and Disease. *Cells* **2015,** *4* (4), 569-95.

80.   Han, W. D.; Mu, Y. M.; Lu, X. C.; Xu, Z. M.; Li, X. J.; Yu, L.; Song, H. J.; Li, M.; Lu, J. M.; Zhao, Y. L.; Pan, C. Y., Up-regulation of LRP16 mRNA by 17beta-estradiol through activation of estrogen receptor alpha (ERalpha), but not ERbeta, and promotion of human breast cancer MCF-7 cell proliferation: a preliminary report. *Endocr Relat Cancer* **2003,** *10* (2), 217-24.

81.   Zhao, Y. L.; Han, W. D.; Li, Q.; Mu, Y. M.; Lu, X. C.; Yu, L.; Song, H. J.; Li, X.; Lu, J. M.; Pan, C. Y., Mechanism of transcriptional regulation of LRP16 gene expression by 17-beta estradiol in MCF-7 human breast cancer cells. *J Mol Endocrinol* **2005,** *34* (1), 77-89.

82.   Liang, J.; Shang, Y., Estrogen and cancer. *Annu Rev Physiol* **2013,** *75*, 225-40.

83.   Dunstan, M. S.; Barkauskaite, E.; Lafite, P.; Knezevic, C. E.; Brassington, A.; Ahel, M.; Hergenrother, P. J.; Leys, D.; Ahel, I., Structure and mechanism of a canonical poly(ADP-ribose) glycohydrolase. *Nat Commun* **2012,** *3*, 878.

84.   Finch, K. E.; Knezevic, C. E.; Nottbohm, A. C.; Partlow, K. C.; Hergenrother, P. J., Selective small molecule inhibition of poly(ADP-ribose) glycohydrolase (PARG). *ACS Chem Biol* **2012,** *7* (3), 563-70.

85.   (a) Hockenbery, D.; Nunez, G.; Milliman, C.; Schreiber, R. D.; Korsmeyer, S. J., Bcl-2 is an inner mitochondrial membrane protein that blocks programmed cell death. *Nature* **1990,** *348* (6299), 334-6; (b) Hockenbery, D. M., The bcl-2 oncogene and apoptosis. *Semin Immunol* **1992,** *4* (6), 413-20; (c) Reed, J. C., Bcl-2 and the regulation of programmed cell death. *J Cell Biol* **1994,** *124* (1-2), 1-6.

86.   Chao, D. T.; Korsmeyer, S. J., BCL-2 family: regulators of cell death. *Annu Rev Immunol* **1998,** *16*, 395-419.

87.   Reed, J. C.; Zha, H.; Aime-Sempe, C.; Takayama, S.; Wang, H. G., Structure-function analysis of Bcl-2 family proteins. Regulators of programmed cell death. *Adv Exp Med Biol* **1996,** *406*, 99-112.

88.   Takayama, S.; Xie, Z.; Reed, J. C., An evolutionarily conserved family of Hsp70/Hsc70 molecular chaperone regulators. *J Biol Chem* **1999,** *274* (2), 781-6.

89.   Coulson, M.; Robert, S.; Saint, R., Drosophila starvin encodes a tissue-specific BAG-domain protein required for larval food uptake. *Genetics* **2005,** *171* (4), 1799-812.

90.   Takayama, S.; Reed, J. C., Molecular chaperone targeting and regulation by BAG family proteins. *Nat Cell Biol* **2001,** *3* (10), E237-41.

91.   Doukhanina, E. V.; Chen, S.; van der Zalm, E.; Godzik, A.; Reed, J.; Dickman, M. B., Identification and functional characterization of the BAG protein family in Arabidopsis thaliana. *J Biol Chem* **2006,** *281* (27), 18793-801.

92.   Fang, S.; Li, L.; Cui, B.; Men, S.; Shen, Y.; Yang, X., Structural insight into plant programmed cell death mediated by BAG proteins in Arabidopsis thaliana. *Acta Crystallogr D Biol Crystallogr* **2013,** *69* (Pt 6), 934-45.

93.   Kabbage, M.; Dickman, M. B., The BAG proteins: a ubiquitous family of chaperone regulators. *Cell Mol Life Sci* **2008,** *65* (9), 1390-402.

94.   Doong, H.; Vrailas, A.; Kohn, E. C., What's in the 'BAG'?--A functional domain analysis of the BAG-family proteins. *Cancer Lett* **2002,** *188* (1-2), 25-32.

95.   Behl, C., Breaking BAG: The Co-Chaperone BAG3 in Health and Disease. *Trends Pharmacol Sci* **2016,** *37* (8), 672-88.

96.   Sondermann, H.; Ho, A. K.; Listenberger, L. L.; Siegers, K.; Moarefi, I.; Wente, S. R.; Hartl, F. U.; Young, J. C., Prediction of novel Bag-1 homologs based on structure/function analysis identifies Snl1p as an Hsp70 co-chaperone in Saccharomyces cerevisiae. *J Biol Chem* **2002,** *277* (36), 33220-7.

97.   Sondermann, H.; Scheufler, C.; Schneider, C.; Hohfeld, J.; Hartl, F. U.; Moarefi, I., Structure of a Bag/Hsc70 complex: convergent functional evolution of Hsp70 nucleotide exchange factors. *Science* **2001,** *291* (5508), 1553-7.

98.   Hohfeld, J.; Jentsch, S., GrpE-like regulation of the hsc70 chaperone by the anti-apoptotic protein BAG-1. *EMBO J* **1997,** *16* (20), 6209-16.

99.   Bukau, B.; Weissman, J.; Horwich, A., Molecular chaperones and protein quality control. *Cell* **2006,** *125* (3), 443-51.

100.   Bimston, D.; Song, J.; Winchester, D.; Takayama, S.; Reed, J. C.; Morimoto, R. I., BAG-1, a negative regulator of Hsp70 chaperone activity, uncouples nucleotide hydrolysis from substrate release. *EMBO J* **1998,** *17* (23), 6871-8.

101.   Zeiner, M.; Gehring, U., A protein that interacts with members of the nuclear hormone receptor family: identification and cDNA cloning. *Proc Natl Acad Sci U S A* **1995,** *92* (25), 11465-9.

102.   Bardelli, A.; Longati, P.; Albero, D.; Goruppi, S.; Schneider, C.; Ponzetto, C.; Comoglio, P. M., HGF receptor associates with the anti-apoptotic protein BAG-1 and prevents cell death. *EMBO J* **1996,** *15* (22), 6205-12.

103.   Song, J.; Takeda, M.; Morimoto, R. I., Bag1-Hsp70 mediates a physiological stress signalling pathway that regulates Raf-1/ERK and cell growth. *Nat Cell Biol* **2001,** *3* (3), 276-82.

104.   Ueda, K.; Kosako, H.; Fukui, Y.; Hattori, S., Proteomic identification of Bcl2-associated athanogene 2 as a novel MAPK-activated protein kinase 2 substrate. *J Biol Chem* **2004,** *279* (40), 41815-21.

105.   Arndt, V.; Daniel, C.; Nastainczyk, W.; Alberti, S.; Hohfeld, J., BAG-2 acts as an inhibitor of the chaperone-associated ubiquitin ligase CHIP. *Mol Biol Cell* **2005,** *16* (12), 5891-900.

106.   Dai, Q.; Qian, S. B.; Li, H. H.; McDonough, H.; Borchers, C.; Huang, D.; Takayama, S.; Younger, J. M.; Ren, H. Y.; Cyr, D. M.; Patterson, C., Regulation of the cytoplasmic quality control protein degradation pathway by BAG2. *J Biol Chem* **2005,** *280* (46), 38673-81.

107.   Kalia, S. K.; Lee, S.; Smith, P. D.; Liu, L.; Crocker, S. J.; Thorarinsdottir, T. E.; Glover, J. R.; Fon, E. A.; Park, D. S.; Lozano, A. M., BAG5 inhibits parkin and enhances dopaminergic neuron degeneration. *Neuron* **2004,** *44* (6), 931-45.

108.   Desmots, F.; Russell, H. R.; Lee, Y.; Boyd, K.; McKinnon, P. J., The reaper-binding protein scythe modulates apoptosis and proliferation during mammalian development. *Mol Cell Biol* **2005,** *25* (23), 10329-37.

109.   Rosati, A.; Graziano, V.; De Laurenzi, V.; Pascale, M.; Turco, M. C., BAG3: a multifaceted protein that regulates major cell pathways. *Cell Death Dis* **2011,** *2*, e141.

110.   Wada, S.; Hamada, M.; Satoh, N., A genomewide analysis of genes for the heat shock protein 70 chaperone system in the ascidian Ciona intestinalis. *Cell Stress Chaperones* **2006,** *11* (1), 23-33.

111.   Gentilella, A.; Khalili, K., Autoregulation of co-chaperone BAG3 gene transcription. *J Cell Biochem* **2009,** *108* (5), 1117-24.

112.   Pagliuca, M. G.; Lerose, R.; Cigliano, S.; Leone, A., Regulation by heavy metals and temperature of the human BAG-3 gene, a modulator of Hsp70 activity. *FEBS Lett* **2003,** *541* (1-3), 11-5.

113.   Rosati, A.; Di Salle, E.; Luberto, L.; Quinto, I.; Scala, G.; Turco, M. C.; Pascale, M., Identification of a Btk-BAG3 complex induced by oxidative stress. *Leukemia* **2009,** *23* (4), 823-4.

114.   Ammirante, M.; Rosati, A.; Arra, C.; Basile, A.; Falco, A.; Festa, M.; Pascale, M.; d'Avenia, M.; Marzullo, L.; Belisario, M. A.; De Marco, M.; Barbieri, A.; Giudice, A.; Chiappetta, G.; Vuttariello, E.; Monaco, M.; Bonelli, P.; Salvatore, G.; Di Benedetto, M.; Deshmane, S. L.; Khalili, K.; Turco, M. C.; Leone, A., IKK{gamma} protein is a target of BAG3 regulatory activity in human tumor growth. *Proc Natl Acad Sci U S A* **2010,** *107* (16), 7497-502.

115.   (a) Franceschelli, S.; Rosati, A.; Lerose, R.; De Nicola, S.; Turco, M. C.; Pascale, M., Bag3 gene expression is regulated by heat shock factor 1. *Journal of cellular physiology* **2008,** *215* (3), 575-7; (b) Song, S.; Kole, S.; Precht, P.; Pazin, M. J.; Bernier, M., Activation of heat shock factor 1 plays a role in pyrrolidine dithiocarbamate-mediated expression of the co-chaperone BAG3. *Int J Biochem Cell Biol* **2010,** *42* (11), 1856-63.

116.   Gamerdinger, M.; Hajieva, P.; Kaya, A. M.; Wolfrum, U.; Hartl, F. U.; Behl, C., Protein quality control during aging involves recruitment of the macroautophagy pathway by BAG3. *EMBO J* **2009,** *28* (7), 889-901.

117.   Romano, M. F.; Festa, M.; Pagliuca, G.; Lerose, R.; Bisogni, R.; Chiurazzi, F.; Storti, G.; Volpe, S.; Venuta, S.; Turco, M. C.; Leone, A., BAG3 protein controls B-chronic lymphocytic leukaemia cell apoptosis. *Cell Death Differ* **2003,** *10* (3), 383-5.

118.   Chiappetta, G.; Ammirante, M.; Basile, A.; Rosati, A.; Festa, M.; Monaco, M.; Vuttariello, E.; Pasquinelli, R.; Arra, C.; Zerilli, M.; Todaro, M.; Stassi, G.; Pezzullo, L.; Gentilella, A.; Tosco, A.; Pascale, M.; Marzullo, L.; Belisario, M. A.; Turco, M. C.; Leone, A., The antiapoptotic protein BAG3 is expressed in thyroid

carcinomas and modulates apoptosis mediated by tumor necrosis factor-related apoptosis-inducing ligand. *J Clin Endocrinol Metab* **2007,** *92* (3), 1159-63.

119. Liu, P.; Xu, B.; Li, J.; Lu, H., BAG3 gene silencing sensitizes leukemic cells to Bortezomib-induced apoptosis. *FEBS Lett* **2009,** *583* (2), 401-6.

120. Rosati, A.; Bersani, S.; Tavano, F.; Dalla Pozza, E.; De Marco, M.; Palmieri, M.; De Laurenzi, V.; Franco, R.; Scognamiglio, G.; Palaia, R.; Fontana, A.; di Sebastiano, P.; Donadelli, M.; Dando, I.; Medema, J. P.; Dijk, F.; Welling, L.; di Mola, F. F.; Pezzilli, R.; Turco, M. C.; Scarpa, A., Expression of the antiapoptotic protein BAG3 is a feature of pancreatic adenocarcinoma and its overexpression is associated with poorer survival. *Am J Pathol* **2012,** *181* (5), 1524-9.

121. De Marco, M.; Turco, M. C.; Rosati, A., BAG3 protein is induced during cardiomyoblast differentiation and modulates myogenin expression. *Cell Cycle* **2011,** *10* (5), 850-2.

122. De Marco, M.; Falco, A.; Basile, A.; Rosati, A.; Festa, M.; d'Avenia, M.; Pascale, M.; Dal Piaz, F.; Bisogni, R.; Barcaroli, D.; Coppola, G.; Piscione, F.; Gigantino, A.; Citro, R.; De Rosa, R.; Vitulano, G.; Virtuoso, N.; Manganelli, F.; Palermo, E.; Siano, F.; Rosato, G.; Hahne, M.; Tiberti, C.; De Laurenzi, V.; Turco, M. C., Detection of soluble BAG3 and anti-BAG3 antibodies in patients with chronic heart failure. *Cell Death Dis* **2013,** *4*, e495.

123. McCollum, A. K.; Casagrande, G.; Kohn, E. C., Caught in the middle: the role of Bag3 in disease. *The Biochemical journal* **2009,** *425* (1), e1-3.

124. Dong, H.; Wade, M.; Williams, A.; Lee, A.; Douglas, G. R.; Yauk, C., Molecular insight into the effects of hypothyroidism on the developing cerebellum. *Biochem Biophys Res Commun* **2005,** *330* (4), 1182-93.

125. Lee, J. H.; Takahashi, T.; Yasuhara, N.; Inazawa, J.; Kamada, S.; Tsujimoto, Y., Bis, a Bcl-2-binding protein that synergizes with Bcl-2 in preventing cell death. *Oncogene* **1999,** *18* (46), 6183-90.

126. Jin, Y. H.; Ahn, S. G.; Kim, S. A., BAG3 affects the nucleocytoplasmic shuttling of HSF1 upon heat stress. *Biochem Biophys Res Commun* **2015,** *464* (2), 561-7.

127. Gout, E.; Gutkowska, M.; Takayama, S.; Reed, J. C.; Chroboczek, J., Co-chaperone BAG3 and adenovirus penton base protein partnership. *J Cell Biochem* **2010,** *111* (3), 699-708.

128. Iwasaki, M.; Tanaka, R.; Hishiya, A.; Homma, S.; Reed, J. C.; Takayama, S., BAG3 directly associates with guanine nucleotide exchange factor of Rap1, PDZGEF2, and regulates cell adhesion. *Biochem Biophys Res Commun* **2010,** *400* (3), 413-8.

129. Kathage, B.; Gehlert, S.; Ulbricht, A.; Ludecke, L.; Tapia, V. E.; Orfanos, Z.; Wenzel, D.; Bloch, W.; Volkmer, R.; Fleischmann, B. K.; Furst, D. O.; Hohfeld, J., The cochaperone BAG3 coordinates protein synthesis and autophagy under mechanical strain through spatial regulation of mTORC1. *Biochim Biophys Acta* **2017,** *1864* (1), 62-75.

130. Carra, S.; Seguin, S. J.; Landry, J., HspB8 and Bag3: a new chaperone complex targeting misfolded proteins to macroautophagy. *Autophagy* **2008,** *4* (2), 237-9.

131. Fuchs, M.; Poirier, D. J.; Seguin, S. J.; Lambert, H.; Carra, S.; Charette, S. J.; Landry, J., Identification of the key structural motifs involved in HspB8/HspB6-Bag3 interaction. *The Biochemical journal* **2009,** *425* (1), 245-55.

132.   Rauch, J. N.; Tse, E.; Freilich, R.; Mok, S. A.; Makley, L. N.; Southworth, D. R.; Gestwicki, J. E., BAG3 Is a Modular, Scaffolding Protein that physically Links Heat Shock Protein 70 (Hsp70) to the Small Heat Shock Proteins. *J Mol Biol* **2017,** *429* (1), 128-141.

133.   Gamerdinger, M.; Carra, S.; Behl, C., Emerging roles of molecular chaperones and co-chaperones in selective autophagy: Focus on BAG proteins. *Journal of Molecular Medicine* **2011,** *89* (12), 1175-1182.

134.   Xu, Z.; Graham, K.; Foote, M.; Liang, F.; Rizkallah, R.; Hurt, M.; Wang, Y.; Wu, Y.; Zhou, Y., 14-3-3 protein targets misfolded chaperone-associated proteins to aggresomes. *Journal of Cell Science* **2013,** *126* (18), 4173-4186.

135.   Virador, V. M.; Davidson, B.; Czechowicz, J.; Mai, A.; Kassis, J.; Kohn, E. C., The anti-apoptotic activity of BAG3 is restricted by caspases and the proteasome. *PloS one* **2009,** *4* (4).

136.   Babu, M. M., The contribution of intrinsically disordered regions to protein function, cellular complexity, and human disease. *Biochem Soc Trans* **2016,** *44* (5), 1185-1200.

137.   Sturner, E.; Behl, C., The Role of the Multifunctional BAG3 Protein in Cellular Protein Quality Control and in Disease. *Front Mol Neurosci* **2017,** *10*, 177.

138.   (a) Merabova, N.; Sariyer, I. K.; Saribas, A. S.; Knezevic, T.; Gordon, J.; Turco, M. C.; Rosati, A.; Weaver, M.; Landry, J.; Khalili, K., WW domain of BAG3 is required for the induction of autophagy in glioma cells. *Journal of cellular physiology* **2015,** *230* (4), 831-41; (b) Crippa, V.; Sau, D.; Rusmini, P.; Boncoraglio, A.; Onesto, E.; Bolzoni, E.; Galbiati, M.; Fontana, E.; Marino, M.; Carra, S.; Bendotti, C.; De Biasi, S.; Poletti, A., The small heat shock protein B8 (HspB8) promotes autophagic removal of misfolded proteins involved in amyotrophic lateral sclerosis (ALS). *Hum Mol Genet* **2010,** *19* (17), 3440-56.

139.   Crippa, V.; Sau, D.; Rusmini, P.; Boncoraglio, A.; Onesto, E.; Bolzoni, E.; Galbiati, M.; Fontana, E.; Marino, M.; Carra, S.; Bendotti, C.; de Biasi, S.; Poletti, A., The small heat shock protein B8 (HspB8) promotes autophagic removal of misfolded proteins involved in amyotrophic lateral sclerosis (ALS). *Human Molecular Genetics* **2010,** *19* (17), 3440-3456.

140.   Kostera-Pruszczyk, A.; Suszek, M.; Ploski, R.; Franaszczyk, M.; Potulska-Chromik, A.; Pruszczyk, P.; Sadurska, E.; Karolczak, J.; Kaminska, A. M.; Redowicz, M. J., BAG3-related myopathy, polyneuropathy and cardiomyopathy with long QT syndrome. *J Muscle Res Cell Motil* **2015,** *36* (6), 423-32.

141.   Feldman, A. M.; Gordon, J.; Wang, J.; Song, J.; Zhang, X. Q.; Myers, V. D.; Tilley, D. G.; Gao, E.; Hoffman, N. E.; Tomar, D.; Madesh, M.; Rabinowitz, J.; Koch, W. J.; Su, F.; Khalili, K.; Cheung, J. Y., BAG3 regulates contractility and Ca(2+) homeostasis in adult mouse ventricular myocytes. *J Mol Cell Cardiol* **2016,** *92*, 10-20.

142.   Knezevic, T.; Myers, V. D.; Gordon, J.; Tilley, D. G.; Sharp, T. E., 3rd; Wang, J.; Khalili, K.; Cheung, J. Y.; Feldman, A. M., BAG3: a new player in the heart failure paradigm. *Heart failure reviews* **2015,** *20* (4), 423-34.

143.   Santoro, A.; Nicolin, V.; Florenzano, F.; Rosati, A.; Capunzo, M.; Nori, S. L., BAG3 is involved in neuronal differentiation and migration. *Cell Tissue Res* **2017,** *368* (2), 249-258.

144.   Bruno, A. P.; Festa, M.; Dal Piaz, F.; Rosati, A.; Turco, M. C.; Giuditta, A.; Marzullo, L., Identification of a synaptosome-associated form of BAG3 protein. *Cell Cycle* **2008,** *7* (19), 3104-3105.

145.   Jaffer, F.; Murphy, S. M.; Scoto, M.; Healy, E.; Rossor, A. M.; Brandner, S.; Phadke, R.; Selcen, D.; Jungbluth, H.; Muntoni, F.; Reilly, M. M., BAG3 mutations: another cause of giant axonal neuropathy. *J Peripher Nerv Syst* **2012,** *17* (2), 210-6.

146.   Carrizzo, A.; Damato, A.; Ambrosio, M.; Falco, A.; Rosati, A.; Capunzo, M.; Madonna, M.; Turco, M. C.; Januzzi, J. L.; De Laurenzi, V.; Vecchione, C., The prosurvival protein BAG3: a new participant in vascular homeostasis. *Cell Death Dis* **2016,** *7* (10), e2431.

147.   Guerriero, L.; Palmieri, G.; De Marco, M.; Cossu, A.; Remondelli, P.; Capunzo, M.; Turco, M. C.; Rosati, A., The anti-apoptotic BAG3 protein is involved in BRAF inhibitor resistance in melanoma cells. *Oncotarget* **2017,** *8* (46), 80393-80404.

148.   Boiani, M.; Daniel, C.; Liu, X.; Hogarty, M. D.; Marnett, L. J., The stress protein BAG3 stabilizes Mcl-1 protein and promotes survival of cancer cells and resistance to antagonist ABT-737. *J Biol Chem* **2013,** *288* (10), 6980-90.

149.   Zhang, Y.; Wang, J. H.; Lu, Q.; Wang, Y. J., Bag3 promotes resistance to apoptosis through Bcl-2 family members in non-small cell lung cancer. *Oncol Rep* **2012,** *27* (1), 109-13.

150.   Cesaro, E.; Montano, G.; Rosati, A.; Crescitelli, R.; Izzo, P.; Turco, M. C.; Costanzo, P., WT1 protein is a transcriptional activator of the antiapoptotic bag3 gene. *Leukemia* **2010,** *24* (6), 1204-1206.

151.   Rosati, A.; Ammirante, M.; Gentilella, A.; Basile, A.; Festa, M.; Pascale, M.; Marzullo, L.; Belisario, M. A.; Tosco, A.; Franceschelli, S.; Moltedo, O.; Pagliuca, G.; Lerose, R.; Turco, M. C., Apoptosis inhibition in cancer cells: A novel molecular pathway that involves BAG3 protein. *International Journal of Biochemistry and Cell Biology* **2007,** *39* (7-8), 1337-1342.

152.   Gentilella, A.; Passiatore, G.; Deshmane, S.; Turco, M. C.; Khalili, K., Activation of BAG3 by Egr-1 in response to FGF-2 in neuroblastoma cells. *Oncogene* **2008,** *27* (37), 5011-5018.

153.   Ammirante, M.; Rosati, A.; Arra, C.; Basile, A.; Falco, A.; Festa, M.; Pascale, M.; D'Avenia, M.; Marzullo, L.; Belisario, M. A.; De Marco, M.; Barbieri, A.; Giudice, A.; Chiappetta, G.; Vuttariello, E.; Monaco, M.; Bonelli, P.; Salvatore, G.; Di Benedetto, M.; Deshmane, S. L.; Khalili, K.; Turco, M. C.; Leone, A., IKKγ protein is a target of BAG3 regulatory activity in human tumor growth. *Proceedings of the National Academy of Sciences of the United States of America* **2010,** *107* (16), 7497-7502.

154.   Festa, M.; Del Valle, L.; Khalili, K.; Franco, R.; Scognamiglio, G.; Graziano, V.; De Laurenzi, V.; Turco, M. C.; Rosati, A., BAG3 protein is overexpressed in human glioblastoma and is a potential target for therapy. *American Journal of Pathology* **2011,** *178* (6), 2504-2512.

155.   Rosati, A.; Graziano, V.; De Laurenzi, V.; Pascale, M.; Turco, M. C., BAG3: A multifaceted protein that regulates major cell pathways. *Cell Death and Disease* **2011,** *2* (4).

156.   Du, Z. X.; Meng, X.; Zhang, H. Y.; Guan, Y.; Wang, H. Q., Caspase-dependent cleavage of BAG3 in proteasome inhibitors-induced apoptosis in thyroid cancer cells. *Biochem Biophys Res Commun* **2008,** *369* (3), 894-8.

157.   Iwasaki, M.; Homma, S.; Hishiya, A.; Dolezal, S. J.; Reed, J. C.; Takayama, S., BAG3 regulates motility and adhesion of epithelial cancer cells. *Cancer Research* **2007,** *67* (21), 10252-10259.

158.   Kassis, J. N.; Virador, V. M.; Guancial, E. A.; Kimm, D.; Ho, A. S.; Mishra, M.; Chuang, E. Y.; Cook, J.; Gius, D.; Kohn, E. C., Genomic and phenotypic analysis reveals a key role for CCN1 (CYR61) in BAG3 - Modulated adhesion and invasion. *Journal of Pathology* **2009,** *218* (4), 495-504.

159.   Fontanella, B.; Birolo, L.; Infusini, G.; Cirulli, C.; Marzullo, L.; Pucci, P.; Turco, M. C.; Tosco, A., The co-chaperone BAG3 interacts with the cytosolic chaperonin CCT: New hints for actin folding. *International Journal of Biochemistry and Cell Biology* **2010,** *42* (5), 641-650.

160.   Kassis, J. N.; Guancial, E. A.; Doong, H.; Virador, V.; Kohn, E. C., CAIR-1/BAG-3 modulates cell adhesion and migration by downregulating activity of focal adhesion proteins. *Experimental Cell Research* **2006,** *312* (15), 2962-2971.

161.   Iwasaki, M.; Tanaka, R.; Hishiya, A.; Homma, S.; Reed, J. C.; Takayama, S., BAG3 directly associates with guanine nucleotide exchange factor of Rap1, PDZGEF2, and regulates cell adhesion. *Biochemical and Biophysical Research Communications* **2010,** *400* (3), 413-418.

162.   Liao, Q.; Ozawa, F.; Friess, H.; Zimmermann, A.; Takayama, S.; Reed, J. C.; Kleeff, J.; Büchler, M. W., The anti-apoptotic protein BAG-3 is overexpressed in pancreatic cancer and induced by heat stress in pancreatic cancer cell lines. *FEBS Letters* **2001,** *503* (2-3), 151-157.

163.   Rosati, A.; Bersani, S.; Tavano, F.; Dalla Pozza, E.; De Marco, M.; Palmieri, M.; De Laurenzi, V.; Franco, R.; Scognamiglio, G.; Palaia, R.; Fontana, A.; Di Sebastiano, P.; Donadelli, M.; Dando, I.; Medema, J. P.; Dijk, F.; Welling, L.; Di Mola, F. F.; Pezzilli, R.; Turco, M. C.; Scarpa, A., Expression of the antiapoptotic protein BAG3 is a feature of pancreatic adenocarcinoma and its overexpression is associated with poorer survival. *American Journal of Pathology* **2012,** *181* (5), 1524-1529.

164.   Franco, R.; Scognamiglio, G.; Salerno, V.; Sebastiani, A.; Cennamo, G.; Ascierto, P. A.; Botti, G.; Turco, M. C.; Rosati, A., Expression of the anti-apoptotic protein BAG3 in human melanomas. *Journal of Investigative Dermatology* **2012,** *132* (1), 252-254.

165.   Guerriero, L.; Chong, K.; Franco, R.; Rosati, A.; De Caro, F.; Capunzo, M.; Turco, M. C.; Hoon, D. S. B., BAG3 protein expression in melanoma metastatic lymph nodes correlates with patients' survival. *Cell Death and Disease* **2014,** *5* (4).

166.   Xiao, H.; Cheng, S.; Tong, R.; Lv, Z.; Ding, C.; Du, C.; Xie, H.; Zhou, L.; Wu, J.; Zheng, S., BAG3 regulates epithelial-mesenchymal transition and angiogenesis in human hepatocellular carcinoma. *Laboratory Investigation* **2014,** *94* (3), 252-261.

167.   Chiappetta, G.; Basile, A.; Barbieri, A.; Falco, A.; Rosati, A.; Festa, M.; Pasquinelli, R.; Califano, D.; Palma, G.; Costanzo, R.; Barcaroli, D.; Capunzo, M.; Franco, R.; Rocco, G.; Pascale, M.; Turco, M. C.; De Laurenzi, V.; Arra, C., The anti-apoptotic BAG3 protein is expressed in lung carcinomas and regulates small cell lung carcinoma (SCLC) tumor growth. *Oncotarget* **2014,** *5* (16), 6846-6853.

168.   Yang, X.; Tian, Z.; Gou, W. F.; Takahashi, H.; Yu, M.; Xing, Y. N.; Takano, Y.; Zheng, H. C., Bag-3 expression is involved in pathogenesis and progression of colorectal carcinomas. *Histology and Histopathology* **2013,** *28* (9), 1147-1156.

169.   Zhu, H.; Wu, W.; Fu, Y.; Shen, W.; Miao, K.; Hong, M.; Xu, W.; Young, K. H.; Liu, P.; Li, J., Overexpressed BAG3 is a potential therapeutic target in chronic lymphocytic leukemia. *Annals of Hematology* **2014,** *93* (3), 425-435.

170.   Sugio, A.; Iwasaki, M.; Habata, S.; Mariya, T.; Suzuki, M.; Osogami, H.; Tamate, M.; Tanaka, R.; Saito, T., BAG3 upregulates Mcl-1 through downregulation of miR-29b to induce anticancer drug resistance in ovarian cancer. *Gynecologic oncology* **2014,** *134* (3), 615-623.

171.   Nourashrafeddin, S.; Aarabi, M.; Modarressi, M. H.; Rahmati, M.; Nouri, M., The Evaluation of WBP2NL-Related Genes Expression in Breast Cancer. *Pathology and Oncology Research* **2015,** *21* (2), 293-300.

172.   Staibano, S.; Mascolo, M.; Di Benedetto, M.; Vecchione, M. L.; Ilardi, G.; Di Lorenzo, G.; Autorino, R.; Salerno, V.; Morena, A.; Rocco, A.; Turco, M. C.; Morelli, E., BAG3 protein delocalisation in prostate carcinoma. *Tumour biology : the journal of the International Society for Oncodevelopmental Biology and Medicine* **2010,** *31* (5), 461-469.

173.   Esposito, V.; Baldi, C.; Zeppa, P.; Festa, M.; Guerriero, L.; d'Avenia, M.; Chetta, M.; Zullo, F.; De Laurenzi, V.; Turco, M. C.; Rosati, A.; Guida, M., BAG3 Protein Is Over-Expressed in Endometrioid Endometrial Adenocarcinomas. *Journal of cellular physiology* **2017,** *232* (2), 309-311.

174.   Rosati, A.; Basile, A.; D'Auria, R.; d'Avenia, M.; De Marco, M.; Falco, A.; Festa, M.; Guerriero, L.; Iorio, V.; Parente, R.; Pascale, M.; Marzullo, L.; Franco, R.; Arra, C.; Barbieri, A.; Rea, D.; Menichini, G.; Hahne, M.; Bijlsma, M.; Barcaroli, D.; Sala, G.; di Mola, F. F.; di Sebastiano, P.; Todoric, J.; Antonucci, L.; Corvest, V.; Jawhari, A.; Firpo, M. A.; Tuveson, D. A.; Capunzo, M.; Karin, M.; De Laurenzi, V.; Turco, M. C., BAG3 promotes pancreatic ductal adenocarcinoma growth by activating stromal macrophages. *Nat Commun* **2015,** *6*, 8695.

175.   Liu, B. Q.; Zhang, S.; Li, S.; An, M. X.; Li, C.; Yan, J.; Wang, J. M.; Wang, H. Q., BAG3 promotes stem cell-like phenotype in breast cancer by upregulation of CXCR4 via interaction with its transcript. *Cell Death Dis* **2017,** *8* (7), e2933.

176.   Ammirante, M.; De Laurenzi, V.; Graziano, V.; Turco, M. C.; Rosati, A., BAG3 is required for IKKa nuclear translocation and emergence of castration resistant prostate cancer. *Cell Death and Disease* **2011,** *2* (3).

177.   Habata, S.; Iwasaki, M.; Sugio, A.; Suzuki, M.; Tamate, M.; Satohisa, S.; Tanaka, R.; Saito, T., BAG3 increases the invasiveness of uterine corpus carcinoma cells by suppressing miR-29b and enhancing MMP2 expression. *Oncology Reports* **2015,** *33* (5), 2613-2621.

178.   Lu, P.; Takai, K.; Weaver, V. M.; Werb, Z., Extracellular matrix degradation and remodeling in development and disease. *Cold Spring Harb Perspect Biol* **2011,** *3* (12).

179.   Yunoki, T.; Tabuchi, Y.; Kondo, T.; Ishii, Y.; Hayashi, A., Overexpression of the anti-apoptotic protein BAG3 in human choroidal melanoma: A case report. *Oncology Letters* **2017,** *13* (6), 4169-4172.

180.   Li, X.; Colvin, T.; Rauch, J. N.; Acosta-Alvear, D.; Kampmann, M.; Dunyak, B.; Hann, B.; Aftab, B. T.; Murnane, M.; Cho, M.; Walter, P.; Weissman, J. S.; Sherman, M. Y.; Gestwicki, J. E., Validation of the Hsp70-Bag3 protein-

protein interaction as a potential therapeutic target in cancer. *Mol Cancer Ther* **2015,** *14* (3), 642-8.

181.   Rauch, J. N.; Gestwicki, J. E., Binding of human nucleotide exchange factors to heat shock protein 70 (Hsp70) generates functionally distinct complexes in vitro. *Journal of Biological Chemistry* **2014,** *289* (3), 1402-1414.

182.   Wang, A. M.; Miyata, Y.; Klinedinst, S.; Peng, H. M.; Chua, J. P.; Komiyama, T.; Li, X.; Morishima, Y.; Merry, D. E.; Pratt, W. B.; Osawa, Y.; Collins, C. A.; Gestwicki, J. E.; Lieberman, A. P., Activation of Hsp70 reduces neurotoxicity by promoting polyglutamine protein degradation. *Nat Chem Biol* **2013,** *9* (2), 112-8.

183.   Li, X.; Colvin, T.; Rauch, J. N.; Acosta-Alvear, D.; Kampmann, M.; Dunyak, B.; Hann, B.; Aftab, B. T.; Murnane, M.; Cho, M.; Walter, P.; Weissman, J. S.; Sherman, M. Y.; Gestwicki, J. E., Validation of the Hsp70-Bag3 protein-protein interaction as a potential therapeutic target in cancer. *Molecular Cancer Therapeutics* **2015,** *14* (3), 642-648.

184.   (a) Rerole, A. L.; Jego, G.; Garrido, C., Hsp70: anti-apoptotic and tumorigenic protein. *Methods Mol Biol* **2011,** *787*, 205-30; (b) Assimon, V. A.; Gillies, A. T.; Rauch, J. N.; Gestwicki, J. E., Hsp70 protein complexes as drug targets. *Curr Pharm Des* **2013,** *19* (3), 404-17.

185.   Massey, A. J., ATPases as drug targets: insights from heat shock proteins 70 and 90. *Journal of medicinal chemistry* **2010,** *53* (20), 7280-6.

186.   Ma, N.; Wang, Y.; Zhao, B. X.; Ye, W. C.; Jiang, S., The application of click chemistry in the synthesis of agents with anticancer activity. *Drug Des Devel Ther* **2015,** *9*, 1585-99.

187.   Bock, V. D.; Hiemstra, H.; van Maarseveen, J. H., Cu-I-catalyzed alkyne-azide "click" cycloadditions from a mechanistic and synthetic perspective. *European Journal of Organic Chemistry* **2006,** (1), 51-68.

188.   Al-Abdullah, E. S.; Asiri, H. H.; Lahsasni, S.; Habib, E. E.; Ibrahim, T. M.; El-Emam, A. A., Synthesis, antimicrobial, and anti-inflammatory activity, of novel S-substituted and N-substituted 5-(1-adamantyl)-1,2,4-triazole-3-thiols. *Drug Des Devel Ther* **2014,** *8*, 505-18.

189.   Schrödinger, L., New York, NY, Maestro, version 10.2,. **(2015).**

190.   Liang, L. Y.; Astruc, D., The copper(I)-catalyzed alkyne-azide cycloaddition (CuAAC) "click" reaction and its applications. An overview. *Coordin Chem Rev* **2011,** *255* (23-24), 2933-2945.

191.   Pokhodylo, N. T.; Savka, R. D.; Pidlypnyi, N. I.; Matiychuk, V. S.; Obushak, M. D., Synthesis of 2-Azido-1,3-thiazoles as 1,2,3-Triazole Precursors. *Synthetic Communications* **2010,** *40* (3), 391-399.

192.   Bernhard Neises; Steglich, P. D. W., Simple Method for the Esterification of Carboxylic Acids. *Angewandte Chemie International edition* **1978,** *17* (7), 522-524.

193.   Morales-Serna, J. A.; Garcia-Rios, E.; Bernal, J.; Paleo, E.; Gavino, R.; Cardenas, J., Reduction of Carboxylic Acids Using Esters of Benzotriazole as High-Reactivity Intermediates. *Synthesis-Stuttgart* **2011,** (9), 1375-1382.

194.   Philpott, M.; Yang, J.; Tumber, T.; Fedorov, O.; Uttarkar, S.; Filippakopoulos, P.; Picaud, S.; Keates, T.; Felletar, I.; Ciulli, A.; Knapp, S.; Heightman, T. D., Bromodomain-peptide displacement assays for interactome mapping and inhibitor discovery. *Mol Biosyst* **2011,** *7* (10), 2899-908.

195. Ju, Y.; Kumar, D.; Varma, R. S., Revisiting nucleophilic substitution reactions: microwave-assisted synthesis of azides, thiocyanates, and sulfones in an aqueous medium. *J Org Chem* **2006,** *71* (17), 6697-700.

196. Rostovtsev, V. V.; Green, L. G.; Fokin, V. V.; Sharpless, K. B., A stepwise huisgen cycloaddition process: copper(I)-catalyzed regioselective "ligation" of azides and terminal alkynes. *Angew Chem Int Ed Engl* **2002,** *41* (14), 2596-9.

197. Savitsky, P.; Bray, J.; Cooper, C. D.; Marsden, B. D.; Mahajan, P.; Burgess-Brown, N. A.; Gileadi, O., High-throughput production of human proteins for crystallization: the SGC experience. *J Struct Biol* **2010,** *172* (1), 3-13.

198. Patel, D.; Bauman, J. D.; Arnold, E., Advantages of crystallographic fragment screening: functional and mechanistic insights from a powerful platform for efficient drug discovery. *Prog Biophys Mol Biol* **2014,** *116* (2-3), 92-100.

199. Danley, D. E., Crystallization to obtain protein-ligand complexes for structure-aided drug design. *Acta Crystallogr D Biol Crystallogr* **2006,** *62* (Pt 6), 569-75.

200. Roessler, C. G.; Agarwal, R.; Allaire, M.; Alonso-Mori, R.; Andi, B.; Bachega, J. F. R.; Bommer, M.; Brewster, A. S.; Browne, M. C.; Chatterjee, R.; Cho, E.; Cohen, A. E.; Cowan, M.; Datwani, S.; Davidson, V. L.; Defever, J.; Eaton, B.; Ellson, R.; Feng, Y.; Ghislain, L. P.; Glownia, J. M.; Han, G.; Hattne, J.; Hellmich, J.; Heroux, A.; Ibrahim, M.; Kern, J.; Kuczewski, A.; Lemke, H. T.; Liu, P.; Majlof, L.; McClintock, W. M.; Myers, S.; Nelsen, S.; Olechno, J.; Orville, A. M.; Sauter, N. K.; Soares, A. S.; Soltis, S. M.; Song, H.; Stearns, R. G.; Tran, R.; Tsai, Y.; Uervirojnangkoorn, M.; Wilmot, C. M.; Yachandra, V.; Yano, J.; Yukl, E. T.; Zhu, D.; Zouni, A., Acoustic Injectors for Drop-On-Demand Serial Femtosecond Crystallography. *Structure* **2016,** *24* (4), 631-640.

201. Ng, J. T.; Dekker, C.; Kroemer, M.; Osborne, M.; von Delft, F., Using textons to rank crystallization droplets by the likely presence of crystals. *Acta Crystallogr D Biol Crystallogr* **2014,** *70* (Pt 10), 2702-18.

202. Cox, O. B.; Krojer, T.; Collins, P.; Monteiro, O.; Talon, R.; Bradley, A.; Fedorov, O.; Amin, J.; Marsden, B. D.; Spencer, J.; von Delft, F.; Brennan, P. E., A poised fragment library enables rapid synthetic expansion yielding the first reported inhibitors of PHIP(2), an atypical bromodomain. *Chemical Science* **2016,** *7* (3), 2322-2330.

203. Winter, G., xia2: an expert system for macromolecular crystallography data reduction. *Journal of Applied Crystallography* **2010,** *43*, 186-190.

204. Krojer, T.; Talon, R.; Pearce, N.; Collins, P.; Douangamath, A.; Brandao-Neto, J.; Dias, A.; Marsden, B.; von Delft, F., The XChemExplorer graphical workflow tool for routine or large-scale protein-ligand structure determination. *Acta Crystallogr D Struct Biol* **2017,** *73* (Pt 3), 267-278.

205. Long, F.; Nicholls, R. A.; Emsley, P.; Graaeulis, S.; Merkys, A.; Vaitkus, A.; Murshudov, G. N., AceDRG: a stereochemical description generator for ligands. *Acta Crystallogr D Struct Biol* **2017,** *73* (Pt 2), 112-122.

206. Murshudov, G. N.; Skubak, P.; Lebedev, A. A.; Pannu, N. S.; Steiner, R. A.; Nicholls, R. A.; Winn, M. D.; Long, F.; Vagin, A. A., REFMAC5 for the refinement of macromolecular crystal structures. *Acta Crystallogr D Biol Crystallogr* **2011,** *67* (Pt 4), 355-67.

207. Emsley, P.; Lohkamp, B.; Scott, W. G.; Cowtan, K., Features and development of Coot. *Acta Crystallogr D Biol Crystallogr* **2010,** *66* (Pt 4), 486-501.

208. Nguyen, H. H.; Park, J.; Kang, S.; Kim, M., Surface plasmon resonance: a versatile technique for biosensor applications. *Sensors (Basel)* **2015,** *15* (5), 10481-510.

209. Tofi, M.; Georgiou, T.; Montagnon, T.; Vassilikogiannakis, G., Regioselective ortho lithiation of 3-aryl and 3-styryl furans. *Org Lett* **2005,** *7* (15), 3347-50.

210. Terracciano, S.; Chini, M. G.; Vaccaro, M. C.; Strocchia, M.; Foglia, A.; Vassallo, A.; Saturnino, C.; Riccio, R.; Bifulco, G.; Bruno, I., Correction: Identification of the key structural elements of a dihydropyrimidinone core driving toward more potent Hsp90 C-terminal inhibitors. *Chemical communications* **2016,** *52* (92), 13515.

211. Rubenstein, D. S.; Lipsius, S. L., Premature beats elicit a phase reversal of mechanoelectrical alternans in cat ventricular myocytes. A possible mechanism for reentrant arrhythmias. *Circulation* **1995,** *91* (1), 201-14.

212. Allan, R. K.; Mok, D.; Ward, B. K.; Ratajczak, T., Modulation of chaperone function and cochaperone interaction by novobiocin in the C-terminal domain of Hsp90: evidence that coumarin antibiotics disrupt Hsp90 dimerization. *J Biol Chem* **2006,** *281* (11), 7161-71.

213. Bruno, G.; Costantino, L.; Curinga, C.; Maccari, R.; Monforte, F.; Nicolo, F.; Ottana, R.; Vigorita, M. G., Synthesis and aldose reductase inhibitory activity of 5-arylidene-2,4-thiazolidinediones. *Bioorg Med Chem* **2002,** *10* (4), 1077-84.

214. De Marco, M.; Basile, A.; Iorio, V.; Festa, M.; Falco, A.; Ranieri, B.; Pascale, M.; Sala, G.; Remondelli, P.; Capunzo, M.; Firpo, M. A.; Pezzilli, R.; Marzullo, L.; Cavallo, P.; De Laurenzi, V.; Turco, M. C.; Rosati, A., Role of BAG3 in cancer progression: A therapeutic opportunity. *Semin Cell Dev Biol* **2017**.

215. Wang, X.; Chen, M.; Zhou, J.; Zhang, X., HSP27, 70 and 90, anti-apoptotic proteins, in clinical cancer therapy (Review). *Int J Oncol* **2014,** *45* (1), 18-30.

216. Moulick, K.; Ahn, J. H.; Zong, H.; Rodina, A.; Cerchietti, L.; Gomes DaGama, E. M.; Caldas-Lopes, E.; Beebe, K.; Perna, F.; Hatzi, K.; Vu, L. P.; Zhao, X.; Zatorska, D.; Taldone, T.; Smith-Jones, P.; Alpaugh, M.; Gross, S. S.; Pillarsetty, N.; Ku, T.; Lewis, J. S.; Larson, S. M.; Levine, R.; Erdjument-Bromage, H.; Guzman, M. L.; Nimer, S. D.; Melnick, A.; Neckers, L.; Chiosis, G., Affinity-based proteomics reveal cancer-specific networks coordinated by Hsp90. *Nat Chem Biol* **2011,** *7* (11), 818-26.

217. (a) Garg, G.; Zhao, H.; Blagg, B. S., Design, synthesis and biological evaluation of alkylamino biphenylamides as Hsp90 C-terminal inhibitors. *Bioorg Med Chem* **2017,** *25* (2), 451-457; (b) Gunaherath, G. M.; Marron, M. T.; Wijeratne, E. M.; Whitesell, L.; Gunatilaka, A. A., Synthesis and biological evaluation of novobiocin analogues as potential heat shock protein 90 inhibitors. *Bioorg Med Chem* **2013,** *21* (17), 5118-29; (c) Garg, G.; Zhao, H.; Blagg, B. S., Design, synthesis, and biological evaluation of ring-constrained novobiocin analogues as hsp90 C-terminal inhibitors. *ACS Med Chem Lett* **2015,** *6* (2), 204-9; (d) Byrd, K. M.; Subramanian, C.; Sanchez, J.; Motiwala, H. F.; Liu, W.; Cohen, M. S.; Holzbeierlein, J.; Blagg, B. S., Synthesis and Biological Evaluation of Novobiocin Core Analogues as Hsp90 Inhibitors. *Chemistry - A European Journal* **2016,** *22*

(20), 6921-31; (e) Kusuma, B. R.; Khandelwal, A.; Gu, W.; Brown, D.; Liu, W.; Vielhauer, G.; Holzbeierlein, J.; Blagg, B. S., Synthesis and biological evaluation of coumarin replacements of novobiocin as Hsp90 inhibitors. *Bioorg Med Chem* **2014,** *22* (4), 1441-9.

218.   Strocchia, M.; Terracciano, S.; Chini, M. G.; Vassallo, A.; Vaccaro, M. C.; Dal Piaz, F.; Leone, A.; Riccio, R.; Bruno, I.; Bifulco, G., Targeting the Hsp90 C-terminal domain by the chemically accessible dihydropyrimidinone scaffold. *Chem Commun* **2015,** *51* (18), 3850-3.

219.   Guo, W.; Reigan, P.; Siegel, D.; Zirrolli, J.; Gustafson, D.; Ross, D., Formation of 17-allylamino-demethoxygeldanamycin (17-AAG) hydroquinone by NAD(P)H:quinone oxidoreductase 1: role of 17-AAG hydroquinone in heat shock protein 90 inhibition. *Cancer Res* **2005,** *65* (21), 10006-15.

List of Abbreviations

17-AAG	17-N-allylamino-17-demethoxygeldanamycin
AAR	O-acetyl-ADP-ribose
ADPr	ADP-ribose
ADPRT	ADP-ribosyl-transferase
AR	Androgen receptor
ARTC	Arginine-specific ecto-enzymes
At	Arabidopsis thaliana
BAG	Bcl-2 associated athanogene
BD	BAG domain
BIR	Biotin ligase
BLI	Biolayer Interferometry
CCT	Chaperonin Containing TCP-1
CDK	Cyclin-Dependent Kinase
CMA	Chaperone-mediated autophagy
DEM	Depletor diethyl maleate
DHPM	3,4-dihydropyrimidin-2-(1H)-one
DIC	*N,N'*-Diisopropylcarbodiimide
DMAP	Dimethylaminopyridine
DMSO	Dimethyl Sulfoxide
DNMT	DNA-methyl-transferase
ER	Estrogen receptor
ESI-MS	Electrospray mass spectrometry
HAT	Histone acetyltransferases
HDAC	Histone deacetylases
Hsc70	Heat shock cognate 70
HSF1	Heat Shock Factor 1
Hsp	Heat Shock Protein
HSR	Heat Shock Response
IC_{50}	Half Maximal Inhibitory Concentration

IFITM-2	Interferon-induced transmembrane protein 2
IKK	IκB kinase
IMAC	Immobilized-metal affinitychromatography
IPTG	β-D-1-thiogalactopyranoside
IPV	Isoleucine–proline–valin
ITC	Isothermal titration calorimetry experiment
K_D	Dissociation Constant
LRP16	Leukemia-related protein 16
MacroD1	Macrodomain protein 1
MacroD2	Macrodomain protein 2
MAR	Mono-ADP-ribose
MARHs	Mono-ADP-ribose-protein hydrolases
MARTs	Mono-ADP-ribose-protein transferases
NAD	Nicotinamide adenine dinucleotide
NMR	Nuclear Magnetic Resonance
OD	Optical density
ODN	Oligodeoxynucleotides
PAR	Poly-ADP-ribose
PARG	PAR glycohydrolases
PARPs	PAR-polymerases
PBMC	Peripheral blood mononuclear cells
PDACs	Pancreatic ductal adenocarcinomas
PDB	Protein Data Bank
PDZGEF2	Guanine nucleotide exchange factor 2
PLC-g	Phospholipase C gamma
PTM	Post translational modification
PXXP	Proline-rich
Rap1	Ras proximate-1
RP-HPLC	Reverse Phase- High Performance Liquid Chromatography
SAR	Structure Activity Relationship
SCLC	Small cell lung cancer
SDS PAGE	Sodium Dodecyl Sulphate -PolyAcrylamide Gel Electrophoresis

SODD	Silencer of death domains
SPR	Surface plasmon resonance
STS	Staurosporine
SUMO	Small-ubiquitine-like modifiers
SYNPO2	Synaptopodin-2
TB	Terrific broth
TEV	Tobacco Etch Virus nuclear-inclusion-endopeptidase
THF	Tetrahydrofuran
TMSCl	Chlorotrimethylsilane
TNF	Tumor necrosis factor